Frequency Domain Temperature Model - A New Method in On-line Temperature Estimation for Power Modules in Drives Applications

Gareth Christopher James

A thesis submitted for the degree of
Engineering Doctorate in Power Electronics,
Machines and Drives

Newcastle University
School of Electrical, Electronic and Computer Engineering

Abstract

The operating temperature of the components within an electronic device has a significant impact on the reliability of a product. In a variable speed drive the power semiconductors in the inverter stage are often operated close to their maximum temperature when the inverter is operating at a low output frequency or during an overload. The temperature of these components must be continuously monitored to prevent them from overheating, but direct measurement of the temperature is only possible if a special test configuration can be used. This is not practicable in a commercial drive and to protect the inverter the temperature of the power semiconductors must be estimated by an on-line thermal model.

The work presented in this thesis describes the development of a novel thermal model that can be implemented using the existing computational resources available in a commercial variable speed drive. The thermal model is based on the transient thermal impedance measured between each device and the internal thermistor in a power module. These form a thermal impedance matrix which can be used to calculate the instantaneous temperature of every device in the inverter. However, with the existing computational resources it is not possible to implement the complete matrix without aliasing. To reduce the risk of aliasing the number of calculations performed during each sample period must be reduced. This is achieved by using a frequency domain model that has been developed to calculate the peak temperature of the hottest devices.

To validate the thermal model it has been implemented in a commercial drive. The drive has been modified to allow the temperature of the power semiconductors in the inverter to be measured using a high speed thermal camera. This allows the temperature estimated by the on-line thermal model to be compared directly with the temperatures measured when the inverter is operating under typical load conditions. Comparisons of the measured and estimated temperatures in several operating conditions are presented. These conditions were chosen to highlight the advantages and disadvantages of the frequency domain model.

Contents

Abstract 2

Contents 3

List of Figures 7

List of Tables 12

Acknowledgements 14

List of Symbols 15

Chapter 1: Introduction 18

1.1 Thermal Protection of the Power Electronics in a Three Phase Inverter 18
1.2 Objectives of the Work 19
1.3 Overview of the Thesis 19
1.4 The Contribution to Knowledge 22

Chapter 2: Background Information 23

2.1 Introduction 23
2.2 Operation of a Variable Speed Drive 23
2.2.1 Typical Power Stage Configuration 24
2.2.2 Motor Control Algorithms 25
2.3 Power Semiconductor Technology 28
2.3.1 Operating Limits and Typical Failure Modes 29
2.4 Power Loss in a Semiconductor 33
2.4.1 Review of Power Loss Models 34
2.4.2 Review of Behaviour Models 35
2.5 Fundamentals of Heat Transfer 37
2.5.1 Thermal Impedance and the Development of Equivalent Thermal Networks 40
2.6 Summary 43

Chapter 3: A Review of Thermal Modelling Techniques 45

3.1 Introduction 45
3.2 Key Requirements for the Inverter Thermal Model 45
3.3 Thermal Modelling Techniques 47
3.3.1 Datasheet Thermal Impedance Model 47
3.3.2 Analytical Solutions 48
3.3.3 Compact Thermal Models 49
3.3.4 Parameter Extraction Network 50
3.3.5 Thermal Impedance Matrix 52
3.3.6 Summary of the Thermal Models 55
3.4 Comparison of the Parameter Extraction and Thermal Impedance Models 57
3.5 Summary 60

Chapter 4: Development of a Thermal Model 61

4.1 Introduction 61
4.2 Steady-State Thermal Model Development 64
4.2.1 Frequency Components of the Current in an IGBT and Anti-Parallel Diode 64
4.2.2 Switching Loss Model 67
4.2.3 Conduction Loss Model 75
4.3 Calculation of the Peak Ripple Temperature 83
4.3.1 Taylor Series Approximation of the Peak Ripple Temperature 83
4.4 Comparison of the Peak Temperature in a Steady-State Operating 89
4.5 Transient Response 92
4.5.1 Calculation of the Transient Response for a General Frequency Component 92
4.5.2 Development of a Continuous Transient Model 96
4.6 Summary 104

Chapter 5: Implementation of the Thermal Model in a Three Phase Inverter 106

5.1 Introduction 106
5.2 Implementation of the Frequency Model for a System Represented by Multiple Foster Network Elements 108
5.3 Development of a Frequency Model for an Inverter 110
5.3.1 Protection of an Inverter Operating in a Stationary Vector Condition 112
5.3.2 Estimated Temperature over a Complete Output Cycle of the Inverter 116
5.4 Simplifying the Frequency Model 117
5.4.1 Single Device Model 118
5.4.2 Single Device Model including the Thermal Coupling between devices 121
5.5 Thermal Parameters used in the Frequency Model 123
5.5.1 Selection of the Elements in each Foster Network 123
5.5.2 Reducing the Number of Mutual Terms in the Frequency Model 124
5.6 Implementation of the Frequency Model and Summary of the Input Parameters 129
5.7 Summary 132

Chapter 6: Measurement of the Power Module Parameters 134

6.1 Introduction 134
6.2 Device Selection and Power Module Preparation 136
6.2.1 Power Module Preparation 136
6.3 Thermal Impedance Measurements 137
6.3.1 Experimental Setup 139
6.3.2 Calculation of the Self Thermal Impedance 141
6.3.3 Calculation of the Mutual Thermal Impedance 147
6.4 Loss Parameter Measurements 152
6.4.1 Experimental Setup 152
6.4.2 Switching Loss Parameters 153
6.4.3 Conduction Loss Parameters 157
6.5 Summary 159

Chapter 7: Calculation of the Thermal Model Input Parameters 161

7.1 Introduction 161
7.2 Calculation of the Coefficients for the Loss Models 162
7.2.1 IGBT turn-on Energy 162
7.2.2 Investigation into the Accuracy of the Power Loss Models 167
7.3 Calculation of the Thermal Impedance Parameters 168
7.3.1 Thermal Network Parameters 169
7.3.2 Thermal Impedance Matrix Simplification 172
7.3.3 Combination of Mutual Thermal Impedance Terms 176
7.4 Summary 179

Chapter 8: Results and Comparison 180

8.1 Introduction 180
8.2 Basic Thermal Model Development 181
8.3 Test Setup 184
8.4 Comparison of the Estimated and Measured Device Temperature 186
8.4.1 Stationary Vector Condition 186
8.4.2 Operation at a Low Output Frequency 189
8.4.3 Operation at a High Output Frequency 193
8.5 Application Case Studies 195
8.5.1 Pick and Place Machine 196
8.5.2 Elevator 198
8.6 Summary 202

Chapter 9: Conclusion 204

9.1 General Overview 204
9.2 Thermal Model for a Single Device 205
9.3 Thermal Model for a Multi-chip Device 206
9.4 Measurements 207
9.5 Comparison of the Thermal Model with Measured Temperatures 208
9.6 Recommendations for Further Work 209

Appendix A: Temperature Response of the Frequency Model 211

A.1 Introduction 211
A.1.1 Calculation of the Frequency Components for a General Term 211
A.1.2 Complete Temperature Response for the Switching Loss Model 216
A.1.3 Complete Temperature Response for the Conduction Loss Model 217

Appendix B: Measured Thermal Parameters for the Inverter 219

B.1 Introduction 219
B.2 Diode Thermal Resistance Comparison 219
B.3 Thermal Impedance Matrix 220
B.4 Curve Fitted Network Parameters for the Transient Thermal Impedance 221
B.4.1 Self Thermal Impedance Network Parameters 221
B.4.2 Mutual Thermal Impedance Network Parameters 222

Appendix C: Pulse Testing Procedure 224

C.1 Introduction 224
C.1.1 Experimental Setup 224
C.1.2 Switching Loss 226
C.1.3 On-State Voltage 227

Appendix D: Switching and Conduction Loss Parameters 228

D.1 Introduction 228
D.2 Switching Loss 229
D.2.1 IGBT Turn-on Energy (E_{on}) 229
D.2.2 IGBT Turn-off Energy (E_{off}) 230
D.2.3 Diode Turn-off Energy (E_{rec}) 231
D.3 Conduction Loss Parameters 232
D.3.1 IGBT on-state Voltage (V_{CE}) 232
D.3.2 Diode Forward Voltage (V_F) 233

Appendix E: Transient Temperature Response 234

E.1 Introduction 234
E.2 IGBT transient response 234
E.3 Diode transient response 236

Appendix F: Temperature Measurements and Comparison 238

F.1 Introduction 238
F.2 Thermal Coupling between Devices 238
F.3 Temperature Distribution in a Stationary Vector Condition 239
F.4 Comparison during an Acceleration, Steady-state and Deceleration Period 240

List of References 243

List of Figures

Figure 2.1: Application of an AC drive 24
Figure 2.2: Typical power stage used in a three phase AC drive 24
Figure 2.3: Sinusoidal modulation 25
Figure 2.4: Load current 27
Figure 2.5: Power semiconductors construction (a) PIN diode (b) PT IGBT 28
Figure 2.6: Typical safe operating areas (a) FBSOA and SCSOA (b) RBSOA 30
Figure 2.7: Power loss in a semiconductor 33
Figure 2.8: Thermal networks with n elements a) Foster b) Cauer 40
Figure 3.1: Case and thermistor temperature measured in a stationary vector condition when a step change in output current is applied to the inverter 48
Figure 3.2: Compact thermal model (a) boundary locations (b) network topology 49
Figure 3.3: Power device construction and the equivalent Cauer network for one layer 51
Figure 3.4: Principle of superposition applied to heat conduction (a) heat spreader with two heat sources (b) temperature measured on the upper surface 53
Figure 3.5: Heat spreader with a single heat source and a constant cooling boundary (a) restricted heat flow (b) heat spread 57
Figure 3.6: Thermal impedance (a) restricted heat flow (b) heat spread 59
Figure 3.7: Comparison of the temperature profile and thermal resistance 60
Figure 4.1: Thermal model implemented in the time domain using the instantaneous phase currents to calculate the temperature of every device in the inverter ... 61
Figure 4.2: Thermal model implemented in the frequency domain using the magnitude of the phase current and output frequency to calculate the temperature of the hottest IGBT and diode in the inverter 62
Figure 4.3: Phase current in an IGBT and an anti-parallel diode 65
Figure 4.4: Switching power loss over a switching frequency cycle (a) IGBT (b) diode 67
Figure 4.5: Comparison of the measured and approximated switching loss for an IGBT and diode over a complete output cycle of an inverter (1 PU = peak IGBT power loss) 68
Figure 4.6: Device switching loss calculated over a complete output cycle of the inverter (a) response of the sinusoidal and frequency model (b) the difference between the frequency and sinusoidal response (1 PU = peak sinusoidal switching loss) 69
Figure 4.7: Sinusoidal switching loss model 74
Figure 4.8: Comparison of the (a) temperature response for the sinusoidal and frequency models at an output frequency of 0.1Hz (b) maximum temperature verses output frequency 75
Figure 4.9: Conduction power loss over a switching frequency cycle 76
Figure 4.10: Comparison of modulation schemes with a unity modulation index (a) SVM (Alt-Rev) and third harmonic (b) third harmonic and sinusoidal approximation 78

Figure 4.11: Sinusoidal conduction loss model 82
Figure 4.12: Temperature response of the sinusoidal and frequency models with an output frequency of 0.1Hz (a) IGBT (b) anti-parallel diode 82
Figure 4.13: Taylor series approximation of the ripple temperature with the peak ripple at an output angle of (a) $\omega t=\pi/2$ (b) $\omega t=0$ 86
Figure 4.14: Taylor series approximation (a) angles between peaks of the harmonic components (b) offset angles used to align the peak ripple with the origin 88
Figure 4.15: Comparison of the peak junction-to-reference temperature calculated for an IGBT (τ_{th}=1s) using the frequency model and the instantaneous sinusoidal approximation at an output frequency of (a) 0Hz (stationary vector condition) (b) 1Hz 90
Figure 4.16: Comparison of the power loss and the resulting temperature rise for a leading and lagging displacement power factor of 0.5 (a) current, duty cycle and power loss (b) temperature rise over a single output cycle of the inverter (1 PU = maximum temperature) 91
Figure 4.17: Transient response (a) steady-state and transient components (b) complete response (1 PU = steady-state ripple temperature) 95
Figure 4.18: Transient response for a step change in (a) switching loss (b) output frequency (1 PU = peak temperature when F_{out} = 0Hz) 97
Figure 4.19: Transient response (a) magnitude of the factor K_{exp} if the ripple temperature is increasing (b) comparison of peak ripple temperature and the transient component 99
Figure 4.20: Implementation of (a) ripple (b) DC components in the continuous model 100
Figure 4.21: Calculation of the transient component (a) original response due to a step change in power loss and output frequency (b) additional response added to remove the steady-state component after 10s (c) complete response (1 PU = steady-state temperature) 100
Figure 4.22: Implementation of the transient component in the continuous model 101
Figure 4.23: Transient model for a step change in power loss (a) DC, ripple and transient components (b) comparison of the instantaneous response and frequency model 102
Figure 4.24: Operating conditions used to compare the frequency model with the instantaneous response (a) operating condition A (b) operating condition B 103
Figure 4.25: Comparison of the frequency model with the instantaneous temperature response for (a) operating condition A (b) operating condition B 103
Figure 5.1: Superposition of the self and mutual thermal impedance 108
Figure 5.2: Flotherm model of a typical power module 110
Figure 5.3: Maximum steady-state junction-to-thermistor temperature (a) selection of the peak temperature for a unity displacement power factor and modulation index (b) peak temperature calculated for all operating conditions 113
Figure 5.4: The devices in which the peak junction-to-thermistor temperature occurs when operating in a stationary vector condition with a constant power loss 114

Figure 5.5: Comparison of the temperature estimated by the frequency model and the maximum steady-state temperature when operating in a stationary vector condition 116
Figure 5.6: Comparison of the single device model developed for I_{UL} when operating with a unity modulation index (a) junction-to-thermistor temperature (b) percentage error 119
Figure 5.7: Error in the single device model when operating in a stationary vector condition (a) IGBT model (b) IGBT and diode models implemented in parallel 120
Figure 5.8: Error in the single device model with thermal coupling when in a stationary vector condition (a) IGBT model (b) IGBT and diode models implemented in parallel 122
Figure 5.9: Combining network elements with the same time constant and offset angle 125
Figure 5.10: Comparison of the step response calculated using the original network parameters and the common time constants in a stationary vector condition with a unity modulation index (a) step response (b) temperature difference 128
Figure 5.11: Control flow diagram for the implementation of the IGBT frequency model for a three phase inverter 130
Figure 6.1: Control Techniques Unidrive SP and power module 136
Figure 6.2: Power module after preparation for thermal testing 137
Figure 6.3: Example of the thermal impedance calculation (a) measured cooling response for the device and thermistor (b) calculated transient thermal impedance 138
Figure 6.4: Equipment setup used to measure the transient thermal impedance 139
Figure 6.5: Test circuit for the thermal impedance measurements 140
Figure 6.6: Example of the measured surface temperature for (a) IGBT and (b) diode 141
Figure 6.7: Self thermal impedance calculations (a) measured cooling temperatures (b) transient thermal impedance between the device and thermistor 142
Figure 6.8: Comparison of the measured ($R_{th,ii(j\text{-}th)}$) and datasheet ($R_{th(j\text{-}c)}$) self thermal resistance for the IGBTs in the inverter 143
Figure 6.9: Definition of the internal parasitic resistance in a single phase of the inverter 145
Figure 6.10: Investigation into the effect of the mutual coupling between the parasitic resistance and a device (a) thermal image with profiles (b) measured profile temperature 147
Figure 6.11: Normalised temperature distribution showing the effects of the (a) distance between the devices (b) operating conditions and power loss in each device 148
Figure 6.12: Heat spreader with two heat sources 149
Figure 6.13: Mutual thermal impedance calculation (a) measured cooling temperature (b) transient thermal impedance between the device and thermistor 150
Figure 6.14: Mutual thermal impedance measured when a power loss is applied to I_{UU} .. 151
Figure 6.15: Test circuit used to measure the switching and conduction loss parameters for the lower IGBT (I_{UL}) and upper diode (D_{UU}) in the U phase of the inverter 152

Figure 6.16: An example of the switching characteristics (I_L=50A, V_{DC}=600V, T_j=25°C) and the measured energy loss (a) IGBT turn-on (b) IGBT turn-off (c) diode turn-off 155
Figure 6.17: Measured on-state voltage (a) IGBT (V_{CE}) (b) diode (V_F) 159
Figure 7.1: Comparison of the measured and curve fitted IGBT turn-on energy verses (a) current (b) temperature (V_{DC} = 600V) 163
Figure 7.2: IGBT turn-on energy (a) measured and curve fitted switching energy verses DC link voltage (b) calculated energy verses current and temperature (V_{DC} = 800V) 166
Figure 7.3: Maximum and average difference between the measured and estimated (a) switching energy (b) on-state voltage 167
Figure 7.4: Foster network with four elements (k=4) 169
Figure 7.5: Comparison of the measured transient thermal impedance with the response of an equivalent Foster network (a) self thermal impedance - $Z_{th}(I_{UU}\text{-}I_{UU})$ (b) mutual thermal impedance - $Z_{th}(I_{UU}\text{-}I_{UL})$ 170
Figure 7.6: Devices in which the peak junction temperature occurs in a stationary vector (a) IGBT (b) diode (I_L=50A, V_{DC}=600V, T_{th}=80°C, F_{SW}=3kHz) 173
Figure 7.7: Error calculated when operating in a stationary vector condition and a high output frequency (a) IGBT model (b) IGBT and diode models implemented in parallel 175
Figure 7.8: Comparison of the step response calculated using the original network parameters and the common time constants in a stationary vector condition with a unity displacement power factor (a) step response (b) temperature difference 177
Figure 8.1: Constants for the basic thermal model calculated at 3kHz (a) K_{50Hz} (b) K_{0Hz} 182
Figure 8.2: Implementation of the basic thermal model (a) K_{Fout} (b) junction-to-thermistor temperature estimated at 75A 183
Figure 8.3: Implementation of the basic thermal model in a continuous system 184
Figure 8.4: Test setup used to measure the temperature under typical operating conditions 185
Figure 8.5: Test setup (a) Unidrive SP with the embedded thermal model (b) power module fitted on a standard heatsink showing the connections between the drive and module 186
Figure 8.6: Comparison in a stationary vector condition (a) load conditions and (b) comparison with peak current in I_{UU} (c) load conditions and (d) comparison with peak current in I_{VU} (e) load conditions and (f) comparison with peak current in I_{WU} 187
Figure 8.7: Comparison at a low output frequency (a) load conditions and (b) comparison for the IGBT model (c) load conditions and (d) comparison for the diode model 190
Figure 8.8: Diode in which the peak junction-to-thermistor temperature occurs in a stationary vector condition (a) operating condition A - I_L=50A, V_{DC}=600V, T_{th}=80°C and F_{SW}=3kHz (b) operating condition B - I_L=16A, V_{DC}=550V, T_{th}=40°C and F_{SW}=16kHz 191
Figure 8.9: Thermal coupling between I_{WU} and D_{VU} (a) thermal image taken with the peak loss in I_{WU} (b) measured profile temperature along the centre of a diode 192

Figure 8.10: Comparison at a high output frequency (a) load conditions and (b) comparison at 16.7Hz (c) load conditions and (d) comparison at 8.3Hz (e) load conditions and (f) comparison at 5Hz 194
Figure 8.11: Typical pick and place machine load profile 196
Figure 8.12: Pick and place machine tool comparison (a) load conditions and (b) comparison over the full profile (c) close up of the acceleration period (d) close up of the deceleration period 197
Figure 8.13: Typical elevator profile with hold at floor operation 199
Figure 8.14: Elevator comparison with a steady state output frequency of 25Hz (a) load conditions and (b) comparison for a single profile (c) load conditions and (d) comparison for two profiles (e) load conditions and (f) comparison with hold at floor current 200
Figure 8.15: Close up of the elevator profile during (a) acceleration (b) deceleration 201
Figure B.1: Comparison of the measured ($R_{th,ii(j-th)}$) and datasheet ($R_{th(j-c)}$) self thermal resistance for the diodes in the inverter 219
Figure C.1: Physical layout used to measured the switching loss and on-state voltage... 224
Figure C.2: Test circuit used to measure the switching loss of the lower IGBT and the upper diode in the U phase of the inverter 225
Figure C.3: Double switching pulse used to control the current magnitude for the switching loss measurements 226
Figure C.4: Single switching pulse used to control the current magnitude for the on-state voltage measurements 227
Figure E.1: Comparison of switching frequencies (a) step response (b) error temperature 234
Figure E.2: Comparison of displacement power factors (a) step response (b) error temperature 235
Figure E.3: Comparison of modulation index (a) step response (b) error temperature ... 236
Figure E.4: Comparison of switching frequencies (a) step response (b) error temperature 236
Figure E.5: Comparison of displacement power factors (a) step response (b) error temperature 237
Figure F.1: Maximum IGBT temperature measured at a switching frequency of 16kHz, load current of 25A and an output frequency of 2.5Hz 238
Figure F.2: Inverter operating in a stationary vector condition at a switching frequency of 16kHz and a current of 19A (a) Infrared image (b) Surface temperature of I_{UU} 239
Figure F.3: Comparison of the measured (maximum) and estimated temperature with the inverter operating in a stationary vector condition at a switching frequency of 16kHz and a load current of 19A (Output frequency = 0Hz) .. 240
Figure F.4: Comparison of the IGBT model with the inverter operating at a switching frequency of 16kHz, load current of 25A and an output frequency = 10Hz (a) complete response (b) acceleration period (c) steady state period (d) deceleration period 241
Figure F.5: Comparison of the diode model with the inverter operating at a switching frequency of 16kHz, load current of 25A and an output frequency = 10Hz (a) complete response (b) acceleration period (c) steady state period (d) deceleration period 242

List of Tables

Table 2.1: Destructive Mechanisms for an IGBT 31
Table 2.2: Power loss calculation for an IGBT and diode 35
Table 3.1: Key features of the thermal models 56
Table 3.2: Thermal Resistance and Capacitance for a Cauer network 58
Table 3.3: Thermal Resistance and Capacitance for a Foster network 58
Table 4.1: Frequency components of the temperature rise due to the device switching loss 73
Table 4.2: Frequency components for the device conduction loss 80
Table 6.1: Internal Resistance 145
Table 6.2: Switching loss measurement conditions 154
Table 6.3: Comparison of the datasheet and measured switching energy with a current of 75A, DC link voltage of 600V and a device temperature of 125°C 156
Table 6.4: Comparison of measured and datasheet on-state voltage for an IGBT and diode 158
Table 7.1: Current loss coefficients for the IGBT turn-on energy 163
Table 7.2: Temperature loss coefficients for the IGBT turn-on energy 164
Table 7.3: Voltage loss coefficients for the IGBT turn-on energy 166
Table 7.4: Foster network parameters for $Z_{th}(I_{UU}\text{-}I_{UU})$ 171
Table 7.5: Foster network parameters for $Z_{th}(I_{UU}\text{-}I_{UL})$ 171
Table 7.6: Network parameters for the equivalent Foster networks for I_{UU} and D_{UU} 174
Table 7.7: IGBT and Diode thermal model parameters 178
Table 8.1: Operating conditions used to calculate the maximum device temperature 182
Table A.1: Components of the temperature response due to the device switching loss 216
Table A.2: Components of the temperature response due to the device conduction loss 218
Table B.1: Steady-state thermal impedances between the junction and thermistor (K/W) 220
Table B.2: IGBT network parameters 221
Table B.3: Diode network parameters 221
Table B.4: IGBT to IGBT network parameters 222
Table B.5: Diode to IGBT network parameters 222
Table B.6: Diode to diode network parameters 223
Table B.7: IGBT to diode network parameters 223
Table D.1: Loss parameters 229
Table D.2: Measured switching energy with a DC Link voltage of 600V (mJ) 229
Table D.3: Calculated switching energy with a DC Link voltage of 600V (mJ) 229
Table D.4: Loss parameters 230
Table D.5: Measured switching energy with a DC Link voltage of 600V (mJ) 230
Table D.6: Calculated switching energy with a DC Link voltage of 600V (mJ) 230
Table D.7: Loss parameters 231

Table D.8: Measured switching energy with a DC Link voltage of 600V (mJ) 231
Table D.9: Calculated switching energy with a DC Link voltage of 600V (mJ) 231
Table D.10: Loss parameters 232
Table D.11: Measured on-state voltage (V) 232
Table D.12: Calculated on-state voltage (V) 232
Table D.13: Loss parameters 233
Table D.14: Measured forward voltage (V) 233
Table D.15: Calculated forward voltage (V) 233

Acknowledgements

First and foremost I would like to thank everybody at Control Techniques for their help. In particular Tom Alexander and Bill Drury for giving me the opportunity to undertake this degree and for their support throughout this project, for this I will be forever grateful. In life there are defining moments and being given this opportunity was one.

I would like to acknowledge the funding provided by Control Techniques and the Engineering and Physical Sciences Research Council, without which this project could not have been undertaken.

Special thanks are due to my supervisors, Mike Cade and Volker Pickert, for the guidance, help and encouragement they have given me over the last four years. I am especially grateful for their patience when reading the initial drafts of my thesis and the detailed and constructive feedback they provided. Without them I would not have learned or achieved so much.

The UG lab at Newcastle University has been a lively, motivating and friendly place to work and I must thank everybody for making it such an enjoyable experience. The unpredictable, expansive and sometimes heated discussions at the dining table were always a highlight of the day. People who deserve a special mention are Chris Bateman and Graeme Hutchinson, their help, advice and friendship has been important.

I would like to convey my heartfelt thanks to my family who have given me so much support and motivation. Above all I would like to thank my wife Jane for her continued love and support, not least for agreeing to move to Newcastle the day after our honeymoon. Finally, thanks are due to my daughter Freya, whose arrival towards the end of this project has been a wonderful distraction.

List of Symbols

A_n	Magnitude of a general n^{th} harmonic frequency component (°C)
A_{cn}	Magnitude of the cosine component for the n^{th} harmonic model (°C)
$A_{con(n)}$	Magnitude of the combined sine and cosine component for the n^{th} harmonic in the conduction loss model (°C)
A_{DC}	Magnitude of the DC component (°C)
A_{Fn}	Magnitude of the filter term for the n^{th} harmonic
A_{sn}	Magnitude of the sine component for the n^{th} harmonic model (°C)
$A_{sw(n)}$	Magnitude of the combined sine and cosine component for the n^{th} harmonic in the switching loss model (°C)
C_{th}	Thermal capacitance (Ws/K)
D_{UL}	Lower diode in the U phase of the inverter
D_{UU}	Upper diode in the U phase of the inverter
D_{VL}	Lower diode in the V phase of the inverter
D_{VU}	Upper diode in the V phase of the inverter
D_{WL}	Lower diode in the W phase of the inverter
D_{WU}	Upper diode in the W phase of the inverter
E_{off}	IGBT turn-off energy loss (mJ)
E_{on}	IGBT turn-on energy loss (mJ)
E_{rec}	Diode reverse recovery (turn-off) energy loss (mJ)
F_{out}	Output frequency of the inverter (Hz)
F_{sw}	Inverter switching frequency (Hz)
iu, iw, iv	Instantaneous inverter output current (A)
I_L	Inverter load current (A)
I_{UL}	Lower IGBT in the U phase of the inverter
I_{UU}	Upper IGBT in the U phase of the inverter
I_{VL}	Lower IGBT in the V phase of the inverter
I_{VU}	Upper IGBT in the V phase of the inverter

I_{WL}	Lower IGBT in the W phase of the inverter
I_{WU}	Upper IGBT in the W phase of the inverter
K_{exp}	Factor used to scale the transient magnitude during increases in the ripple temperature
L_s	Stray inductance in the switching circuit (H)
m	Modulation index
$m_{(DC)}$	Modulation index associated with the DC component of the approximate scheme
P_{con}	Conduction power loss (W)
$P_{con(\delta m=1)}$	Conduction power loss with a unity duty cycle (W)
P_{sw}	Switching power loss (W)
R_g	Gate resistance (Ω)
R_{th}	Thermal resistance (K/W)
T_a	Ambient temperature (°C)
T_{con}	Temperature rise due to the conduction loss (°C)
T_{DC}	Temperature rise due to the DC component of the response (°C)
T_{exp}	Magnitude of the transient component in the response (°C)
T_j	Absolute junction temperature (°C)
$T_{j\text{-}ref}$	Temperature between the junction and reference value (°C)
T_{ripple}	Temperature rise due to the steady-state component of the response (°C)
T_{ss}	Steady-state temperature (°C)
T_{sw}	Temperature rise due to the switching loss (°C)
T_{th}	Thermistor temperature (°C)
T_{tran}	Transient temperature (°C)
V_{CE}	IGBT on-state voltage (V)
V_{ge}	Gate Emitter voltage (V)
V_{DC}	DC link voltage (V)
V_F	Diode on-state voltage (V)
Z_{th}	Thermal impedance (K/W)
$Z_{th,j\text{-}ref}$	Thermal impedance between the junction and reference value (K/W)

α	Device offset angle (radians)
β_n	Phase shift due to the thermal time constant (radians)
δ_m	Duty cycle
$\delta_{m(IGBT)}$	IGBT duty cycle
$\delta_{m(diode)}$	Diode duty cycle
θ	Power factor angle (radians)
σ_n	Phase angle for the n^{th} harmonic for the combined response of the switching and conduction loss (radians)
ψ	Offset angle for the first harmonic used to align the peak ripple with the origin (radians)
τ_{th}	Thermal time constant (s)
τ_{IGBT}	Thermal time constant for the Foster network element used to represent all of the mutual thermal coupling from the IGBTs in the inverter(s)
τ_{diode}	Thermal time constant for the Foster network element used to represent all of the mutual thermal coupling from the diodes in the inverter(s)
ϕ	Angle between the peaks of the first and second harmonics in the ripple temperature (radians)
ϕ_{min}	Minimum angle between the peaks of the first and second harmonics in the ripple temperature (radians)
ω	Output frequency of the inverter (radians/s)
ωt_{max}	Location of the maximum turning point in the ripple temperature (radians)
ωt_{min}	Location of the minimum turning point in the ripple temperature (radians)

Chapter 1: Introduction

1.1 Thermal Protection of the Power Electronics in a Three Phase Inverter

To ensure the reliable operation of a variable speed drive it is important that the power electronic components are prevented from exceeding their maximum operating temperature. If this is not done it can lead to a premature failure. However, when designing an inverter it is desirable to allow these components to operate as close as possible to their maximum temperature since this has a positive impact of the performance, size and cost of a product. Consequently, in some operating conditions, especially during overloads, it is possible that these components could exceed their maximum junction temperature. In a commercial product this temperature cannot be measured directly and in most applications only the case temperature of a power module is measured. Therefore, a 'real-time' thermal model must be used to estimate the transient temperature response between the junction of a device and the case temperature.

This project was initiated because several weaknesses were identified in the existing thermal model employed by Control Techniques. These can result in the temperature of the power electronics being underestimated. Furthermore, by improving the accuracy of the thermal model and minimising any overestimation of the temperature an opportunity to improve the maximum current rating of an inverter was identified.

One of the present trends in the power electronic industry is to increase the current density of a multi-chip power module by reducing the size of the individual chips and/or packaging. As the size of a chip is reduced its self thermal impedance is increased and for a given power loss the operating temperature will be higher. In addition, in a smaller package the chips are closer together and they will begin to thermally interact with one another. This can have a significant effect on the temperature of a device when the inverter is operating at an output frequency of 0Hz (often referred to as a stationary vector condition or a DC condition). In this condition there is no filtering effect due to the thermal time constants

associated with the thermal impedance between the devices. Consequently, the operating temperature of a device can be much higher than the temperature calculated using the self thermal impedance provided by the manufacturer, which is usually the only thermal impedance given in a datasheet. This effect is described in [1] and is one of the major limitations of existing approaches that rely on the datasheet values to develop a thermal model for an inverter application.

1.2 Objectives of the Work

The main objective of this work is to develop a thermal model that can be used to estimate the transient temperature response between the junction of the hottest device in an inverter and a reference temperature measured by a thermistor. This model must include the thermal interaction between all of the devices in the inverter, the impact of the thermistor location, and the effect of the operating conditions on the power loss generated in a device. One of the most important requirements is that it must be possible to implement the thermal model using the existing computational resources without introducing the risk of aliasing.

1.3 Overview of the Thesis

This thesis is divided into nine chapters with Chapter one providing a general introduction to the project and identifying the key aims and objectives.

Chapter two describes the key principles that must be understood in order to develop a thermal model. This includes a brief description of a variable speed drive, the operation of an inverter, construction of the power semiconductors and the heat transfer mechanisms. The latter includes the definition of thermal resistance and capacitance and describes how these values can be used to form an equivalent thermal network.

Chapter three reviews the different approaches that can be used to develop a thermal model for a multi-chip device and provides a review of published work in this area. In this review the strengths and weaknesses of the different methods are covered and these are used to select a suitable design approach.

Chapter four covers the development of a unique thermal model based on the representation of the power loss generated in a device by its frequency components. These frequency

components are developed by assuming that the power loss in a device is proportional to its current and in an inverter this can be approximated by a half wave rectified sinusoid. These frequency components are then used to calculate the temperature response due to the switching and conduction loss. The procedure described in Chapter four is summarised below:

1. Determine the power loss of a device over a complete output cycle due to its switching characteristics and represent this loss as a series of frequency components.
2. Apply the frequency components for the switching loss to an equivalent thermal network and calculate the resulting temperature rise in the frequency domain.
3. Determine the power loss of a device over a complete output cycle due to its conduction characteristics and represent this loss as a series of frequency components.
4. Apply the frequency components of the conduction loss to an equivalent thermal network and calculate the resulting temperature rise in the frequency domain.
5. Combine the frequency components for the switching and conduction loss.

By following the procedure outlined above the steady-state temperature of one device can be calculated. However, an additional step is performed to determine the peak temperature that occurs over one complete output cycle of the inverter:

6. Use the magnitude and phase of the combined frequency components to calculate the peak steady-state temperature between the junction of the device and the measured reference temperature.

If the peak temperature is known it is not necessary to calculate the temperature at each sample point and this reduces the number of calculations that must be performed in order to protect an inverter. Consequently, calculating the peak temperature is one of the key steps used to development the thermal model proposed in this work. In the final section of Chapter four the transient response of the thermal model is investigated and the method used to implement the transient component for a single device is proposed.

Chapter five describes the adaption of the thermal model developed in chapter four to a power module containing the twelve devices (six IGBTs and six freewheeling diodes) used in the inverter stage of a variable speed drive. This model is based on the use of a thermal impedance matrix and the principle of superposition, which allows the effect of the self and mutual thermal impedance to be included in the model. The implementation of the complete matrix is described at the beginning of the chapter. However, to implement the thermal model on-line some level of simplification is required and different approaches are compared. From this investigation a thermal model that can be used to protect the devices in the inverter is proposed and the complete model is presented in the form of a control diagram.

Chapter six includes a description of the test methods that have been used to measure the input data required by the thermal model. This data includes the on-state voltage and switching energy of an IGBT and diode, along with the self and mutual transient thermal impedances that form the complete thermal impedance matrix for the inverter.

Chapter seven uses the data measured in chapter six to develop the behaviour models that are used to estimate the change in the on-state voltage and switching energy with temperature, voltage and current. Furthermore, the measured thermal impedances are converted into an equivalent thermal network and these are used to identify the hottest IGBT and diode under a defined operating condition. From this investigation the thermal parameters used in the thermal model are selected.

Chapter eight compares the instantaneous IGBT and diode temperatures measured by an infrared camera with the temperature estimated by the thermal model developed in this work and the existing thermal model used in a Control Techniques, Unidrive SP. These are compared under typical operating conditions for the inverter and include operation in a stationary vector condition. From these comparisons the advantages and disadvantages of the new thermal model are highlighted.

Chapter nine describes the major achievements and shortcomings of the research and the extent to which the initial aims have been fulfilled. This chapter also covers some suggestions for further work.

1.4 The Contribution to Knowledge

This section outlines the areas of work in this thesis that the author believes have not been previous published:

Chapter Four

- The development of a thermal model based on the representation of the power loss generated in a device (over a complete output cycle of an inverter) by its frequency components.
- The modification of the frequency components to minimise the number of calculations required to implement the model.
- A method of calculating the peak temperature response over an output cycle using the Taylor series approximation of the frequency components.
- The identification and modelling of the transient components of the thermal model.

Chapter Five

- The calculation of the temperature rise of a multi-chip device represented by more than one equivalent Foster network by combining frequency components with different offset values.

Chapter Six

- The investigation into the effect of the fan speed on the measured self and mutual thermal impedance measured between the junction of a device and the internal thermistor in the power module.

Chapter 2: Background Information

2.1 Introduction

This chapter describes the key principles that must be understood in order to develop a thermal model to protect the power semiconductors in the inverter stage of an industrial variable speed drive (VSD). These principles include:

a) Operating theory of an industrial variable speed drive
b) Electrical characteristics of the power semiconductors
c) Factors limiting the maximum operating conditions
d) The power loss generated in a device
e) Thermal characteristics of a power module and drive system

The operating theory of an industrial VSD has a significant impact on the development of a thermal model since it defines the conditions in which the power semiconductors must operate. To show how a drive works, the configuration of a typical power stage is described in Section 2.2. In this section the power semiconductors and the control algorithms used to produce the required output voltages are introduced. The electrical characteristics of the power semiconductors are then described in more detail in Section 2.3. This section includes a review of the key failure mechanisms and the restrictions these place on the device ratings, including the maximum current, voltage and temperature. The estimation of the power loss is then covered in Section 2.4. Finally, the basic heat transfer mechanisms and the development of an equivalent thermal network are described in Section 2.5.

2.2 Operation of a Variable Speed Drive

A variable speed drive can be used to control the current, torque and speed of a motor [2]. In an AC drive a supply voltage with a fixed frequency and magnitude is converted into an output voltage with a variable frequency and magnitude. This concept is illustrated in Figure 2.1.

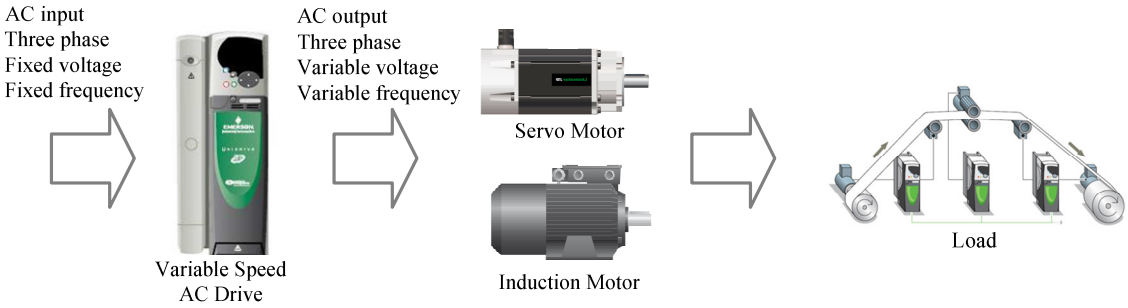

Figure 2.1: Application of an AC drive

In an application a drive offers the ability to accurately control a process over a wide speed range. Common applications that utilise the versatility of a drive include test rigs, pumps, fans, cranes, elevators and escalators.

2.2.1 Typical Power Stage Configuration

To understand how a drive works, the basic operation of a typical power stage is described. A typical configuration is shown Figure 2.2. This power stage consists of a rectifier, DC link filter and a voltage source inverter.

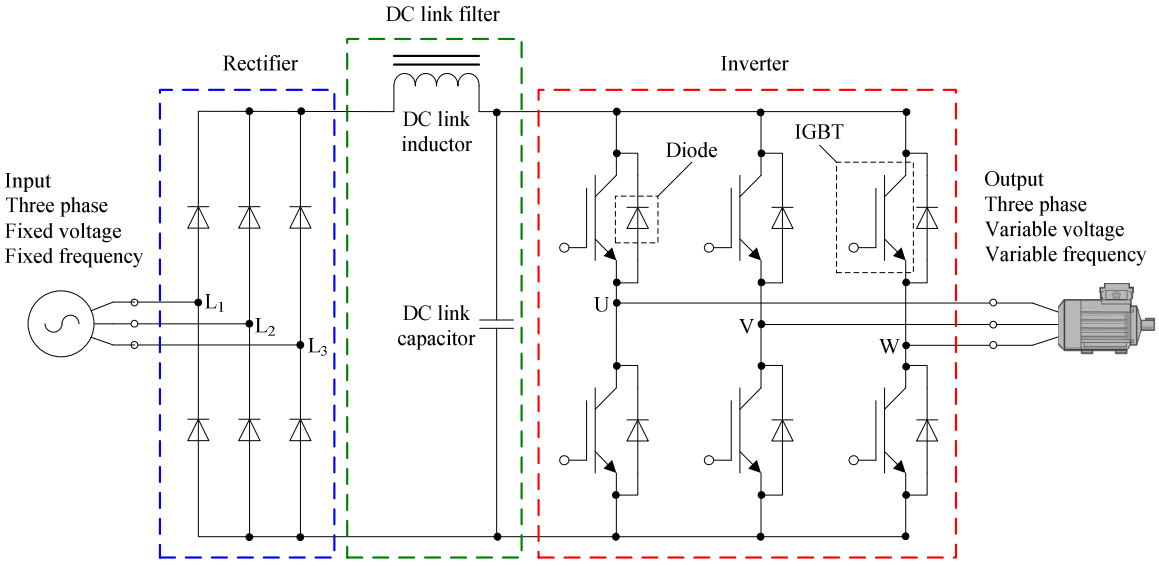

Figure 2.2: Typical power stage used in a three phase AC drive

As discussed, the input voltage to the diode rectifier has a fixed voltage and frequency and this is converted by the rectifier into a DC voltage (V_{DC}). This voltage then becomes the

input to the inverter stage. The inverter consists of six switching devices, normally Insulated Gate Bipolar Transistors (IGBTs), and six anti-parallel (freewheeling) diodes. The IGBTs in the inverter are controlled (modulated) to produce a sinusoidal output voltage with a variable voltage and frequency. The control scheme used in this process is important as it determines the number of switching events (switching loss) and the on-time or the conduction time (conduction loss) of each device. Therefore, the basic principles of a modulation scheme are reviewed in the following section.

2.2.2 Motor Control Algorithms

An output voltage with a sinusoidal component can be generated using Pulse Width Modulation (PWM). To illustrate this technique an example of sinusoidal modulation is shown in Figure 2.3. This figure shows the switching patterns over one output cycle of the inverter ($1/F_{out}$).

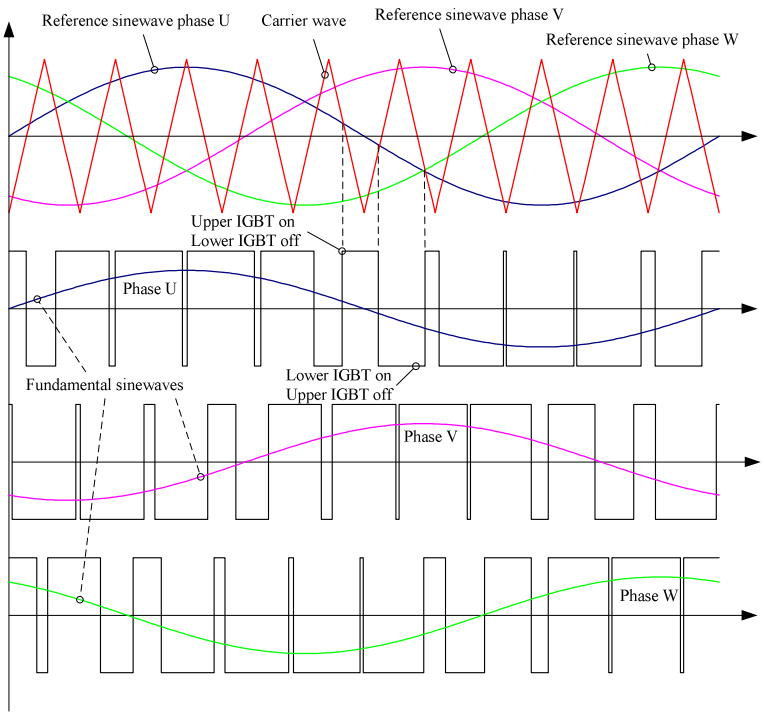

Figure 2.3: Sinusoidal modulation

To generate the switching pattern for the IGBTs a reference sine wave $V_{ref}(\omega t)$ is compared with a triangular carrier wave $V_c(\omega t)$. If the reference signal is higher than the carrier wave

the upper IGBT in the appropriate phase of the inverter is turned on and the lower IGBT is turned off. If the reference signal is lower than the carrier wave the opposite applies. This simple process produces an output voltage with a sinusoidal component. The frequency of the fundamental voltage can be changed by adjusting the frequency of the reference waveform. Furthermore, the magnitude of the voltage is changed by modifying the magnitude of the reference waveform in relation to the carrier wave. The ratio of the reference and carrier waveforms is defined as the modulation index (m):

$$m = \frac{\hat{V}_c}{\hat{V}_{ref}} \tag{2.1}$$

For linear modulation (m≤1) the magnitude of the fundamental component of the output voltage is proportional to the modulation index. However, if over-modulation (m>1) is permitted the maximum output voltage can be increased, but in this instance it is no longer proportional to the modulation index [3]. When using sinusoidal PWM the peak phase (Line-to-Neutral) voltage is:

$$\hat{V}_{L-N} = \frac{1}{2} m V_{DC} \tag{2.2}$$

and the peak line-line voltage is:

$$\hat{V}_{L-L} = \frac{\sqrt{3}}{2} m V_{DC} \tag{2.3}$$

This equation shows that sinusoidal PWM does not fully utilise the available DC link voltage. Therefore, in order to increase the peak voltage other modulation schemes are normally employed. The most popular of these schemes is Space Vector Modulation (SVM) and the implementation of the this scheme and its variants is well documented [4-7]. In general, when using SVM the IGBTs are controlled to produce eight unique voltage vectors and combinations of these vectors can be used to produce a rotating voltage vector.

The key advantage of this scheme over sinusoidal modulation is that the peak of the fundamental phase voltage is increased:

$$\hat{V}_{L-N} = \frac{1}{\sqrt{3}} m V_{DC} \tag{2.4}$$

Therefore, in this instance the peak line-line voltage is:

$$\hat{V}_{L-L} = m V_{DC} \tag{2.5}$$

The choice of modulation scheme determines the number of switching events (switching frequency) and the on-time (modulation index) of each device which have a significant effect on the power loss generated in an IGBT or diode. However, since an IGBT can only conduct current in the forward direction the conduction loss is also dependant on the direction of the load current. This effect is illustrated in Figure 2.4. This figure shows how the output current from an inverter with an inductive load changes over a complete cycle.

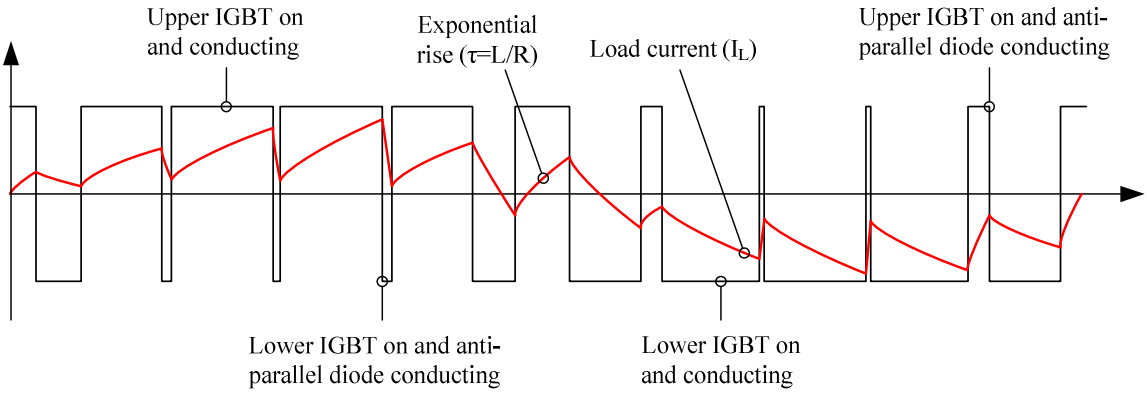

Figure 2.4: Load current

In this example the frequency of the carrier waveform (switching frequency) is very low and the ripple current is significant, but as the switching frequency is increased the output current will become more sinusoidal. For this reason, in a drive application it is common to use a switching frequency (F_{sw}) in the order 1 kHz and above. By definition, when the phase current (I_L) is positive it will flow in the upper IGBT (when on) or the lower anti-

parallel diode. Alternatively, when the phase current is negative it will flow in the lower IGBT (when on) or the upper anti-parallel diode. Thus, in addition to the switching frequency and modulation index, the power loss is dependant on the type of load, specifically the displacement angle (θ). Before reviewing the methods that can be used to estimate this loss, the structure and operation of the power semiconductors are described.

2.3 Power Semiconductor Technology

The use of IGBTs (with an anti-parallel diode) in an inverter is well established. The IGBT was first proposed in the 1980's and was introduced to the market place in 1983 [8]. The advantage of an IGBT is that it combines the low conduction loss of a BJT with the lower switching energy and the simpler gate drive requirements of a MOSFET [9]. Since its first development, the desire for improved operating characteristics, higher ratings and lower cost has seen the introduction of Punch Through (PT), Non Punch Through (NPT) and Field Stop (FS) chip technology [10-14]. Importantly, this development has coincided with several advances in freewheeling diode [15] and packaging technologies [16]. The construction of a PIN diode and a PT IGBT are shown in Figure 2.5.

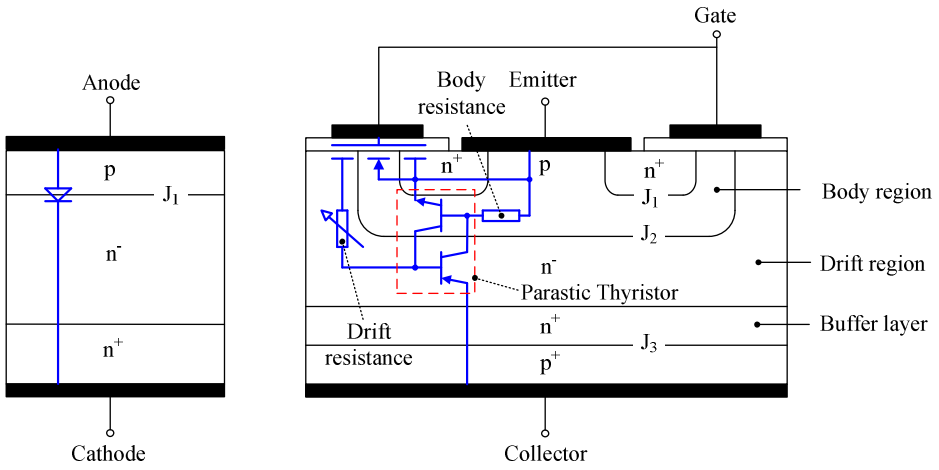

(a) (b)

Figure 2.5: Power semiconductors construction (a) PIN diode (b) PT IGBT

A PIN diode has a lightly doped n^- layer positioned between heavily doped p and n layers. This lightly doped layer is often referred to as the intrinsic or I-region, which gives the diode its name. When the junction of the diode is forward biased, electrons and holes are injected into this layer reducing its resistance and allowing a current to flow between the

terminals. This is known as conductivity modulation [9]. When the junction is reversed biased, the depletion layer extends into the intrinsic layer. If this depletion layer contacts the n^+ layer the diode is referred to as a punch through device, otherwise it is a non punch through device. The addition of this wide depletion layer reduces the electric field allowing a high voltage to be applied across the terminals of the device without causing impact ionization.

As shown in Figure 2.5(b), an IGBT is a four layers (PNPN) structure with a parasitic NPN and PNP transistor. These transistors from a parasitic thyristor and this can have a significant influence on the robustness of a device. The state (on/off) of an IGBT is controlled by the voltage applied to the gate. If the gate voltage (V_{GE}) is below the threshold voltage ($V_{GE(th)}$) no inversion layer is created under the gate (body region). When in the forward blocking state, the applied voltage is supported by the reversed biased p-n junction J_2 (PIN diode). Otherwise, in the reverse blocking state the applied voltage is supported by the reversed biased p-n junction J_3. This junction prevents any current flow in the reverse direction, but due to the doping levels can only support a low voltage. Therefore, an anti-parallel diode is required to conduct the reverse current (inductive load) and restrict the reverse voltage seen by the IGBT. To turn the IGBT on, the gate voltage must be greater than the threshold voltage. In this condition an inversion layer is created under the gate and electrons are injected into the drift region. At the same time holes are injected from the forward biased junction J_3. Consequently, conductivity modulation takes place allowing a current to flow between the collector and emitter. When the gate voltage is removed electrons are no longer injected into the drift region. However, a current temporarily flows in the device due to the recombination of the minority carriers (holes) in the drift region and this current is often referred to as the tail current.

2.3.1 Operating Limits and Typical Failure Modes

When switching an inductive load the IGBTs and diodes in the inverter are subjected to a high electrical and thermal stress. Therefore, to avoid damaging the devices they must be operated within the limits (ratings) provided by the manufacturer. The maximum ratings for a semiconductor are often defined in the form of a Safe Operating Area (SOA). For an IGBT, the safe operating area is enveloped by the maximum collector-to-emitter voltage

(V_{CE}) and collector-to-emitter current (I_{CE}). Typically, the following can be found in the datasheet of a device:

1. Forward Bias Safe Operating Area (FBSOA)
2. Reverse Bias Safe Operating Area (RBSOA)
3. Short Circuit Safe Operating Area (SCSOA)

The use of a SOA to describe the maximum ratings for a diode is less common, but in some instances a dynamic SOA is defined. The safe operating area for a diode is enveloped by the maximum reverse voltage (V_D) and forward current (I_R). In general, the SOA of a diode in a power module is larger than the corresponding IGBT and does not limit the maximum ratings. Even so, care must be taken to avoid overheating as this can increase the risk of dynamic avalanche.

To describe how the SOA for an IGBT impacts the maximum ratings of a drive examples are shown in Figure 2.6. The FBSOA determines the maximum ratings when the IGBT is in the on state. Normal operation (non fault conditions) is confined by the peak repetitive collector current (I_{CRM}) and the breakdown voltage (BV_{CES}).

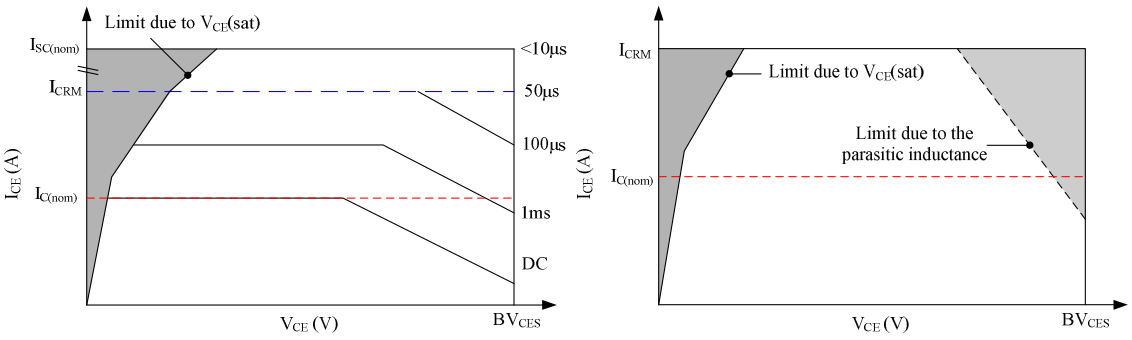

Figure 2.6: Typical safe operating areas (a) FBSOA and SCSOA (b) RBSOA

Repetitive operation anywhere within this boundary is permitted, although continuous operation is limited by the maximum operating temperature. An indication of this limitation is provided in the form of a series of simple curves with a maximum pulse length (on-time), where the diagonal part of the curve corresponds to a constant power loss. However, these

curves can only be applied under constant operating conditions. Furthermore, the ability to operate over the full area enclosed by the maximum voltage and current ratings is desirable as this has a positive impact on the performance, size and cost of a product [17]. Therefore, in this instance the device temperature is the limiting factor. However, it is not possible to directly measure the junction temperature in an online application and in order to protect the inverter this temperature must be estimated by a thermal model. Operating with a current higher than I_{CRM} is only permitted under short circuit conditions (non-periodic) and this boundary is commonly referred to as the SCSOA. Under a short circuit condition the current ($I_{SC(nom)}$) can be up to five times greater than $I_{C(nom)}$. Therefore, in order to avoid overheating this current can only be tolerated for a short period (typically less than 10μs). The RBSOA is shown in Figure 2.6(b), this defines the maximum voltage and current that the device can tolerate when turning off. In modern devices this SOA is often square, although the maximum voltage applied to the terminals of a power module can be limited by the voltage induced in the internal parasitic inductance during the switching event. Once again, operation anywhere within the boundary is permitted as long as the temperature is maintained below the maximum value.

Exceeding the limits defined by the SOA can lead to the failure of the device and in general, the boundary is defined by the destructive mechanisms shown below:

Table 2.1: Destructive Mechanisms for an IGBT

	V_{CE}	**I_{CE}**	**Failure Mechanism**
1	High	Low	Breakdown voltage
2	Low	High	Latch up
3	High	High	Power limitations of the device and package

A brief description of these failure modes is given below:

1) If the breakdown voltage is exceeded avalanche breakdown of the reversed bias p-n junction J_2 can occur. This is itself not a destructive mechanism, but with a high voltage the current quickly rises increasing the power loss generated in the device. Consequently, this condition can lead to the thermal failure of the chip, connections or packaging [9].

2) Latch up is a failure mode where an IGBT enters a state of continuous conduction in which the gate voltage has no influence on the collector current. In general, two kinds of latch up can be distinguished [9].

a) Static
b) Dynamic

Static latch up occurs when the IGBT is in its forward conduction state (steady-state), whereas dynamic latch up occurs during the turn-off transient. Latch up can occur if the current and the corresponding voltage drop across the body resistance is sufficient to forward bias the p-n junction J_1. If the sum of the NPN and PNP current gains are greater than unity the parasitic thyristor is activated (latch up) and the IGBT can no longer be controlled by the gate. In modern devices the latching current is in the order of five times larger than the nominal collector current and does not pose a problem under normal operating conditions. However, at elevated temperatures the current gain of the transistors increases, reducing the latching current and increasing the risk of latch up occurring [18].

3) Operating at a high voltage and current can cause an excessive temperature rise, which can lead to thermal runaway and ultimately the thermal breakdown of the device [9]. In this condition, thermal assisted carrier multiplication can take place causing current crowding and the generation of a localized hot spot. However, in [19] it was shown that it is possible to operate a typical IGBT (maximum temperature of 150˚C) at a temperature of up to 200˚C. However, clear limitations were identified. These include a significant increase in the leakage current that can lead to thermal runaway [20] and a reduction in the allowable short circuit time.

In addition to the failure mechanisms described above, the effect of power cycling must be considered. Power cycling refers to the repeated operation of a device over a wide temperature range, but within the normal operating limits. In this type of operation shear stress is generated at the interface between the different materials in the power module (e.g. silicon, solder, copper etc) due to the mismatch in the coefficients of thermal expansion [21]. This can lead to the degradation of the solder layers and the bond wire connections,

and ultimately device failure [22-25]. However, if the temperature is known appropriate action can be taken to minimise this effect and prolong the operational lifetime of the product.

In summary, to ensure reliable operation a power semiconductor must be operated within the voltage and current boundaries defined by the safe operating area. Furthermore, it must not exceed its maximum temperature. Given that this temperature cannot be measured directly it must be estimated by a thermal model and the development of a suitable model is the focus of this research. A thermal model can be broken down into two key requirements, the estimation of the power loss and the approximation of the thermal characteristics; both of these are discussed in the following sections.

2.4 Power Loss in a Semiconductor

In order to estimate the device temperature the total power loss must be known. In general, the power loss in a semiconductor can be divided into the following categories:

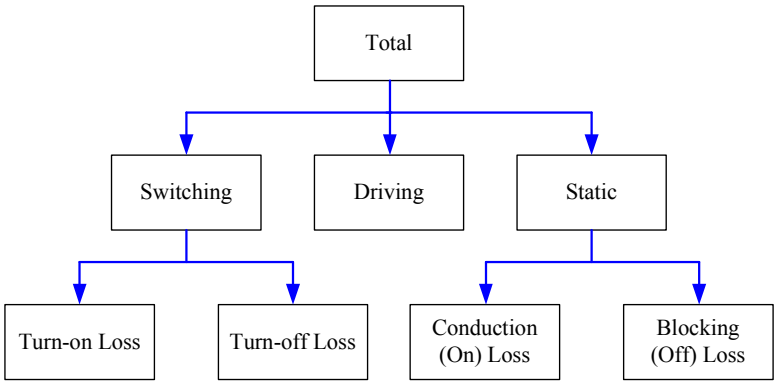

Figure 2.7: Power loss in a semiconductor

However, under normal operating conditions, the blocking and driving losses are negligible [26, 27]. Furthermore, when compared to the reverse recovery loss (turn-off) the turn-on loss of a diode is insignificant. Therefore, these losses can usually be ignored.

2.4.1 Review of Power Loss Models

Various methods of predicting the power loss in an IGBT and a diode exist. A comprehensive review was provided in [28]. In this review the power loss models were divided into four main categories:

- Mathematical or Analytical
- Semi-mathematical
- Behavioural
- Semi-numerical

Mathematical models are based on solving physics equations with some level of simplification. A review of mathematical models was presented in [29] and two common IGBT models were compared in [30]. Using a mathematical model in conjunction with circuit simulators allows a flexible design approach, although simulations can be slow [31]. Furthermore, various parameters must be extracted from electrical measurements [32-40] making these models difficult to develop.

Semi-mathematical models are based partly on physics equations but utilise existing models for other components, such as the MOSFET and BJT, while including the specific effects of an IGBT. This type of model is less common and is often not as accurate as the purely mathematical models.

Behavioural models are based on measured characteristics as opposed to physical mechanisms. The advantage of these models is that simple expressions for the power loss can be developed from experimental results [31] or alternatively the measured data can be stored directly in lookup tables [41, 42]. The disadvantage of behaviour models is that a new set of measured data is required if the operating conditions (i.e. the gate resistance) are changed. Therefore, these models are not as flexible as those used in circuit simulators.

Semi-numerical models combine finite element methods with existing analytical models to improve the modelling of some key characteristics. These models are capable of

modelling accurate transient operation, but are significantly slower than other models and can be difficult to implement.

In general, it is recognised that the best results can be gained by combining well defined mathematical models with curve fitting techniques [43]. An example of this approach is given in [44]. This model uses the simulation of an ideal device to determine the dependency of the voltage and current with time, while using lookup tables to calculate the power loss. However, it is difficult to implement this type of model in an on-line application. In contrast, a simple behaviour model allows the power loss to be estimated with sufficient accuracy with the benefit of very fast calculation times, making them ideal for online applications.

2.4.2 Review of Behaviour Models

The equations that form the basis of the power loss calculations for an IGBT and diode are shown in Table 2.2. In this table it can be seen that the switching loss is calculated using the turn-on (E_{on}) and turn off energy (E_{off} or E_{rec}) measured during a single switching event.

Table 2.2: Power loss calculation for an IGBT and diode

Power Loss (W)		**IGBT**	**Diode**
Conduction		$P_{con} = I_L V_{CE(sat)}$	$P_{con} = I_L V_F$
Switching	Turn-on	$P_{sw\ (on)} = F_{sw} E_{on}$	
	Turn-off	$P_{sw\ (off)} = F_{sw} E_{off}$	$P_{sw\ (rec)} = F_{sw} E_{rec}$

The power loss is defined as the average power over a switching period ($1/F_{sw}$). For this approach to be valid the switching period must be significantly shorter than the thermal time constant of the device. In addition, the equations in Table 2.2 assume that the device is conducting the load current for the complete period and do not include the effect of the modulation index or displacement power factor. The incorporation of these operating parameters into the power loss model is described in Chapter 4. To calculate the power loss under a defined operating condition the following parameters must be known:

- Turn-on switching energy of an IGBT (E_{on})
- Turn-off switching energy of an IGBT (E_{off})
- On-state voltage of an IGBT (V_{CE})
- Turn-off (reverse recovery) switching energy of a diode (E_{rec})
- On-state voltage of a diode (V_F)

The on-state voltage for a device is dependant on the device temperature (T_j) and load current (I_L), although it is common to ignore the effect of temperature and assume a linear relationship between V_{CE} and I_C:

$$V_{CE(sat)} = V_{CE(ZERO)} + A \cdot I_C(t) \tag{2.6}$$

However, the relationship between V_{CE} and I_C is rarely linear [43] and in [45-48] an additional parameter (B) is included, although the effect of temperature is still ignored:

$$V_{CE(sat)} = V_{CE(ZERO)} + A \cdot I_C(t)^B \tag{2.7}$$

A similar approach has been used for the switching loss [49-51]. However, this loss is also dependant on the device temperature and the DC link voltage (V_{DC}). In [46] an extended loss model was proposed to account for the variation due to these parameters:

$$E_{sw} = A \cdot I_C(t)^B \cdot \left[\frac{V_{DC}}{V_{DC,Nom}}\right]^C \cdot \left[\frac{T_j}{T_{j,Nom}}\right]^D \tag{2.8}$$

Another approach which has been widely used to estimate the on-state voltage and switching energy is to use a second order polynomial [52-54]:

$$E_{sw}(I_C) = A + B \cdot I_C(t) + C \cdot I_C{}^2(t) \tag{2.9}$$

The parameters (A, B and C) in this equation can be calculated from the measured results using standard curve fitting software, and if necessary the equation can be extended to

higher order polynomials [55]. In [56] the dependency of the parameters with voltage are themselves represented by a first order polynomial, although in this model the effect of temperature is ignored. While, in [52, 54] the same approach is used to represent the dependency of the parameters with temperature, but at a constant DC link voltage. However, in order to develop an accurate thermal model none of the dependencies can be ignored. Therefore, an alternative model is proposed in Chapter 7. This model is based on a series of polynomial expressions and includes the effect of the current, temperature and voltage.

2.5 Fundamentals of Heat Transfer

The second part of a thermal model, and often the most difficult to develop, is the approximation of the thermal characteristics. In any system the propagation of heat can take place in three different ways, conduction, convection and radiation.

Conduction: When a temperature gradient exists in a body there is an energy transfer from the high temperature region to the low temperature region. The heat transfer rate is proportional to the gradient of the temperature and can be expressed by Fourier's law of heat conduction:

$$q = -kA\frac{\partial T}{\partial x} \tag{2.10}$$

Where, q is the heat transfer rate (W or J s), k is the thermal conductivity (W/m K), A is the cross section area (m^2), T is the temperature (K) and x is the distance in the direction of heat flow (m). The rate of heat transfer is restricted by the thermal conductivity, the thickness of the material and the surface area. If the heat flow is one-dimensional the energy transfer rate can be expressed by the thermal resistance (R_{th}):

$$R_{th(Conduction)} = \frac{\Delta x}{kA} = \frac{T_1 - T_2}{q} \tag{2.11}$$

This equation is only valid if the temperatures of the hotter (T_1) and cooler (T_2) surfaces are isothermal and all of the heat flux entering the hotter surface leaves via the cooler surface

[57]. However, in a power module it is unlikely that the surface temperature of the silicon chip, case or heatsink will be isothermal. As a consequence the thermal resistance will be dependant on the boundary conditions and the location where the temperature is measured. Despite this, thermal resistance is widely used by manufacturers to describe the steady-state thermal properties of a power module.

For transient conduction, the temperature at any point within a solid is given by the heat conduction equation, which is developed using the principles of energy conservation. The three-dimensional heat (diffusion) equation for an isotropic material without an internal energy source is:

$$\underbrace{\rho \times c \frac{\partial T}{\partial t}}_{\text{Stored Energy}} = \underbrace{k\left(\frac{\partial^2 T}{\partial x^2} + \frac{\partial^2 T}{\partial y^2} + \frac{\partial^2 T}{\partial z^2}\right)}_{\text{Energy conducted in and out}} \tag{2.12}$$

Where c is the specific heat (kJ/Kg K), ρ is the material density (kg/m^3) and t is the time (s). If the specific heat capacity ($c_p=\rho \times c$) is multiplied by the volume (V) of the element or structure being examined the resulting term can be defined as the thermal capacitance (C_{th}) and this has units of J/K:

$$C_{th} = \rho c V \tag{2.13}$$

This term is often used in conjunction with the thermal resistance to form an equivalent RC network of a device. A thermal network can be used to describe the transient thermal impedance (Z_{th}) and allows the transient temperature response to be calculated using electrical equivalents of the thermal parameters. This approach is widely used in the development of a thermal model. The properties of an equivalent thermal network are described in more detail in Section 2.5.1.

Convection: Heat energy can also be transferred between a solid and a fluid if there is a temperature difference between them. This process is known as convection. The

temperature gradient that defines the heat transfer rate is dependant on the velocity of the fluid, the higher the velocity the higher the temperature gradient. However, the velocity of the fluid at the surface of a solid is reduced to zero due to viscous friction [58] and the heat is transferred to the fluid by conduction. The effect of convection on the system is specified by Newton's law of cooling [59]:

$$q = hA(T_s - T_\infty) \tag{2.14}$$

Where h is the convection heat transfer coefficient (W/m^2K) and is a function of the velocity, density, specific heat and the thermal conductivity, A is the surface area (m^2), T_∞ is the fluid temperature (K) and T_s is the surface temperature (K). For convection the restriction to heat transfer can also be represented by a thermal resistance:

$$R_{th(Convection)} = \frac{1}{hA} \tag{2.15}$$

To calculate this thermal resistance the convection heat transfer coefficient is required and for most systems an average value is used. This value is usually determined experimentally.

Radiation: Unlike conduction and convection, heat transfer between objects by radiation does not require any matter to exist between the two bodies. In contrast to conduction and convection, the amount of energy transferred via radiation is related to a power term of the temperature difference, making it the main form of heat transfer in very hot objects. The exchange of heat between two surfaces (gray bodies) via radiation is given by:

$$q = S\varepsilon\sigma A\left(T_1^4 - T_2^4\right) \tag{2.16}$$

Where S is the geometric view factor, ε is the emissivity and σ is the Stefan-Boltzmann constant which has a value of 5.669×10^{-8} (W/m^2K^4). This equation can be used to show that for an electronic component with a relatively small surface area the effect of radiation can be ignored without introducing any significant errors.

2.5.1 Thermal Impedance and the Development of Equivalent Thermal Networks

As explained, the thermal characteristics of a system can be described by its thermal impedance and this is often represented in the form of an equivalent thermal network. A thermal network is capable of describing a one-dimensional, two-dimensional or three-dimensional problem [60] and can be easily implemented in circuit simulators. Therefore, they are ideal for electro-thermal simulations [61]. Many different thermal networks have been used to describe the thermal characteristics of a system, but there are two dominant topologies; the Foster and Cauer networks. These networks are illustrated in Figure 2.8.

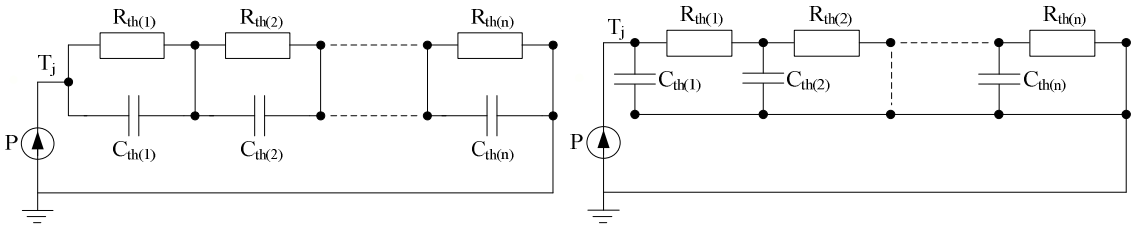

Figure 2.8: Thermal networks with n elements a) Foster b) Cauer

To use these networks it must be assumed that the heat is generated uniformly at the upper surface of the device and all of the heat flows perpendicular to this surface [62], i.e. towards the heatsink. Furthermore, the networks shown can only be used to calculate the temperature of a single device. To estimate the temperature of more than one device the networks must be combined with other modelling techniques. This is a key requirement for the thermal model of the inverter (twelve devices) and existing methods that have been used to model a multi-chip device are described in Chapter 3.

To calculate the temperature of a device using a thermal network a known power loss (P), which is equivalent to an electrical current, is applied to the first node in the network. The transient temperature response of the device (equivalent to electrical voltage) can then be measured. Before using a network the thermal parameters (R_{th} and C_{th}) must be calculated and there are two distinct approaches than can be used:

a) Parameterization of the elements in the equivalent network based on measurements and curve fitting techniques
b) Calculation of the individual component values from the known material parameters and geometry of the device

Both of these methods have advantages and disadvantages and lend themselves to a particular type of network. This is discussed in more detail in the following sections.

2.5.1.1 Foster Network

The Foster network is based on a set (theoretically infinite) of exponential time constants equivalent to a step response with zero initial conditions:

$$Z_{th}(t) = \sum_{i=1}^{n} R_{th,i}\left(1 - e^{-\frac{t}{\tau_{th,i}}}\right) \tag{2.17}$$

The thermal time constant (τ_{th}) is equal to the sum of the thermal resistance and capacitance in each element. Typically, four terms are enough to describe the thermal impedance with sufficient accuracy. However, when the thermal impedance is modelled by a finite number of elements there will always be an additional (shorter) time constant that is not included [63]. The transfer function for a Foster network can be found by applying Laplace transforms to the response of the network in the time domain:

$$Z_{th}(s) = \sum_{i=1}^{n} \frac{R_{th,i}}{1 + sR_{th,i}C_{th,i}} \tag{2.18}$$

This transfer function only applies to a linear model i.e. a model where the variation of the conductivity and the specific heat with temperature can be ignored [64]. Since each element in the Foster network can be treated individually, the Foster network is very simple to implement. Furthermore, it is possible to use standard curve fitting algorithms (method A) to determine the individual component values from the measured thermal impedance [63, 65]. However, although the Foster network is able to describe the thermal behaviour at the input node (device junction or upper surface) it cannot be used to determine the temperature

distribution within the device, nor is it possible to extend this network to include other components. This is because in an electrical circuit the current flow is equal on both sides of the capacitor, while in a thermal equivalent circuit only the flow on one side has a meaningful effect. Likewise, the stored thermal energy in an element of a device is proportional to the absolute temperature of the material, rather than the temperature difference between two layers. However, in the Foster network the energy stored in the capacitance is proportional to the voltage difference between two nodes [66] rather than their absolute temperature.

2.5.1.2 Cauer Network

The component values of the Cauer networks can be determined from the direct application of the heat equation [66]. If the heat flow is one-dimensional the values of the thermal resistance and capacitance can be derived directly from the material parameters of the structure [67]. Unlike the Foster network, the Cauer network can correctly describe the internal temperature distribution in a system since the thermal capacitances are connected to the electrical or thermal ground. Therefore, the stored energy in the capacitors is proportional to the temperature rise above the temperature of the environment and as in the physical structure heat takes time to propagate between the nodes of the network. The transfer function for the Cauer network can be expressed by continued fractions:

$$Z_{th}(s) = \cfrac{1}{sC_{th,1} + \cfrac{1}{R_{th,1} + \cfrac{1}{sC_{th,2} .... + \cfrac{1}{R_n}}}} \tag{2.18}$$

In general, the Cauer network has some key advantages compared to the Foster network, specifically the ability to extend the model and estimate intermediate temperatures. However, to achieve this, the thermal parameters must be calculated using the material properties of the device. If the heat flow in any layer of the device is not one-dimensional this becomes very difficult and can lead to significant errors. If required, the Cauer network can be transformed to the equivalent Foster network and vice versa using standard circuit

transformations [68], but in this process the characteristics of the individual layers in a device is lost.

2.5.1.3 The Effect of Nonlinearities on the Development of an Equivalent Network

To develop an equivalent thermal network for a device the thermal properties must be considered linear, that is independent of the operating conditions [69]. However, there are various material parameters that are not linear. In terms of semiconductors, one of the major nonlinearities is the thermal conductivity of silicon, which falls rapidly with increasing temperature [70]. The thermal conductivity of silicon for a given temperature can be expressed by [61]:

$$k(T) = 154.86\left(\frac{300}{T}\right)^{\frac{4}{3}} \tag{2.19}$$

For dynamic models, the temperature dependence of the heat capacity may also be an important factor, although its effects are relatively small over the normal operating range of a power semiconductor. In [70] it was recommend that a nonlinear model should be used for a temperature rise of 80°C to 100°C. While in [64], it was shown that if the thermal conductivity is fixed at the mid point of the operating range (i.e. at 125°C for an operating range of 27°C-200°C) the resultant deviations are ±26% and ±7% for thermal conductivity and specific heat respectively. Therefore, since the thermal conductivity falls as it is heated, to avoid significantly underestimating the device temperature the parameters of a linear thermal network should always be calculated or measured at the maximum operating temperature, i.e. the conditions that give the highest thermal impedance.

2.6 Summary

The aims of this chapter were to introduce some of the key principles that are used to develop a thermal model that can protect the power semiconductors in the inverter stage of an industrial drive and identify the key operating limits for these components. In this chapter the development of a thermal model was divided into two stages, the estimation of the power loss and the approximation of the thermal characteristics. The methods that could be used to estimate the power loss were reviewed in Section 2.4.1. Of the methods

reviewed, a behaviour model is most suited to online (real time) applications due to the fast calculation times. Using a behaviour model the on-state voltage and switching energy can be calculated. These values are highly dependant on the operating conditions of the inverter and the following parameters must be included in the power loss estimation:

- Junction temperature (T_j)
- DC link voltage (V_{DC})
- Output current (I_L)
- Switching frequency (F_{sw})
- Modulation index (m)
- Displacement angle (θ)

The power loss model (based on the basic loss equations) is developed in Chapter 4 and the methods used to measure the on-state voltage and switching energy is covered in Chapter 6. To implement this model the parameters of the behaviour model must be generated from these measurements and this process is described in Chapter 7.

In addition to the power loss estimation, the thermal properties of the power module must be represented in a form that allows the transient temperature response to be calculated quickly and efficiently. In the review of the heat transfer mechanisms a thermal resistance and capacitance were defined. These thermal parameters can be used to form an equivalent thermal network which can be used to represent the transient thermal impedance of a device. However, the networks described in this chapter can only be used to estimate the temperature of a single device (single thermal impedance). Therefore, in an inverter where multiple devices can be included in a single power module an alternative thermal network or modelling technique must be used to account for the thermal interaction between these devices. These methods are reviewed in the next chapter.

Chapter 3: A Review of Thermal Modelling Techniques

3.1 Introduction

The aims of this chapter are to review the methods that can be used to develop and implement a thermal model, identify their strengths and weaknesses and highlight those that have been or can be applied to an inverter. In this chapter the thermal models have been divided into five categories:

1. Basic thermal impedance model provided in the datasheet of a power module.
2. Analytical models where the effective heat flow area is calculated using the known geometry of a device and this area is used to calculate the total thermal resistance.
3. Compact thermal models where the parameters of a thermal network are calculated to give the best temperature estimation under a range of boundary conditions.
4. Parameter extraction network where the thermal parameters of a Cauer network are calculated from the known material properties.
5. Thermal impedance model based on the development of a thermal impedance matrix, where each element is represented by an equivalent Foster network.

After the brief review of the key requirements for the thermal model in Section 3.2, the five model types are described in Sections 3.3.1 to 3.3.5. The main features of each model are then summarised in Section 3.3.6. From this summary the methods that are best suited to an inverter application are selected. In Section 0 the selected models are developed for a simple heat spreader and are compared with simulation results.

3.2 Key Requirements for the Inverter Thermal Model

A comprehensive thermal model must include the following effects:

- Transient heat exchange via conduction, convection and radiation
- Thermal interaction between devices in a multi-chip power module
- The effect of the location of the internal thermistor in the power module
- The variation of material properties with temperature
- Non-uniform heat paths caused by imperfections in a device (e.g. solder voids)
- The degradation of the heat path over the lifetime of the device
- Variations in the cooling conditions (e.g. fan speed)

Most of these factors can be modelled by sophisticated simulation packages, but for on-line applications a simplified approach is required. Using a simplified model reduces the computational resource required to implement the model, speeds up the calculation time and reduces the number of input parameters [64]. If the model is difficult to implement the calculation time will be slow and aliasing may occur. In order to protect the inverter this must be avoided. In the simplest models most of the effects listed above are ignored. As a result the temperature can be significantly underestimated and this is usually more evident when operating in specific (worst case) conditions.

One of the known problem areas with the existing thermal model used in a Control Techniques, Unidrive SP is prolonged operation in a stationary vector condition (also referred to as a DC condition). The model implemented in this drive is based on the thermal data provided by the manufacturer of the power module. Relying on this data alone can result in the temperature being significantly underestimated. This effect has been highlighted by the work presented in [1]. Operating in a stationary vector condition causes a particular problem in an inverter application because the output current and power loss generated in a device (ignoring any temperature dependency) is constant. Therefore, there is no filtering effect due to the thermal capacity of the materials in the power module. Consequently, the effect of the thermal interaction between each device, which cannot be modelled by the single thermal impedance used in the Unidrive SP thermal model, is at its maximum. This can have a significant impact on the operating temperature of the power semiconductors in the inverter.

3.3 Thermal Modelling Techniques

Various techniques have been used to develop a simplified thermal model that can be used to estimate the junction temperature of a device. Five of the most common approaches are reviewed in the following sections.

3.3.1 Datasheet Thermal Impedance Model

Using a thermal impedance to estimate the temperature of a device is well established [63] and in the datasheet of most power modules two thermal impedances are defined. These are usually presented in the form of an equivalent Foster network and are measured between the junction of an IGBT and a diode, and the case directly under the device. This measurement is described in [71]. In [60] a single thermal impedance is used to estimate the temperature of the IGBTs in a multi-chip power module in which power is applied to all of the devices simultaneously. In this instance the thermal impedance is measured in the same condition. Therefore, the effect of the thermal coupling between each device is included in the single measurement. In this instance the temperature calculated using this thermal impedance will never be underestimated. However, this is not an operating condition that is found in an inverter.

In an inverter the power loss in each device varies over an output cycle. Therefore, the effect of the thermal coupling on the temperature of a device is not constant and cannot be modelled by the single thermal impedance in the datasheet. Furthermore, this thermal impedance is measured between the junction and the case directly under a device, but in an application this case temperature is not accessible. Due to this it is common to assume that the temperature measured by the internal thermistor in a power module is the same as the case temperature under the device. The impact of this assumption is dependant on the operating conditions and the location of the thermistor. To show the potential error of this approximation the temperature difference between the thermistor and the case directly under an IGBT has been measured when an inverter is operating in a stationary vector condition. The measured temperatures are shown in Figure 3.1. These results show that the error due to this assumption can be significant and for the operating conditions examined (a step in power loss) a temperature difference of 17˚C was observed. These results are similar to those presented in [1].

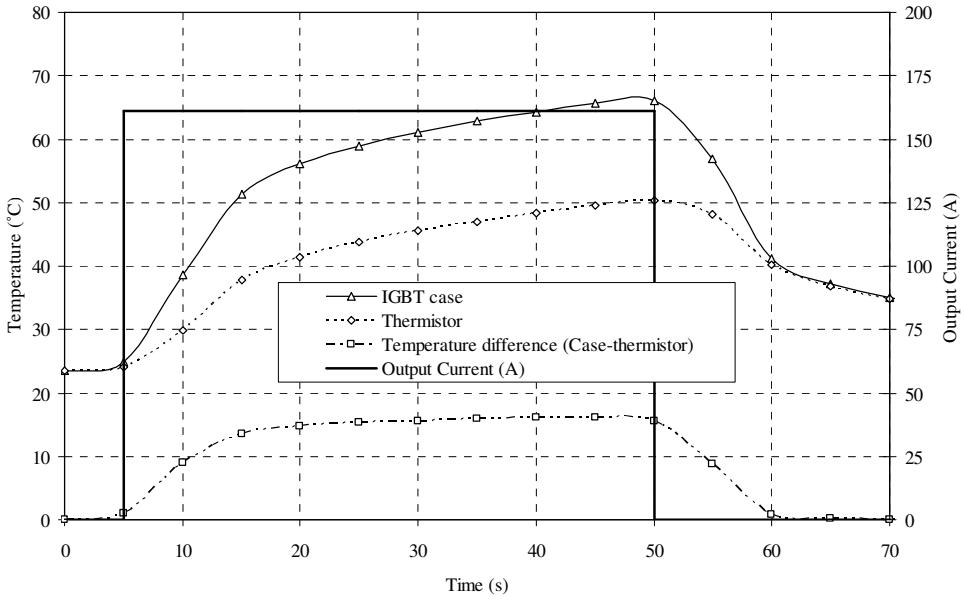

Figure 3.1: Case and thermistor temperature measured in a stationary vector condition when a step change in output current is applied to the inverter

Although these results show that this model cannot be guaranteed to protect the devices in an inverter operating in a stationary vector condition, it is the common method suggested by manufacturers. When using this type of model widespread failures are only prevented by the safety margins added to the thermal impedance. These margins are added to account for the variations in the manufacturing procedure and to give some overall margin in an application, but can result in the temperature being significantly overestimated in other operating conditions. For these reasons the datasheet values cannot be used on their own.

3.3.2 Analytical Solutions

An analytical solution can be used to calculate the thermal characteristics of a device, but in general they are restricted to simple geometries (i.e. a heat spreader or flux channel) with a single heat source operating under steady state conditions. In the simplest models the total thermal resistance is calculated using the area of heat flow defined by a constant spreading angle, which is independent of the geometry and boundary conditions [72, 73]. When using this approach it is common to use a spreading angle of 45°. However, this is an arbitrary selection and is only correct when a semi-infinite, circular heat spreader is considered [73]. The constant angle model can be improved by including some compensation for the geometry of the source and heat spreader. In [74-76] this is achieved by calculating the

spreading angle using various factors that influence the heat spread. Even so, the accuracy of this variable angle approach can be poor.

Alternative methods are based on the solution to the heat equation. Various solutions have been developed for a range of simple geometries with specified boundary conditions in both rectangular [77-83] and cylindrical coordinates [84-87]. These models give an exact solution and allow the temperature to be calculated at any point in the system, but once again they are restricted to simple geometries operating under steady-state conditions. This makes them unsuitable for an inverter application. Therefore, this type of model will not be discussed any further.

3.3.3 Compact Thermal Models

The term Compact Thermal Model (CTM) normally refers to a simplified network model intended to reproduce the thermal behaviour of a component in a wide variety of operating conditions [88-90]. This type of model is primarily used to estimate the temperature of a component under steady state conditions (thermal resistor network), although the development of dynamic models (thermal resistor and capacitor network) have been described [91, 92]. At present, this approach has only been applied to integrated circuits and has been primarily used with simulation software to estimate the temperature of components on a printed circuit board during the design phase. The thermal network used in a compact model consists of several nodes that represent the thermal boundaries of a device where a significant heat transfer occurs. An example of a typical steady–state compact model is shown in Figure 3.2 [93].

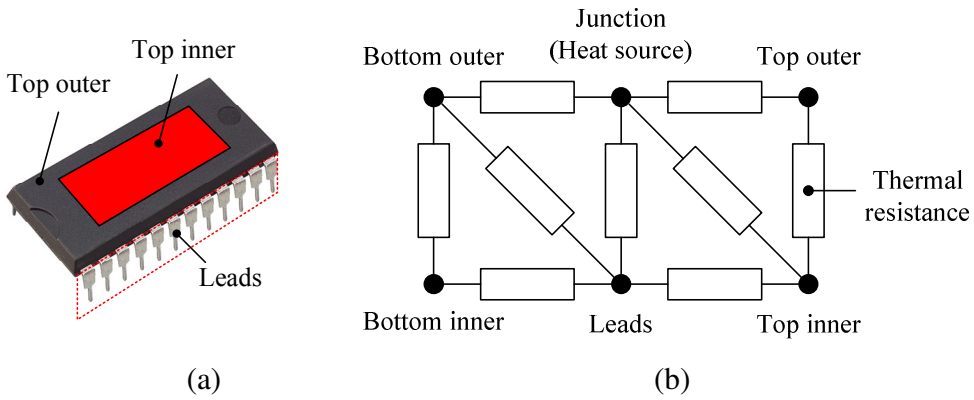

Figure 3.2: Compact thermal model (a) boundary locations (b) network topology

In this instance the network has five cooling boundaries and these include the heat flow through the upper surface of the chip (top outer and top inner), lower surface of the chip (bottom outer and bottom inner) and the package leads.

The parameters of a CTM are calculated using an optimisation process and the standard procedure is described below [94]:

1. Develop a detailed thermal model of a device in a simulation package (e.g. Flotherm) and validate this model using test results
2. Use the simulation model to calculate the junction temperature for a range of boundary conditions (e.g. different heat transfer coefficients)
3. Select a network topology for the compact thermal model
4. Optimise the network parameters to minimise the error in the estimated junction temperature under each boundary condition
5. Evaluate the accuracy of the model using test or simulations results that are different to those used to generate the network parameters

In [91] the accuracy of a compact thermal model was examined for three different package styles over a range of boundary conditions and it was shown that the maximum error in the estimated junction temperature was 6%. However, a compact thermal model has several limitations that prevent them from being applied to a power module. These include the need to develop a detailed simulation model of the power module, the complexity of the network required to model multiple heat sources and the modification of the network (i.e. the addition of the thermal capacitances) to allow the estimation of the transient response.

3.3.4 Parameter Extraction Network

In a parameter extraction network the thermal properties of an equivalent network, often based on a Cauer network, are calculated using the geometry of a device, its material properties and the known heat flow area and volume. An example of how this model is developed for a power semiconductor is illustrated in Figure 3.3. In this figure the ceramic layer has been divided into two parts and the area, volume and material properties of these are used to calculate the parameters of the equivalent Cauer network. In this model the

temperature dependency of the materials can be included, i.e. the thermal parameters can be variable. This process must be repeated for each layer (e.g. silicon, solder, copper, etc) and the complete thermal network can then be constructed by placing each of the Cauer networks in series.

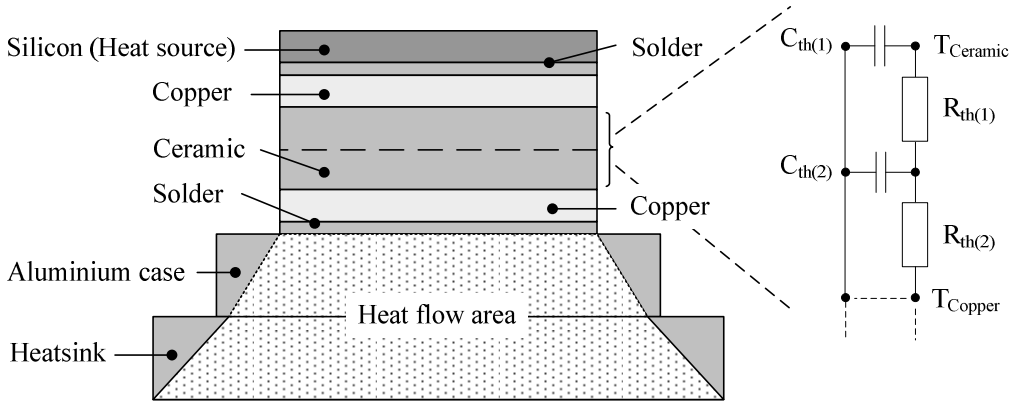

Figure 3.3: Power device construction and the equivalent Cauer network for one layer

In this example the heat flow in the first few layers is one-dimensional and the effective heat flow area and volume of each layer can be easily calculated. However, heat spreading occurs in the aluminium case and heatsink. Thus, in order to calculate the network parameters for these layers the effective heat flow area must be estimated.

One approach is to use the constant heat flow angle that was described in Section 3.3.2. In [95] a Cauer network was developed for the silicon layer of an IGBT using a constant spreading angle of 45˚. This network was then used within a circuit simulator to estimate the temperature rise during a short circuit event. However, no comparisons were provided making it impossible to assess the accuracy of this model.

In [96, 97] the effective heat flow area for the devices in an inverter were calculated using the cylindrical heat spreading along the edges, the spherical heat flow at the corners and the rectangular heat flow under the device. The area and volume of these elements are used to calculate the thermal parameters of an equivalent Cauer network that represents the heat flow in the vertical direction. To incorporate the lateral heat spread, additional thermal resistors are connected between each of the vertical networks at the ceramic and case

nodes. The method used to calculate the value of these resistors is described in [98]. This model was validated for a single IGBT by comparing the estimated and measured temperature during a short heating period (less than 10ms). In these comparisons the estimated temperature was shown to be in agreement with the measured response. However, this comparison ignores the impact of the thermal coupling between the devices and the effect of the longer time constants associated with the case of the power module. Therefore, it is not clear if the coupling resistors are capable of modelling the thermal coupling between the devices in an inverter application. In [99] the same approach was applied to a silicon carbide power module with four devices. In this model all of the devices are operated in parallel and it is assumed that the power loss in each device is identical. Therefore, a reflective boundary is defined between the devices. This allows the temperature to be estimated using a single Cauer network with no coupling resistors, but once again this cannot be applied to an inverter.

From the review of the parameter extraction models two areas have been identified that make it difficult to develop this model for an inverter:

a) Calculating the effective heat flow area under different operating conditions
b) Modelling the thermal coupling between the devices in the power module

Although possible solutions to these problems have been discussed, insufficient comparisons have been provided to assess the suitability of this technique.

3.3.5 Thermal Impedance Matrix

The thermal impedance matrix is based on the principle of linear superposition. For heat conduction this principle states that the total temperature response at a given place and time due to one or more heat sources is the same as the sum of the responses if each heat source is treated individually. In Figure 3.4 the concept of superposition is illustrated using the temperature measured along the upper surface of a simple heat spreader with two heat sources. In this example the temperatures measured when a power loss (P) is applied to a single source are:

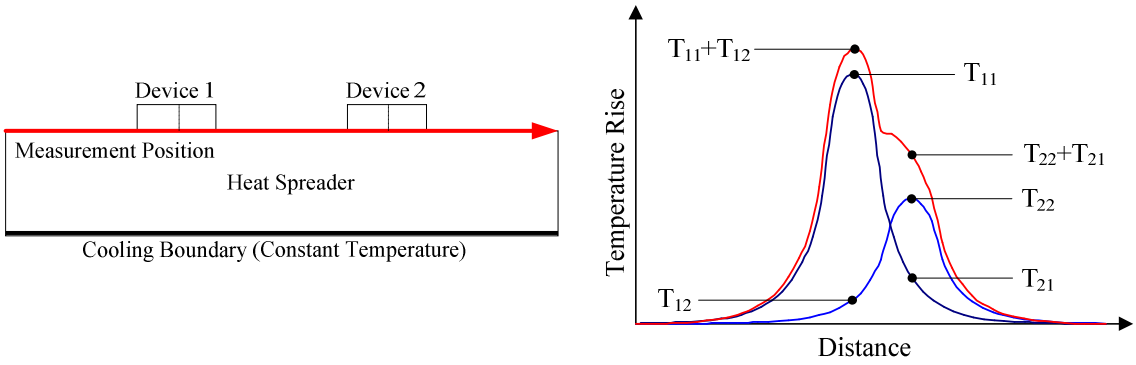

(a) (b)

Figure 3.4: Principle of superposition applied to heat conduction (a) heat spreader with two heat sources (b) temperature measured on the upper surface

T_{11} = temperature of device 1 when a power loss is applied to device 1

T_{22} = temperature of device 2 when a power loss is applied to device 2

T_{12} = temperature of device 1 when a power loss is applied to device 2

T_{21} = temperature of device 2 when a power loss is applied to device 1

The temperatures measured when the power loss is applied to both sources simultaneously are:

$T_1 = T_{11} + T_{12}$ = temperature of device 1 when a power loss is applied to device 1 and 2

$T_2 = T_{22} + T_{21}$ = temperature of device 2 when a power loss is applied to device 1 and 2

For transient conditions these temperatures can be represented in the form of a matrix containing the transient thermal impedance (Z_{th}). Therefore, taking a system with n heat sources the temperature of each device can be calculated using:

$$\begin{bmatrix} T_1 \\ T_2 \\ \vdots \\ T_n \end{bmatrix} = \begin{bmatrix} Z_{th,11} & Z_{th,12} & \cdots & Z_{th,1n} \\ Z_{th,21} & Z_{th,22} & \cdots & Z_{th,2n} \\ \vdots & \vdots & \ddots & \vdots \\ Z_{th,n1} & Z_{th,n2} & \cdots & Z_{th,nn} \end{bmatrix} \cdot \begin{bmatrix} P_1 \\ P_2 \\ \vdots \\ P_n \end{bmatrix} \tag{3.1}$$

The thermal impedance matrix consists of the self and mutual thermal impedances. The self thermal impedance (diagonal elements) represents the temperature rise of a device due to its own power loss, whereas the mutual thermal impedance (off diagonal elements) represents the temperature rise of a device when the power loss is applied to another device in the power module. These thermal impedances can be measured or derived from simulation results, but to use superposition it must be assumed that they are linear. However, in practice there are several non-linear effects, including the temperature dependency of the materials and the effect of cooling via convection and radiation. If there are significant non-linear effects the thermal impedances can be made linear by defining them at a chosen operating point, normally this is the condition that gives the highest steady-state temperature [100]. To implement the matrix the thermal impedance is often represented by a Foster network since they can be easily applied in a microprocessor. The number of elements selected in these networks has a direct impact on the number of calculations that must be performed and this has been discussed in [101].

The thermal impedance matrix has been used in a wide variety of applications and was first applied to a multi-chip power module in [102]. It was then used to model the impact of the thermal coupling (i.e. the mutual thermal impedance) in an IGBT module operating as an inverter [103, 104]. In [105] the method used to construct a complete thermal impedance matrix for a commercially available IGBT module was described. This model was then used to compare the estimated and measured temperature of the IGBTs and diodes in an inverter operating with a load profile representative of an electric vehicle [106]. Further comparisons of a thermal impedance model with measured or simulation results have been shown in [107-109]. Overall, these comparisons show that a thermal impedance matrix can be used to estimate the steady-state or transient temperature of one or more devices in an inverter.

In each of the above papers the temperature was calculated off-line using the complete thermal impedance matrix with n^2 elements. However, to implement the complete model in real-time a significant computational resource would be required and as of yet this is not available in a commercially available drive. Consequently, the thermal impedance matrix must be simplified and a potential method was identified in [1]. In this model the number of

terms in the matrix was reduced using a near neighbour approach, where only the mutual thermal impedance between a device and its nearest neighbour(s) were considered. Furthermore, the thermal impedances used in this model were measured between the junction of an IGBT or diode and the internal thermistor. This model was compared with temperature measured in a stationary vector condition over a full output cycle of the inverter. This comparison was used to highlight the significant impact that the thermal coupling can have on the device temperature.

The main advantages of the thermal impedance matrix are that all of the thermal coupling between devices and the effect of the thermistor position are inherently included. In addition, no material properties are required to generate the model and as long as the heat transfer is dominated by conduction, the same approach can be applied to any device or configuration. However, to develop this model it must be possible to measure the transient temperature response of every device in the power module, and this is not straightforward when using encapsulated power modules.

3.3.6 Summary of the Thermal Models

The key features of the thermal models that were reviewed in sections 3.3.1 to 3.3.5 are summarised in Table 3.1. Apart from the ability to model the basic heat flow, the key requirement for the thermal model for an inverter is the ability to model the thermal coupling between each device. From this summary it is clear that only the parameter extraction network and the thermal impedance matrix can be used. Therefore, to select the model that is best suited to an inverter both of these techniques are used to develop a thermal model for a simple heat spreader. The process used to develop these models and a comparison with simulation results are presented in the next section.

Table 3.1: Key features of the thermal models

	Datasheet Model	Analytical	Compact[1]	Parameter Extraction Network	Thermal Impedance Matrix
Temperature Estimation					
Steady-state	Yes	Yes	Yes	Yes	Yes
Transient	Yes	No	Possible	Yes	Yes
Internal nodes	No	Yes	No	Yes	No
Temperature Feedback					
Ambient	No	Yes	Yes	Yes	Yes
Case	Yes	No	No	Yes	Yes
Internal thermistor	No	No	No	Possible	Yes
Multi-chip Device					
Thermal coupling	No	No	Possible	Yes	Yes
Non-Linear Effects					
Material properties	No	Yes	No	Yes	No
Material degradation	No	No	No	Possible	No
Cooling conditions	No	Possible	Yes	Possible	No
Model Generation					
Measurements	Yes	No	Yes	No	Yes
Material properties	No	Yes	No	Yes	No
Applications					
Simple heat spreader	N/A	Yes	Yes	Yes	Yes
Integrated circuits	N/A	No	Yes	Yes	Yes
Power module	Yes	No	Possible	Yes	Yes

[1] The term compact model is commonly used in the literature to specifically describe network models used to estimate the junction temperature of an integrated circuit, although the term compact applies to any simplified or reduced order model.

Note: Table entries indicate the characteristics that can be included in a model initially developed to estimate the junction temperature of a device and are based on a review of models implemented in the literature. Where the inclusion of a characteristic is indicated as possible a method has been discussed but not implemented.

3.4 Comparison of the Parameter Extraction and Thermal Impedance Models

In this section the parameter extraction and thermal impedance models are compared using the simple heat spreader shown in Figure 3.5. Two different conditions are examined, one where the flow of heat is restricted to the area directly under the source (one-dimensional heat flow) and another where the heat is allowed to spread.

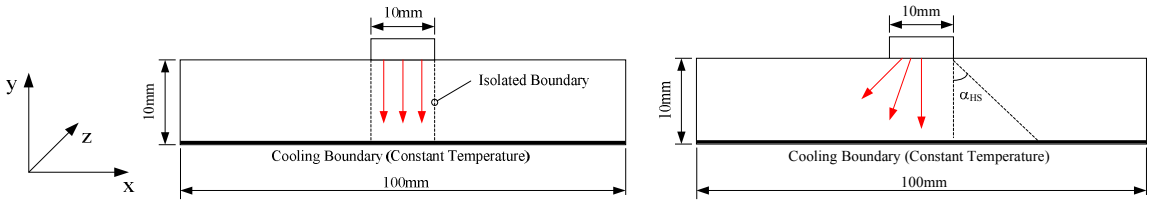

Figure 3.5: Heat spreader with a single heat source and a constant cooling boundary (a) restricted heat flow (b) heat spread

For this comparison arbitrary material properties have been selected for the heat spreader and these are:

- Thermal conductivity (k) = 10 W/K·m
- Mass density (ρ) = 800Kg/m^3
- Specific heat (c) = 1600J/K·Kg

To calculate the thermal resistance and capacitance in the equivalent Cauer network (parameter extraction) the heat flow area and volume must be known. For the case where the heat flow is one-dimensional the area (assuming a uniform heat source) is equal to the area of the source. This applies at any height (Y axis). Therefore, for a unit depth (Z axis) the heat flow area is 0.01m^2. In this comparison the heat spreader is divided into six sections and the thermal resistance and capacitance of each section is shown in Table 3.2. When the heat is allowed to spread the heat flow area is approximated by a constant angle (α_{HS}=36°). In this instance the angle has been selected so that the total thermal resistance is the same as the simulation results, this is a combination of the curve fitting and parameters extraction techniques. This approach is only possible if the thermal resistance is known.

Table 3.2: Thermal Resistance and Capacitance for a Cauer network

Height (mm)	Restricted Heat Flow		Heat Spread	
	Resistance (K/W)	Capacitance (J/K)	Resistance (K/W)	Capacitance (J/K)
0-1	0.01	12.8	0.00932	13.73
1-2	0.01	12.8	0.00821	15.59
2-4	0.02	25.6	0.01390	36.76
4-6	0.02	25.6	0.01158	44.19
6-8	0.02	25.6	0.00992	51.64
8-10	0.02	25.6	0.00867	59.07

For the thermal impedance model the parameters of an equivalent Foster network are calculated by curve fitting the characteristic of the network to the transient thermal impedance determined from the simulation of the heat spreader in Flotherm. For this model the same approach is used for both conditions. The parameters (thermal resistance and time constant) of a forth order network (four network elements) are shown in Table 3.3.

Table 3.3: Thermal Resistance and Capacitance for a Foster network

Network Element	Restricted Heat Flow		Heat Spread	
	Resistance (K/W)	Time constant (s)	Resistance (K/W)	Time constant (s)
1	0.01	4.90	0.010	5.30
2	0.01	5.60	0.012	0.15
3	0.03	1.00	0.020	4.00
4	0.05	0.12	0.020	1.25

The transient thermal impedance calculated using the Cauer and Foster networks are compared with the simulation results in Figure 3.6. From these results it can be seen that the response of the Foster network and the simulation results are in agreement. However, the response of the Cauer network is much slower during the initial rise. For the one-dimensional heat flow this effect is caused entirely by the use of lumped parameters and can be reduced by increasing the number of elements in the network. When heat spreading occurs, it is assumed that the effective heat flow area at any depth is constant with time and that this area increases linearly in the direction of heat flow (i.e. this uses the constant angle model). However, neither of these assumptions is true and both have a significant impact on the transient response. From the results shown in Figure 3.6(b) it is clear that when using a

constant heat flow angle the estimated temperature rise is initially much slower than the simulation response, although due to the calculation of the heat flow angle the steady state impedance is the same.

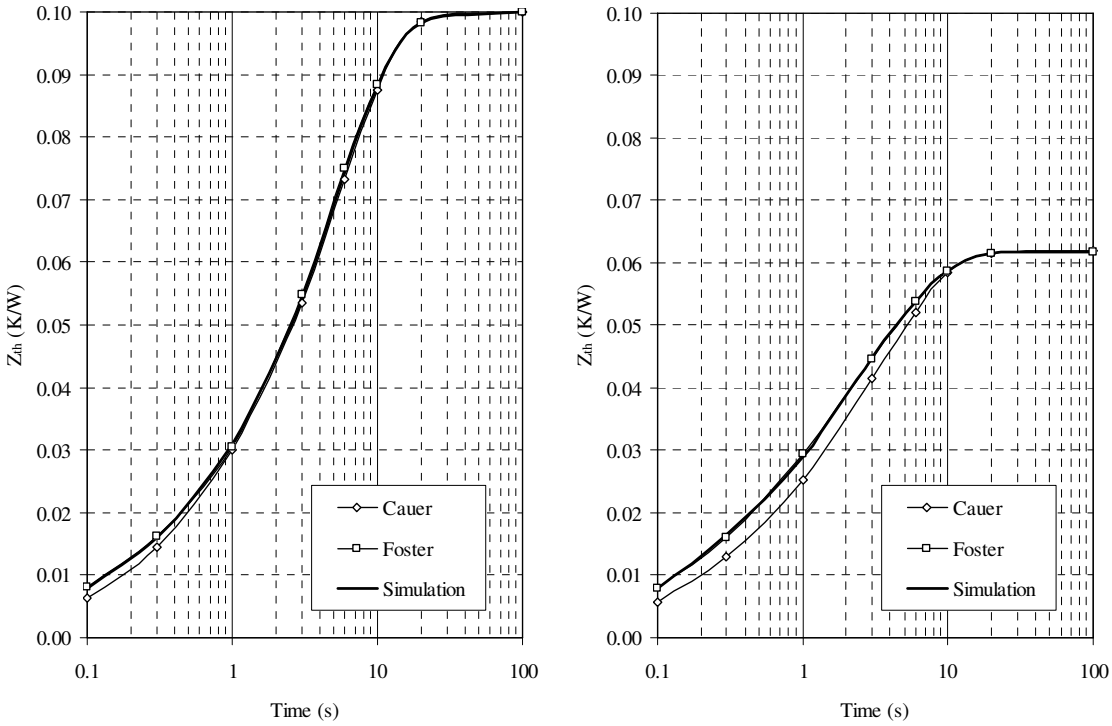

Figure 3.6: Thermal impedance (a) restricted heat flow (b) heat spread

This simple comparison highlights the difficulty in developing an accurate model using the parameter extraction technique, especially when heat spreading occurs. Furthermore, in this instance the heat flow angle has been selected from the known thermal resistance. If an angle of 45° was selected the heat flow area would have been larger causing an underestimation of steady-state temperature. This is shown in Figure 3.7. In this figure the thermal resistance at the upper surface of the heat spreader (i.e. the sum of the resistance in the Cauer network) is calculated using the full analytical solution for a rectangular heat spreader, the variable angle model and the constant angle model.

From the results presented in this section it is clear that when using a parameter extraction model it is very difficult to achieve the required accuracy. This will become more evident if the model is applied to a power module with multiple layers of different materials.

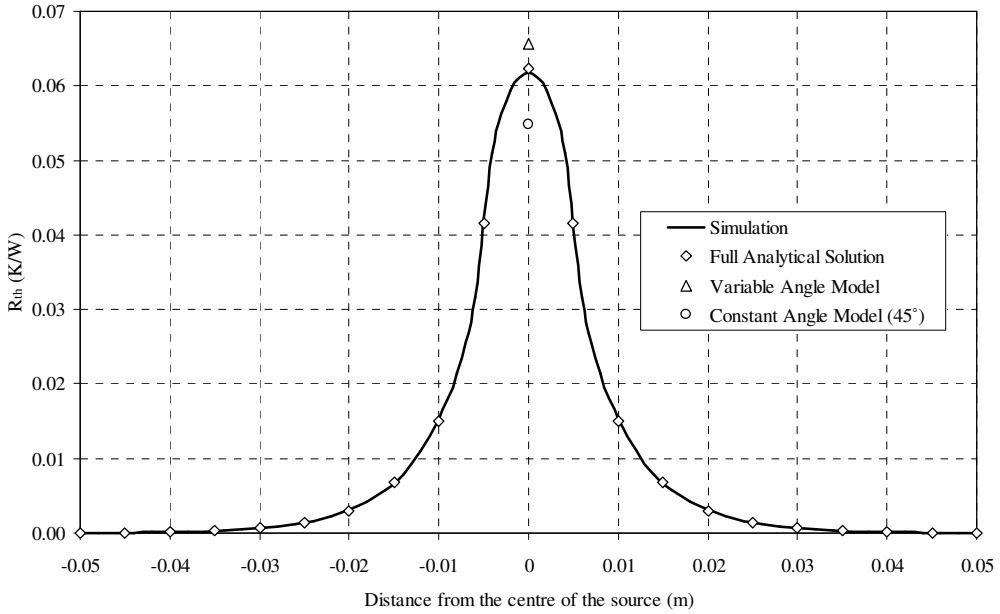

Figure 3.7: Comparison of the temperature profile and thermal resistance

In contrast, curve fitting a Foster network to the measured thermal impedance provides a good approximation of the thermal characteristics and by using linear superposition the same approach can be applied to a multi-chip device. Therefore, of the models reviewed in this chapter the thermal impedance matrix is the only model that can achieve the required accuracy and be implemented efficiently in a microprocessor.

3.5 Summary

In this chapter five methods that can be used to develop a thermal model have been reviewed. From this review it is clear that the parameter extraction network and thermal impedance matrix can be applied to a multi-chip power module. Therefore, these models were compared using a simple heat spreader. This comparison showed that when heat spreading occurs, calculating an effective heat flow area is very difficult and the approximations used in this calculation can lead to a significant error. In contrast the parameters of the thermal impedance matrix can be calculated easily by curve fitting the response of a Foster network to the measured thermal impedance. Furthermore, the effect of the thermal coupling between each device and the location of the thermistor is included. The main disadvantage of the thermal impedance matrix is that it must be possible to measure the temperature of every device in the inverter and a number of measurements must be performed, which can be time consuming.

Chapter 4: Development of a Thermal Model

4.1 Introduction

The power semiconductors in the inverter stage of a typical industrial drive are often operated close to their maximum temperature during an overload or if the inverter is operating at a low output frequency. Therefore, to ensure the drive is reliable the temperature of these components must be monitored to prevent them from overheating as this can lead to an instant failure of the component, or a reduced lifetime. However, the junction temperature (T_j) of the power semiconductors cannot be measured directly. Therefore, the temperature rise between the junction of a device and a measured reference temperature (T_{ref}) has to be estimated using a real-time thermal model. In this work, a general thermal model is developed to protect the six IGBTs and freewheeling diodes in an inverter. As shown in Figure 4.1, a real-time thermal model based on the full thermal impedance matrix and the measured instantaneous phase currents could be used to calculate the temperature between the junction of each device and the measured reference temperature.

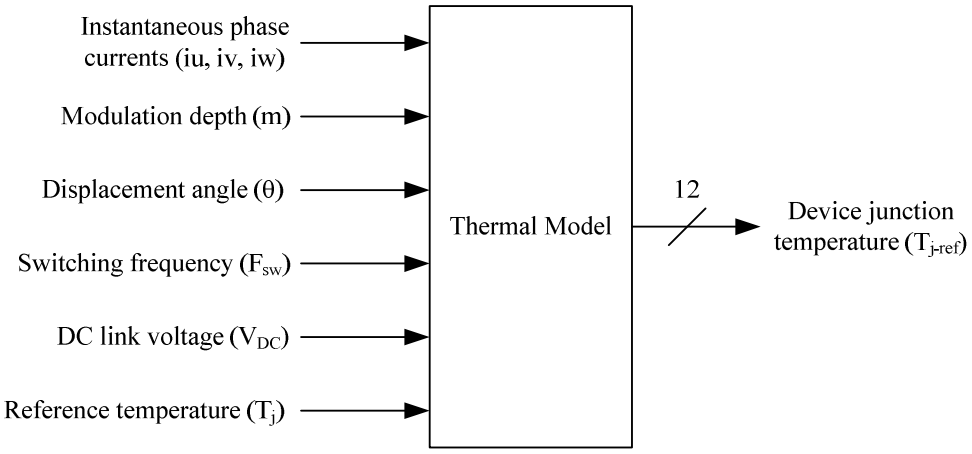

Figure 4.1: Thermal model implemented in the time domain using the instantaneous phase currents to calculate the temperature of every device in the inverter

However, to implement this type of model a considerable number of calculations must be performed by the microprocessor during each sample period, and since these are carried out in the time domain, the sample rate must be high enough to prevent aliasing when the inverter is operating at high output frequencies. To achieve this, a significant computational resource is required and as yet this is not available in a commercial drive control system. In this chapter an alternative model is proposed which is based on the calculation of the peak steady-state junction-to-reference temperature in the frequency domain. In a steady-state operating condition, this type of model will not be affected by aliasing and can be implemented using a moderate sample frequency. Furthermore, to protect all of the devices in the inverter it is only necessary to calculate the peak temperature of the hottest IGBT and diode. In the frequency domain model shown below, the current magnitude and output frequency are used in place of the three instantaneous phase currents.

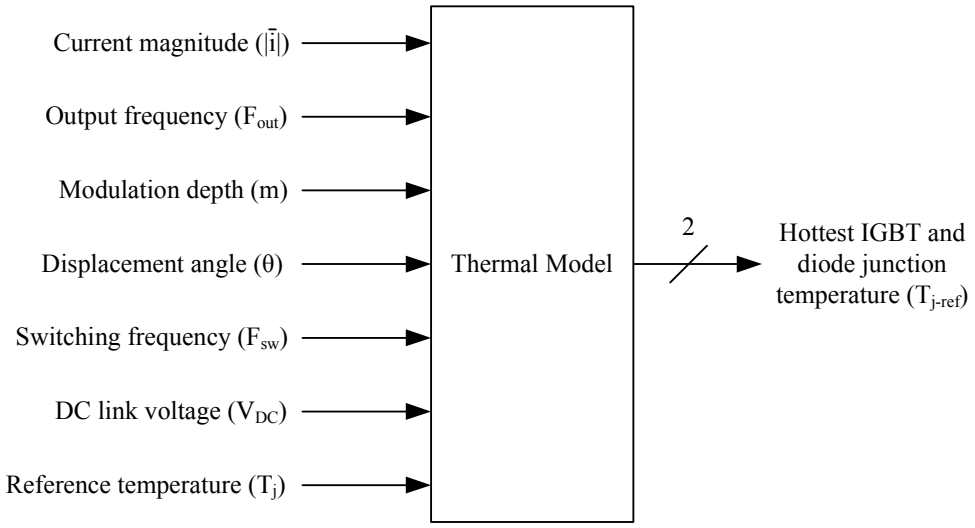

Figure 4.2: Thermal model implemented in the frequency domain using the magnitude of the phase current and output frequency to calculate the temperature of the hottest IGBT and diode in the inverter

In this model, the magnitude of the output current is used to calculate the temperature between the junction of a device and the measured reference temperature over a complete output cycle of the inverter ($1/F_{out}$). This temperature is represented by a series of frequency components, including the DC component (0Hz), the fundamental of the output frequency and a number of harmonics terms. These frequency components are used to calculate the

steady-state temperature of the hottest IGBT and diode at every sample. Therefore, the output of the steady-state model is the temperature that would occur if the input parameters were held constant over a period of time. The steps used to develop the steady-state model are summarized below:

1. Determine the power loss of a device over a complete output cycle due to its switching characteristics and represent this loss as a series of frequency components. For the switching loss, these components are dependant on the current magnitude, switching frequency and DC link voltage.
2. Apply the frequency components for the switching loss to an equivalent Foster network and calculate the resulting temperature rise in the frequency domain.
3. Determine the power loss of a device over a complete output cycle due to its conduction characteristics and represent this loss as a series of frequency components. For the conduction loss, these components are dependant on the current magnitude, modulation index and the angle between the fundamental output voltage and current (displacement angle).
4. Apply the frequency components of the conduction loss to an equivalent Foster network and calculate the resulting temperature rise in the frequency domain.
5. Combine the frequency components for the switching and conduction loss.
6. Use the magnitude and phase of the combined frequency components to calculate the peak steady-state temperature between the junction of the device and the measured reference temperature.

The frequency components used to calculate the steady-state temperature response over a complete output cycle of the inverter are developed in Section 4.2. The frequency components are divided into those representing the temperature rise due to the switching loss (steps 1 and 2), which is covered in Section 4.2.2, and the conduction loss (steps 3 and 4), covered in Section 4.2.3. The calculation of the peak temperature (steps 5 and 6) between the junction and reference is described in Section 4.3.

Throughout the development of the steady-state thermal model, the frequency components used to represent the power loss and duty cycle are selected to minimize the number of

calculations required to estimate the device temperature. In this process care is taken to ensure that the temperature calculated using the self thermal impedance of a device is never underestimated. However, in many operating conditions it is the thermal model for the inverter that restricts the maximum performance of a drive. Thus, care must also be taken to prevent excessive overestimation of the device temperature since this can lead to a reduction in the maximum output current available from the inverter and ultimately an uncompetitive product. The impact of any approximations made during the development of the frequency model is investigated in Section 4.4.

In addition to the steady-state temperature it is important that the thermal model is capable of estimating the transient response due to changes in power loss or output frequency. The transient model is developed from the steady-state model and is described in Section 4.5.

4.2 Steady-State Thermal Model Development

The thermal model developed in this chapter is based on the calculation of the steady-state temperature over a complete output cycle of the inverter. This calculation is carried out in the frequency domain. Therefore, the first step in the procedure is to calculate the frequency components for the power loss due to the switching and conduction losses in an IGBT and diode. These losses are related to the current flowing in a device and in the next section, this current is approximated by a number of frequency components. These frequency components are then used to develop the switching and conduction loss models.

4.2.1 Frequency Components of the Current in an IGBT and Anti-Parallel Diode

In an inverter the IGBTs are switched to control the magnitude of the voltage applied to a motor and as a result, the current in a device is discontinuous. However, the sum of the current in an IGBT and the complementary anti-parallel diode is equal to the positive (upper IGBT and lower diode) or the negative (lower IGBT and upper diode) phase current (I_L). Thus, in order to represent the current in the frequency domain, it is assumed that the phase current flowing in an IGBT and anti-parallel diode is a half-wave rectified sinusoid. This concept is illustrated in Figure 4.3.

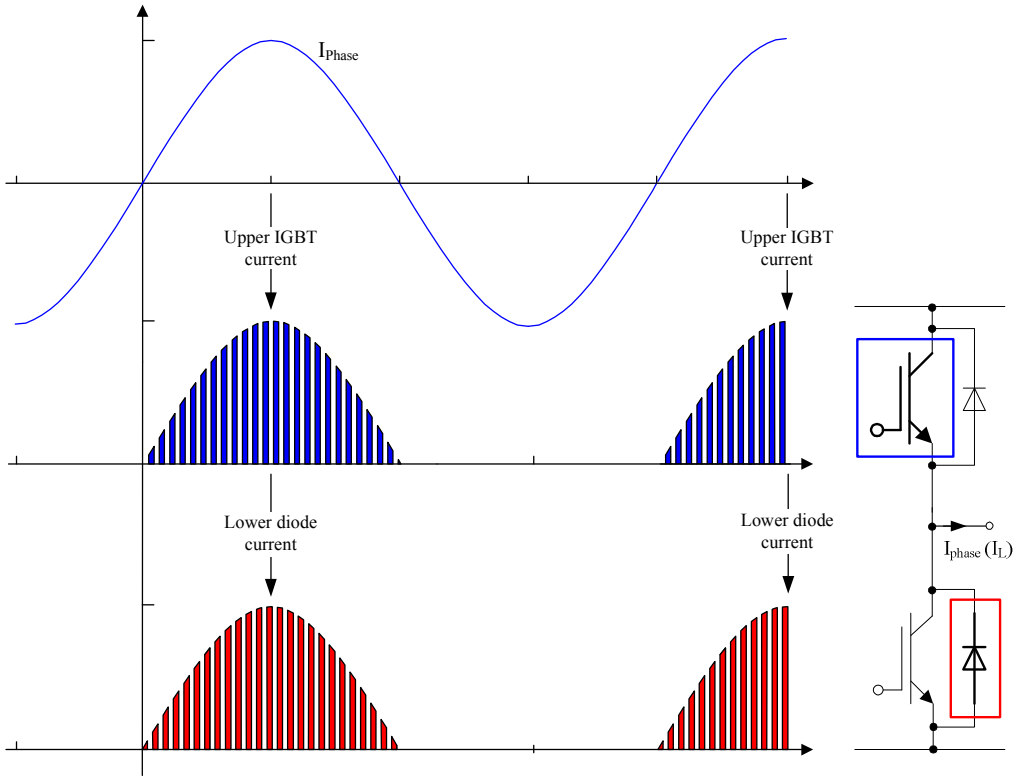

Figure 4.3: Phase current in an IGBT and an anti-parallel diode

The frequency components for the phase current in these devices can be expressed by the Fourier series:

$$I_L(\omega t) = a_0 + \sum_{n=1}^{\infty} a_n \cos(n\omega t) + b_n \sin(n\omega t) \tag{4.1}$$

and for a half-wave rectified sinusoid, the Fourier coefficients are as follows:

$$a_0 = \frac{\hat{I}_L}{\pi} \tag{4.2}$$

$$a_n = \begin{cases} \dfrac{-2\hat{I}_L}{\pi(n^2-1)} \rightarrow n = \{2,4,\ldots\} \\ \\ 0 \quad \rightarrow \quad n = odd \end{cases} \tag{4.3}$$

$$b_n = \begin{cases} \dfrac{\hat{I}_L}{2} \rightarrow n = 1 \\ 0 \rightarrow n \geq 2 \end{cases} \tag{4.4}$$

As the number of harmonics (n) in the Fourier series is increased, the response of the Fourier series will become a more accurate representation of the original current waveform in the time domain, although more calculations must be performed by the microprocessor. Therefore, to develop a thermal model that can be implemented using the available computational resources the load current is approximated using only three Fourier coefficients, these are a_0, a_2 and b_1. Thus, in this model the phase current flowing in an IGBT and the anti-parallel diode is approximated by:

$$I_L(\omega t) = \hat{I}_L\left(\frac{1}{\pi} + \frac{1}{2}\sin(\omega t) - \frac{2}{3\pi}\cos(2\omega t)\right) \tag{4.5}$$

The impact of this approximation is investigated later in this section. To model the current in an upper and lower device in the same phase or the devices in other phases of the inverter an offset angle (α) is required. In addition, to develop the model for the conduction loss, the displacement angle (θ) must also be included. This angle defines the relationship between the applied voltage, which is directly related to the duty cycle of a device, and the resultant output current. Including these angles, the phase current is represented by:

$$I_L(\omega t) = \hat{I}_L\left(\frac{1}{\pi} + \frac{1}{2}\sin(\omega t + \theta + \alpha) - \frac{2}{3\pi}\cos(2\omega t + 2\theta + 2\alpha)\right) \tag{4.6}$$

By definition, for the device being modelled (α=0), the peak phase voltage occurs when $\omega t=\pi/2$. The current in this device (I_L) is referenced to this point by the displacement angle, i.e. the current is in phase with the voltage when the displacement power factor $\cos(\theta)$ is unity. The output voltage and the corresponding current in the other devices is then

referenced to the modelled device by the offset angle (α), i.e. there is 120° between the peak voltage in each phase and 180° between the upper and lower devices.

4.2.2 Switching Loss Model

To develop a frequency model for the switching loss, the power loss due to the switching energy is defined as the average power loss (P_{sw}) over a switching period ($1/F_{SW}$). For an IGBT, this loss is dependant on the switching energy when the device is turning on (E_{on}) and off (E_{off}). For a diode the only significant switching energy is due to the reverse recovery (E_{rec}) as the diode is turning off. The definition of the switching loss for an IGBT and diode is illustrated in Figure 4.4.

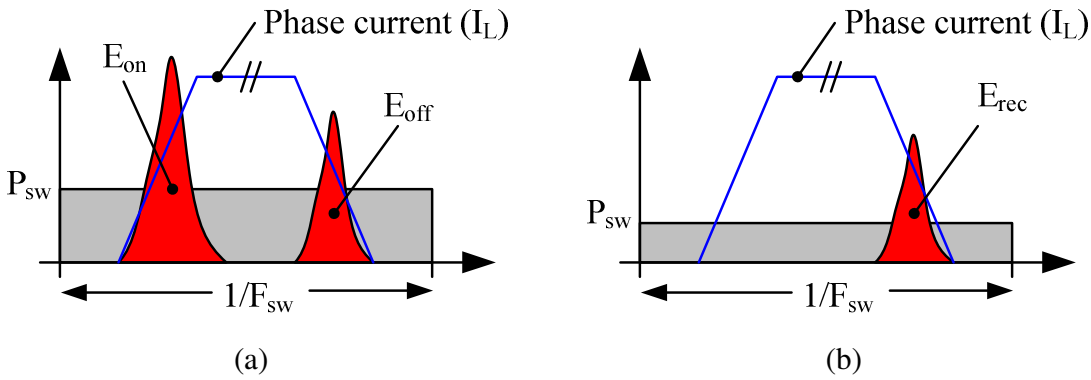

Figure 4.4: Switching power loss over a switching frequency cycle (a) IGBT (b) diode

In this approximation it is assumed every device switches on and off during each switching period and there is no significant temperature ripple due to the peak loss that occurs when the devices are actually switching, i.e. the effect of the instantaneous power loss is filtered by the thermal time constants. Using this approach, the peak switching loss ($\hat{P}_{sw}$) is defined as the power loss calculated when the device switches the peak phase current. For an IGBT the peak switching loss (averaged over the switching period) is given by:

$$\hat{P}_{sw} = F_{sw}E_{on}(\hat{I}_L, T_j, V_{dc}) + F_{sw}E_{off}(\hat{I}_L, T_j, V_{dc}) \tag{4.7}$$

and for a diode:

$$\hat{P}_{sw} = F_{sw} E_{rec}(\hat{I}_L, T_j, V_{DC}) \tag{4.8}$$

To represent the switching loss over the entire output cycle of the inverter (ωt = 0 to 2π) it is assumed that the switching loss is proportional to the phase current. This allows the switching loss to be approximated using the same frequency components:

$$P_{sw}(\omega t) = \hat{P}_{sw}\left(\frac{1}{\pi} + \frac{1}{2}\sin(\omega t + \theta + \alpha) - \frac{2}{3\pi}\cos(2\omega t + 2\theta + 2\alpha)\right) \tag{4.9}$$

However, the switching energy in a device is not directly proportional to the phase current and the actual switching loss will not be sinusoidal. This is shown in the Figure below.

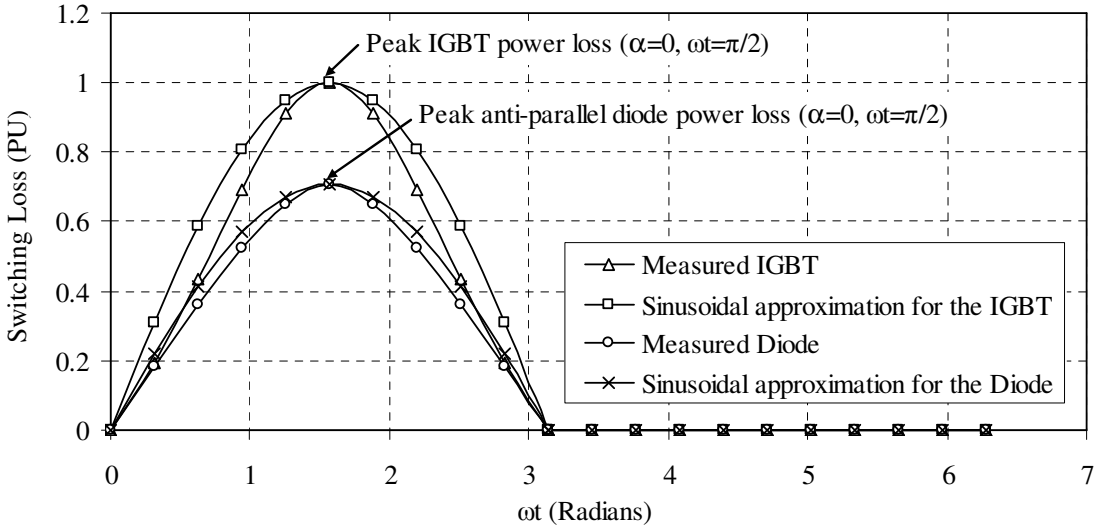

Figure 4.5: Comparison of the measured and approximated switching loss for an IGBT and diode over a complete output cycle of an inverter (1 PU = peak IGBT power loss)

In this figure, the switching loss calculated using the measured characteristics from an actual device is compared with the sinusoidal approximation (with the same peak value) over a complete output cycle. Apart from the peak switching loss, the power loss estimated by the sinusoidal approximation for the IGBT and diode is higher than the measured loss.

As a result, the device temperature will be overestimated. However, the power loss is approximated by only three Fourier coefficients (Equation 4.9) and this simplification will introduce an additional error. To show the effect of this approximation, the power loss calculated using the frequency model is compared directly with the sinusoidal approximation, i.e. the response of the frequency model if all of the harmonic terms (n =1 to ∞) could be used. A comparison is shown in Figure 4.6(a) and the difference between these responses (sinusoidal – frequency model) can be seen in the Figure 4.6(b).

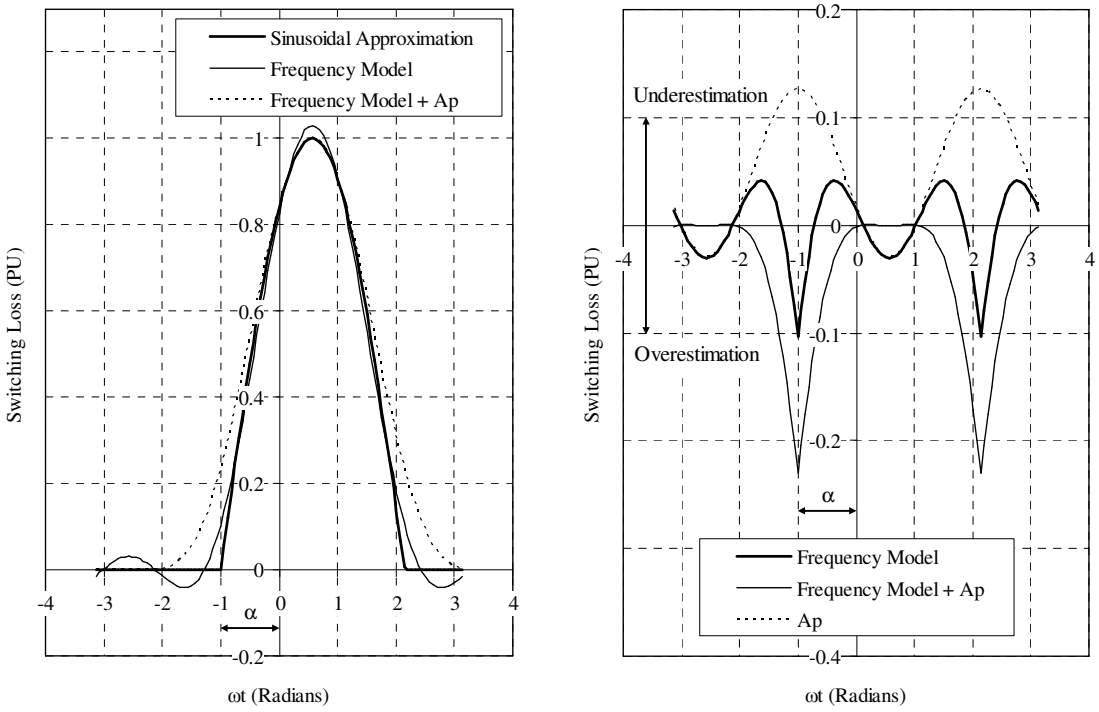

(a) (b)

Figure 4.6: Device switching loss calculated over a complete output cycle of the inverter (a) response of the sinusoidal and frequency model (b) the difference between the frequency and sinusoidal response (1 PU = peak sinusoidal switching loss)

From the comparison it is evident that power loss calculated by the frequency model can be negative. This is highlighted in Figure 4.6(b). In this figure a positive value indicates that the magnitude of the frequency model is smaller than the sinusoidal approximation, i.e. the instantaneous power loss is underestimated. However, the output of the thermal model is

the peak steady-state junction-to-reference temperature and the negative power loss will have little effect on the estimated temperature of a single device. Although, when frequency components from neighbouring devices are combined the negative power loss could be aligned with the peak loss in one of the other devices. In this instance the negative power loss will reduce the estimated temperature. Furthermore, the peak loss in the frequency model is 3% higher than the sinusoidal approximation and this will have a direct impact on the temperature estimated at low output frequencies.

To improve the approximation of the power loss, the magnitude of the Fourier coefficients in Equation 4.9 (a_0 and a_2) are modified in order to remove the negative power loss and the peak error. The additional component (A_P) added to the initial frequency model is:

$$A_p(\omega t) = \hat{P}_{sw}\left[A_{p(DC)} + A_{p(ac)}\cos(2\omega t + 2\theta + 2\alpha)\right] \tag{4.10}$$

The constants used in this equation were determined from the inspection of the error characteristics. The chosen magnitude for these constants is:

$A_{p(DC)} = 0.048$
$A_{p(ac)} = 0.077$

The response of Equation 4.10 is shown in Figure 4.6(b). By combining Equations 4.9 and 4.10, the switching loss in a device is approximated by:

$$P_{sw}(\omega t) = \hat{P}_{sw}\left(\begin{array}{l}\left(\frac{1}{\pi} + A_{p(DC)}\right) + \frac{1}{2}\sin(\omega t + \theta + \alpha) \\ -\left(\frac{2}{3\pi} - A_{p(ac)}\right)\cos(2\omega t + 2\theta + 2\alpha)\end{array}\right) \tag{4.11}$$

As shown in Figure 4.6(a), when compared to the initial sinusoidal approximation, the switching loss estimated by Equation 4.11 (Frequency model + A_p) is never underestimated and the peak value in both responses is identical. This equation is used in the following section to calculate the temperature response of a device due to its switching characteristics.

4.2.2.1 Temperature Response

The methods that can be used to represent the thermal characteristics of a device in a power module were reviewed in Chapter 3. In this review it was shown that the simplest method is to use the measured or calculated thermal impedance in the form of an equivalent Foster network. The characteristics of this network can be easily implemented in a microprocessor and by using linear superposition the thermal coupling from any neighbouring devices can be included. The response of a Foster network element (first order filter) in the Laplace domain is given by:

$$Z_{th}(s) = \frac{R_{th}}{(1 + \tau s)} \tag{4.12}$$

To calculate the temperature response due to the switching loss (T_{sw}) the following equation must be solved:

$$T_{sw}(s) = P_{sw}(s) Z_{th}(s) \tag{4.13}$$

The complete solution for this equation is shown in Appendix A. In the steady-state, the device temperature is given by:

$$T_{sw}(t) = T_{DC} + T_{ripple}(t) \tag{4.14}$$

With a fixed power loss the temperature rise due to the steady-state DC component (T_{DC}) will be constant. However, the ripple temperature (T_{ripple}) is the sum of the frequency components and the magnitudes of these components are dependant on the output frequency of the inverter. For example, if the general sinusoid term:

$$A_{\sin}(\omega t) = A_n \sin(n\omega t) \tag{4.15}$$

is applied to a first order filter the magnitude of the output response is reduced by the filter magnitude A_{Fn} and is phase shifted by the angle β_n. Therefore, the output of the filter is given by:

$$A_{\sin(Filter)}(\omega t) = A_n A_{Fn} \sin(n\omega t + \beta_n) \tag{4.16}$$

where

$$A_{Fn} = \frac{1}{\sqrt{1+(n\omega\tau)^2}} \tag{4.17}$$

and

$$\beta_n = -\tan^{-1}(n\omega\tau) \tag{4.18}$$

The fundamental and harmonic terms for the ripple temperature due to the switching loss in a device (solution of Equation 4.13), including the effect of the filter element on the magnitude and phase shift of these components, are shown in Table 4.1.

As discussed, where possible any overestimation of the temperature should be avoided since this will have a direct impact on the maximum output current that can be achieved. As the output frequency is increased the contribution from the harmonics is reduced and the term A_p is no longer required. Therefore, the constant $A_{p(DC)}$, which was added to ensure that the peak junction-to-reference temperature is correct at a low output frequency, is itself multiplied by the magnitude of a first order filter (Equation 4.17) calculated for a first harmonic term (n=1). Thus, as the output frequency is increased the magnitude of the DC component in the frequency model tends towards the calculated Fourier coefficient a_0 (i.e. $1/\pi$). This approximation prevents the temperature from being overestimated at higher output frequencies. As shown in Table 4.1, the constant $A_{p(ac)}$ is naturally reduced by the filter associated with the second harmonic (A_{F2}).

Table 4.1: Frequency components of the temperature rise due to the device switching loss

Frequency Component	Magnitude	
DC	A_{DC}	$\hat{P}_{sw}R_{th}\left(\frac{1}{\pi}+A_{p(DC)}A_{F1}\right)$
sin(ωt)	A_{s1}	$\frac{\hat{P}_{sw}R_{th}A_{F1}}{2}\cos(\theta+\alpha+\beta_1)$
sin(2ωt)	A_{s2}	$\hat{P}_{sw}R_{th}A_{F2}\left(\frac{2}{3\pi}-A_{p(ac)}\right)\sin(2\theta+2\alpha+\beta_2)$
cos(ωt)	A_{c1}	$\frac{\hat{P}_{sw}R_{th}A_{F1}}{2}\sin(\theta+\alpha+\beta_1)$
cos(2ωt)	A_{c2}	$-\hat{P}_{sw}R_{th}A_{F2}\left(\frac{2}{3\pi}-A_{p(ac)}\right)\cos(2\theta+2\alpha+\beta_2)$

Once calculated, the sine and cosine components for the fundamental and second harmonic can be combined into a single term and the ripple temperature can be calculated using:

$$T_{ripple(sw)} = A_{sw1}\cos(\omega t+\sigma_1)+A_{sw2}\cos(2\omega t+2\sigma_2) \tag{4.19}$$

where, A_{sw1} and A_{sw2} are the combined magnitude of the sine and cosine components in the fundamental and second harmonic terms and σ_n is the resulting phase shift. This process can be used to combine the frequency response for any number of devices (self and mutual) or network elements. Therefore, the ripple component of the temperature response due to the switching loss in multiple devices can be represented by just two frequency components; this concept is described in more detail in Chapter 5.

4.2.2.2 Comparison of the Temperature Response

To compare the temperature response, the frequency components for the switching loss model (Table 4.1) are implemented in Matlab. This is compared with the temperature calculated using the sinusoidal approximation. The response of this model is calculated

using Simulink and the basic model for a single device and Foster network element is shown in the figure below:

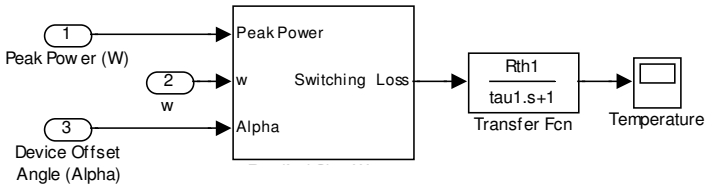

Figure 4.7: Sinusoidal switching loss model

This model allows the power loss ($\hat{P}_{sw}$), output frequency ($\omega=2\pi F_{out}$) and the offset angle (α) along with the thermal resistance (R_{th}) and the time constant (τ) of the network element to be defined. The temperatures calculated using the frequency model (Matlab) and the sinusoidal approximation (Simulink) are compared using the following parameters:

- R_{th} = 1K/W
- τ = 1s
- P_{sw} = 20W
- ω = 0.628 radians/s or F_{out} = 0.1Hz
- α = 0 radians

The steady-state temperatures calculated using these parameters are compared in Figure 4.8(a). As intended, the temperature estimated by the frequency model is never lower than the sinusoidal response and the peak temperatures are identical. However, if the factor A_p was ignored, the peak temperature calculated using the frequency model would have been higher than the sinusoidal response. This effect can be seen in Figure 4.8(b). Although the temperature is initially overestimated by the frequency model without A_p, the results show that as the output frequency is increased the peak magnitude of this model tends towards the peak of the sinusoidal response. This is caused by the reduction in the magnitude of the higher harmonic terms that have not been included in the frequency model.

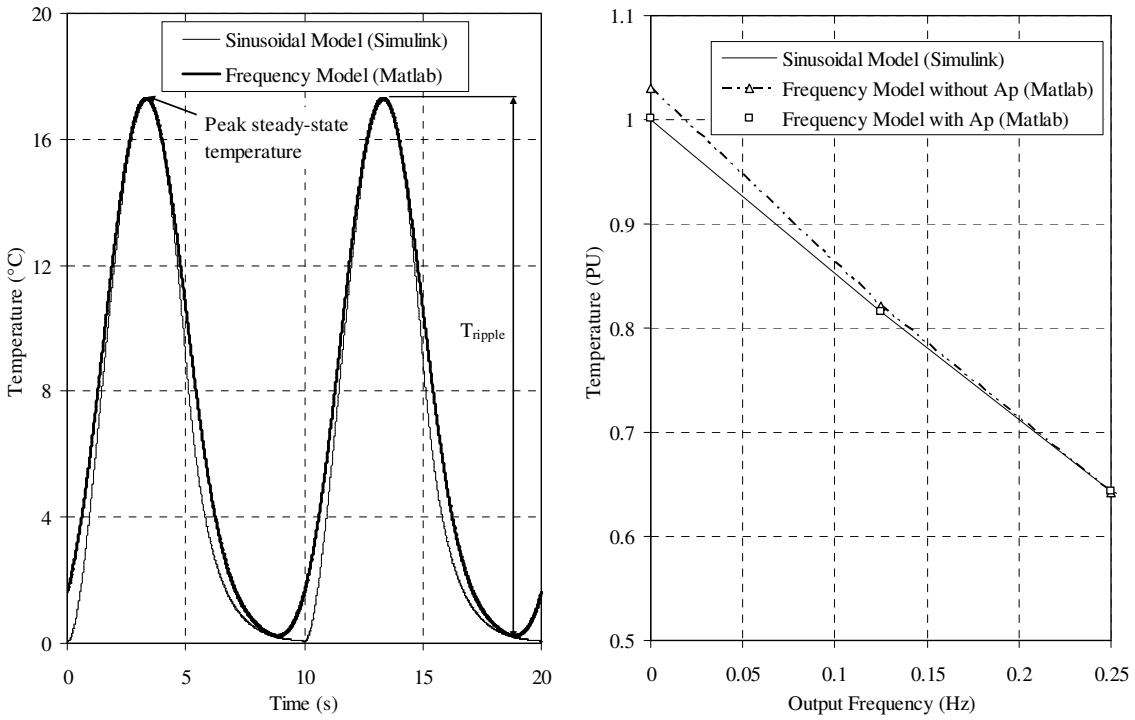

(a) (b)

Figure 4.8: Comparison of the (a) temperature response for the sinusoidal and frequency models at an output frequency of 0.1Hz (b) maximum temperature verses output frequency

In summary, the frequency components developed in this section allow the steady-state temperature response of a Foster network element to be calculated in the frequency domain when the switching loss of either an IGBT or diode is applied. However, the impact of the conduction loss on the temperature response cannot be ignored and the frequency components for this model are developed in the following sections.

4.2.3 Conduction Loss Model

The conduction loss in a device is dependant on the current, displacement angle (θ) and the modulation index (m). However, to develop the conduction loss model, it is initially assumed that the current in a device is sinusoidal (not discontinuous) and the device conducts for the entire switching period, i.e. the duty cycle (δ_m) is unity. Therefore, under this condition, the power loss can be derived in a similar way to the switching loss and will have the same form as Equation 4.11:

$$P_{con(\delta_m=1)}(\omega t) = \hat{P}_{con}\begin{pmatrix}\left(\frac{1}{\pi}+A_{p(DC)}\right)+\frac{1}{2}\sin(\omega t+\theta+\alpha)\\ -\left(\frac{2}{3\pi}-A_{p(ac)}\right)\cos(2\omega t+2\theta+2\alpha)\end{pmatrix} \tag{4.20}$$

where $\hat{P}_{con}$ is the peak conduction loss. For an IGBT this loss is given by:

$$\hat{P}_{con} = \hat{I}_L V_{CE}(\hat{I}_L, T_j) \tag{4.21}$$

or for a diode:

$$\hat{P}_{con} = \hat{I}_L V_F(\hat{I}_L, T_j) \tag{4.22}$$

However, in order to generate the required output voltage the on-time (t_{on}) of each IGBT in the inverter is modulated and the duty cycle for a device must vary over an output cycle. This modulation will have a significant impact on the average conduction loss over a switching period. This is illustrated in the figure below.

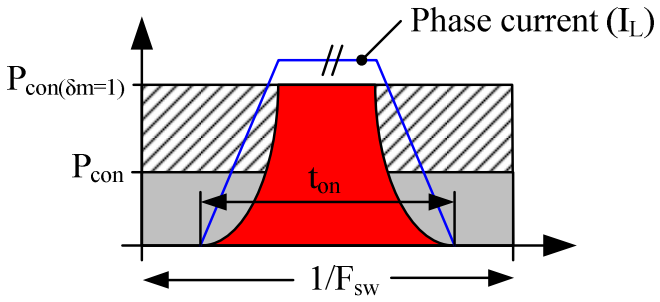

Figure 4.9: Conduction power loss over a switching frequency cycle

The average power loss over a switching period (P_{con}) is dependant on the conduction loss calculated for a unity duty cycle and the actual on-time of the device. For a switching frequency cycle, the duty cycle can be defined as:

$$\delta_m = F_{sw} t_{on} \tag{4.23}$$

and the average conduction loss over a switching period can be calculated using:

$$P_{con} = \delta_m P_{con(\delta_m=1)} \tag{4.24}$$

The temperature rise due to the conduction loss in a device is given by:

$$T_{con}(s) = P_{con}(s) Z_{th}(s) \tag{4.25}$$

In order to solve Equation 4.25, a modulation scheme must be chosen and the resulting duty cycle must be represented by its frequency components. This selection is described in the next section.

4.2.3.1 Modulation Schemes

Possible modulation schemes were briefly reviewed in Chapter 2. In a modern drive, the most common modulation scheme is Space Vector Modulation (SVM). As described, this scheme is based on switching the IGBTs in the inverter to produce eight unique output vectors (voltage) and by simply changing the time spent at each vector an output voltage with any magnitude (limited by the DC bus voltage) or angle can be produced. Variations of the SVM are based on the selection of the null vectors and a number of different techniques are compared in [7]. The most popular of these is the Alternating-Reversing (Alt-Rev) sequence. In this scheme, the null vectors are alternated in each sequence and then reversed. When using SVM the duty cycle cannot be calculated using a closed form expression and six equations are required to calculate the duty cycle over the complete output cycle of the inverter. Thus, to calculate the frequency components an approximation of this scheme is required. Prior to the advent of SVM, the third harmonic modulation scheme was popular due to the increased bus utilisation when compared to a sinusoidal modulation [110]. In this scheme the duty cycle is calculated using a sine wave modulation with a third harmonic component:

$$\delta_m = 0.5 + \frac{m}{\sqrt{3}}\sin(\omega t + \alpha) + \frac{m}{6\sqrt{3}}\sin(3\omega t + 3\alpha) \tag{4.26}$$

The duty cycle calculated using the third harmonic and SVM (Alt-Rev) schemes are compared in Figure 4.10(a). From this comparison it is evident that the duty cycle for both schemes is similar.

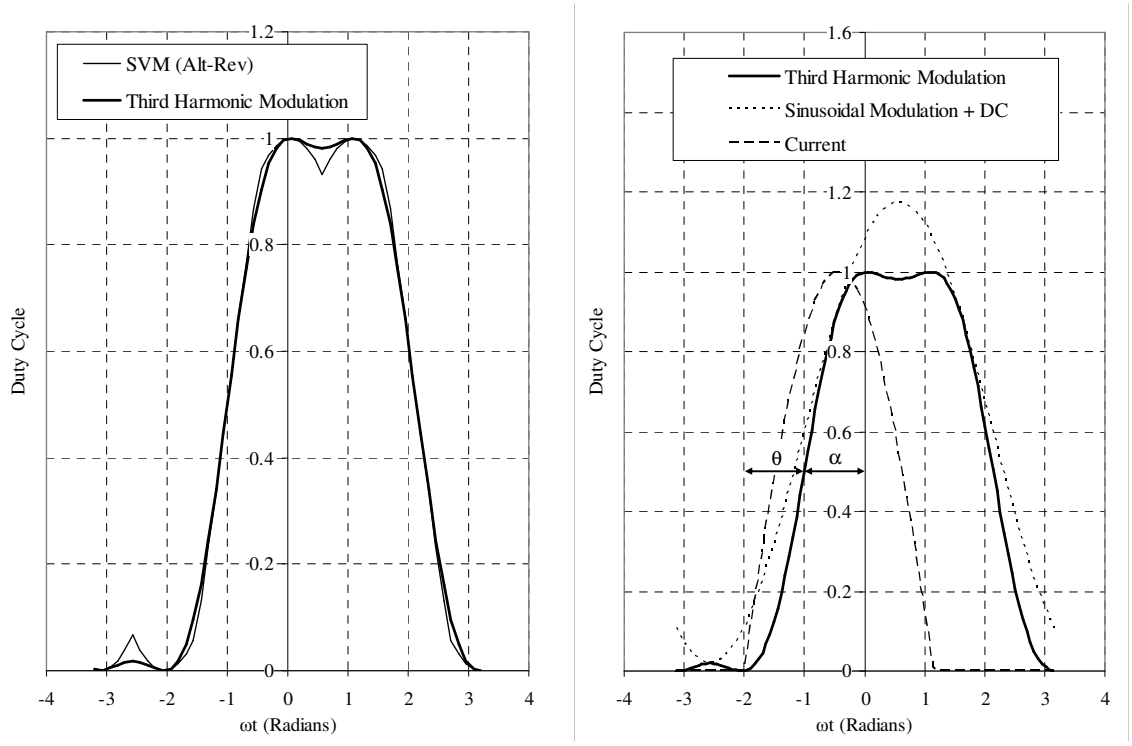

(a) (b)

Figure 4.10: Comparison of modulation schemes with a unity modulation index (a) SVM (Alt-Rev) and third harmonic (b) third harmonic and sinusoidal approximation

If the third harmonic modulation scheme is used to calculate the frequency components for the conduction loss, the solution will have five harmonic terms (i.e. the DC, 1st and 2nd harmonics in Equation 4.20 combined with DC, 1st and 3rd harmonics in Equation 4.26). Thus, when compared to the switching loss more calculations must be performed to estimate the corresponding temperature rise. Therefore, to simplify the model the modulation scheme used to calculate the temperature rise due to the conduction loss is:

$$\delta_m = \left(0.5 + \frac{m_{(DC)} A_{F3}}{6\sqrt{3}}\right) + \frac{m}{\sqrt{3}} \sin(\omega t + \alpha) \tag{4.27}$$

This approximation is based on the third harmonic modulation scheme shown in Equation 4.26, but the magnitude of the third harmonic term is added to the DC term, i.e. the duty cycle only has a fundamental and DC component. As with the switching loss model, to avoid overestimating the conduction loss at high output frequencies, the magnitude of the additional DC term is multiplied by the magnitude of a first order filter (Equation 4.17) and in this instance, this is calculated for a third harmonic term (n=3).

The duty cycle calculated using Equation 4.27 (sinusoidal modulation + DC) is shown in Figure 4.10(b). As intended, the duty cycle calculated using this approximation is always higher than the third harmonic scheme. Although, if the modulation index is high when the output frequency is low the peak duty cycle can be greater than unity, which by definition is an impossible operating condition. Consequently, the temperature rise due to the conduction loss can be significantly overestimated. However, this is not a common operating condition for a drive running a motor (low output frequency = low output voltage = low modulation index). Even so, the accuracy of the model can be improved by limiting the maximum temperature using:

$$T_{con} \leq \hat{P}_{con} R_{th} (0.5 + 0.5m) \tag{4.28}$$

This equation is based on the calculation of the maximum steady-state temperature when operating in a stationary vector condition with a unity displacement power factor, i.e. the temperature calculated when the loss in the device is at its maximum.

4.2.3.2 Steady-State Temperature Response

The full solution for Equation 4.25 is shown in Appendix A. The steady-state frequency components for the conduction loss model are shown in Table 4.2. These can be used to calculate the temperature rise of an IGBT or diode with any displacement power factor or modulation index; although for an anti-parallel diode the duty cycle is normally defined as:

Table 4.2: Frequency components for the device conduction loss

Frequency Component	Magnitude	
DC	A_{DC}	$\hat{P}_{con}R_{th}\left[\frac{m}{4\sqrt{3}}\cos(\theta)+\left(\frac{1}{\pi}+A_{P(DC)}A_{F(DC)}\right)\left(\frac{1}{2}+\frac{m_{(DC)}A_{F3}}{6\sqrt{3}}\right)\right]$
sin(ωt)	A_{s1}	$\hat{P}_{con}R_{th}A_{F1}\left[\begin{array}{l}\frac{1}{2}\left(\frac{1}{2}+\frac{m_{(DC)}A_{F3}}{6\sqrt{3}}\right)\cos(\theta+\alpha+\beta_1)\\+\left(\frac{2}{3\pi}-A_{p(ac)}\right)\frac{m}{2\sqrt{3}}\cos(2\theta+\alpha+\beta_1)\\+\left(\frac{1}{\pi}+A_{p(DC)}\right)\frac{m}{\sqrt{3}}\cos(\alpha+\beta_1)\end{array}\right]$
sin(2ωt)	A_{s2}	$\hat{P}_{con}R_{th}A_{F2}\left[\begin{array}{l}\left(\frac{2}{3\pi}-A_{P(ac)}\right)\left(\frac{1}{2}+\frac{m_{(DC)}A_{F3}}{6\sqrt{3}}\right)\sin(2\theta+2\alpha+\beta_2)\\+\frac{m}{4\sqrt{3}}\sin(\theta+2\alpha+\beta_2)\end{array}\right]$
sin(3ωt)	A_{s3}	$-\hat{P}_{con}R_{th}A_{F3}\left(\frac{2}{3\pi}-A_{P(ac)}\right)\frac{m}{2\sqrt{3}}\cos(2\theta+3\alpha+\beta_3)$
cos(ωt)	A_{c1}	$\hat{P}_{con}R_{th}A_{F1}\left[\begin{array}{l}\frac{1}{2}\left(\frac{1}{2}+\frac{m_{(DC)}A_{F3}}{6\sqrt{3}}\right)\sin(\theta+\alpha+\beta_1)\\+\left(\frac{2}{3\pi}-A_{p(ac)}\right)\frac{m}{2\sqrt{3}}\sin(2\theta+\alpha+\beta_1)\\+\left(\frac{1}{\pi}+A_{p(DC)}\right)\frac{m}{\sqrt{3}}\sin(\alpha+\beta_1)\end{array}\right]$
cos(2ωt)	A_{c2}	$-\hat{P}_{con}R_{th}A_{F2}\left[\begin{array}{l}\left(\frac{2}{3\pi}-A_{P(ac)}\right)\left(\frac{1}{2}+\frac{m_{(DC)}A_{F3}}{6\sqrt{3}}\right)\cos(2\theta+2\alpha+\beta_2)\\+\frac{m}{4\sqrt{3}}\cos(\theta+2\delta+\beta_2)\end{array}\right]$
cos(3ωt)	A_{c3}	$-\hat{P}_{con}R_{th}A_{F3}\left(\frac{2}{3\pi}-A_{P(ac)}\right)\frac{m}{2\sqrt{3}}\sin(2\theta+3\alpha+\beta_3)$

$$\delta_{m(Diode)} = 1 - \delta_{m(IGBT)} \tag{4.29}$$

However, unlike the standard modulation schemes, the DC component in Equation 4.27 is greater than 0.5. Thus, only the fundamental component in this equation is made negative:

$$\delta_{m(IGBT)} = \left(0.5 + \frac{m_{(DC)} A_{F3}}{6\sqrt{3}}\right) - \frac{m}{\sqrt{3}} \sin(\omega t + \alpha) \tag{4.30}$$

Therefore, to calculate the temperature of a diode using the equations outlined in Table 4.2, the modulation index (m) must be defined as a negative value, while the term $m_{(DC)}$ remains positive for an IGBT or diode. As with the switching loss model, the magnitude of the sine and cosine components for each harmonic can be combined into a single term. Thus, the ripple temperature due to the conduction loss is given by:

$$T_{ripple(con)} = \begin{pmatrix} A_{con1} \cos(\omega t + \sigma_1) + \\ A_{con2} \cos(2\omega t + 2\sigma_2) + \\ A_{con3} \cos(3\omega t + 3\sigma_3) \end{pmatrix} \tag{4.31}$$

4.2.3.2.1 Comparison of the Temperature Response

The equations developed for the conduction loss (Table 4.2) are implemented in Matlab and the response of this model is compared with the sinusoidal approximation, which is calculated using Simulink. The model used for the conduction loss comparison is shown in Figure 4.11. To compare the temperature response the duty cycle in this model is calculated using the standard third harmonic modulation scheme given in Equation 4.26. The operating parameters used in this comparison are the same as those used to compare the switching loss models in Section 4.2.2.2, although for the conduction loss model the following displacement power factor and modulation index are used:

- DPF = 0.707 (lagging)
- m = 0.5

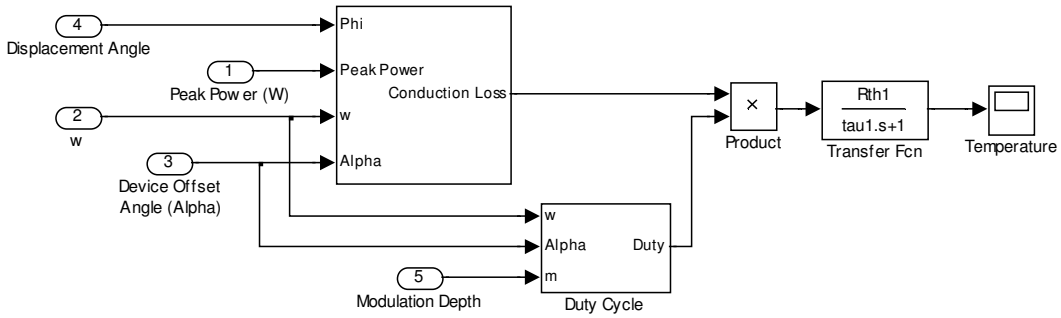

Figure 4.11: Sinusoidal conduction loss model

In an inverter the maximum conduction loss will occur when a device conducts the peak current for the maximum length of time. For an IGBT this occurs when the displacement power factor (DPF) is unity. However, as shown by Equation 4.29, in this condition an anti-parallel diode will only conduct for a short period. Therefore, unlike the switching loss, the chosen operating conditions will have a different impact on the temperature response of an IGBT and diode. The comparison of the steady-state temperatures are shown below:

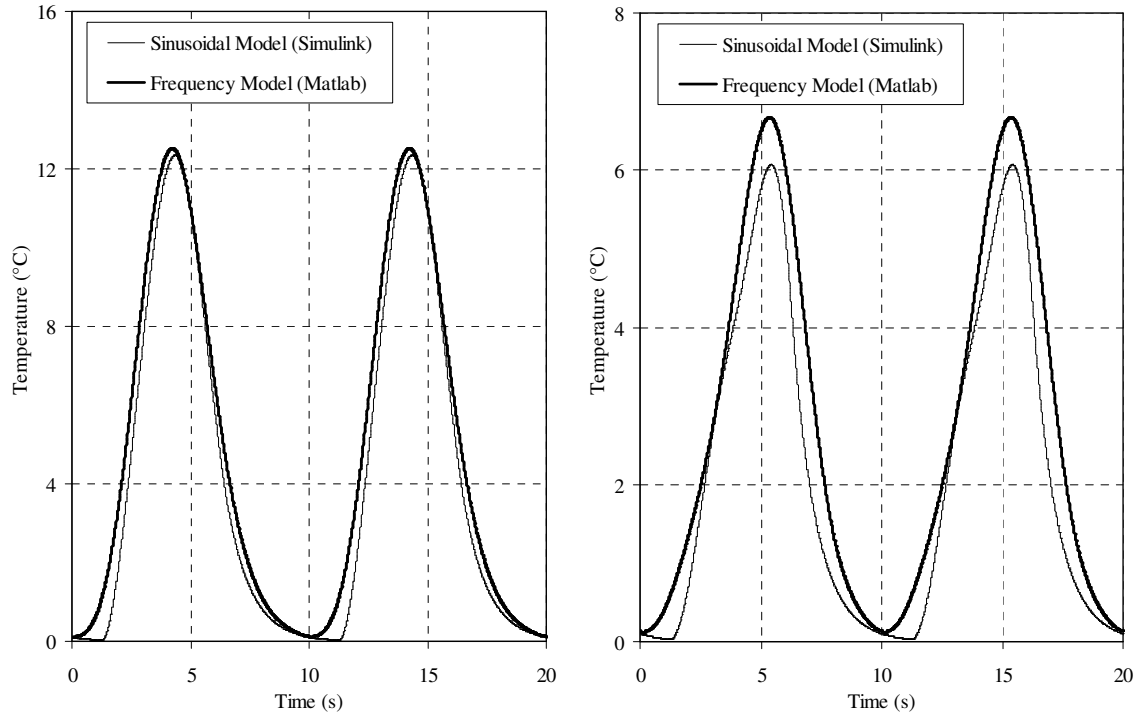

(a) (b)

Figure 4.12: Temperature response of the sinusoidal and frequency models with an output frequency of 0.1Hz (a) IGBT (b) anti-parallel diode

As expected, even though both devices have the same thermal characteristics, with a displacement power factor of 0.707 the resulting temperature rise in the IGBT is higher than the anti-parallel diode. Once again, because of the selection of the frequency components used to represent the current and duty cycle, it can be seen that the temperature response calculated using the frequency model is always higher than the Simulink model. Although for the conduction loss, the peak temperature is overestimated. This is caused by the approximation of the power loss and duty cycle in the region where the peak power loss occurs, i.e. the instantaneous power loss is overestimated.

In summary, the frequency components for the switching loss (Table 4.1) and conduction loss (Table 4.2) models have been developed. However, in order to implement these equations the output angle of the inverter (ωt) must still be known. Therefore, as discussed in the introduction, the frequency components are used to calculate the peak steady-state junction-to-reference temperature over a complete output cycle of the inverter. This temperature will then become the output of the steady-state frequency model. The method used to calculate the peak temperature is described in the following sections.

4.3 Calculation of the Peak Ripple Temperature

The peak ripple temperature is calculated from the sum of the fundamental and harmonic components. The magnitude and phase of these components is dependant on a number of input variables, including the peak power loss, modulation index, displacement power factor, output frequency and the thermal properties of the network element. This is a complex problem and one that cannot be solved directly using standard trigonometric relationships. Therefore, a method that can be used to estimate the output angle where the peak temperature occurs is required, and it must be possible to implement the chosen method efficiently in a microprocessor.

4.3.1 Taylor Series Approximation of the Peak Ripple Temperature

The method described in this section is based on the approximation of the frequency components by an equivalent Taylor series. In order to calculate the peak of the complete temperature response the frequency components for the switching and conduction loss must first be combined. The resulting ripple temperature will consist of the fundamental and

second harmonic terms due to the combined effect of the switching and conduction loss, and a third harmonic due entirely to the conduction loss. However, as shown in Table 4.2, the magnitude of the third harmonic is much smaller than the other terms and to simplify the calculation, the third harmonic is treated as a constant value:

$$T_{ripple} = A_1 \cos(\omega t + \sigma_1) + A_2 \cos(2\omega t + 2\sigma_2) + A_3 \tag{4.32}$$

where A_n is the magnitude of the n^{th} harmonic due to the combination of the components in the switching and conduction loss models. To represent the harmonic terms by a Taylor series approximation they must be represented in the form:

$$A_n \cos(n\omega t + n\sigma_n) = A_n [\cos(\omega t)\cos(n\sigma_n) - \sin(\omega t)\sin(n\sigma_n)] \tag{4.33}$$

The Taylor series approximation of the general harmonic term, using only the first two terms in the series for the sine and cosine components, is then given by:

$$A_n \cos(n\omega t + n\sigma_n) = A_n \left[\begin{array}{l} \left(1 - \frac{(n\omega t)^2}{2!}\right)\cos(n\sigma_n) \\ -\left(n\omega t - \frac{(n\omega t)^3}{3!}\right)\sin(n\sigma_n) \end{array} \right] \tag{4.34}$$

From this expression, the location of the turning points can be found by solving:

$$\frac{d}{d\omega t} A_n \cos(n\omega t + n\sigma_n) = 0 \tag{4.35}$$

For the Taylor series approximation in Equation 4.34, the turning points are found by solving:

$$A_n\left[\left(-\frac{2n^2(\omega t)}{2!}\right)\cos(n\sigma_n)-\left(n-\frac{3n^3(\omega t)^2}{3!}\right)\sin(n\sigma_n)\right]=0 \tag{4.36}$$

By limiting the Taylor series approximation to the first two terms, it can be seen that Equation 4.36 is a quadratic and this can be expressed in the form:

$$a(\omega t)^2+b\omega t+c=0 \tag{4.37}$$

This equation has two turning points and these can be found using the standard quadratic formula:

$$\omega t=\frac{-b\pm\sqrt{b^2-4ac}}{2a} \tag{4.38}$$

As shown in Equation 4.32, the ripple temperature has two harmonic components and to calculate the turning points the coefficients of the quadratic equation for the fundamental (n=1) and second harmonic (n=2) terms must be combined. Thus, the coefficients for the full response (ignoring the third harmonic component) are:

$$a=\sum_{n=1}^{2}\frac{A_n n^3}{2}\sin(n\sigma_n) \tag{4.39}$$

$$b=-\sum_{n=1}^{2}A_n n^2\cos(n\sigma_n) \tag{4.40}$$

$$c=-\sum_{n=1}^{2}A_n n\sin(n\sigma_n) \tag{4.41}$$

The two turning points are calculated by substituting these coefficients into Equation 4.38. To identify which of the turning points is the minimum (ωt_{min}) and maximum (ωt_{max}), the

coefficients and the turning points can be substituted into the derivative of Equation 4.36, which can be represented in the form:

$$\frac{d^2}{d(\omega t)^2} a(\omega t)^2 + b\omega t + c = 2a(\omega t) + b \tag{4.42}$$

If the result of this calculation is positive, the turning point is a maximum. The procedure outlined above is used to determine the location of the peak ripple, but to calculate the actual peak ripple temperature this location (ωt_{max}) must be substituted into Equation 4.32. However, by using only the first two terms of the Taylor series the accuracy of the approximated ripple temperature falls as the output angle of the inverter moves away from the origin ($\omega t=0$). By definition, when the inverter is operating in a stationary vector condition with a unity displacement power factor, the peak temperature will occur at an output angle of $\omega t=\pi/2$. Therefore, as shown in Figure 4.13(a), the Taylor series approximation cannot be used to calculate the peak ripple temperature in this condition.

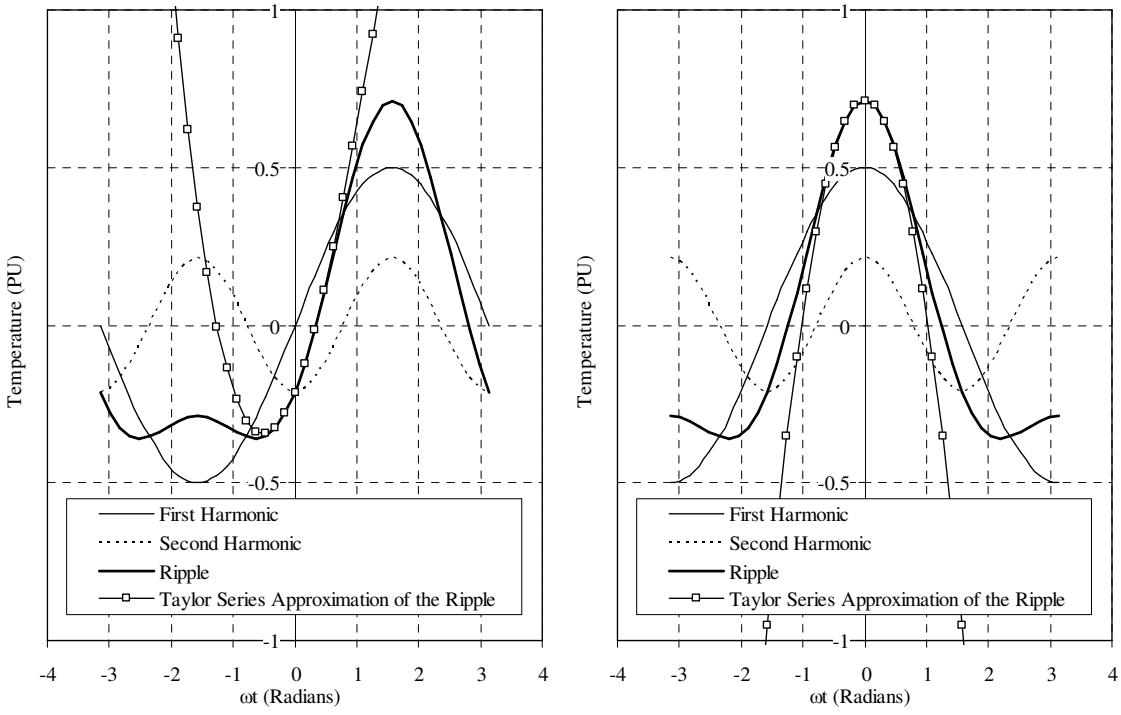

(a) (b)

Figure 4.13: Taylor series approximation of the ripple temperature with the peak ripple at an output angle of (a) $\omega t=\pi/2$ (b) $\omega t=0$

Consequently, in order to use this approach, the phase angles (σ_1 and σ_2) of the harmonics in Equation 4.32 must be modified (maintaining the same phase relationship between the 1st and 2nd harmonics) so that the peak ripple occurs near the origin. The effect of this process on the accuracy of the Taylor series approximation can be seen in Figure 4.13(b). In this figure the harmonics have been shifted so that the peak ripple occurs when $\omega t=0$. The results show that the peak ripple calculated using the frequency components and the Taylor series approximation is identical. Therefore, the phase shift required to ensure that the peak ripple occurs near the origin must be calculated. This procedure is described below.

In any operating condition the peak of the ripple temperature will occur between the positive peaks of the first and second harmonics that are closest together, i.e. the peaks with the smallest angle between them. The two angles (ϕ_1 and ϕ_2) between the peaks are calculated using the phase angles for the combined response:

$$\phi_1 = \sigma_1 - \sigma_2 \tag{4.43}$$

$$\phi_2 = \phi_1 + \pi \tag{4.44}$$

The angles for a general operating condition where the peaks of the first and second harmonics are not in phase are shown in Figure 4.14(a). By observation the angle where the peak ripple occurs can be approximated using:

$$\psi = \phi_{\min} \frac{1.5A_2}{A_1} \tag{4.45}$$

where ϕ_{min} is the smallest angle between the two peaks. Therefore, the fundamental and second harmonic terms are shifted using the angles ψ and ψ-ϕ_{min}. This process is illustrated in Figure 4.14(b). For the frequency components in this figure, ωt_{max} is close to zero and the ripple temperature can be calculated using:

$$T_{ripple} = A_1 \cos(\omega t + \psi) + A_2 \cos(2\omega t + 2[\psi - \phi_{\min}]) + A_3 \tag{4.46}$$

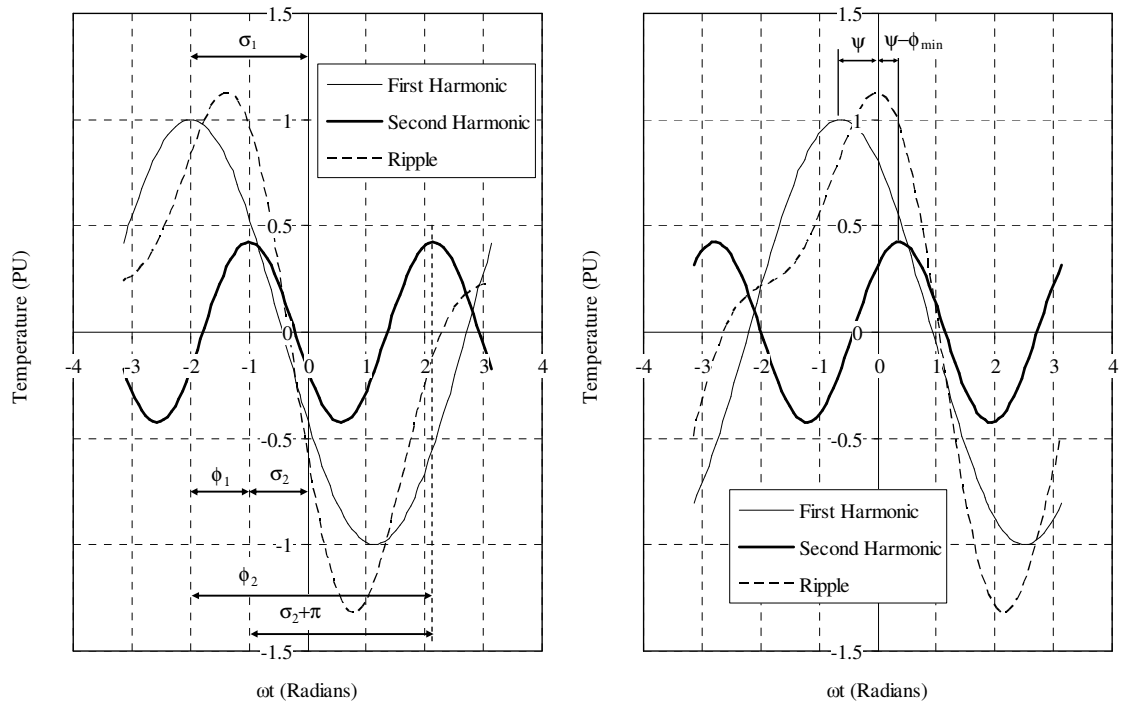

(a) (b)

Figure 4.14: Taylor series approximation (a) angles between peaks of the harmonic components (b) offset angles used to align the peak ripple with the origin

In summary, the peak ripple temperature is calculated using the following steps:

1. Calculate the smallest angle (ϕ_{min}) between the positive peaks for the first and second harmonics (Equation 4.32).
2. Use this angle to determine the phase shift for the first harmonic (ψ).
3. Calculate the phase shift for the second harmonic required to maintain the same phase relationship (ψ-ϕ_{min}) as the original response.
4. Calculate the coefficients of the quadratic formula for the frequency model with the new phase angles (Equation 4.46).
5. Use the quadratic formula to calculate the two turning points and identify which of these is the peak (ωt_{max}).
6. Substitute ωt_{max} into Equation 4.46 and calculate the peak ripple temperature.

To check the accuracy of the Taylor series approximation it has been used to calculate the peak of the following ripple temperature:

$$T_{ripple} = A_1 \cos(\omega t) + A_2 \cos(2\omega t + 2\sigma_2) \tag{4.47}$$

Using the approximation the peak ripple temperature is calculated over the full range of possible magnitudes (A_2=0 to A_1) and phase shifts (σ_2=0 to 2π). This is compared with the actual peak temperature of the combined harmonics calculated using Simulink. From this investigation it was found that for all possible operating conditions, the maximum error in the estimated peak temperature is less than 1%. However, this comparison only validates the method used to calculate the peak ripple temperature and does not show the effects of ignoring the third harmonic term or the assumptions used to generate the frequency components. Therefore, in the next section the peak junction-to-reference temperature estimated by the frequency model (using the Taylor series approximation) is compared against the peak junction-to-reference temperature calculated using the initial sinusoidal approximation in various operating conditions.

4.4 Comparison of the Peak Temperature in a Steady-State Operating Condition

As shown in Equation 4.32, in order to use the Taylor series approximation to calculate the peak ripple temperature the magnitude of the third harmonic term is treated as a constant value. This assumption, combined with the approximation of the duty cycle and power loss, will have an impact on the accuracy of the estimated peak junction-to-reference temperature. To show the effect of these approximations, the peak steady-state temperature is calculated using the frequency model and this temperature is given by:

$$\hat{T}_{ss} = T_{dc} + \hat{T}_{ripple} \tag{4.48}$$

This equation is then used to calculated the temperature over the full range of the modulation index (m=0 to 1) with a leading and lagging displacement power factor. This is then compared with the peak instantaneous temperature calculated using the sinusoidal approximation (Simulink model). The results from this comparison are represented as a percentage of the peak instantaneous temperature. A positive value indicates that the

temperature is overestimated by the frequency model, but the devices are protected. The results for an IGBT operating at 0Hz (in a stationary vector condition) and at an output frequency of 1Hz are shown in Figure 4.15(a) and Figure 4.15(b) respectively. The operating conditions used to generate these results are the same as those used in the comparison of the switching loss model in Section 4.2.2.2.

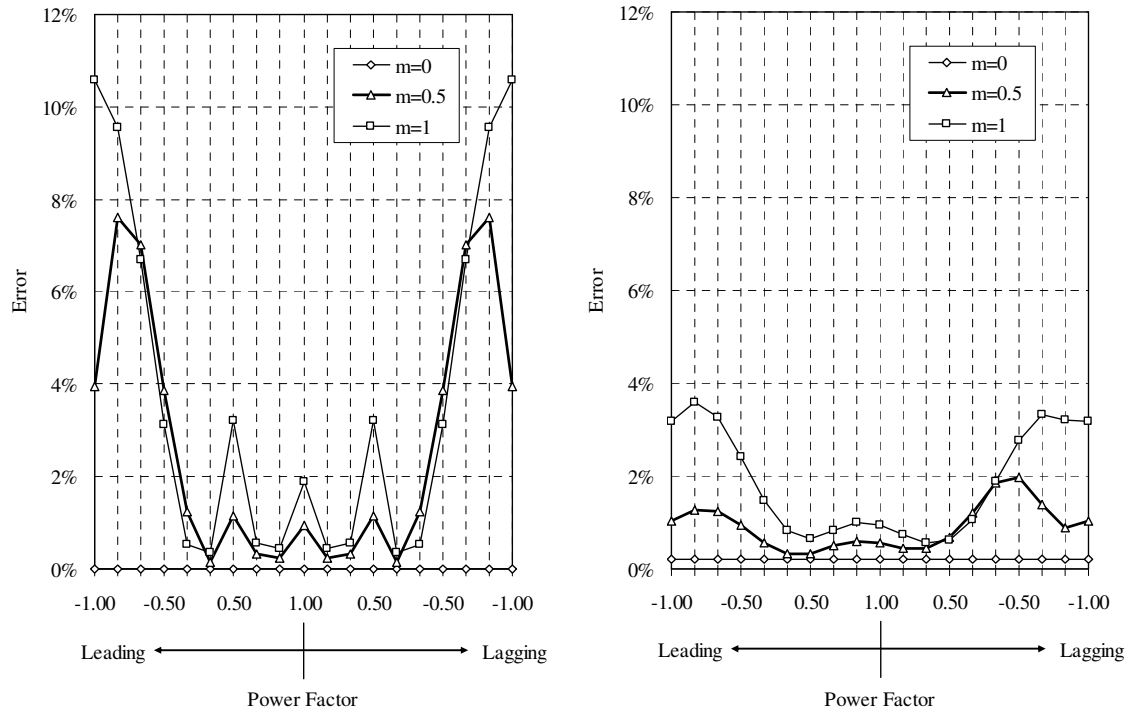

Figure 4.15: Comparison of the peak junction-to-reference temperature calculated for an IGBT (τ_{th}=1s) using the frequency model and the instantaneous sinusoidal approximation at an output frequency of (a) 0Hz (stationary vector condition) (b) 1Hz

When operating in a stationary vector condition with a modulation index of zero, the approximation of the duty cycle and the peak power loss in both models is the same, i.e. the duty cycle is 0.5 over the complete output cycle of the inverter. Consequently, there is no error in this condition. However, the error increases as the modulation index approaches unity and the displacement power factor becomes negative. This error is caused by the approximations used to generate the frequency components for the power loss and duty cycle.

As the output frequency of the inverter is increased the harmonic components will no longer be in phase. Therefore, treating the third harmonic as a constant value (Equation 4.32) will contribute towards the total error. In Figure 4.15(b) it can be seen that at an output frequency of 1Hz there is a small error when the modulation index is zero. This is caused by the decay of the higher harmonics that are not included in the approximation of the power loss. As a result, there is a small difference (~0.2%) between the magnitudes of the peak loss in both models. This difference was not shown in Figure 4.8(b). Furthermore, it can be seen that the errors calculated with a leading and lagging displacement power factor are different. This is caused by the shape of the power loss that is applied to the Foster network element. To show this effect an example of the conduction loss calculated with a leading and lagging displacement power factor of 0.5 is shown in Figure 4.16(a).

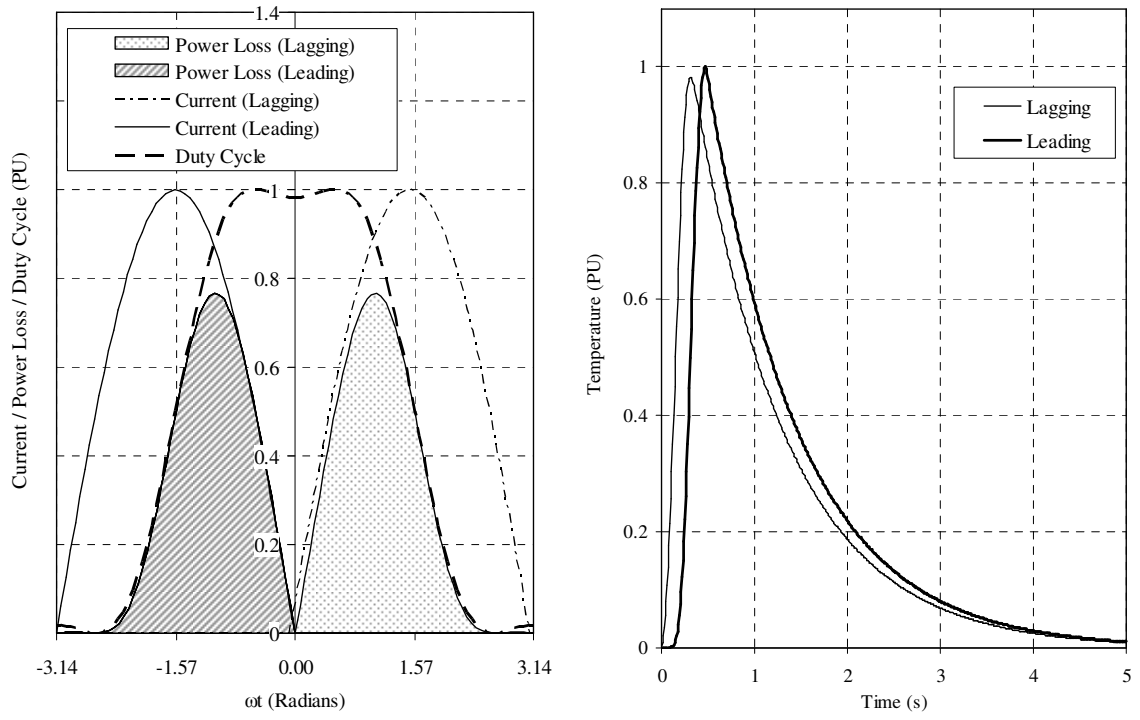

(a) (b)

Figure 4.16: Comparison of the power loss and the resulting temperature rise for a leading and lagging displacement power factor of 0.5 (a) current, duty cycle and power loss (b) temperature rise over a single output cycle of the inverter (1 PU = maximum temperature)

This figure shows that the area of the power loss calculated with a leading and lagging displacement power factor is identical. However, for a leading displacement power factor

the area between the initial rise in the power loss and its peak value is slightly larger. Consequently, the peak temperature, which is shown in Figure 4.16(b), is higher.

Overall, the results described in this section show that the accuracy of the steady-state temperature calculated in the key operating conditions for the inverter is acceptable and importantly, the temperature of a device is never underestimated by the frequency model. However, the transient response due to changes in power loss and output frequency cannot be ignored. The development of a transient model is described in the next section.

4.5 Transient Response

To maximise the performance of a drive, it is essential that the transient response due to any changes in power loss or output frequency can be accurately modelled. Furthermore, it is important that the maximum temperature of a device cannot be exceeded during a transient period. The model developed in this section is an extension of the steady-state model developed in the previous sections. The calculation of the additional transient component for a general frequency term is described in Section 4.5.1. This analysis is then used in Section 4.5.2 to develop a model that can be implemented in a continuous system. This component is developed to predict the maximum possible temperature for any transient condition and is based on the analysis of a system with initial conditions of zero.

4.5.1 Calculation of the Transient Response for a General Frequency Component

In this section, the transient temperature response of a Foster network element (first order filter) is calculated when a general frequency component of the power loss is applied to the network. The following analysis applies for a step change in magnitude due to a change in the peak power loss (A_n) and output frequency (ω). Taking a general frequency component (n^{th} harmonic):

$$P(\omega t) = A_n \sin(n\omega t) \tag{4.51}$$

and representing this in the Laplace domain gives:

$$P(s) = \frac{A_n \omega}{s^2 + (n\omega)^2} \tag{4.52}$$

This can then be applied to the transfer function for a first order filter (Equation 4.12). With a unity magnitude (R_{th}=1) the temperature response is given by:

$$T(s) = \frac{A_n \omega}{s^2 + (n\omega)^2} \cdot \frac{1}{1 + \tau s} = \frac{A}{s - jn\omega} + \frac{B}{s + jn\omega} + \frac{C}{1 + \tau s} \tag{4.53}$$

The combination of the first two partial fractions (A and B) in this response represents the steady-state component (defined as T_{ripple}), which in the time domain is a sinusoid with a filtered magnitude ($A_n A_{Fn}$) and a phase shift (β_n). Until now, this is the only part of the response that has been considered. The final partial fraction (C) represents the transient component of the temperature response (T_{exp}), and in the time domain the magnitude of this component is given by:

$$T_{\exp(\sin)}(\omega t) = A_n \left[\frac{n\tau\omega}{1 + (n\tau\omega)^2} \right] \cdot e^{\frac{-t}{\tau}} \tag{4.54}$$

Similarly, for a cosine component, it can be shown that the transient term is:

$$T_{\exp(\cos)}(\omega t) = A_n \left[-\frac{1}{1 + (n\tau\omega)^2} \right] \cdot e^{\frac{-t}{\tau}} \tag{4.55}$$

The calculation of these components is outlined in Appendix A. These equations can be used to calculate the transient response for a general frequency component with an offset (σ_n):

$$P(\omega t) = A_n \cos(n\omega t + n\sigma_n) = A_n [\cos(\omega t)\cos(n\sigma_n) - \sin(\omega t)\sin(n\sigma_n)] \tag{4.56}$$

For this power loss the magnitude of the transient component (A_{exp}) is given by:

$$A_{\exp} = -A_{cn}\left[\left(\frac{1}{1+(n\tau\omega)^2}\right)\cos(n\sigma_n)+\left(\frac{n\tau\omega}{1+(n\tau\omega)^2}\right)\sin(n\sigma_n)\right] \tag{4.57}$$

From this equation it can be seen that the magnitude of the transient term is dependant on the offset angle and this will be a maximum when:

$$n\sigma_n = \tan^{-1}(n\omega\tau)+\pi \tag{4.58}$$

This offset is equal to π plus the phase shift in the steady-state output due to the filtering effect (β_n). Consequently, at this angle the magnitude of the exponential term is equal to the maximum ripple temperature. The importance of this characteristic is highlighted in the following example.

To show the effect of the transient component, the temperature response has been calculated for a fundamental frequency term (F_{out}=0.25Hz, τ=1s and n=1) during a step change in power loss (A_1=0 to 1PU). For this condition the magnitude of the transient term will be a maximum when σ_1=4.14rads (calculated using Equation 4.58). The individual steady-state and transient components of the complete response are shown in Figure 4.17(a). At t=0 the magnitude of the transient component is equal to the negative peak of the steady-state component ($-A_n$) and the combined response is initially zero. Therefore, the transient component ensures that the output of the filter does not change instantaneously. Using these characteristics for a single step with initial conditions of zero, the highest transient temperature (i.e. the worst case for any starting angle) can be approximated using:

$$T_{tran} = \hat{T}_{ripple}\left(1+e^{\frac{-t}{\tau}}\right) \tag{4.59}$$

The temperature estimated using this equation is compared against the instantaneous response (steady-state + transient component) in Figure 4.17(b).

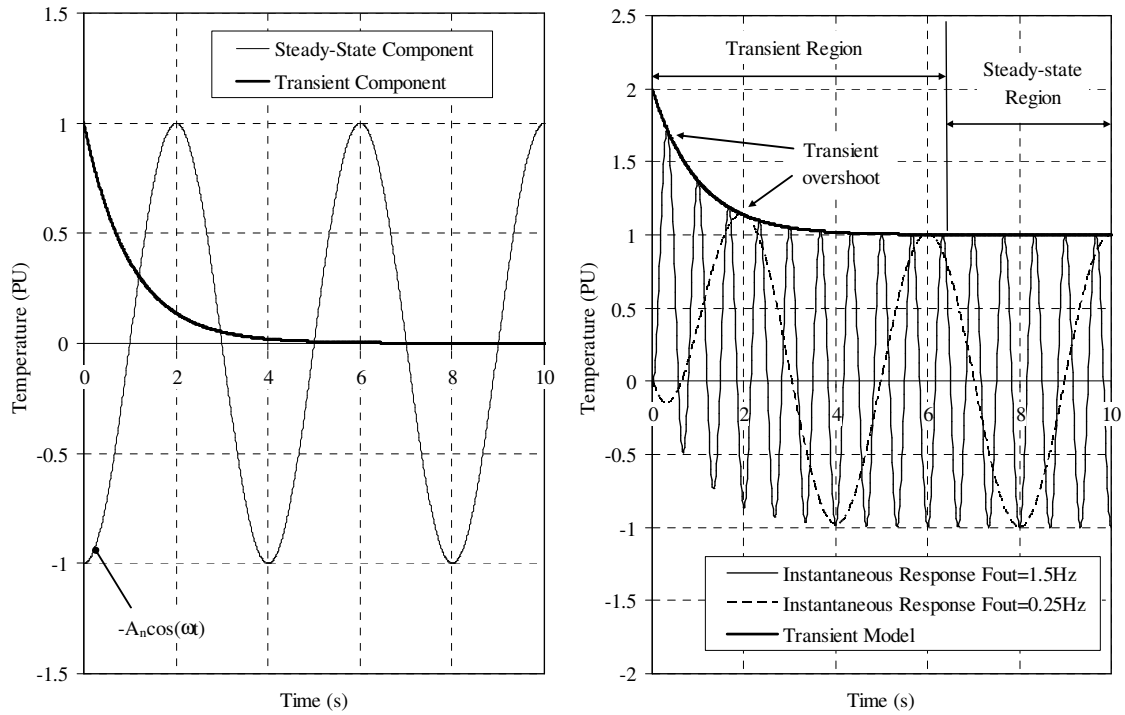

Figure 4.17: Transient response (a) steady-state and transient components (b) complete response (1 PU = steady-state ripple temperature)

The transient term ensures that the frequency model does not underestimate the temperature during the transient period. In addition, the results show that for a given time constant, the overshoot above the steady-state magnitude is dependant on the output frequency. As the frequency is reduced this overshoot becomes negligible. Consequently, if Equation 4.59 is used to estimate the transient response the temperature can be significantly overestimated in some operating conditions. In summary, the transient model developed in this section has the following limitations which are addressed in the next section:

1. At low output frequencies the temperature can be significantly overestimated during the initial part of the transient period.
2. The transient component in Equation 4.59 only applies for a single step change from zero and cannot be implemented directly in a continuous system.

4.5.2 Development of a Continuous Transient Model

This section is divided into four parts:

1. The calculation of the magnitude of the transient component
2. An investigation into the effect of the output frequency on the peak overshoot
3. The implementation of a continuous frequency model
4. A comparison of the frequency model with the instantaneous device temperature

By the end of this section, a transient model that can be used to estimate the temperature response of a single IGBT or diode in any operating condition is defined.

4.5.2.1 Magnitude of the Transient Component

In Section 4.5.1 it was shown that for a step change in power loss and output frequency, where the initial conditions are zero, the maximum magnitude of the transient component for a single harmonic is equal to the peak magnitude of the steady-state component. This is equivalent to the change in the ripple temperature. However, this does not apply for a continuous system. To illustrate this, the complete response and the individual steady-state and transient components have been calculated during a step change in the switching loss and output frequency. The results are shown in Figure 4.18(a) and Figure 4.18(b) respectively.

For a step change in power loss, the magnitude of the transient component is equal to the change in the peak steady-state response and as in Equation 4.59, this can be determined from the known peak ripple temperature. Whereas, for a step change in the output frequency, the magnitude of the transient component can be higher than the change in the peak ripple temperature due to the resulting phase shift in the harmonic terms. However, it is unlikely that a step change in output frequency will occur without a corresponding change in the output current. Thus, the magnitude of the transient component in the frequency model is determined directly from the change in the peak ripple temperature. This approximation applies for both an increase and decrease in ripple. Using this approach simplifies the calculation of the transient component, but can result in an underestimation of the temperature during rapid changes in output frequency.

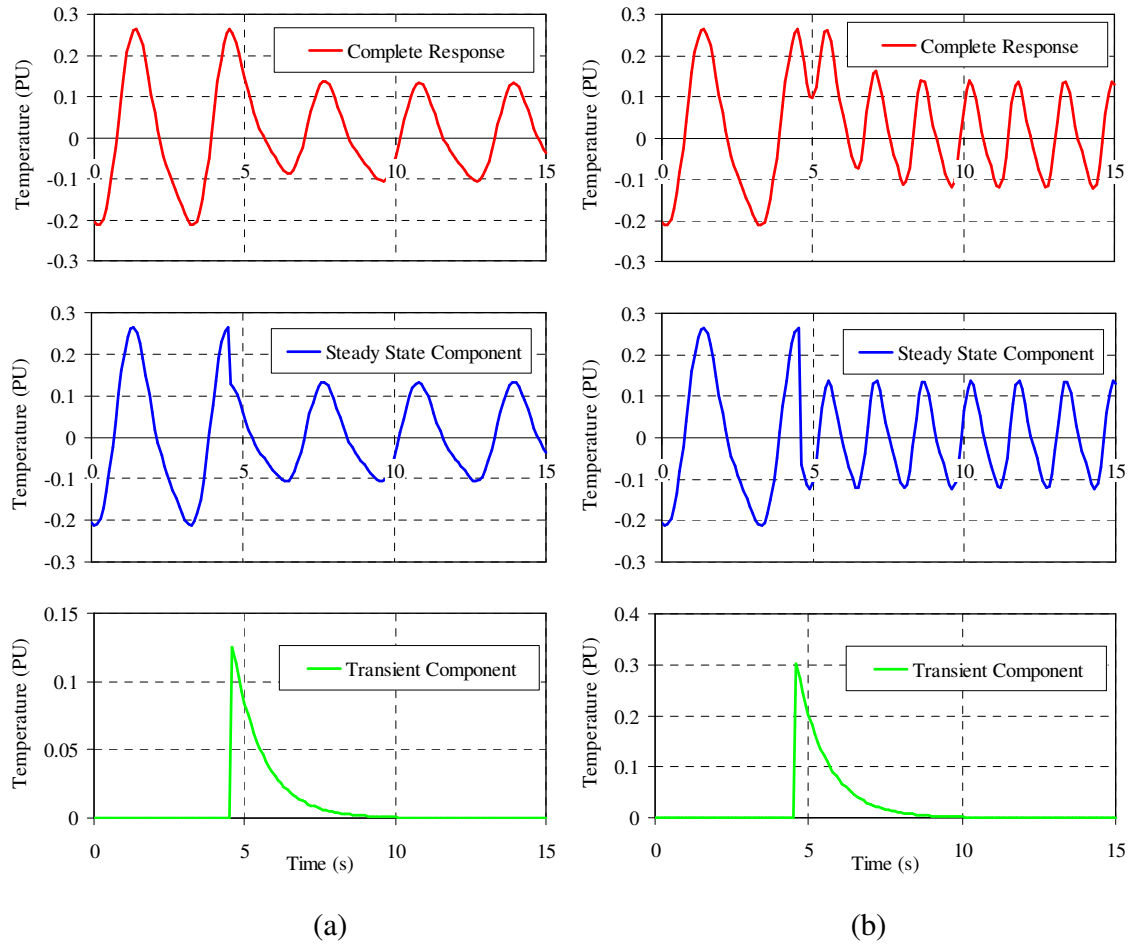

Figure 4.18: Transient response for a step change in (a) switching loss (b) output frequency (1 PU = peak temperature when F_{out} = 0Hz)

4.5.2.2 Effect of the Output Frequency on the Transient Magnitude

When the output frequency (F_{out}) is low in relation to the thermal time constant the transient component will decay to zero before the ripple component reaches its peak value. In this condition the transient component will cause a significant overestimation of the device temperature. Therefore, a method of estimating the magnitude of the transient component during an increase in the ripple temperature, which is based on the known output frequency and time constant, is required. This method is described below.

From the inspection of the transient characteristics for the switching loss model measured during a step increase in power loss, it was found that the first peak in the ripple temperature which is higher than the steady-state temperature always occurs after:

$$T_{peak} = \frac{0.85}{4F_{out}} \tag{4.60}$$

The actual location of the first peak is dependant on the output frequency and the time constant. Using this equation, it can be shown that there will be no overshoot when:

$$\frac{0.85}{4F_{out}} \geq 5\tau_{th} \tag{4.61}$$

In this condition the first peak in the ripple temperature will occur after the transient component has already decayed to a negligible value (i.e. if $t > 5\tau_{th}$) and it is not necessary to add a transient component to the model if the peak ripple temperature is increasing. However, as the output frequency is increased the magnitude of the overshoot will tend towards the change in the peak ripple temperature and this cannot be ignored. To model this effect, the magnitude of the transient component is changed with the output frequency:

$$A_{\exp} = K_{\exp}(\omega)\Delta\hat{T}_{ripple} \tag{4.62}$$

The characteristic of K_{exp} is shown in Figure 4.19(a). The slope of this characteristic has been determined by comparing the transient model of the switching loss with the instantaneous response. To show the effect of using this characteristic, the peak ripple and magnitude of the transient component are compared at different output frequencies. This is shown in Figure 4.19(b). The difference between these characteristics is the amount that the temperature would have been overestimated by if the transient component was made equal to the change in the peak ripple. When using Equation 4.62 the transient temperature calculated during a step change in power loss is never underestimated by more than 1.5% of the peak ripple. Furthermore, the significant overestimation at low frequencies has been reduced. Therefore, in the continuous model, K_{exp} is used to modify the magnitude of the transient component, but only when the ripple temperature is increasing.

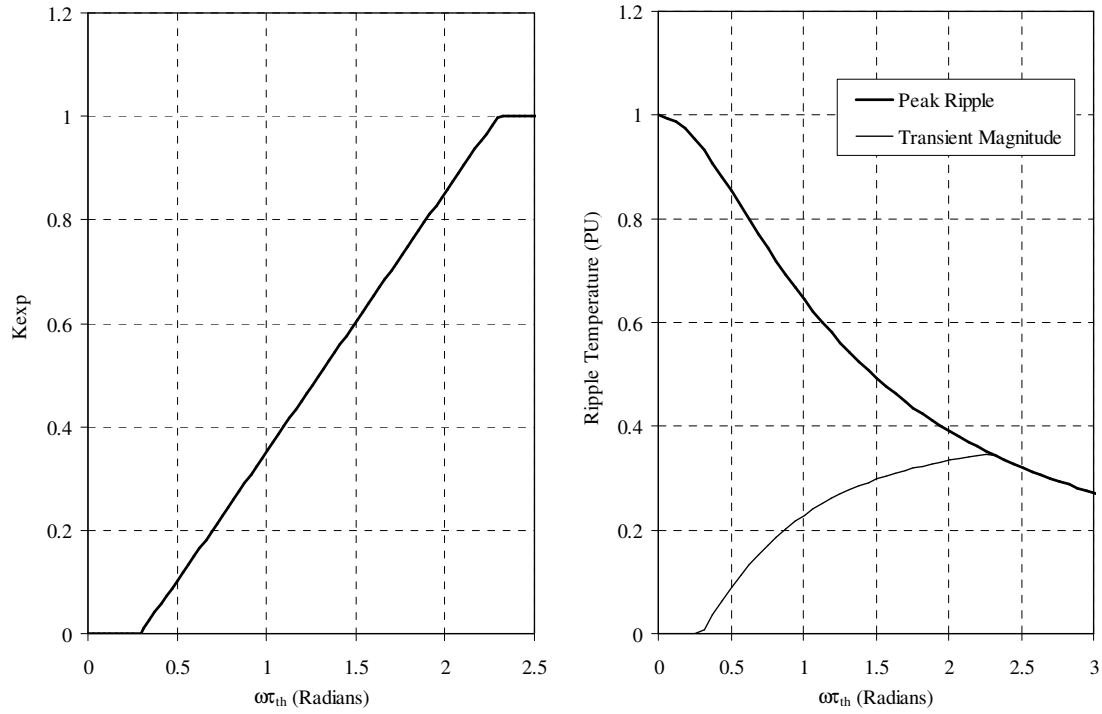

(a) (b)

Figure 4.19: Transient response (a) magnitude of the factor K_{exp} if the ripple temperature is increasing (b) comparison of peak ripple temperature and the transient component (1 PU = peak temperature when F_{out} = 0Hz)

4.5.2.3 Implementation of a Continuous Frequency Model

The complete transient model consists of the following components:

1. Steady-state (peak ripple)
2. DC
3. Transient

As described, the peak ripple temperature is calculated using the Taylor series approximation and this is applied in the model as a constant value. Whereas, the magnitude of the DC component is applied to the transfer function of a first order filter with a unity magnitude, the time constant used in this transfer function is taken directly from the Foster network element. The implementation of these components is shown in Figure 4.20.

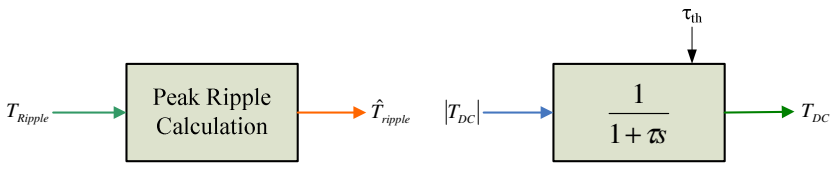

(a) (b)

Figure 4.20: Implementation of (a) ripple (b) DC components in the continuous model

To show how the transient component of the model is implemented in a continuous system, a change in power loss and output frequency is modelled by adding an additional frequency component with the original response. This approach is illustrated in Figure 4.21. In this example, a step in power loss and output frequency is applied at t=0s. The resulting temperature response and the magnitude of the transient component (ignoring the effect of K_{exp}) are shown in Figure 4.21(a).

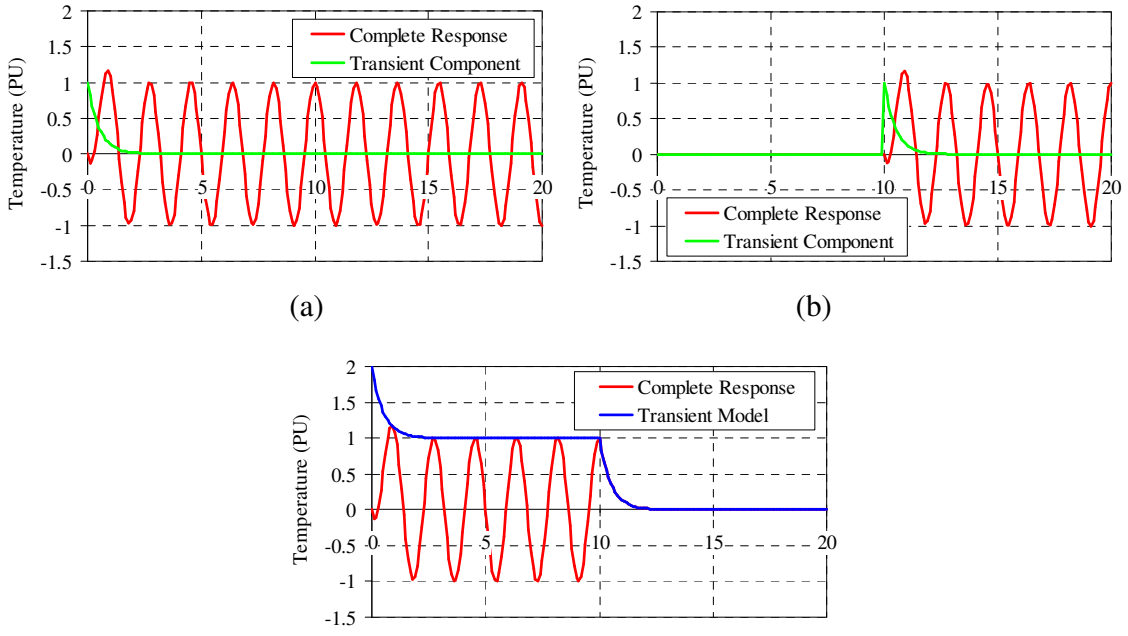

(a) (b)

(c)

Figure 4.21: Calculation of the transient component (a) original response due to a step change in power loss and output frequency (b) additional response added to remove the steady-state component after 10s (c) complete response (1 PU = steady-state temperature)

After operating in this condition for 10s, the power loss is removed. To model this change an additional frequency component, which is out of phase with the original, is added to the

Foster network element. This component is shown in Figure 4.21(b). Adding the two frequency components removes the steady-state component in the output response, leaving the transient component to decay to zero. The resulting instantaneous response and the temperature estimated by the frequency model, which for this condition is the sum of the transient component and the peak ripple temperature, are shown in Figure 4.21(c).

The method used to implement the transient component in a continuous model is shown in Figure 4.22. As described in Section 4.5.2.2, to avoid overestimating the temperature when the ripple is increasing the input to the transient component is multiplied by the factor K_{exp}, when decreasing K_{exp} is always unity. The resulting magnitude (A_{exp}) is then applied to a high pass filter. The time constant of this filter is once again taken directly from the Foster network element.

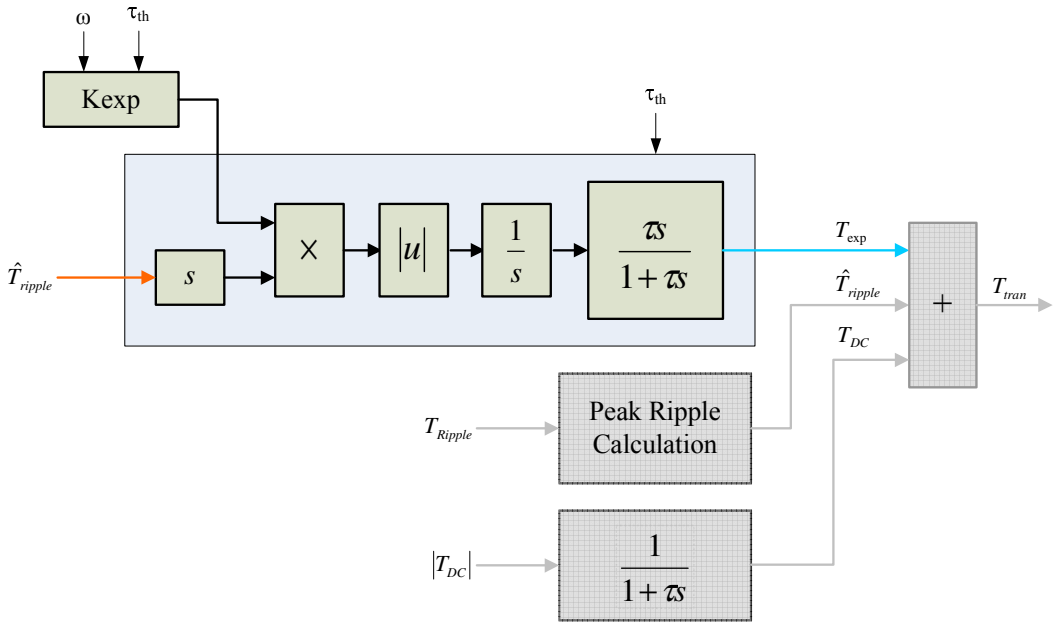

Figure 4.22: Implementation of the transient component in the continuous model

The total output (T_{tran}) of the continuous model is calculated by adding the transient (T_{exp}), peak ripple (T_{ripple}) and DC (T_{DC}) components together. An example of the individual components calculated after a step change in power loss (t=0s) are shown in Figure 4.23(a). The complete transient response, with and without the transient component, is compared against the instantaneous response in Figure 4.23(b). This comparison shows the importance of the transient component during both an increase and decrease in temperature.

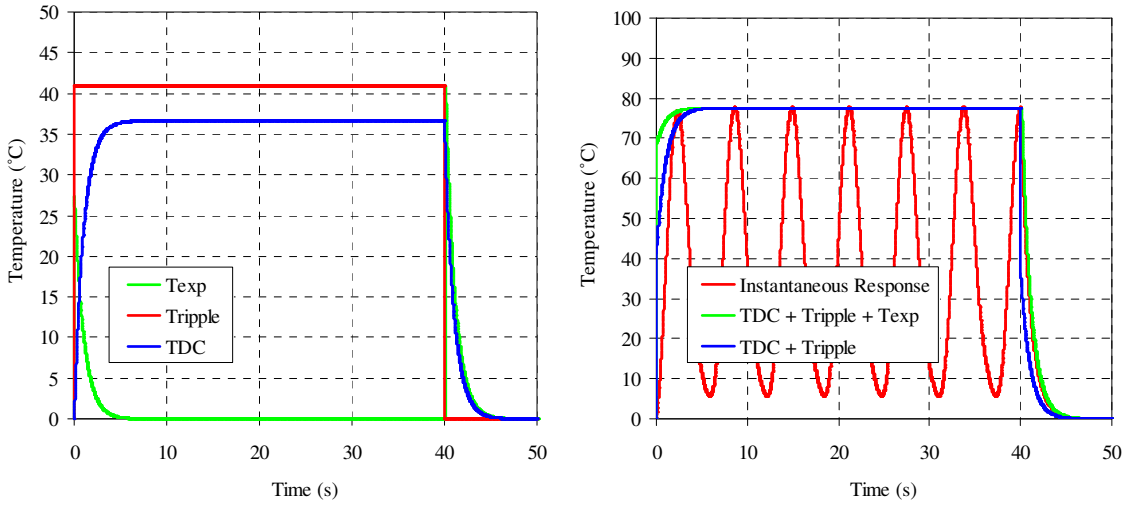

(a) (b)

Figure 4.23: Transient model for a step change in power loss (a) DC, ripple and transient components (b) comparison of the instantaneous response and frequency model

One limitation of the method used to implement the transient component (Figure 4.22) is the response that would occur if a significant change in the peak ripple occurred repeatedly. As described in Section 4.5.1, the magnitude of the transient component is dependant on the output angle of the inverter, but the maximum magnitude is applied to the transient component every time the ripple temperature changes. If this component does not have time to decay the output will continuously increase and can result in the thermal model tripping the drive prematurely. This limitation may prevent the thermal model from being applied in some applications and a solution to this problem will be investigated as part of the further work.

4.5.2.4 Comparison of the Transient Frequency Model

In this section, the methods used to implement the steady-state, DC and transient components are combined to estimate the temperature rise due to the switching loss in a device. This temperature is then compared with the instantaneous response for the two operating conditions defined in Figure 4.24. Although these profiles are similar, operating condition B highlights the key weaknesses in the frequency model.

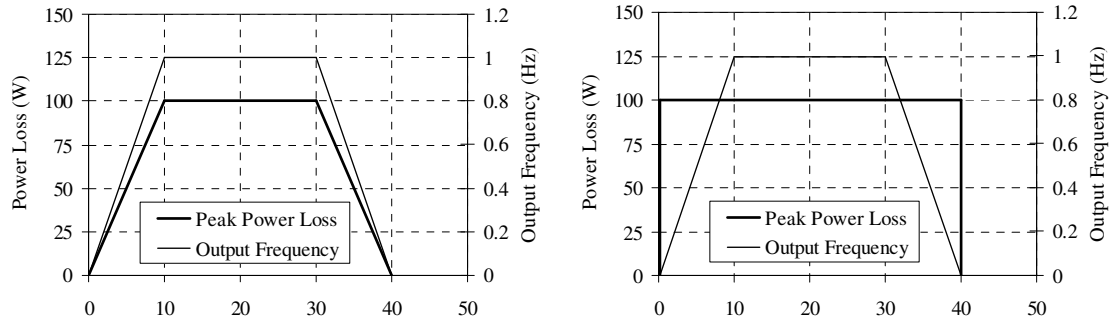

Figure 4.24: Operating conditions used to compare the frequency model with the instantaneous response (a) operating condition A (b) operating condition B

The comparisons of the temperature response for both operating conditions are shown in Figure 4.25. For operating condition A, the temperature estimated by the frequency model accurately follows the profile of the instantaneous response and the model protects the device without significantly overestimating the temperature.

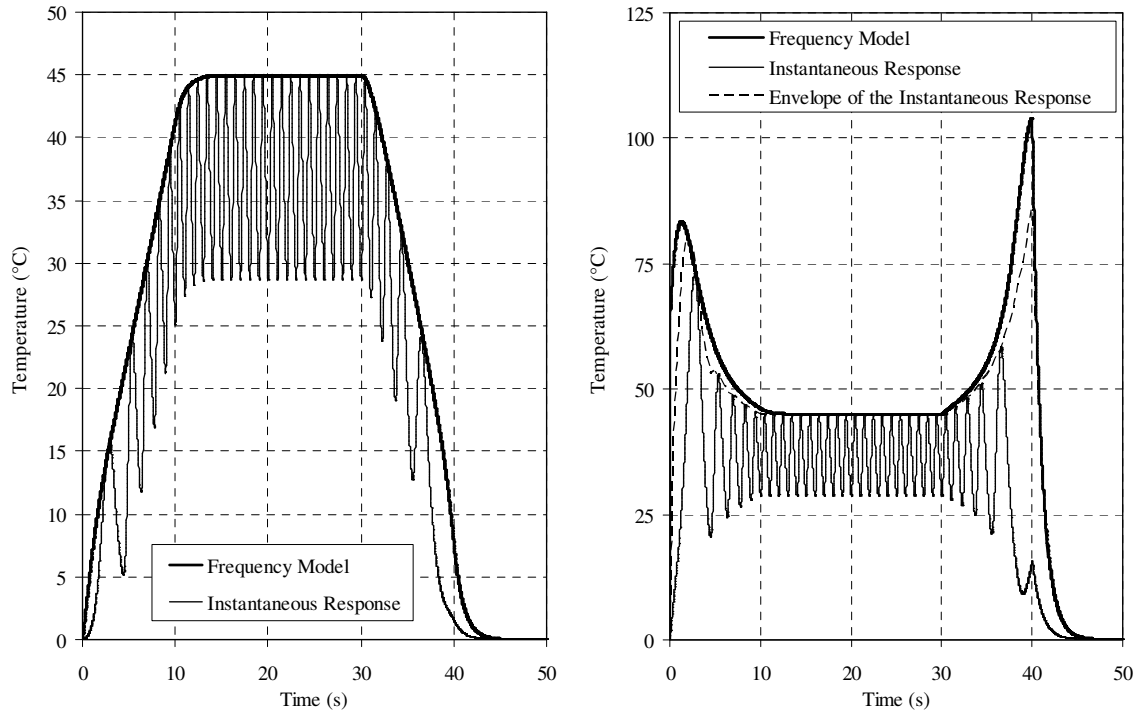

Figure 4.25: Comparison of the frequency model with the instantaneous temperature response for (a) operating condition A (b) operating condition B

For operating condition B, the characteristics of the temperature response are dependant on the offset angle. Therefore, in order to make a fair comparison, the instantaneous response is calculated over the full range of offset angles (α = 0 to 2π). This is equivalent to the inverter starting at each possible output angle. The maximum instantaneous temperature that occurs at any offset angle is then found by calculating the upper envelope of these responses. This is included in the comparison in Figure 4.25(b). In this comparison it can be seen that the inverter is protected by the frequency model, but the temperature is overestimated when the output frequency is low. The main cause of this effect is the implementation of the ripple component, which is applied as a constant value. The reason why this has a greater impact on the accuracy of the estimated temperature at low output frequencies is that it takes longer for the instantaneous ripple temperature to reach its peak value. Therefore, if the power loss is removed before this occurs, the frequency model will overestimate the temperature, although this temperature will occur if the conditions are maintained for a longer period.

Overall, the comparisons in this section show that the transient frequency model can be used to estimate the temperature response for a Foster network element during changes in output frequency and power loss. Although, in order to maximize the performance of the inverter the overestimation caused by the implementation of the ripple component at low output frequencies must be removed. This is an area for further work.

4.6 Summary

The aim of this chapter was to develop a thermal model that can be implemented using the available computational resources. This was divided into three distinct stages, the first of these covered the development of the steady-state model and this procedure is summarised below:

1. Determine the frequency components for the phase current and duty cycle.
2. Calculate the power loss in a device over an output cycle of the inverter.
3. Multiply the frequency components of the power loss with the transfer function of a single element of a Foster network.

In each of these steps all of the calculations can be performed off-line. However, several approximations were made in order to reduce the number of harmonics in the final solution and the number of on-line calculations that are required. After performing these steps, several equations were developed that describe the steady-state temperature response of an IGBT or diode. These equations are dependant on the output angle of the inverter (ωt), which is not known by the thermal model. Therefore, the second part of this chapter described a method that can be used to calculate the peak steady-state junction-to-reference temperature that occurs over an output cycle. This is not a straightforward calculation and the method developed is based on the Taylor series approximation of the dominate frequency components. The temperature calculated using this method forms the basis of the thermal model. This is a novel approach, which when compared to a model implemented in the time domain, has several key advantages. These include the following:

1. A reduction in the number of calculations that must be performed on-line which allows the model to be implemented at a moderate sample frequency while being capable of estimating the temperature at high fundamental output frequencies.
2. The ability to estimate the temperature under a wide range of operating conditions using minimal computational resources.
3. The adaptability of the model, which when combined with the principles of linear superposition can be used to model a complete inverter.

The final part of this chapter covered the development of the transient model. The transient model includes the steady-state (T_{ripple}), DC (T_{DC}) and transient (T_{exp}) components. The transient model has been shown to protect the devices in the inverter under typical operating conditions. However, due to the methods used to implement each component, the model overestimates the temperature during rapid changes in output frequency when operating at a high load current. Therefore, these factors must be addressed before the model can be considered an optimum solution.

Overall, the solution presented in this chapter provides the basis of a thermal model that can be used to estimate the temperature of any device in an inverter over a wide range of operating conditions, during steady-state and transient operation.

Chapter 5: Implementation of the Thermal Model in a Three Phase Inverter

5.1 Introduction

In the previous chapter the temperature estimated by the frequency model was compared against the instantaneous response calculated for a single element of a Foster network. One or more of these network elements can be used to represent the thermal characteristics (thermal impedance) measured between the junction of a device and a defined reference point, typically the external ambient (T_a) or the temperature measured by the internal thermistor (T_{th}) in the power module. However, the thermal coupling between each device in an inverter can have a significant impact on the temperature of any neighbouring devices. Thus, to model the devices in an inverter the self and mutual transient thermal impedances are required. These are defined as:

- **Self thermal impedance –** represents the change in the temperature between the junction of a device (i) and a reference point due to its own power loss.
- **Mutual thermal impedance –** represents the change in the temperature between the junction of a device (i) and a reference point due to a power loss applied to another device (j) in the inverter.

To calculate the temperature of a single device in the inverter (six IGBTs and diodes) the frequency components in the switching and conduction loss models must be calculated for each element in the equivalent Foster networks. For an inverter, these include the eleven mutual thermal impedances associated with the device being modelled. However, the magnitude of the sine and cosine components calculated for each network element (at the same frequency) can be added together and combined into a single term. This allows the peak steady-state junction-to-reference temperature to be calculated using the method developed for a single element (i.e. the Taylor series approximation). This procedure is described in Section 5.2.

The frequency model could be used to calculate the temperature of every device in the inverter, including the effect of the self and all of the mutual thermal impedances, but the number of calculations that can be performed is limited by the available computational resources. Consequently, in order to allow the model to be implemented in a drive, some level of simplification is required. This is described in the remainder of the chapter. In order to evaluate these simplifications, a model of a typical power module is developed in Flotherm and this is described in Section 5.3. This model is used to calculate all of the self and mutual transient thermal impedances (144 values) for the inverter. The equivalent Foster network for each of these is used to form the complete thermal impedance matrix, which is used to calculate the instantaneous temperature of every device under a range of operating conditions. This temperature is then used to identify the devices in the inverter that have the greatest risk of overheating. To protect the inverter, the temperature of these devices must then be estimated using the frequency model. In Section 5.3.1, this procedure is outlined using the temperature calculated in a stationary vector condition. The temperature of one of the chosen devices is then compared against the instantaneous response over a complete output cycle of the inverter and this is shown in Section 5.3.2.

The simplifications required to implement the frequency model are reviewed in Section 5.4 and these include the following approximations:

1. The temperature of a device is calculated using only the self thermal impedance, and any thermal coupling that exists between the devices in the inverter is ignored (Section 5.4.1).
2. The temperature of a single IGBT and diode is calculated using the self and mutual thermal impedances, and it is assumed that in any operating condition, either the chosen IGBT or diode is the hottest device in the inverter (Section 5.4.2).

To implement the frequency model, the parameters of an equivalent Foster network must be calculated for every one of the thermal impedances in the simplified model. These are reviewed in Section 5.5. The number of elements in each of these networks is defined in Section 5.5.1, while methods that can be used to reduce the number of networks are discussed in Section 5.5.2. Finally, the implementation of the frequency model in a

commercial drive control system, including a definition of the input, feedback and calculated parameters, is reviewed in Section 5.6.

5.2 Implementation of the Frequency Model for a System Represented by Multiple Foster Network Elements

Using superposition, the frequency model developed for a single element of a Foster network can be used to calculate the temperature response due to the self (α=0) and mutual ($\alpha\neq0$) thermal impedances in an inverter. To describe this process, the steady-state temperature is calculated for a basic system with two devices (p=2). In this, the self and mutual thermal impedances are represented by an equivalent network with two elements (k=2). Each of these elements has a unique thermal resistance (R_{th}), thermal capacitance (C_{th}) and time constant ($\tau_{th}=R_{th}C_{th}$). The method used to calculate the temperature of device 1 (T_1) is illustrated in the figure below:

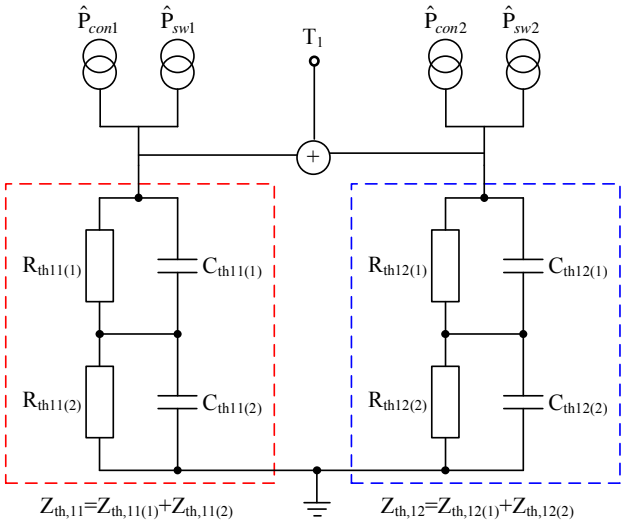

Figure 5.1: Superposition of the self and mutual thermal impedance

To calculate the temperature, the magnitude of each term in the frequency model for the switching loss (Table 4.1) and conduction loss (Table 4.2) must be calculated for each network element. In order to do this, the terms for the self thermal impedance ($Z_{th,11}$) are calculated using the corresponding peak power losses for device 1, while the terms for the mutual thermal impedance ($Z_{th,12}$) are calculated using the losses for device 2. Therefore, given that there are four network elements and two peak losses, each term (A_{s1}, A_{c1}, etc) in the complete frequency model must be calculated eight times. By separating each of the

harmonics in the frequency model into its sine and cosine components the effect of the phase shift, which will be different for each element, is included in the magnitude of these components. Consequently, the magnitude of the like terms calculated for each element can be added together directly. For example, in the switching loss model the magnitude of the fundamental term A_{s1} (taken from Table 4.1) calculated for the first element of the self thermal impedance is given by:

$$A_{s1(sw),11,(1)} = \frac{\hat{P}_{sw} R_{th,11(1)} A_{F1}}{2} \cos(\theta + \alpha + \beta_1) \tag{5.1}$$

where A_{F1} and β_1 are both dependant on the time constant $\tau_{th,11(1)}$. Therefore, for the four network elements in this model, the total magnitude of this term is:

$$A_{s1(sw)} = \sum_{j=1}^{p} \sum_{m=1}^{k} A_{s1(sw),1j(m)} = A_{s1(sw),11(1)} + A_{s1(sw),11(2)} + A_{s1(sw),12(1)} + A_{s1(sw),12(2)} \tag{5.2}$$

where $A_{s1(sw),1j(m)}$ is the magnitude calculated for element *m* of the thermal impedance $Z_{th,1j}$. Hence, in the complete model, the magnitude of the sine component for the n^{th} harmonic is calculated using:

$$A_{sn(sw+con)} = \sum_{j=1}^{p} \sum_{m=1}^{k} A_{sn(sw),1j(m)} + \sum_{j=1}^{p} \sum_{m=1}^{k} A_{sn(con),1j(m)} \tag{5.3}$$

Once every term in the frequency model has been calculated, the sine and cosine components for the first and second harmonics can be combined and, as for a single element, the ripple temperature (ignoring the third harmonic component) is given by:

$$T_{ripple(sw+con)} = A_{1(sw+con)} \cos(\omega t + \sigma_1) + A_{2(sw+con)} \cos(2\omega t + 2\sigma_2) \tag{5.4}$$

where $A_{n(sw+con)}$ is the magnitude of the combined sine and cosine components for the n^{th} harmonic and σ_n is the resultant phase shift. Using this process, the ripple component of the

complete response for any number of devices or network elements can be represented by just two harmonic terms, and the peak of this ripple can be calculated using the Taylor series approximation. Therefore, the frequency model can now be used to calculate the steady-state temperature of one or more devices in an inverter.

5.3 Development of a Frequency Model for an Inverter

A separate frequency model could be used to estimate the temperature of every device in an inverter. However, this is not possible due to the limited computational resources. Furthermore, in order to protect all of the devices it is only necessary to calculate the temperature of the hottest device. The hottest device is dependant on the operating conditions and the thermal properties, including the thermal coupling between each device, which is dependant on the layout (chip positions) and configuration (one or more power modules) of the inverter. Therefore, to develop the frequency model the complete thermal impedance matrix is required, and although any values could be used, they should have similar characteristics to an actual power module. Consequently, the frequency model is developed using the transient thermal impedances determined using the model of a typical power module implemented in the simulation package Flotherm. A diagram of this model showing the position of each device can be seen in Figure 5.2.

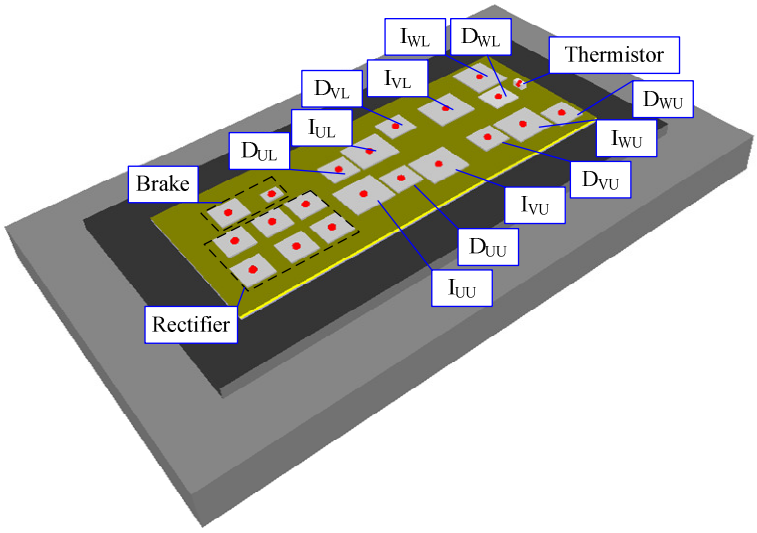

Figure 5.2: Flotherm model of a typical power module

Although the power module used in this simulation contains a rectifier, inverter and brake, the frequency model has been developed to only protect the devices in an inverter. Thus, the Flotherm model is used to generate the typical self and mutual transient thermal impedance curves for the six IGBTs and freewheeling diodes (p=12). These are represented by an equivalent Foster network, which form the complete thermal impedance matrix for the inverter:

$$\left[Z_{th,j-ref}\right]=\begin{bmatrix} Z_{th,11} & \cdots & Z_{th,1p} \\ \vdots & \ddots & \vdots \\ Z_{th,i1} & \ddots & Z_{th,ip} \\ \vdots & \ddots & \vdots \\ Z_{th,p1} & \cdots & Z_{th,pp} \end{bmatrix} \tag{5.5}$$

The methods used to calculate the transient thermal impedance and the parameters of an equivalent Foster network are described in Chapter 7. Using the simulation model, the thermal impedances can be calculated between the junction of a device (T_j) and any reference point. In practice, most models that have been developed use the ambient temperature (T_a) or the temperature measured by the internal thermistor in the power module (T_{th}). Therefore, the simulation model has been used to generate the complete thermal impedance matrix using both of these reference temperatures. The absolute temperature of the devices can be calculated using either:

$$\left[T\right]=\left[Z_{th,j-a}\right]\cdot\left[P\right]+T_a \tag{5.6}$$

or

$$\left[T\right]=\left[Z_{th,j-th}\right]\cdot\left[P\right]+T_{th} \tag{5.7}$$

To identify the hottest device in the inverter under any operating condition and to allow the frequency model to be compared against the instantaneous response, Equations 5.6 and 5.7 have been implemented in Simulink. In this model, it is assumed that the power loss in a device is sinusoidal and the duty cycle is approximated by the third harmonic modulation

scheme. These are the initial assumptions used to develop the frequency model. Therefore, in order to calculate the temperature of a device the following operating parameters must first be defined:

- IGBT and diode peak conduction loss (W) $\hat{P}_{con(IGBT)}$ and $\hat{P}_{con(diode)}$
- IGBT and diode peak switching loss (W) $\hat{P}_{sw(IGBT)}$ and $\hat{P}_{sw(diode)}$
- Displacement Power factor DPF or $\cos(\theta)$
- Modulation index m
- Output frequency (radians/s or Hz) ω or F_{out}

However, when an inverter is operating at an output frequency of 0Hz, which is defined as a stationary vector condition, a device can be continuously operating at the output angle (ωt) where its peak power loss occurs (i.e. switching the peak load current). At this frequency there is no filtering effect ($A_{Fn}=1$) due to the thermal time constants. Consequently, for a constant power loss, the resulting steady-state temperature will be higher in a stationary vector condition than at any other frequency. Hence, a device is more likely to exceed its maximum operating temperature. Therefore, this chapter is focused on the development of a frequency model that will protect an inverter operating in a stationary vector condition.

5.3.1 Protection of an Inverter Operating in a Stationary Vector Condition

The output of the steady-state frequency model is equivalent to the peak junction-to-reference temperature of a device calculated over a complete output cycle of the inverter, i.e. the peak ripple temperature is calculated using the Taylor series approximation. Therefore, in order to protect every device in the inverter under a specific operating condition, the frequency model must be used to estimate the temperature of the device in which the highest peak junction-to-reference temperature occurs. Using this approach, the temperature estimated by the frequency model will be equal to or higher than the hottest device in the inverter. However, due to the thermal coupling between devices, the peak junction-to-reference temperature and the device in which this temperature occurs will depend on the operating conditions. Consequently, more than one frequency model may be required.

In this section, an example is used to describe the procedure for identifying the devices that must be modelled. In this example, the temperature is calculated using the equivalent Foster networks in the junction-to-thermistor thermal impedance matrix. Therefore, to calculate the instantaneous temperature, Equation 5.7 is implemented in the Simulink model. The peak switching and conduction loss for the IGBTs (68W) and diodes (34W) has been selected to ensure that no device can exceed 150°C when operating at any displacement power factor or modulation index. The first step in the procedure is to calculate the steady-state temperature (junction-to-thermistor) of each device over a complete output cycle (ωt=0 to 2π). By definition, when operating in a stationary vector condition, the output vector does not rotate and the steady-state temperature can be calculated directly using the sum of the thermal resistances in each network. After completing this calculation, the peak temperature that occurs over the output cycle ($\hat{T}_{j-th}$) can be selected. This process is illustrated in Figure 5.3(a).

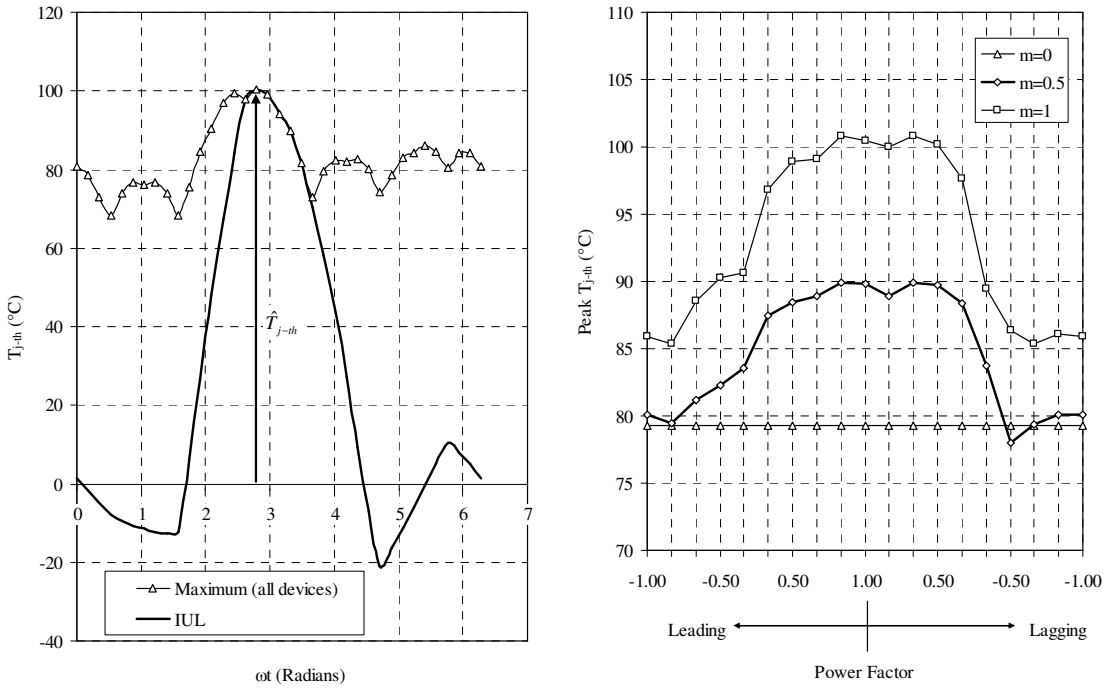

(a) (b)

Figure 5.3: Maximum steady-state junction-to-thermistor temperature (a) selection of the peak temperature for a unity displacement power factor and modulation index (b) peak temperature calculated for all operating conditions

In this figure, the maximum steady-state temperature between each device and the internal thermistor is calculated over a complete output cycle when the inverter is operating with a unity displacement power factor and modulation index. As shown, the peak junction-to-thermistor temperature calculated over the cycle can then be selected. This process is repeated at each displacement power factor and modulation index. Although some of these conditions do not reflect a true operating condition, they provide a good indication of the thermal interaction in the power module. The peak steady-state junction-to-thermistor temperature calculated in each of these conditions is shown in Figure 5.3(b). The next step is to identify the device in which this peak temperature occurs. For example, in Figure 5.3(a) the device selected is the lower IGBT in the U phase (I_{UL}). Therefore, when the displacement power factor and modulation index are unity, estimating the temperature of I_{UL} (single frequency model) will ensure that the inverter is protected regardless of the output angle (ωt). However, as discussed, the device in which the peak junction-to-thermistor temperature occurs is dependant on the operating conditions and this can be seen in the figure below:

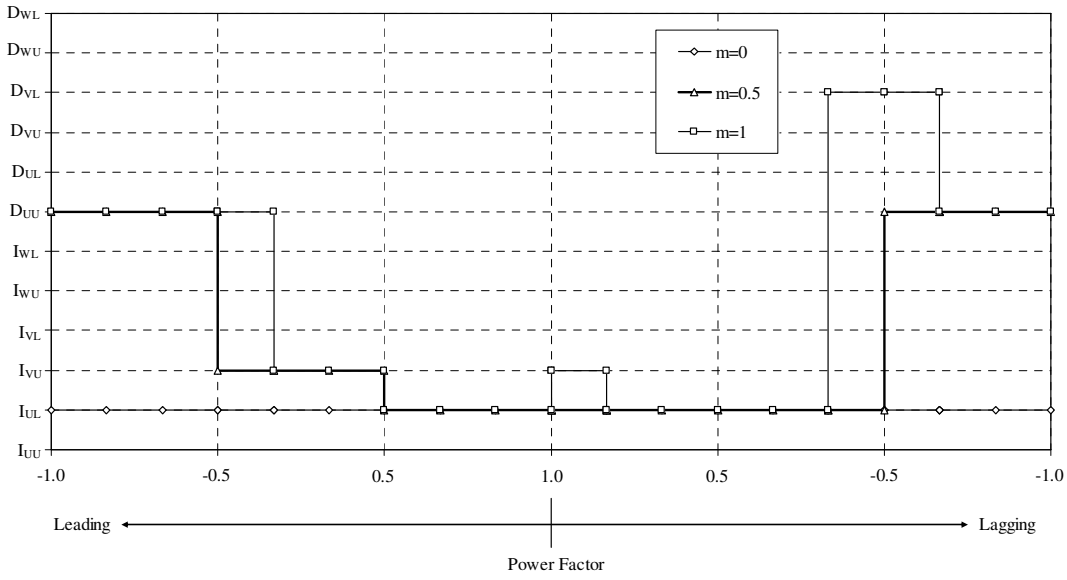

Figure 5.4: The devices in which the peak junction-to-thermistor temperature occurs when operating in a stationary vector condition with a constant power loss

From these results, it can be seen that in order to protect every device in the inverter the frequency model must be used to estimate the temperature of four devices; these are I_{UL}, I_{VU}, D_{UU} and D_{VL}. This is because in at least one of the operating conditions examined the peak junction-to-thermistor temperature occurs in one of these devices. These results show that when using the frequency model to protect the inverter in a stationary vector condition it is not necessary to implement the complete thermal impedance matrix. However, in a power module, the thermal coupling between the devices has a considerable impact on the device temperature, and this coupling is dependant on the layout of the power module. Therefore, if the frequency model is developed for a power module where the position of the devices and/or the internal thermistor are different (e.g. a power module produced by a different manufacturer) more or less devices may need to be modelled to ensure the inverter is protected under all possible operating conditions.

The procedure outlined in this section has been used to identify the devices that must be modelled to protect an inverter operating in a stationary vector condition with a constant power loss. The same procedure can be used to identify the devices that must be modelled at different output frequencies and with different peak losses. In summary, to select the devices the following steps must be performed:

1. Calculate the instantaneous temperature over a complete output cycle of the inverter using the self and mutual thermal impedances defined between the junction of a device and the chosen reference point.
2. Repeat this calculation for each device and operating condition. These can include the output frequency, displacement power factor, modulation index and the peak switching and conduction losses for the IGBTs and diodes.
3. Select the maximum temperature that occurs over the output cycle ($\hat{T}_{j-ref}$).
4. Identify the device in which the peak junction-to-thermistor temperature occurs.

As described, for a given power loss a device is more likely to exceed its maximum temperature when operating at low output frequencies. Therefore, in the remainder of this chapter, the steps outlined above are used to select the devices that are required to protect

the inverter in a stationary vector condition and the effect of operating at different output frequencies is ignored.

5.3.2 Estimated Temperature over a Complete Output Cycle of the Inverter

In an inverter the reference temperature is usually measured by a thermistor and many manufacturers now include a thermistor within a standard power module. Therefore, the reference temperature used in the thermal model is an instantaneous value. Combining this with the output of the steady-state frequency model (constant value) will have a significant impact on the accuracy of the estimated temperature at low output frequencies. To show this effect, the temperature estimated using the frequency model is compared against the temperature of the hottest device in the inverter. A comparison for an inverter operating in a stationary vector condition is shown in Figure 5.5.

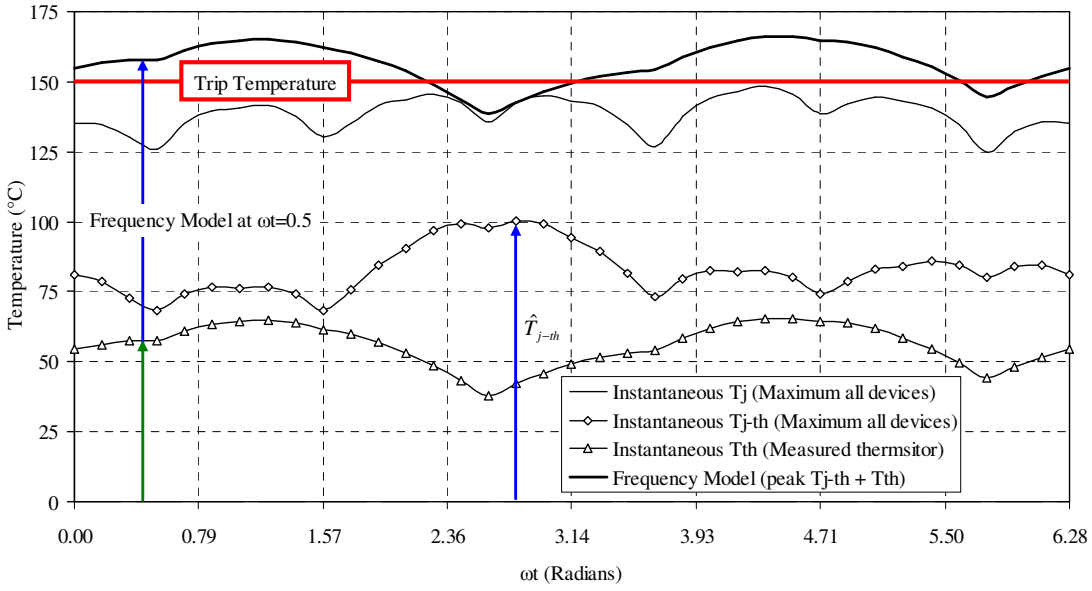

Figure 5.5: Comparison of the temperature estimated by the frequency model and the maximum steady-state temperature when operating in a stationary vector condition

For these operating conditions, the peak junction-to-thermistor temperature occurs at an output angle of 2.79rads. At this angle the temperature estimated by the frequency model is identical to the maximum instantaneous temperature. However, over an output cycle the temperature measured by the thermistor changes due to the thermal coupling between the thermistor and the devices in the inverter (IGBTs and diodes). Therefore, since the output

of the frequency model is equivalent to the peak junction-to-thermistor temperature, when the inverter is operating at any other output angle, the temperature estimated by the frequency model will be higher than the hottest device. If this exceeds the maximum operating temperature, the drive will enter an error or trip condition, which will prevent any further increase in temperature. In this condition the performance will be restricted by the thermal model rather than the true operating temperature of the devices and this will have a direct impact on the rating of the inverter. For example, the results in Figure 5.5 show that the temperature of the hottest device is always below 150°C. Even so, to ensure that the temperature estimated by the thermal model does not exceed the maximum temperature the peak power loss in the IGBTs must be reduced from 68W to 62.5W. This decrease in power loss corresponds to a reduction in the maximum output current available from the inverter, which is an undesirable effect.

However, as the output frequency is increased the ripple present in the measured thermistor temperature will be reduced. Eventually this will become a constant value, which is independent of the output angle. From tests carried out on a typical power module [111], it was found that the measured ripple temperature was negligible when the output frequency was above 5Hz. Therefore, using the frequency model to protect the inverter will only have a significant effect on the maximum output current available from the inverter at low output frequencies.

5.4 Simplifying the Frequency Model

In the previous section, it was shown that when using the frequency model to protect the inverter it is not necessary to calculate the temperature of every device. Therefore, compared to the implementation of the complete thermal impedance matrix the number of calculations that must be performed by the thermal model is significantly reduced. Even so, to implement the thermal model using the available resources further assumptions must be made in order to reduce the number of network elements (i.e. thermal impedances) used in the model.

To show the effect of any assumptions, the temperature estimated by the frequency model is compared with the maximum instantaneous temperature calculated using the Simulink

model, which includes all of the mutual coupling in the power module. In the Simulink model it is assumed that the power loss for each device is a rectified sinusoid and the duty cycle is approximated using the third harmonic scheme. Thus, if the instantaneous temperature is compared directly with the output of the frequency model the differences between the calculated temperatures will be due to one or both of the following:

a) The assumptions used to develop the frequency components for the switching and conduction loss models, i.e. the number of harmonic components used in the approximation of the power loss and duty cycle.
b) The elements in the thermal impedance matrix not included in the model.

The impact of the assumptions used to develop the frequency components for the models were reviewed in Chapter 4. Therefore, in order to isolate the effect of the simplifications made to the thermal impedance matrix, the temperature estimated by the steady-state frequency model is approximated by:

$$T_{ss(n=\infty)} = \hat{T}_{j-ref\,(n=\infty)} + T_{ref} \tag{5.8}$$

The temperature calculated using this equation is equal to the output of the frequency model if all of the harmonics (n=0 to ∞) were included. Therefore, any differences in the comparisons will be due to the selection of the device being modelled and/or any of the mutual impedances that have been ignored. In the following comparisons the frequency model is developed using the thermal impedance measured between the junction of a device and the internal thermistor in the power module, while the operating conditions are the same as those defined in Section 5.3.1.

5.4.1 Single Device Model

In this section the temperature of a device is calculated using the self thermal impedance and any coupling that exists between the devices in the inverter is ignored. Therefore, the terms in the frequency model are calculated for the elements in a single equivalent Foster network. To implement this model the self impedance for a device must be selected from the complete thermal impedance matrix.

When an inverter is operating with a positive displacement power factor the power loss in an IGBT will normally be much higher than a parallel diode. Consequently, in this condition, the largest temperature difference measured between the junction of a device and the internal thermistor will occur in one of the IGBTs. However, the opposite applies when the displacement power factor is negative and in this condition, it is likely that the peak temperature will occur in one of the diodes. Therefore, because the effect of the operating conditions on an IGBT and diode are different, estimating the temperature of a single device will inevitably lead to a significant underestimation of the temperature in some operating conditions. To show this effect, the frequency model is used to estimate the temperature of the lower IGBT in the U phase (I_{UL}) of the inverter. This device is selected from the results shown in Figure 5.4, which shows that the peak junction-to-thermistor temperature occurs more often in this IGBT.

In Figure 5.6(a), the temperature estimated using the self thermal impedance (simplified frequency model) is compared with the maximum IGBT and diode temperature calculated using the complete thermal impedance matrix.

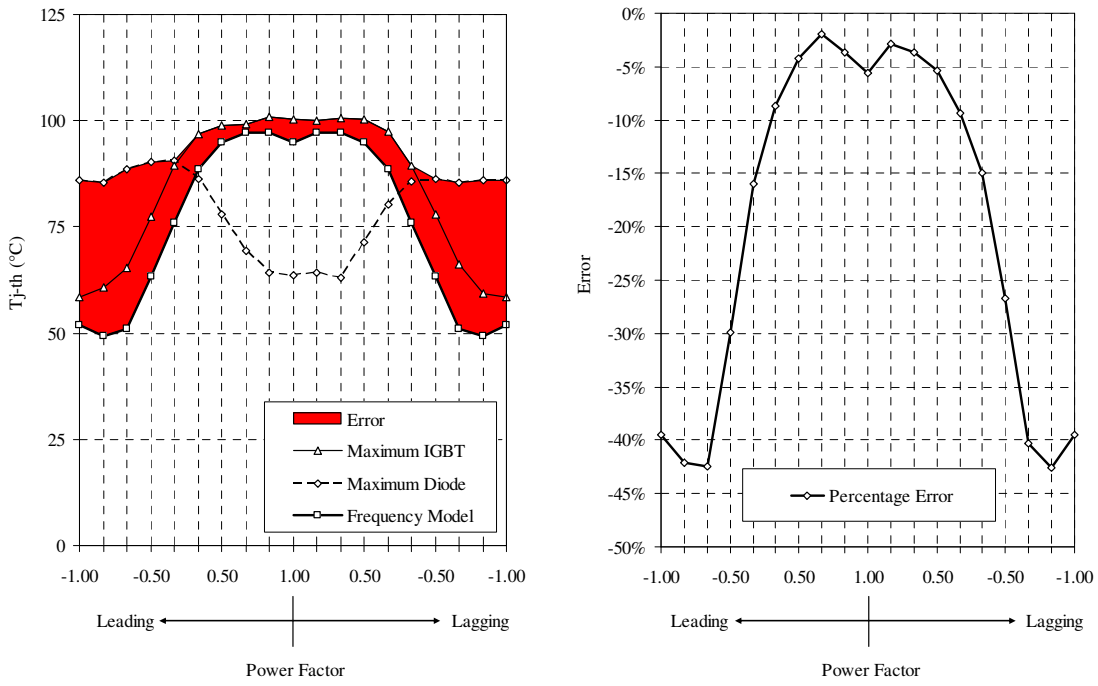

Figure 5.6: Comparison of the single device model developed for I_{UL} when operating with a unity modulation index (a) junction-to-thermistor temperature (b) percentage error

In this figure, it is evident that in most operating conditions the temperature estimated by the frequency model is considerably lower than the maximum device temperature. As expected, the error is larger when the peak temperature occurs in one of the diodes. In Figure 5.6(b) the error is represented as a percentage of the maximum device temperature and since this is underestimated by the frequency model, the error is negative. The percentage error shown in this figure is an important indication of the error that could be expected when operating with a unity modulation index. However, the modulation index will have a significant effect on the accuracy of the simplified frequency model. Consequently, the error must be calculated over the full range of the modulation index (m=0 to 1). These results are shown in Figure 5.7(a).

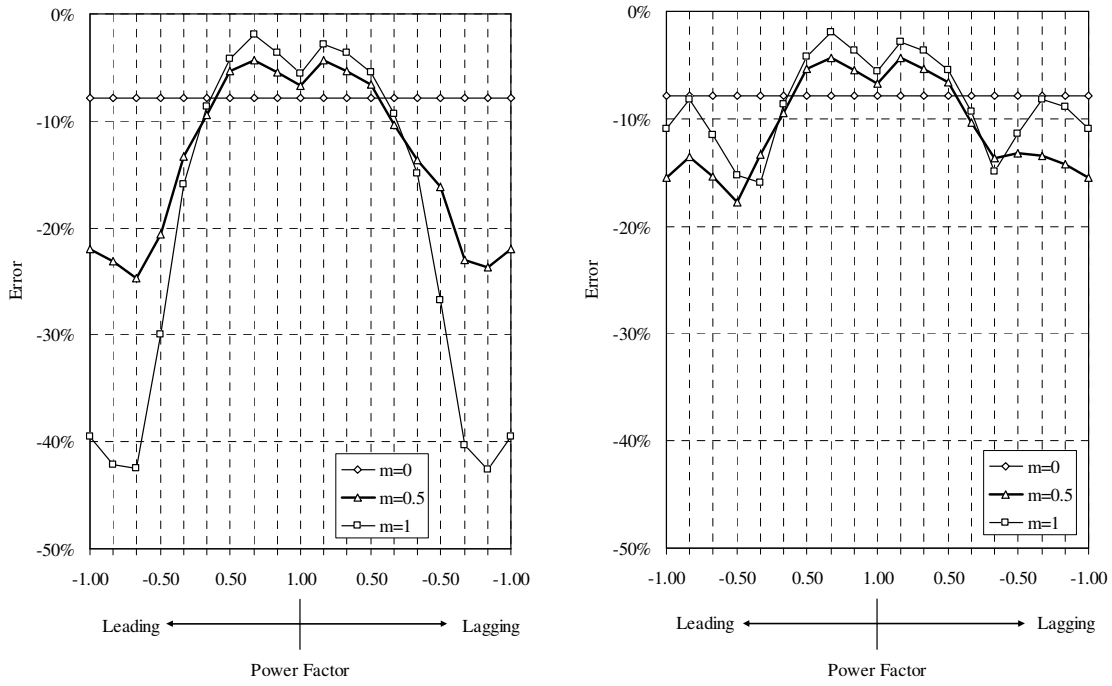

Figure 5.7: Error in the single device model when operating in a stationary vector condition (a) IGBT model (b) IGBT and diode models implemented in parallel

These results show that when using a single IGBT model with no coupling, the temperature is significantly underestimated in most operating conditions. Therefore, at minimum, the frequency model must be used to estimate the temperature of one IGBT and one diode in the inverter. Furthermore, if these models are implemented in parallel, the devices in the

inverter are protected by the model that estimates the highest temperature and this can improve the level of protection. As with the IGBT model, the diode is selected using the results in Figure 5.4. The diode used in the model is the upper diode (D_{UU}) in the U phase of the inverter. The error calculated using the highest temperature estimated by the IGBT and diode model is shown in Figure 5.7(b). By running both models in parallel the maximum error has been considerably reduced, although it is still significant in many operating conditions. Consequently, this model cannot be used to protect an inverter operating at low output frequencies and an alternative model is required. Furthermore, the results presented in this section highlight the limitation of a model developed using the thermal impedances provided in the datasheet of a device. These are normally limited to the self thermal impedance for an IGBT and diode measured between the junction of the device and the case of the power model [71].

5.4.2 Single Device Model including the Thermal Coupling between devices

In order to reduce the error in the estimated temperature and develop a model that can be used to provide sufficient protection for the inverter, the thermal coupling from the neighbouring devices must be included. In this section, the temperature of I_{UL} and D_{UU} are calculated using the self and all of the mutual thermal impedances associated with these devices. Therefore, in this model, the temperature will only be underestimated if the peak junction-to-thermistor temperature does not occur in either of these devices. As previously, Figure 5.8(a) shows the error that would be expected if only the IGBT model (I_{UL}) was used, whereas Figure 5.8(b) shows the error calculated when the IGBT and diode models are implemented in parallel. This allows a direct comparison to be made with the results in Figure 5.7, which shows the error calculated when only the self thermal impedance is used.

As shown in Figure 5.8(a), when using the IGBT model there is no error in the operating conditions where the peak junction-to-thermistor temperature occurs in I_{UL}. However, the error is still significant when the inverter is operating with a negative displacement power factor. Therefore, both models must be implemented in parallel. The error for this model is shown in Figure 5.8(b). This figure shows that the maximum error is reduced to 11% and where an error occurs, the peak junction-to-thermistor temperature does not occur either in I_{UL} or D_{UU}.

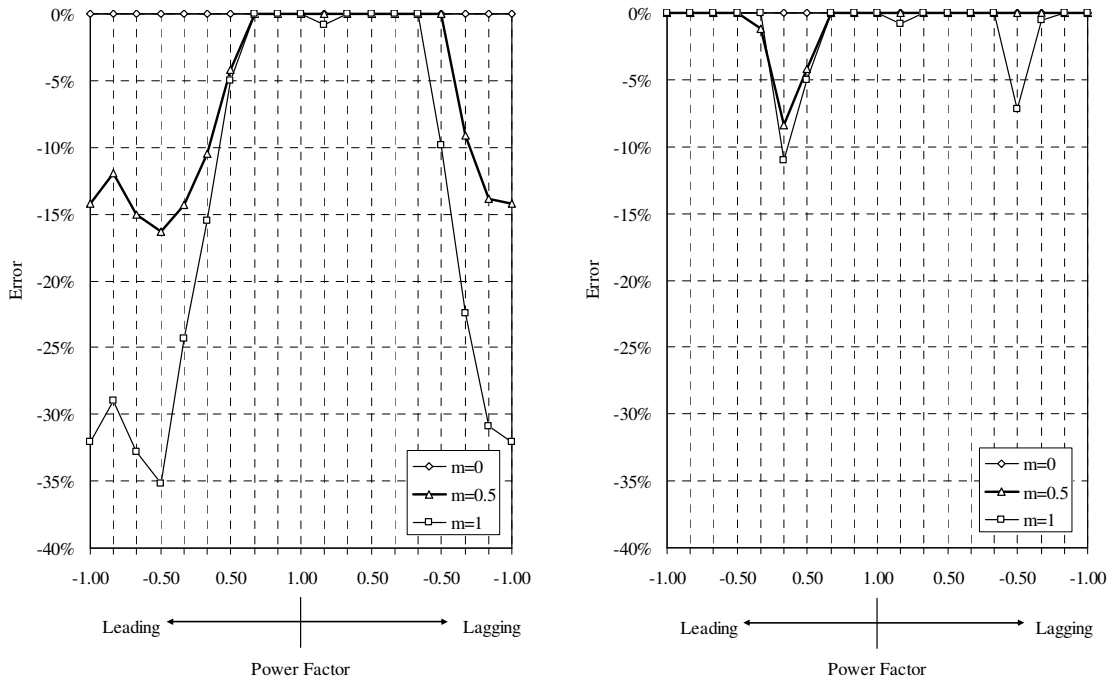

Figure 5.8: Error in the single device model with thermal coupling when in a stationary vector condition (a) IGBT model (b) IGBT and diode models implemented in parallel

Although incorporating the mutual thermal coupling into the model has been shown to reduce the error, any error in the thermal model is undesirable, especially if it could result in a device exceeding its maximum temperature. However, the error has been calculated using a single IGBT and diode with the inverter operating in a stationary vector condition, and when assessing the impact of this error the following factors should be considered:

- If there are sufficient computational resources, more devices can be modelled to prevent any underestimation of the temperature (as described in Section 5.3.1).
- The operating conditions where the error is significant are not practical in an inverter driving a motor load, i.e. operating at a low frequency with a high modulation index and displacement angle. Thus, the error calculated with a unity displacement factor is the most important.
- The error will be different for each power module and will be considerably lower for a power module where the thermal coupling between devices is less significant.

Taking these factors into account the frequency model developed in the following chapters is based on the self and mutual thermal impedances for a single IGBT and diode. Where a significant error occurs due to the approximation of the power loss, duty cycle or the thermal characteristics, this must be incorporated into the final protection scheme in the form of a constant or variable (dependant on the operating conditions) safety margin.

5.5 Thermal Parameters used in the Frequency Model

In the simplified model described in Section 5.4.2, the temperature of one IGBT and one diode is estimated using the self and all of the mutual thermal impedances associated with these devices. To implement this model, these thermal impedances must be represented by an equivalent Foster network with one or more elements. The following parameters must be defined:

- **Thermal resistance** (R_{th}) – This defines the magnitude of the frequency terms in a stationary vector condition.
- **Time constant** (τ_{th}) – This defines the change in magnitude with the output frequency of the inverter.
- **Offset angle** (α) – This is the phase shift used to represent the power loss in each device in the inverter with reference to the modelled device. This determines the magnitude of the corresponding sine and cosine components for each harmonic.

The number of network elements that are used to represent the self and mutual thermal impedances are selected in the next section.

5.5.1 Selection of the Elements in each Foster Network

The number of elements used in the frequency model will have a direct impact on the number of calculations required to estimate the device temperature, but will also have an effect on the following:

a) The magnitude of the steady-state frequency components
b) The transient response

If possible, an equivalent network should have enough elements to ensure that the response of the network is an accurate representation of the measured impedance. In general, to achieve this no more than four elements are required [101, 112]. However, in this model, the number of elements that can be used is restricted by the available computational resource and at present, implementing a model with four elements in each network is not possible.

In any power module, the temperature of an active device will be dominated by its self thermal impedance. By definition, this includes the impedance measured between the junction of the device and the case of the power module, e.g. the silicon chip, solder, case, etc. Therefore, there will be multiple time constants associated with this impendence and as a result, more elements must be used in these networks to provide a reasonable approximation. With these limitations in mind, the following elements have been chosen:

- **Self thermal impedance –** Two network elements
- **Mutual thermal impedance –** Single network element

As discussed, the number of elements is constrained by the computational resource and if possible, more elements should be used to improve the transient response. In summary, to estimate the temperature of one device, each term in the switching and conduction loss models must be calculated for thirteen elements (two self and eleven mutual elements).

5.5.2 Reducing the Number of Mutual Terms in the Frequency Model

Several approaches that can be used to reduce the number of mutual impedances in a model based on the thermal impedance matrix have been described in the literature, and these include the following:

a) Ignore any of the mutual thermal impedances that are negligible when compared to the self thermal impedance of the device.
b) Use only the thermal impedances from the nearest neighbour to the device being modelled, and ignore the coupling from all other devices in the power module [1].

By ignoring the thermal impedances that are negligible, the number of elements in the model can be reduced without significantly affecting the accuracy of the estimated temperature. However, when the temperature measured by the internal thermistor is used as the reference for the model, devices that are positioned close to either the modelled device or the thermistor have a significant effect. Therefore, using only the coupling from the nearest neighbours to the device can lead to a considerable under or overestimation of the temperature. An alternative method that is unique to the frequency model developed in this work is described below.

If the time constant of two or more of the elements that are used to represent the mutual thermal impedance are the same, the magnitude of the terms in the frequency model will change at the same rate, i.e. they will have the same phase shift (β) and filter magnitude (A_{Fn}). If these elements are in the same network (same offset angle), the combined response can be represented by a single element by simply adding the thermal resistances together. This process is equivalent to adding two frequency components that are in phase, but with different magnitudes. This is illustrated in Figure 5.9.

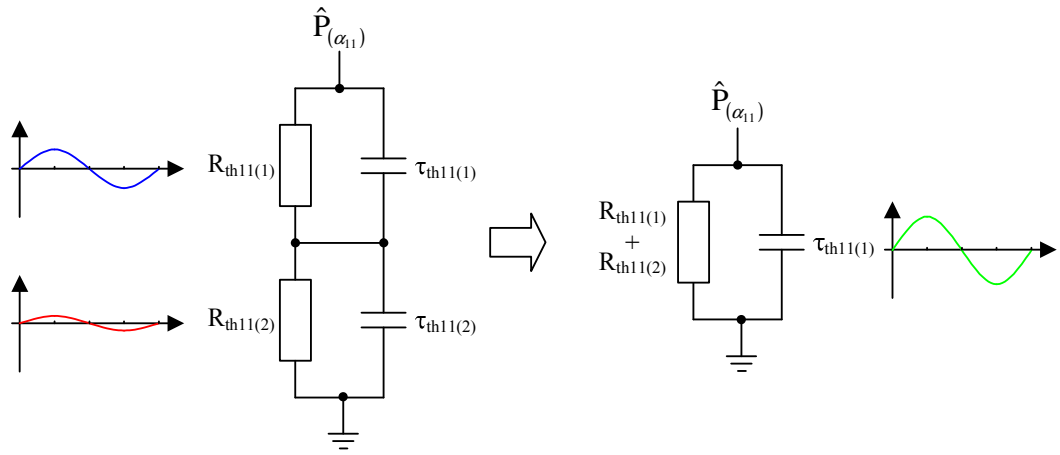

Figure 5.9: Combining network elements with the same time constant and offset angle

With this approach, instead of calculating the frequency terms for each element separately, the magnitude can be calculated once by using the combined network parameters. This is similar to the method that was described in Section 5.2, although the calculations in this section can be performed off-line. The method illustrated in Figure 5.9 can also be used to

combine network elements in different networks (different offset angles). This is equivalent to adding two or more frequency components that are not in phase. As a result, a different thermal resistance and offset angle must be used for each harmonic (n) in the frequency model. Even so, each term must still only be calculated once. The magnitude of the combined thermal resistance for the n^{th} harmonic is given by:

$$R_{th,i(n)} = \sqrt{\left[\sum_{\substack{j=1 \\ j\neq i}}^{m} R_{th,ij\,(k)} \cos(n\alpha)\right]^2 + \left[\sum_{\substack{j=1 \\ j\neq i}}^{m} R_{th,ij\,(k)} \sin(n\alpha)\right]^2} \tag{5.9}$$

and the corresponding offset angle is calculated using:

$$n\alpha_{i(n)} = \cos^{-1}\left(\frac{\sum_{\substack{j=1 \\ j\neq i}}^{m} R_{th,ij(k)} \cos(n\alpha)}{\left|R_{th,i(n)}\right|}\right) \tag{5.10}$$

where $R_{th,i(n)}$ and $\alpha_{i(n)}$ are the magnitude and phase shift for device *i* and the n^{th} harmonic, *m* is the number of network elements with the same time constant and *k* is the position of the element in each network.

Due to the implementation of the duty cycle, the terms in the frequency model for an IGBT and diode are different. Consequently, the network elements representing the coupling due to the loss in an IGBT and diode cannot be combined. Nevertheless, if the mutual thermal impedances from the IGBTs and diodes could be represented by a common time constant, all of the coupling in an inverter could be modelled by just two network elements, with one representing the coupling from the IGBTs and the other from the diodes. Using this approximation, the steady-state temperature in a stationary vector condition will remain the same, but the transient response will change. The effect this has on the accuracy of the estimated temperature will depend largely on the thermal properties of the inverter, specifically the ratio between the self and mutual thermal impedances. Furthermore, the

method used to select the common time constants for the combined network elements will have a significant effect. This is described in the following section.

5.5.2.1 Calculation of the Common Time Constants for the Combined IGBT and Diode Networks

In order to combine the equivalent networks for the mutual thermal impedances, a common time constant must be selected for the network elements used to represent the coupling from the IGBTs ($\tau_{th,IGBT}$) and diodes ($\tau_{th,diode}$) in the inverter. In order to select these time constants, a Simulink model is used to calculate the instantaneous temperature response of the modelled devices (I_{UL} and D_{UU}) during a step change in the peak power loss. This calculation is repeated using the original network parameters determined from the Flotherm model and the common time constants, which are selected to minimise any differences between the responses.

An example of the step response calculated for the IGBT model operating in a stationary vector condition is shown in Figure 5.10(a). The time constants used in this comparison are:

$\tau_{th,IGBT} = 3.5s$

$\tau_{th,diode} = 3s$

The difference between the temperature responses is shown in Figure 5.10(b). In this figure a negative value indicates that the temperature is underestimated. For the chosen operating conditions, which are the same as those defined in Section 5.3.1, the temperature is never underestimated (negative value) by more than 2°C. As well as the transient response, this approximation will also have an effect on the steady-state temperature calculated at higher output frequencies. However, because the time constants associated with the mutual coupling are relatively long, the effect that these terms have on the device temperature falls rapidly as the output frequency is increased and any error will be negligible. Therefore, the time constants for the combined networks used in the thermal model are selected using this procedure. This is covered in Chapter 7.

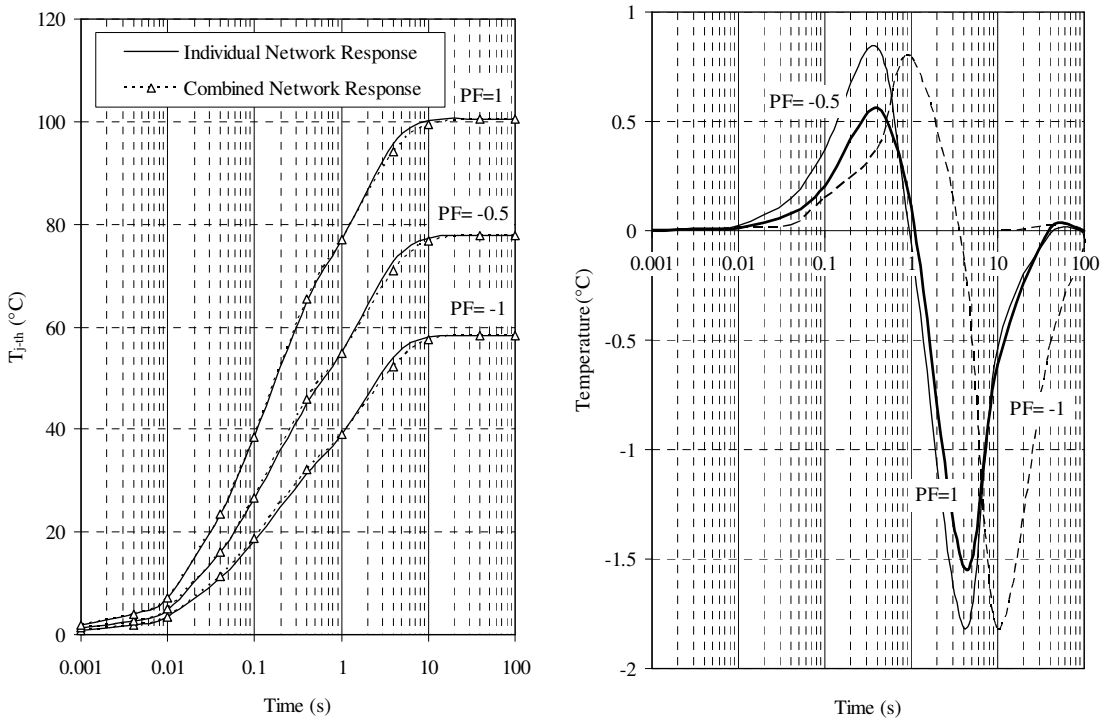

(a) (b)

Figure 5.10: Comparison of the step response calculated using the original network parameters and the common time constants in a stationary vector condition with a unity modulation index (a) step response (b) temperature difference

The procedure used to calculate the thermal parameters for one device is summarised below, all of these calculations can be completed off-line:

1. Calculate the thermal resistance, time constant and offset angle for the two network elements used to represent the self impedance for the chosen device.
2. Calculate the thermal resistance, time constant and offset angle for the eleven mutual impedances for the chosen device.
3. Use Equations 5.9 and 5.10 to calculate the thermal resistance and offset angle for the combined networks representing the coupling from the IGBTs and diodes in the inverter, and repeat this for each harmonic (n=1 to 3).
4. Select the common time constant for the combined IGBT ($\tau_{th,IGBT}$) and diode ($\tau_{th,diode}$) networks.

Using this procedure, the parameters of four Foster network elements are calculated. These represent the self and all of the mutual thermal impedances associated with one device. Therefore, the terms in the frequency model only need to be calculated eight times, once for each peak loss (switching and conduction) applied to each network element (two self and two mutual elements).

5.6 Implementation of the Frequency Model and Summary of the Input Parameters

To implement the frequency model the following temperatures must be calculated:

- **Steady-State (T_{ripple})** – The peak ripple temperature is calculated from the frequency components using the Taylor series approximation and this component is applied as a constant value.
- **DC (T_{DC})** – The magnitude of the DC terms for each network element in the model are calculated separately. These magnitudes are applied to an individual transfer function of a first order filter with a unity magnitude (1K/W) and the time constant of the associated network element.
- **Transient (T_{exp}) –** This magnitude is calculated from the change in the peak ripple temperature and this is applied to a high pass filter. The time constant (τ_{exp}) used in this filter is selected from one of the four network elements.

The control diagram for the frequency model is shown in Figure 5.11. This diagram shows how the thermal model is implemented in the drive. It includes all of the input parameters that are required to calculate the peak loss in an IGBT or diode, and the resulting steady-state, DC and transient components of the temperature response. The input parameters in this diagram are separated into the following categories:

1. → Measured device parameters
2. → Thermal parameters calculated off-line
3. → Internal feedback parameters

The main parameters that are calculated on-line are shown at the output of the various control blocks.

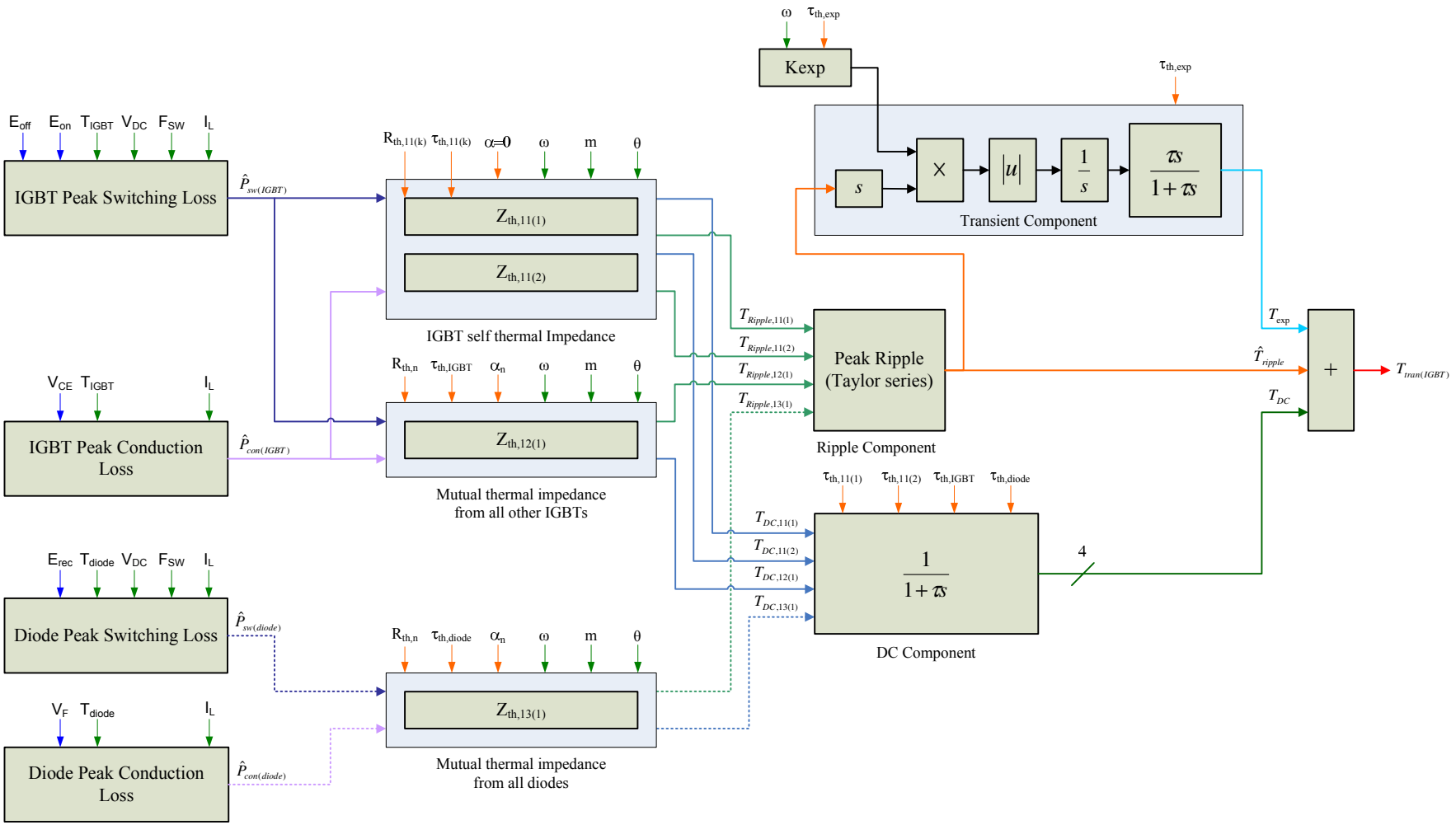

Figure 5.11: Control flow diagram for the implementation of the IGBT frequency model for a three phase inverter

The model shown in the control diagram is used in Chapter eight to compare the estimated and measured device temperatures and is implemented in the control microprocessor of the drive described in the next chapter. In this drive the thermal model runs in a background routine operating at a cycle rate of 250Hz and the input parameters are sampled at the beginning of each cycle.

The model implementation combines the frequency analysis used to calculate the magnitude of the ripple components with the time domain implementation of the DC and transient components. The frequency components developed in the previous section are used to calculate the ripple temperature for each of the four network elements. These ripple components are combined to calculate the peak ripple temperature and this is used as the input to the transient component. To ensure the transient component calculates the maximum temperature it is assumed that the exponential output (T_{exp}) is positive regardless of the direction of the change in the peak ripple. To implement this, the magnitude of the change in the peak ripple is calculated and this is applied to the high pass filter which is implemented in the time domain. The output of this filter is always a positive component that decays exponentially.

Out of the parameters shown in the control diagram the only parameter that has not yet been defined is the time constant (τ_{exp}) used in the transient component. The magnitude of the transient component is determined directly from the change in the ripple temperature, which is a function of the thermal parameters in each of the network elements (i.e. the self and mutual impedances). In order to implement more than one transient component, the terms in the frequency model would have to be recalculated for each individual element using the location of the peak ripple (ωt_{max}) found from the combined response. From this, the change in the ripple temperature associated with each of the elements could be used to determine the magnitude of the individual transient components. However, these additional calculations cannot be performed using the existing computational resource and the transient component must be approximated by a single characteristic. The effect that this has on the estimated temperature will depend largely on the thermal properties of each network and the chosen time constant. As a compromise between protection and performance, the time constant used in the model is the longest time constant in the

equivalent network of the self thermal impedance. However, this time constant is often much shorter than the time constants associated with the mutual thermal impedances. Consequently, at a low output frequency where the effect of the mutual thermal impedance is more significant, this approximation may result in a slight underestimation of the device temperature because the transient term will decay too fast.

In the following chapters, the complete thermal model illustrated in Figure 5.11 is used to estimate the temperature of an IGBT and diode in a production drive. The methods used to measure the electrical and thermal characteristics of the power module used in this drive are described in Chapter 6. These measurements are then used in Chapter 7 to calculate the input parameters required by the frequency model. Finally, in Chapter 8 the temperature estimated by this model is compared with the temperature measured using a thermal camera.

5.7 Summary

In this chapter the thermal model was applied to a typical power module. In order to estimate the temperature of a device in this module the thermal model has been extended to allow the thermal characteristics to be represented by multiple Foster networks with one or more elements. However, using the available computational resources it is not possible to implement the full model (thermal impedance matrix) on-line. Consequently, the main focus of this chapter was to develop a simplified thermal model and this was achieved by selecting only the key thermal impedances. To show how the selection of the thermal impedance impacts the protection provided by the thermal model, the effects of the following simplifications were investigated with the inverter operating in a stationary vector condition:

1. Multiple device model using the self and mutual thermal impedance of each device in which the peak junction-to-thermistor temperature occurs.
2. Single device model using the self thermal impedance of one IGBT and diode
3. Single device model using the self and mutual thermal impedance of one IGBT and diode

The first of these was shown to protect all of the devices in the inverter. However, this model uses the self and mutual thermal impedances associated with several devices and for this reason, it cannot be implemented on-line. In contrast, using only the self thermal impedance significantly reduces the number of on-line calculations, but results in a significant underestimation of the temperature. As a compromise, the final model includes all of the mutual thermal impedances associated with a single IGBT and diode, which significantly improved the protection for the inverter. Therefore, this model was chosen to form the basis of the final solution.

Even though the complexity of the chosen model has been significantly reduced when compared to the complete thermal impedance matrix, it is still not possible to implement this using the available resources. Thus, in the remainder of this chapter a procedure that can be used to combine the frequency components of the network elements that represent the mutual thermal impedance between devices was described. This procedure can only be applied in conjunction with the frequency model and importantly, all of these calculations can be performed off-line. Finally, the method used to implement the on-line thermal model was presented in the form of a control diagram and from this all of the input parameters were defined.

Chapter 6: Measurement of the Power Module Parameters

6.1 Introduction

The thermal model that was developed in Chapters 4 and 5 requires a number of thermal and electrical device parameters that cannot be obtained directly from the datasheet, or that are not specified in sufficient detail. Consequently, before the thermal model can be implemented in a drive, the transient thermal impedance together with the switching and conduction loss parameters for every device in the inverter must be measured. The methods used to measure these parameters and the key results are described in this chapter.

The drive used to evaluate the thermal model has been selected from the existing range of products that are offered by Control Techniques. A description of this drive and the integrated power module is included in Section 6.2. Where possible, the parameters required by the thermal model are measured using a standard power module. However, in order to use an infrared camera to measure the temperature of the devices in the inverter stage the power module must be modified. This procedure is described in section 6.2.1. The temperature measured by the infrared camera (T_j) and the internal thermistor (T_{th}) in the power module are used in the calculation of the transient thermal impedance. The following thermal impedances are calculated in Section 6.3:

- Self thermal impedance measured between a device (i) and the internal thermistor in the power module – $Z_{th,ii(j\text{-}th)}$
- Mutual thermal impedance measured between a device (i) and the internal thermistor in the power module – $Z_{th,i\neq j(j\text{-}th)}$

These cannot be determined from the datasheet of the device since typically, only the self thermal impedance measured between the junction of a device and the case of the power model is defined. Furthermore, as described in Chapter 5, in order to select the devices used in the frequency model the temperature of every device in the inverter is calculated using

the complete thermal impedance matrix. Therefore, although the parameters required to implement the model are calculated from the thermal impedances associated with a single IGBT and diode, the self and mutual thermal impedances must be measured for every device in the inverter. The factors that affect these calculations and the key results are presented in Section 6.3.2 and 6.3.3.

As well as the thermal parameters, in order to calculate the temperature response the total power loss in each device must be known and in the thermal model, this is calculated on-line. To calculate the power loss, a number of parameters that are dependant on the configuration of the inverter (e.g. the gate resistance, stray inductance, etc) are required. Consequently, these parameters cannot be determined directly from the datasheet of the device and must instead be measured in the same configuration that will be used to evaluate the thermal model. The experimental setup that is used to measure the parameters for an IGBT and diode is described in Section 6.4.1. Using this method, the following switching loss parameters are measured:

- Turn-on switching energy of an IGBT – E_{on}
- Turn-off switching energy of an IGBT – E_{off}
- Turn-off switching energy of a diode – E_{rec}

An example of the waveforms measured during these tests and the resulting energy loss are shown in Section 6.4.2. The following parameters are required to calculate the conduction loss in a device and these are measured in Section 6.4.3:

- On-state voltage of an IGBT – V_{CE}
- On-state voltage of a diode – V_F

The loss parameters listed above are not constant values, but are dependant on the device current (I_L), temperature (T_j) and DC link voltage (V_{DC}). Therefore, the loss parameters are measured over the full range of operating conditions and this requires multiple tests to be performed.

6.2 Device Selection and Power Module Preparation

To evaluate the thermal model under typical operating conditions the model is implemented in a standard production drive. The drive selected for this evaluation is a Control Techniques Unidrive SP [113], which has a rated continuous output power of 15kW. A picture of this drive and an unmodified power module are shown in Figure 6.1.

Figure 6.1: Control Techniques Unidrive SP and power module

As well as the devices in the inverter stage, the power module used in this drive includes a three phase rectifier and brake IGBT [111]. The rated current of this module is 75A. This rating refers to the maximum continuous output current that is available from the inverter for a given case temperature. As shown, the devices are enclosed within the power module. Therefore, to allow an infrared camera to be used the module must be modified and this is described in the following section.

6.2.1 Power Module Preparation

In the experimental methods described in this chapter the temperature of the devices in the inverter are measured using an infrared camera. To prepare the power module for thermal testing the lid of the module and the internal silicone gel is removed. Afterwards a thin layer of black paint is applied to the surface in order to provide a known and uniform emissivity. A picture of the power module prepared by the manufacturer is shown in Figure

6.2. This figure shows the positions of the devices in the inverter, which are protected by the thermal model, and the internal thermistor used to provide the temperature feedback.

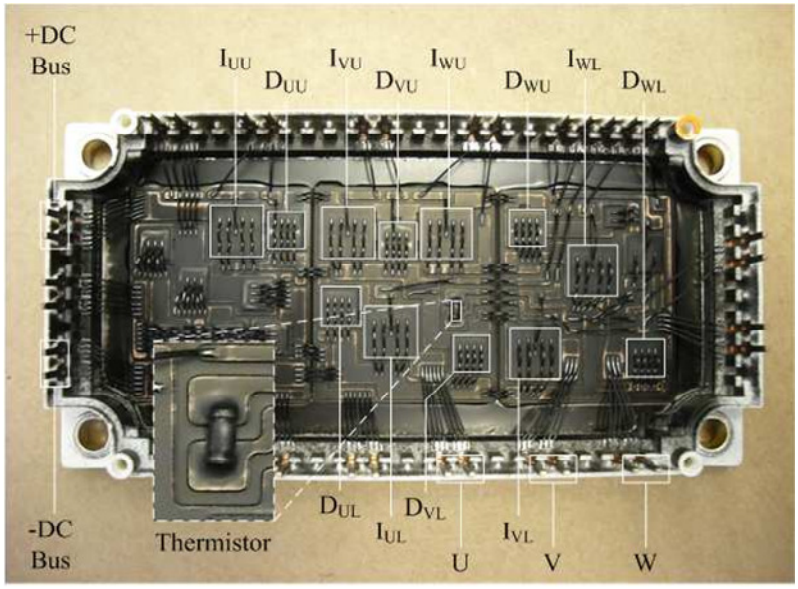

Figure 6.2: Power module after preparation for thermal testing

After the module has been prepared, it is assumed that the emissivity of the surface of each device is constant and has a value of 0.95, which is a typical emissivity for matt black paint [114-116].

6.3 Thermal Impedance Measurements

In the thermal model, the temperature feedback is provided by the internal thermistor in the power module (T_{th}). Using this measurement, the junction temperature (T_j) is estimated using the known power loss (P) and the transient thermal impedance between the device and the thermistor. For example, the self impedance of device *i* can be calculated using:

$$Z_{th,ii(j-th)} = \frac{T_{j(i)} - T_{th}}{P_{(i)}} \quad \text{(K/W)} \tag{6.1}$$

This transient thermal impedance can be calculated from the measured heating or cooling response due to a step change in power loss. However, the properties of an IGBT and diode are highly dependant on the device temperature and this makes it difficult to maintain a

constant power loss in the device as it is being heated [117]. Therefore, in this work, the thermal impedance is calculated from the cooling response, the same technique is used by most manufacturers [118]. In this approach a known power loss is used to heat the device to the desired steady-state temperature. As this temperature is increased the thermal conductivity of the different materials in the device and module fall [119]. Consequently, to ensure that the maximum steady-state thermal impedance (i.e. the thermal resistance) is measured the device is heated to the maximum operating temperature (150°C). Once the temperature has stabilised, the power loss is removed (t=0s) and the temperature of every device, including the internal thermistor, are measured as they decay towards the ambient temperature. An example of a typical cooling response is shown in Figure 6.3(a).

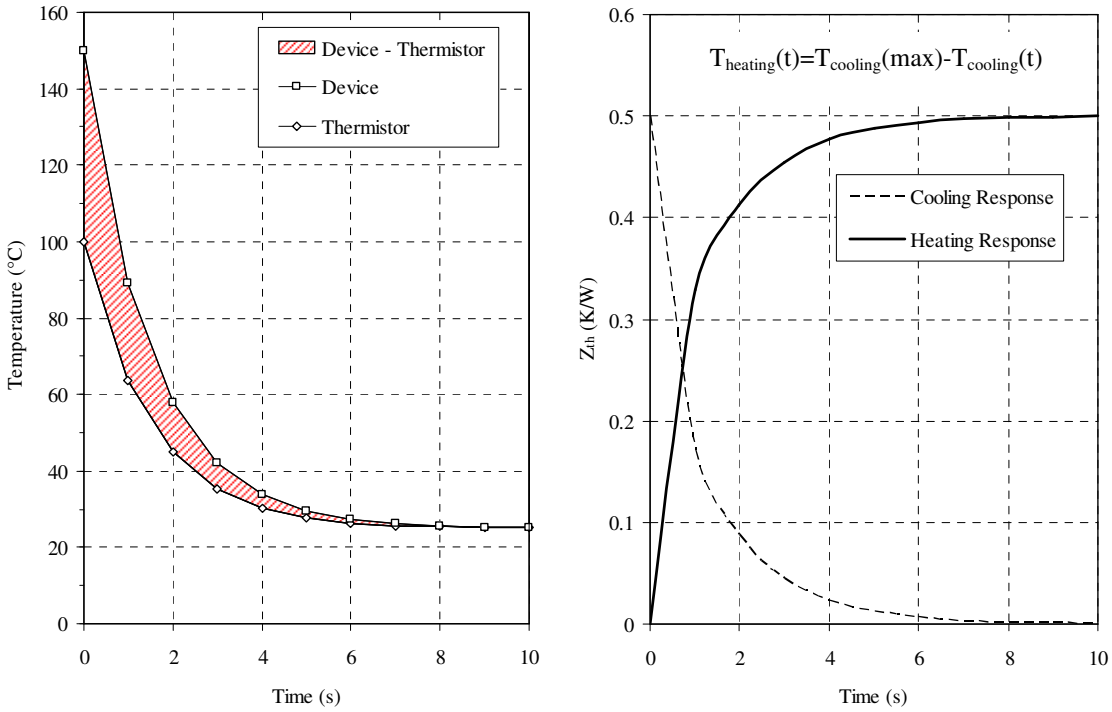

(a) (b)

Figure 6.3: Example of the thermal impedance calculation (a) measured cooling response for the device and thermistor (b) calculated transient thermal impedance

To calculate the transient thermal impedance, the temperature difference measured between the device and the thermistor, which is highlighted in this figure, is divided by the power loss required to heat the device to its maximum temperature. The transient thermal

impedance calculated using the measured cooling response is shown in Figure 6.3(b). However, it is more conventional to present the results in the form of a heating response and both are compared in this figure. In this example, a power loss of 100W is used to heat the device. As a result, the steady-state thermal impedance is 0.5K/W.

6.3.1 Experimental Setup

When measuring the thermal impedance it is important that the thermal characteristics of the system are as close as possible to those that will be experienced by the device during normal operation. Therefore, the heatsink, fan and fan speed used in the thermal impedance measurements must be the same as those used in a standard drive. However, to measure the device temperature using an infrared camera the lid of the power module and the internal silicone gel has been removed. The silicone gel in a module is not intended to provide an additional cooling path, and typically has a relatively low thermal conductivity of between 0.2 and 0.3W/mK [120]. However, removing the gel will allow the convection of heat from the surface of a device, changing its thermal characteristics. Nevertheless, in this work, the thermal impedance is measured using the same power module that is used to evaluate the thermal model. Therefore, in both of these experiments the thermal characteristics will be identical. Even so, when applying the thermal model to a standard power module the thermal impedances may be different. This effect will be reviewed as part of the further work. A schematic diagram of the experimental setup used to measure the thermal impedances in the inverter stage of the power module is shown in Figure 6.4.

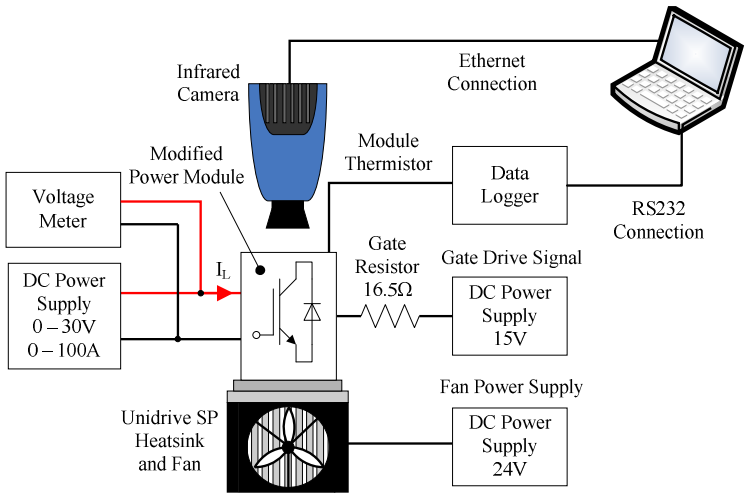

Figure 6.4: Equipment setup used to measure the transient thermal impedance

In this diagram, it can be seen that an external power supply is used to apply a DC current (I_L) to the device under test. This current and the resulting conduction loss in the device, which is calculated using the voltage and current measured at the terminals of the power module, is used to heat the device to its maximum operating temperature. When measuring the thermal characteristics of an IGBT, the device is turned on by a constant gate voltage (+15V) from a second power supply. This is shown in the circuit diagram in Figure 6.5.

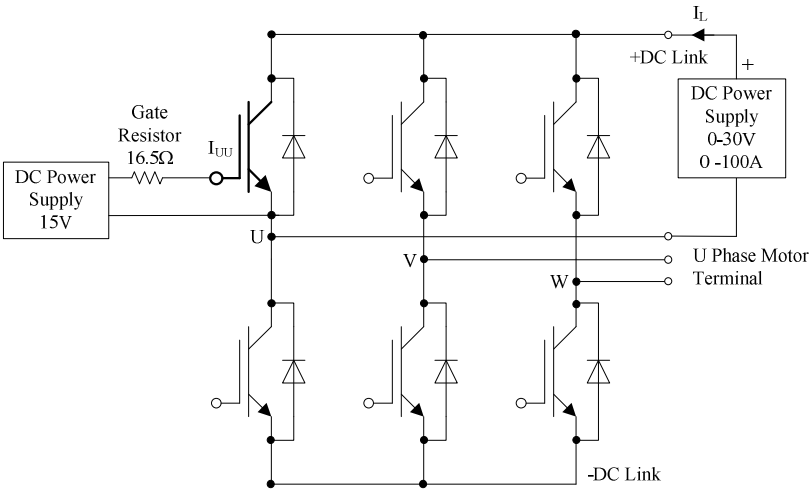

Figure 6.5: Test circuit for the thermal impedance measurements

In this example the external power supply is connected between the +DC link and the U phase motor terminals (current flows into the +DC link) and the circuit is configured to measure the thermal impedance of I_{UU}. In order to measure the thermal impedance of the parallel diode associated with this IGBT (D_{UU}) the connections on the supply are reversed.

6.3.1.1 Temperature Measurements

In the thermal impedance measurements the temperature of the thermistor and the devices in the inverter are measured using the following methods.

Thermistor Temperature

The temperature of the thermistor (T_{th}) is calculated from the measured resistance using the resistance-temperature characteristics provided by the manufacturer [121]. In the transient measurements, this resistance is measured using a data logger [122] and is recorded at a sample frequency of 4Hz.

Device Temperature

The surface temperature of the IGBTs and diodes are measured using an infrared camera [123] and in the calculation of the thermal impedance, this temperature is referred to as the junction temperature of the device (T_j). In these measurements, the maximum sample rate of the camera is limited to approximately 500Hz. An example of the thermal image for an IGBT and diode measured during steady-state operating conditions is shown in the figure below:

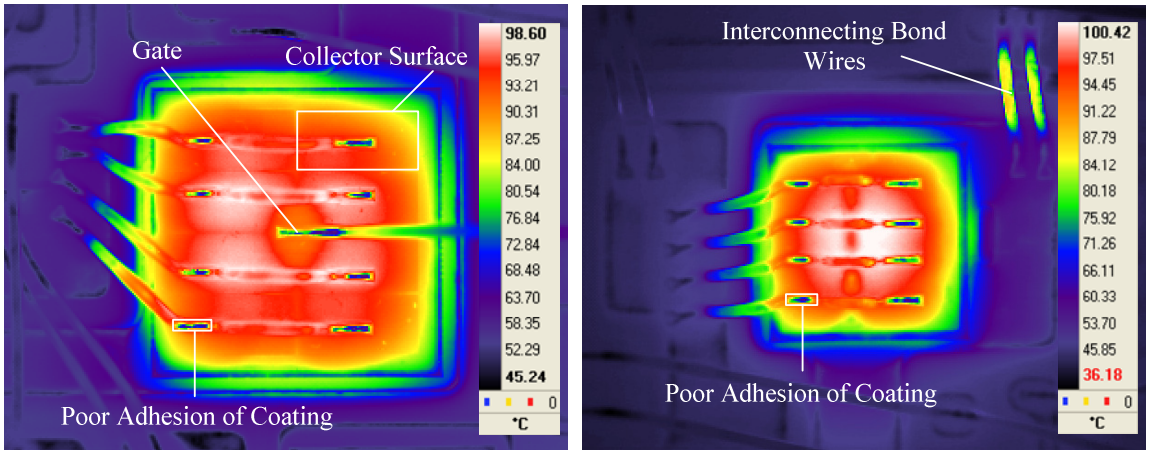

(a) (b)

Figure 6.6: Example of the measured surface temperature for (a) IGBT and (b) diode

In the image of the IGBT, the cooler region of the gate, which is located at the centre of the device, and the individual elements of the collector metallization to which the bond wires are attached is just visible. The cooler regions (dark blue) seen on the bond wires in both images are caused by the poor adhesion of the black coating in the areas where they are soldered to the surface of the device. This reduces the emissivity in these areas and subsequently the temperature measured by the infrared camera.

6.3.2 Calculation of the Self Thermal Impedance

As shown in the previous example, using an infrared camera allows the temperature at any point on the surface of a device to be measured. Nevertheless, in order to calculate the thermal impedance a discrete temperature must be selected. When using an infrared camera, this temperature can be the mean or maximum temperature measured over a

specified area of the device. However, given that the main aim of the thermal model is to protect the inverter by preventing a device from exceeding its maximum temperature, the self thermal impedance is calculated using the maximum temperature measured over the entire surface of a device (i.e. the hotspot). This will give the highest thermal impedance.

6.3.2.1 Results and Comparison

The measured cooling temperatures and the calculated self transient thermal impedance for the upper IGBT in the U phase of the inverter (I_{UU}) are shown in Figure 6.7. During the initial cooling period the temperature of the IGBT falls rapidly, although due to the longer thermal time constants associated with the case of the power module, the temperature of the thermistor is almost constant over this initial period (t<2s).

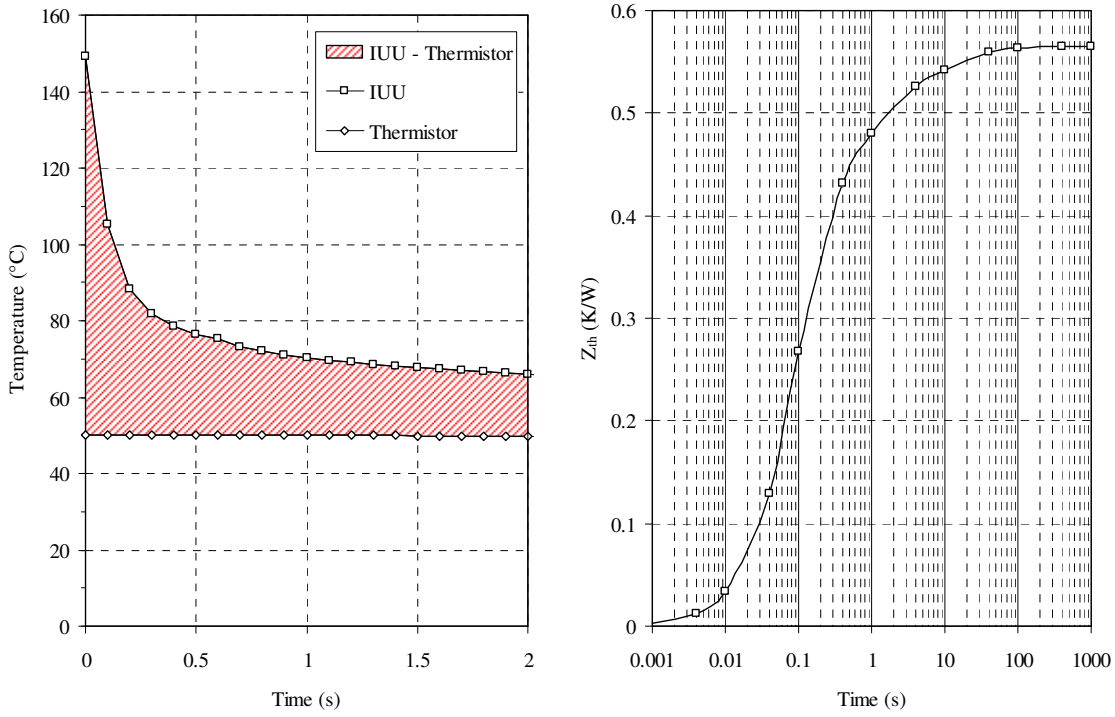

(a) (b)

Figure 6.7: Self thermal impedance calculations (a) measured cooling temperatures (b) transient thermal impedance between the device and thermistor

The self thermal impedance calculated from the measured cooling response is shown in Figure 6.7(b). From this figure, it can be seen that the steady-state thermal impedance or thermal resistance for I_{UU} is 0.56K/W. However, the thermal impedance used in the thermal

model is dependant on the distance between a device and the internal thermistor. Therefore, for most power modules the thermal impedance of each device will be different. To show this, the thermal resistance between the IGBTs and the internal thermistor, measured with the cooling fan on and off, are compared against the published datasheet value and this comparison is shown in the figure below:

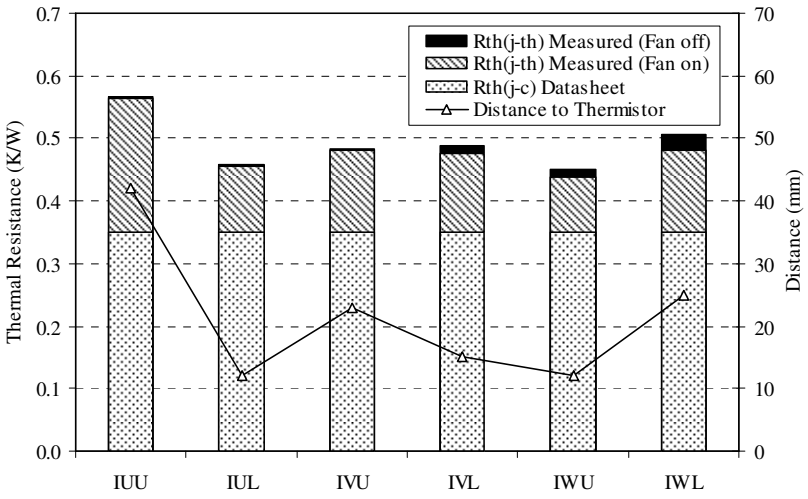

Figure 6.8: Comparison of the measured ($R_{th,ii(j-th)}$) and datasheet ($R_{th(j-c)}$) self thermal resistance for the IGBTs in the inverter

The thermal impedance in the datasheet of a device is normally measured between the junction and the case directly under the device [71, 124]. Consequently, when using this value it must be assumed that the temperature of the case and the thermistor are identical. Furthermore, due to the expected degradation of the thermal resistance over the lifetime of the device the thermal resistance in the datasheet will include a safety margin in the order of 20% [125, 126]. However, despite this margin, the results in Figure 6.8 show that the thermal resistance measured between an IGBT and the thermistor is significantly higher than the datasheet value. This indicates that the temperature measured by the thermistor is much lower than the temperature of the case directly under the device. Thus, when developing a thermal model it should never be assumed that the temperature of the case and the thermistor are the same. This comparison highlights the major limitation of the thermal impedance quoted in a datasheet and a similar conclusion was made in [1].

Despite a significant change in the heatsink temperature, the results in Figure 6.8 show that when the cooling fan is turned off the thermal resistance measured between the device and the thermistor is only slightly increased. Consequently, in this power module, the effect of the fan speed can be ignored and the thermal model is developed using the values measured with the fan operating at its nominal speed. However, in different power modules and/or configurations, the fan speed may have a significant effect on the measured thermal impedances. If this is true, this effect cannot be ignored.

The self thermal impedances for the diodes in the inverter are measured using the same approach and for completeness, a similar comparison is shown in Appendix B.

6.3.2.2 Internal Parasitic Resistance

As discussed, the power loss in a device is calculated using the voltage and current measured at the terminals of the power module. However, in a power module there will be an internal parasitic resistance between each device and the terminals. This includes the resistance of the terminals, copper tracks, aluminium bond wires and the various connections within the module. When calculating the thermal impedance the parasitic resistance will have the following effects:

a) The power loss that is calculated using the voltage and current measured at the terminals of the power module will include the power loss in the parasitic resistance.
b) The measured device temperature will include the temperature rise due to any mutual thermal coupling between the parasitic resistance and a device.

Because of the parasitic resistance, some manufacturers provide two on-state voltages for an IGBT in the datasheet, one measured directly across the device and another measured across the terminals of the module. Comparing these values will give an indication of the internal resistance in the power module. However, the parasitic resistance is highly dependant on the position of a device and more specifically, its proximity to the terminals of the module. Therefore, in order to calculate the power loss in a device, the parasitic resistance between each device and the terminals must be measured. This resistance is

measured using the same experimental setup as the thermal impedance, although in these measurements the voltage is measured between a device and the terminals. These tests were performed with a device conducting the rated current of the module, which in this instance is 75A. The locations of the resistances measured in a single phase of the inverter are shown in the figure below:

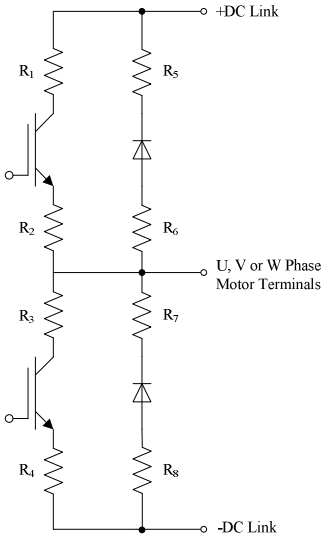

Figure 6.9: Definition of the internal parasitic resistance in a single phase of the inverter

From this figure, it can be seen that if the on-state voltage is measured at the terminals of the module, each measurement will include the voltage drop across two parasitic resistances. The resistances (R_1 to R_8) measured in each phase are shown the table below:

Table 6.1: Internal Resistance

Motor Output	Resistance (mΩ)							
	R_1	R_2	R_3	R_4	R_5	R_6	R_7	R_8
U	0.81	2.03	0.74	2.09	0.88	1.81	0.83	1.85
V	1.93	2.36	0.83	3.41	1.93	2.23	1.89	2.37
W	2.55	2.09	1.09	4.08	1.59	1.42	0.75	4.15

For the module used in this drive, the maximum parasitic resistance is measured between the terminals and the lower IGBT in the W phase of the inverter (R_3 and R_4). The total resistance for this device is 5.17mΩ. At rated current, the voltage drop across this resistance will be 0.39V. This equates to an additional power loss of 29W. Therefore, if the voltage

drop across the parasitic resistance is ignored, the power loss used in the thermal impedance calculations will be significantly higher than the true power loss in the device. Consequently, the calculated thermal impedance will be reduced and will result in an underestimation of the device temperature. Thus, to calculate the power loss in a device, the voltage drop across the parasitic resistance must be subtracted from the voltage measured at the terminal of the power module. This voltage drop can be calculated using the resistances in Table 6.1, which were measured at an ambient temperature of 23°C and at the rated current of the module. However, the temperature coefficient of resistance, for both copper and aluminium is $3.9e^{-3}K^{-1}$ [127] and a change in temperature of 25°C will result in a 10% change in the internal resistance. Although, even at rated current, this equates to no more than 2.2% of the nominal on-state voltage of a device. A detailed analysis of the parasitic resistance in a power module, which includes the effect of temperature is given in [128]. In this work the dependency of the parasitic resistance with temperature is ignored. This approximation allows the values in Table 6.1 to be used in the power loss calculation.

In addition to the voltage drop, any thermal coupling that exists between a device and the internal resistance (mutual thermal coupling) will be incorporated into the measured thermal impedance, i.e. the measured temperature will include the temperature rise due to the mutual coupling from the parasitic resistances. The impact that this has on the measured thermal impedance will depend on the magnitude of this coupling. To investigate this, the temperature of the interconnecting bond wires has been measured when one of the diodes in the inverter is operating at the rated current of the module. Under this condition, the power loss in the bond wires will be at its maximum. The thermal image taken using the infrared camera and the temperature profiles measured along the upper surface of the DCB and diode are shown in Figure 6.10. From the temperature measured along profile A, it can be seen that although the power loss in the parasitic resistance is sufficient to significantly increase the temperature of the bond wires, the temperature measured either side of the connections to the DCB falls rapidly. Therefore, from the results shown in Figure 6.10(b), it can be concluded that the thermal coupling between the parasitic resistance and a device does not have a significant effect on the measured device temperature. As a result, when calculating the thermal impedance the effect of the thermal coupling between the parasitic resistance and a device can be ignored.

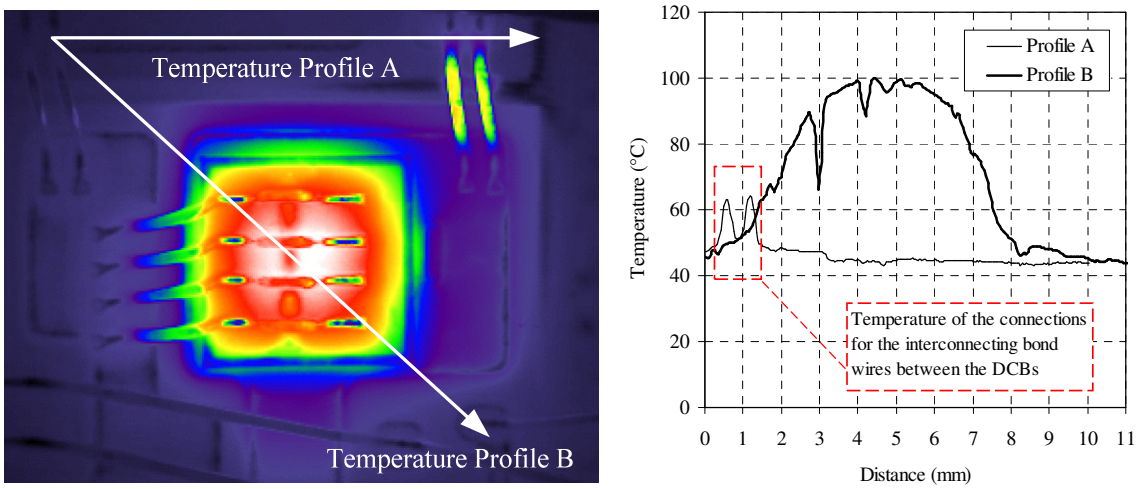

(a) (b)

Figure 6.10: Investigation into the effect of the mutual coupling between the parasitic resistance and a device (a) thermal image with profiles (b) measured profile temperature

In summary, to calculate the thermal impedance using the voltage and current measured at the terminals of the power module, the following factors are considered:

a) **Device power loss** – To avoid underestimating the device temperature, the voltage drop across the internal parasitic resistance is subtracted from the voltage measured at the terminals of the module. This voltage is then used to calculate the power loss.
b) **Change of resistance with temperature** – Compared to the on-state voltage of the device, the voltage drop attributed to the change in the internal resistance with temperature is negligible. Therefore, the voltage drop across the parasitic resistances is calculated using the measured resistances in Table 6.1.
c) **Mutual thermal coupling** – The temperature rise due to the thermal coupling between the parasitic resistance and a device (including the thermistor) does not have a significant effect on the calculated thermal impedance and this is ignored.

6.3.3 Calculation of the Mutual Thermal Impedance

To measure the mutual thermal impedance an infrared camera is used to measure the temperature of every device in the inverter simultaneously. To calculate the mutual thermal impedance a discrete device temperature must be selected. However, due to the thermal

coupling between the neighbouring device(s) in the power module the temperature distribution measured over the surface of a device is dependant on the following:

a) Distance between the devices and the location of the thermistor
b) Operating conditions and the resulting power loss in each device (e.g. current, voltage and temperature)

To illustrate the effect that the distance between the devices has on the temperature distribution, the temperature is measured across the centre of the upper IGBT in the U phase (I_{UU}) of the inverter when it is operating under self and mutual heating conditions. The measured temperatures, which are normalised to the maximum temperature measured over the complete surface of the device (T_{max}), are compared in Figure 6.11(a). In this figure, the temperature rise due to the mutual heating from a neighbouring device is measured when a power loss is applied to the diodes D_{UU} and D_{WL}.

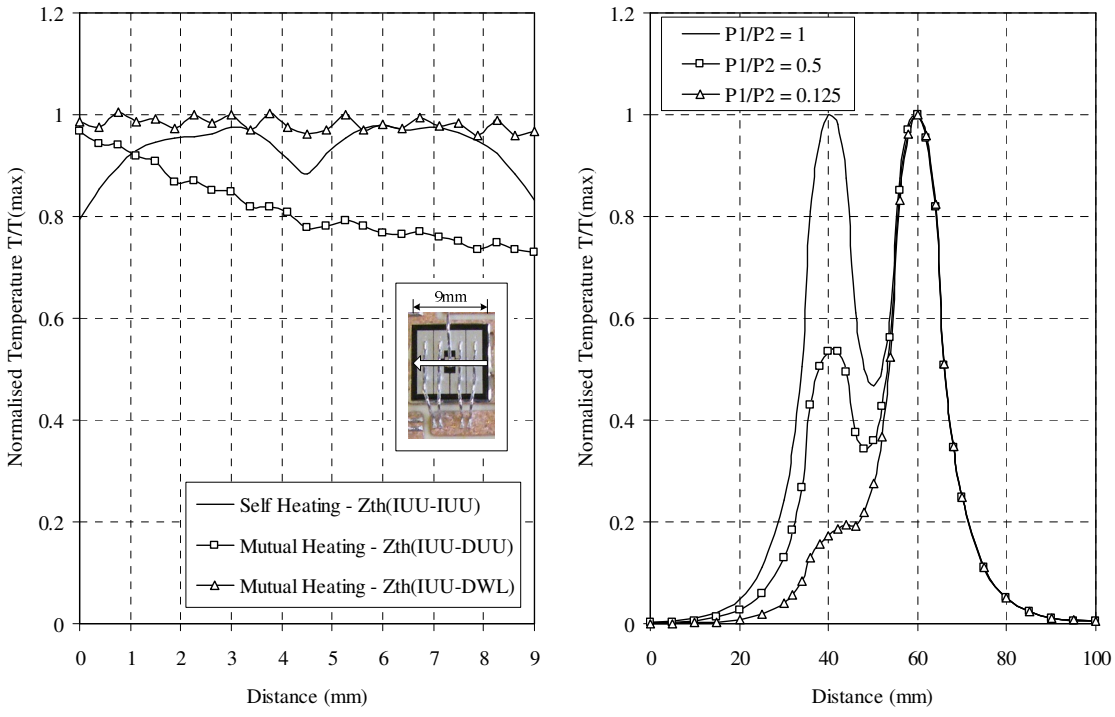

(a) (b)

Figure 6.11: Normalised temperature distribution showing the effects of the (a) distance between the devices (b) operating conditions and power loss in each device

Under the self heating conditions where the power loss is applied to I_{UU}, the maximum temperature is measured between the gate located at the centre of the IGBT and the edge of the device. However, when the power loss is applied to D_{UU}, which is the nearest device to I_{UU}, a significant temperature gradient exists across the device and the maximum temperature is measured at the edge closest to D_{UU}. Alternatively, when the power loss is applied to D_{WL}, which is the device furthest from I_{UU}, the temperature profile is almost constant. Consequently, if the maximum temperature is used to define the mutual thermal impedance, under some conditions the thermal model will significantly overestimate the device temperature. Furthermore, the power loss in each device will have an effect on the temperature distribution. In order to show this effect, the temperature along the upper surface of the simple heat spreader in Figure 6.12 is calculated under different power loss conditions. The results from this investigation are shown in Figure 6.11(b).

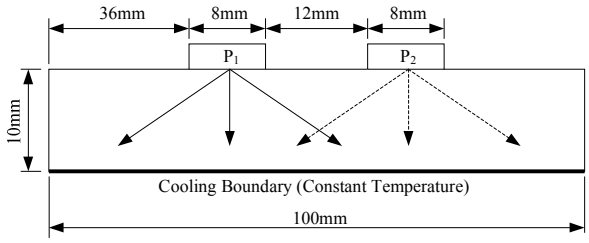

Figure 6.12: Heat spreader with two heat sources

Initially, when the power loss in each device is the same (P_1=P_2) the self heating in the device dominates the temperature rise and the maximum temperature is measured at the centre of device 1 (40mm). However, the temperature profile changes as the effect of mutual coupling between the devices becomes more significant (P_1<<P_2). In this condition, the location of the maximum temperature moves towards the edge of the device (44mm).

In summary, the results in this section show that the temperature distribution for each device in the inverter is different and will continuously change with the operating conditions. However, the temperature of an active device is dominated by its self heating (self thermal impedance). Thus, any error caused by the definition of the mutual thermal impedance is less significant. Therefore, to allow a simple and consistent definition to be used for every device, the mutual thermal impedance is calculated using the mean surface

temperature. This definition is a compromise between the protection offered by the thermal model and the maximum performance of the drive.

6.3.3.1 Comparison and Results

An example of the measured cooling temperature and the mutual transient thermal impedance measured when a power loss is applied to the upper IGBT in the U phase (I_{UU}) is shown in Figure 6.13. Unlike the self thermal impedance, when calculating the mutual thermal impedance the temperature of every device in the inverter is measured simultaneously, although in this example the temperature of only two devices is shown.

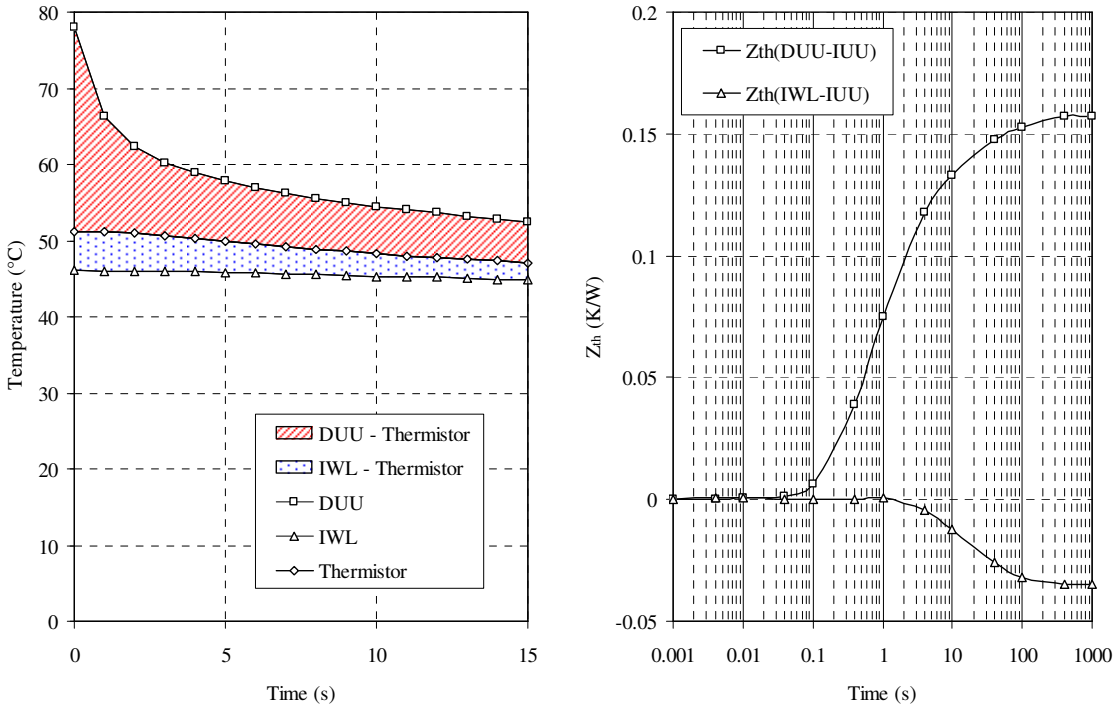

(a) (b)

Figure 6.13: Mutual thermal impedance calculation (a) measured cooling temperature (b) transient thermal impedance between the device and thermistor

In Figure 6.13(a), it can be seen that when a power loss is applied to I_{UU} the mean temperature measured on the surface of D_{UU} is higher than the thermistor. Consequently, the thermal impedance calculated between this device and the internal thermistor is positive. However, as shown in Figure 6.2, the distance between I_{UU} and the thermistor is

smaller than the distance between I_{UU} and I_{WL}. Thus, when I_{UU} is heated the temperature measured by the thermistor will be higher than I_{WL}. As a result, the calculated mutual thermal impedance will be negative.

The mutual thermal resistance between I_{UU} and the five other IGBTs in the inverter are shown in Figure 6.14. In this figure, it can be seen that the mutual thermal impedance is negative for any device that is further from I_{UU} than the thermistor, i.e. a distance between devices greater than 42mm. In addition, the results show that the fan speed has a greater impact on the measured thermal resistance as the distance between the devices is increased. This characteristic is caused by the change in the temperature gradient across the surface of the heatsink and the case of the power module, which is dependant on the speed of the cooling fan.

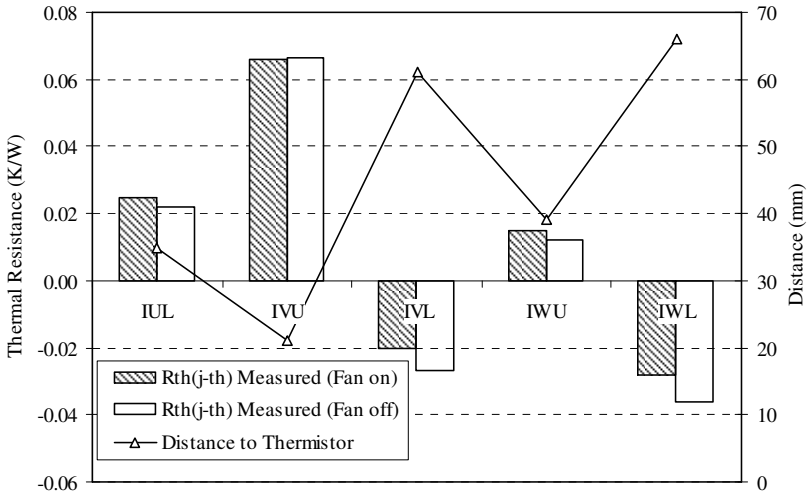

Figure 6.14: Mutual thermal impedance measured when a power loss is applied to I_{UU}

When the fan is turned off, the measured mutual thermal impedance is in general smaller than the impedance measured with the fan operating at its nominal speed. Therefore, if it is assumed that the fan is always on the thermal model will overestimate the device temperature. Consequently, as with the self thermal impedance, the thermal model is developed using the thermal impedances measured with the fan on. The mutual thermal resistance for every device in the inverter is compared in Appendix B.

In the previous sections, the procedures used to calculate the self and mutual transient thermal impedances have been described and the key results have been compared. In order to calculate the thermal impedance several decisions have been made that could have a significant effect on the calculated values; these include the choice of the discrete device temperature, the use of the cooling or heating response and the parameters used to calculate the power loss. Where possible, the values used to calculate the thermal impedance have been selected to avoid any significant under or overestimation of the device temperature.

6.4 Loss Parameter Measurements

The loss parameters measured for a device are used by the thermal model to calculate the conduction and switching loss under any operating condition and these calculations are performed on-line. The parameters required by the thermal model are measured using the experimental setup described in the next section.

6.4.1 Experimental Setup

In an inverter, the measured turn-on energy of an IGBT must include the additional switching energy due to the reverse recovery current in the anti-parallel diode and this requirement defines the test circuit and procedure. The test circuit used to measure the loss parameters is shown in Figure 6.15. In this figure, a load inductor is connected between the U phase motor terminal and the positive DC link terminal of the power module; this inductor is required to provide a constant load current during the switching event.

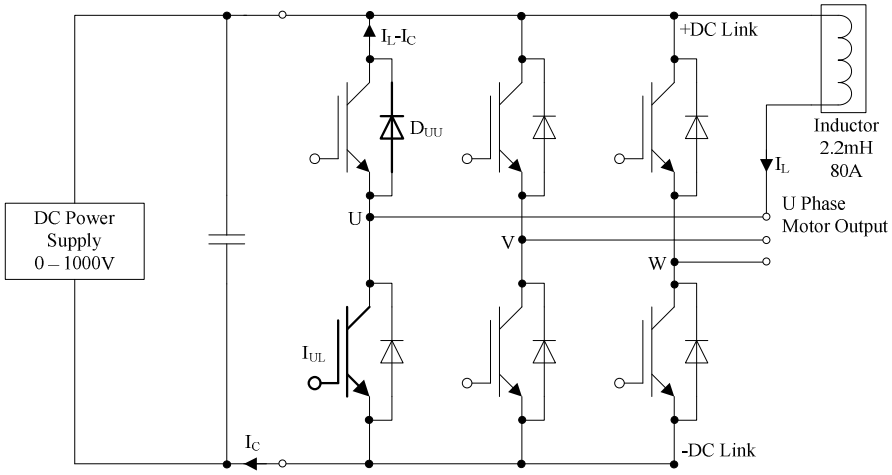

Figure 6.15: Test circuit used to measure the switching and conduction loss parameters for the lower IGBT (I_{UL}) and upper diode (D_{UU}) in the U phase of the inverter

This particular configuration allows the loss parameters to be measured in the lower IGBT and the upper diode in the U phase. The loss parameters must be measured over the full range of operating conditions and in the experimental setup the DC link voltage, temperature and switching current are controlled using the following methods:

- **DC link voltage (V_{DC})** – The voltage is controlled by a high voltage power supply connected directly to the DC link terminals of the power module (0-1000V).
- **Temperature (T_j)** – The entire power module is heated by a power resistor attached to the case of the module (I^2R heating).
- **Current (I_L)** – The current is controlled by varying the on-time of the IGBT in the test circuit. In Figure 6.15 the active IGBT is I_{UL}.

In the circuit configuration shown in Figure 6.15, the current in the IGBT (I_C) is measured directly using a current transducer placed in the negative DC link connection between the inverter and the DC link capacitance. During these tests, the current in the anti-parallel diode cannot be measured directly and is calculated by subtracting the IGBT current from the measured load current (I_L). Unlike the thermal impedance measurements, the voltage across the device is measured between the emitter terminal of the IGBT and the power terminal of the module (DC link or motor). This minimises the effect that any internal stray inductance in the power module has on the voltage measured during the switching events.

6.4.2 Switching Loss Parameters

As discussed in Chapter 2, when compared to the other losses in the inverter the turn-on loss in a diode is insignificant and is usually ignored. Therefore, the switching loss parameters used in the thermal model are:

- Turn-on switching energy of an IGBT – E_{on}
- Turn-off switching energy of an IGBT – E_{off}
- Turn-off switching energy of a diode – E_{rec}

To allow the power loss to be calculated in any operating condition, these parameters are measured over the range of conditions shown in Table 6.2. In each of these, the switching

energy is measured several times and the average energy is used to generate the input parameters for the thermal model, which is described in the next chapter.

Table 6.2: Switching loss measurement conditions

Parameter			Minimum	Step	Maximum
Current	I_L	(A)	5	5	75
Voltage	V_{DC}	(V)	500	25	800
Temperature	T_j	(°C)	25	25	150

As well as the parameters that are shown in Table 6.2, the switching loss in an inverter is highly dependant on the stray inductance in the switching circuit and the gate drive parameters, in particular the gate resistance (R_G) and the gate-to-emitter voltage (V_{GE}). Therefore, when measuring the switching energy it is important that the circuit configuration (i.e. the stray parameters) and gate drive parameters are as close as possible to the values used in the final application. In this work, the temperature of the devices in the power module are measured using an infrared camera and in order to provide visual access to the devices, the module is operated outside of the drive. Thus, in order to compare the measured temperature with the output of the thermal model (these results are shown in Chapter 8) the switching energy must be measured in this exact configuration. However, if the thermal model is to be implemented in a standard drive the switching energy must be recalculated, although the thermal parameters will not change.

6.4.2.1 Measurement and Comparison

To measure the switching energy the load current in the inductor is increased to the desired level by turning on the IGBT in the test circuit for a specified period. The IGBT is then switched and the current and voltage in both the IGBT and diode are measured during the switching event, this process is described in more detail in Appendix C. To minimise the risk of damaging the modified power module during these tests, the switching energy and on-state voltage are measured using a standard module. These measurements are taken from the lower IGBT (I_{UL}) and the upper diode (D_{UU}) in the U phase of the inverter. In order to validate these, tests are repeated on the modified power module in a few key operating conditions. An example of the measured switching waveforms and the resulting switching energy for the IGBT and diode are shown in Figure 6.16.

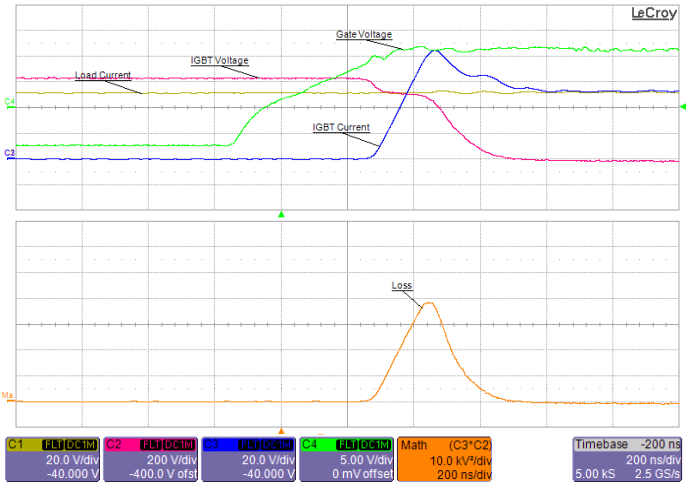

(a)

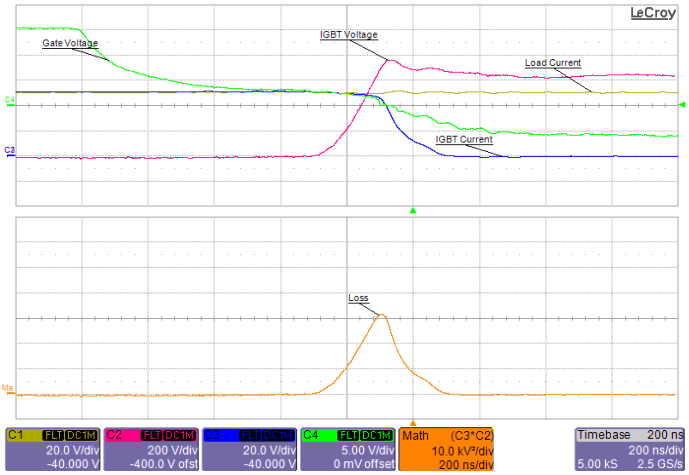

(b)

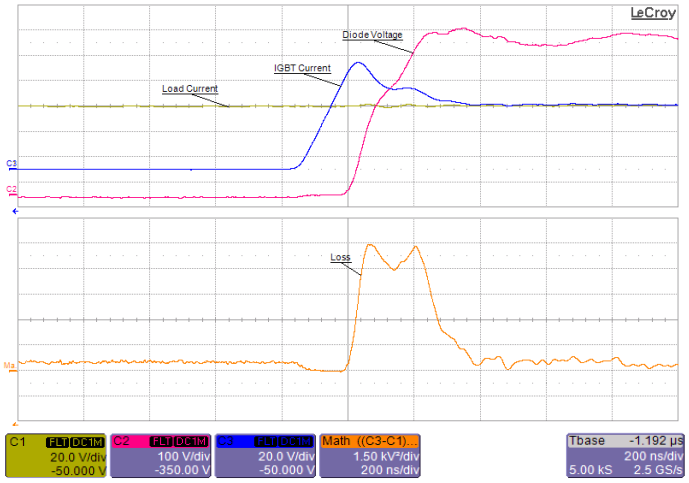

(c)

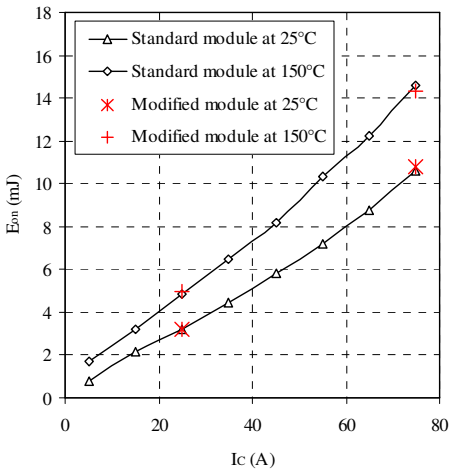

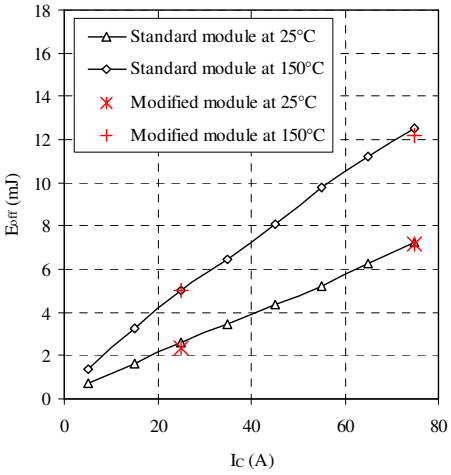

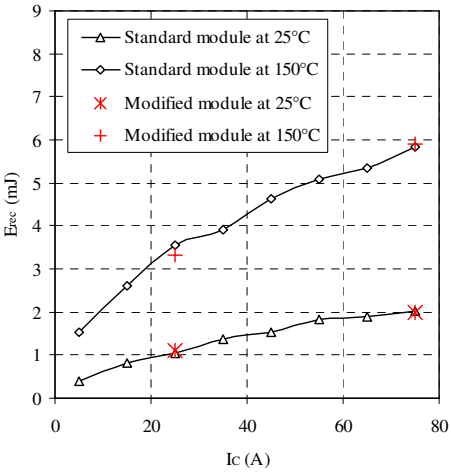

Note: Measurements made using Lecroy Wave Runner 6050A Oscilloscope and Person 411 current monitor

Figure 6.16: An example of the switching characteristics (I_L=50A, V_{DC}=600V, T_j=25°C) and the measured energy loss (a) IGBT turn-on (b) IGBT turn-off (c) diode turn-off

This figure includes a comparison of the switching energy measured on a standard and modified power module. From this comparison, it is evident that the measured switching energy in both modules is similar. Therefore, in order to evaluate the thermal model the values measured using the standard power module can be used to estimate the power loss. However, the switching energy measured in the IGBT is significantly higher than the values in the datasheet of the device. These are compared in the table below:

Table 6.3: Comparison of the datasheet and measured switching energy with a current of 75A, DC link voltage of 600V and a device temperature of 125°C

Loss Parameter	Energy Loss (mJ)	
	Datasheet Value R_G=5Ω L_s = 45nH	15kW Unidrive SP with external IGBT R_G=16.5Ω L_s = 225nH
E_{on}	9.4	13.3
E_{off}	9.4	11.2
E_{rec}	6.5	4.6

The reasons for the higher switching energy seen in the IGBT are the larger gate resistance and stray inductance in the test circuit, which have a significant effect on the switching characteristics. Although, as shown, slowing the IGBT reduces the peak reverse recovery current in the diode, and subsequently the turn-off energy in this device. The full results from the switching loss measurements are shown in Appendix D.

As expected, due to the temperature dependency of the device parameters, the switching energy increases with temperature. The key device parameters that affect the switching loss include the switching times, tail current of the IGBT and the reverse recovery current of the diode, which all increase with temperature. However, as shown in the datasheet of the device [111], the turn-on time of an IGBT does not change significantly. Therefore, the increase in the measured turn-on energy of the IGBT is due almost entirely to the increase in the reverse recovery current of the anti-parallel diode [129]. Therefore, the switching energy estimated from the experimental results will only be correct when the temperature of an IGBT and the anti-parallel diode are identical. In most applications the IGBT will be much hotter than the diode and the power loss and temperature will be overestimated. However, it is not possible to heat each device individually and this makes it difficult to

separate the effect that the characteristic of the diode has on the turn-on energy in the IGBT. Consequently, this error is unavoidable.

As illustrated in Figure 6.16, the switching loss is measured using a standard power module and these results are compared with those taken from the modified module in some key operating conditions. For these power modules, the measured switching energy is comparable. However, due to the variations in the internal stray inductance and the manufacturing tolerances in the devices, the switching loss can vary between devices. An indication of the potential tolerances can be seen in the datasheet of a device, where normally the manufacturer provides a typical and maximum switching loss. In some instances, the maximum loss can be up to 35% higher than the typical value [130]. Whereas, using the typical values could result in the underestimation of this temperature. Therefore, before the thermal model can be implemented in a production drive, where it is not practical to measure the characteristics of each device in every power module, the tolerances associated with the switching losses and the other key parameters must be understood and incorporated into the thermal model.

6.4.3 Conduction Loss Parameters

In the thermal model, the conduction loss is calculated on-line and the following device parameters must be known:

- On-state voltage of an IGBT – V_{CE}
- On-state voltage of a diode – V_F

In normal operating conditions the power loss due to the leakage current in a device (blocking state) is insignificant and in this work it is ignored. Although, when operating at elevated temperatures (normally outside of the recommended limits) this loss can lead to thermal runaway and the failure of the device [20].

The on-state voltage of an IGBT and diode is measured as the load current is increased to its rated value. This test must be repeated at each temperature. This process is described in more detail in Appendix C. In these measurements, an oscilloscope is used to measure the

on-state voltage and the device current at the terminals of the modified power module. However, in an inverter, the blocking voltage is significantly higher than the on-state voltage of a device, making it difficult to measure this voltage directly. Therefore, in these measurements the input to the oscilloscope is clamped using a saturation voltage tester, which is connected between the terminals of the device and the oscilloscope. The saturation tester used in these measurements was built to the specifications outlined in [131].

6.4.3.1 Measurement and Comparison

To calculate the on-state voltage of a device from the voltage measured at the terminal of the module, the voltage drop across the parasitic resistance (between the collector and power terminal) is calculated using the resistances in Table 6.1. As in the thermal impedance measurements, this voltage is then subtracted from the terminal voltage. However, the dependency of the parasitic resistance with temperature will have an impact on the accuracy of these measurements. As described in Section 6.3.2.2, when compared to the on-state voltage of the device the change in the voltage drop across the internal resistance due to a change in temperature is insignificant. Even so, to validate these measurements the on-state voltage for the IGBT and diode, measured at the rated current, are compared against the typical datasheet values. This comparison is shown in the table below:

Table 6.4: Comparison of measured and datasheet on-state voltage for an IGBT and diode

	IGBT $V_{CE(sat)}$ (V)		Diode V_F (V)	
Temperature (°C)	25	125	25	125
Measured	1.77	2.04	1.59	1.66
Datasheet	1.7	2	1.65	1.65

The results in this table show that the measured on-state voltage and the values presented in the datasheet for the power module are in agreement. Therefore, the measured values are used to estimate the conduction loss in the thermal model.

An example of the measured on-state voltage for the IGBT and diode is shown in Figure 6.17. The IGBT used in the power module is a Trench-cell (Field-Stop) [132, 133]. This type of device exhibits similar characteristics to those of an NPT device.

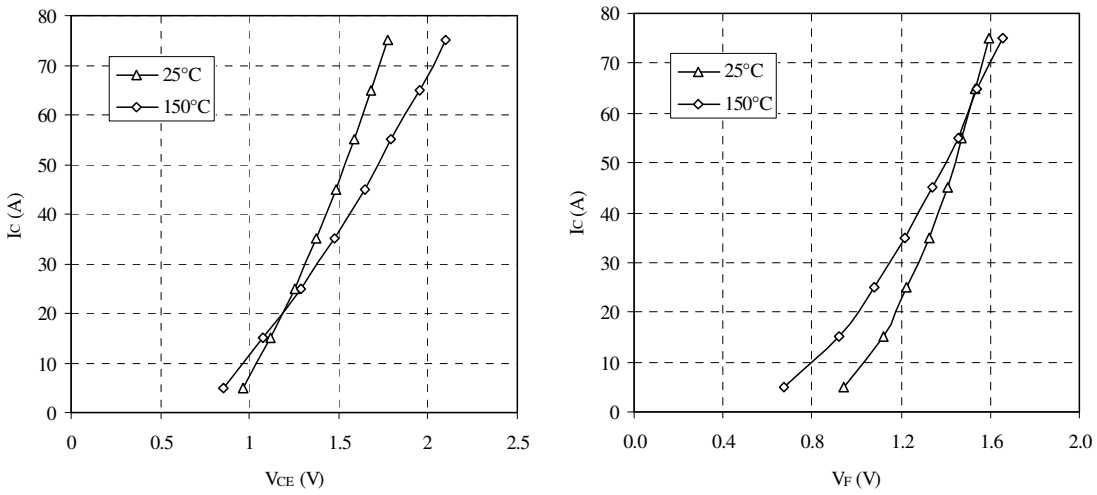

(a) (b)

Figure 6.17: Measured on-state voltage (a) IGBT (V_{CE}) (b) diode (V_F)

These results show that apart from when operating at a low current ($I_c \leq 20A$), the on-state voltage of the IGBT increases with temperature, i.e. the device has a positive temperature coefficient. Conversely, apart from at high currents ($I_c \leq 65A$), the diode has a negative temperature coefficient. The full tables of the measured on-state voltage for an IGBT and diode are shown in Appendix D.

6.5 Summary

To implement the thermal model a number of input parameters that cannot be determined directly from the datasheet of a device are required. Therefore, in this chapter the test methods used to measure the following parameters were described:

Thermal Impedance Parameters

- 12 self thermal impedances $Z_{th,ii(j\text{-}th)}$
- 132 mutual thermal impedances $Z_{th,i\neq i(j\text{-}th)}$

Electrical Parameters

- IGBT turn-on energy $E_{on}(I_L,T_j,V_{DC})$
- IGBT turn-off energy $E_{off}(I_L,T_j,V_{DC})$
- Diode turn-off energy $E_{rec}(I_L,T_j,V_{DC})$
- IGBT on-state voltage $V_{ce}(I_L,T_j)$
- Diode on-state voltage $V_f(I_L,T_j)$

In the measurement of these parameters some key decisions were made that can have a significant impact on the temperature estimated by the thermal model. This includes the definition of the temperature used to calculate the self and mutual thermal impedance, which due to the thermal coupling between the devices is not straightforward. Therefore, based on the analysis performed in this chapter, the self and mutual thermal impedances have been calculated using the maximum and mean surface temperatures respectively. Furthermore, results have shown that the fan speed has an impact on the temperature measured between a device and the internal thermistor. However, for the power module used in this investigation this effect was shown to be negligible. Consequently, the thermal impedances were calculated using the temperature measured with the fan operating at its nominal speed.

Using the methods outlined in this chapter, all of the parameters were measured over the full range of operating conditions that the inverter might experience during normal operation. However, many of the measured parameters cannot be used directly by the thermal model and the methods used to process these measurements are described in the next chapter.

Chapter 7: Calculation of the Thermal Model Input Parameters

7.1 Introduction

In the previous chapter, the experimental methods used to measure the transient thermal impedance and the loss parameters for every device in the inverter were described. However, the measured values cannot be used directly by the thermal model. Therefore, in this chapter the methods used to process the measured data and calculate the input parameters required by the thermal model are discussed.

In the thermal model, the power loss in an IGBT and diode is calculated on-line. This calculation is divided into two parts, the calculation of the switching and conduction loss. By using interpolation, these losses could be estimated directly from the measured values, which have been measured over the full range of operating temperature, DC link voltage and current. However, the available resource restricts the amount of input data that can be used in the thermal model. Thus, it is not possible to use large tables of input data. Therefore, in order to calculate the power loss the measured switching loss (3x624 values) and on-state voltage (2x48 values) are each represented by a polynomial expression with 12 coefficients. The method used to calculate the coefficients in the polynomial expressions is described within Section 7.2. A detailed example of the calculations used to define the coefficients for the IGBT turn-on energy (E_{on}) is outlined in Section 7.2.1. The accuracy of the polynomial expressions for each of the loss parameters is examined in Section 7.2.2.

Like the measured power loss data, the self and mutual thermal impedance curves cannot be used directly in the thermal model. These must be curve fitted to an equivalent Foster network with one or more elements. The configuration of this network is reviewed in Section 7.3.1. The method used to calculate the parameters of an equivalent Foster network is described in Section 7.3.2. These parameters form the complete thermal impedance matrix for the inverter and this is used to estimate the temperature of every device under a range of operating conditions. The procedure outlined in Chapter 5 is then used to select the

IGBT and diode that offer the best protection for the inverter at low output frequencies and this is covered in Section 7.3.2. Finally, the input parameters required by the thermal model are defined in Section 7.3.3.

7.2 Calculation of the Coefficients for the Loss Models

The existing methods that have been used to estimate the switching energy and the on-state voltage of an IGBT and diode were reviewed in Chapter 2. In this review, it was shown that due to the fast calculation speed, a behaviour model is well suited to online (real-time) applications. Therefore, in this work, a series of polynomial expressions are used to estimate the loss parameters for the IGBT and diode. These are then used to estimate the total power loss in a device. This approach is similar to the methods discussed in [43, 52, 54, 56]. The steps used to calculate the coefficients for the IGBT turn-on energy (E_{on}) are described in the next section, although the same approach is used to calculate the coefficients for the other switching and conduction loss parameters.

7.2.1 IGBT turn-on Energy

The loss models used in the thermal model are developed in three stages. At each stage an additional dependency is incorporated into the model, i.e. the operating current (I_C), temperature (T_j) and DC link voltage (V_{DC}). The calculations that must be performed in each stage are described below.

Stage 1 – Current

In the first stage, the coefficients of the second order polynomial:

$$E_{on}(I_C) = k_1 \cdot {I_C}^2 + k_2 \cdot I_C + k_3 \quad \text{(mJ)} \tag{7.1}$$

are curve fitted (using the method of least squares) to the switching energy measured over the full range of operating current (I_C=0A to 75A) at the following temperatures and voltage:

- Device temperature of 25°C and 150°C
- DC link voltage of 600V

The coefficients calculated by curve fitting Equation 7.1 to the switching energy measured at these temperatures are shown in the table below.

Table 7.1: Current loss coefficients for the IGBT turn-on energy

T_j (°C)	k_1 (mJ/A^2)	k_2 (mJ/A)	k_3 (mJ)
25	0.472	99.409	393.05
150	0.637	132.18	1061.7

A comparison of the measured and curve fitted switching energy is shown in Figure 7.1(a). This comparison shows that for the selected operating conditions, the second order polynomial provides a good approximation of the measured switching energy.

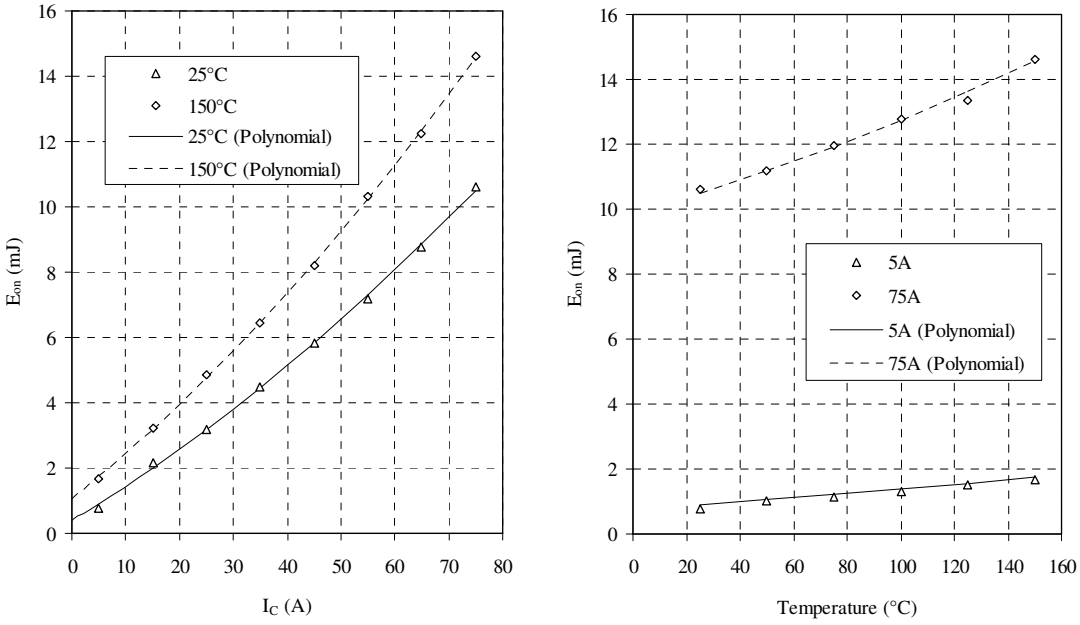

(a) (b)

Figure 7.1: Comparison of the measured and curve fitted IGBT turn-on energy verses (a) current (b) temperature (V_{DC} = 600V)

The coefficients in Table 7.1 can only be used to estimate the switching energy in the selected operating conditions, i.e. with a fixed temperature and voltage. Therefore, additional stages are required to develop the complete power loss model, and these are described in the following pages.

Stage 2 – Temperature

The second stage in the development of the power loss model is to incorporate the dependency of the device temperature. To achieve this, the coefficients in Equation 7.1 are themselves represented by a second order polynomial:

$$k_1 = k_{11} \cdot T_j^{\,2} + k_{12} \cdot T_j + k_{13} \quad (\text{mJ/A}^2) \tag{7.2}$$

$$k_2 = k_{21} \cdot T_j^{\,2} + k_{22} \cdot T_j + k_{23} \quad (\text{mJ/A}) \tag{7.3}$$

$$k_3 = k_{31} \cdot T_j^{\,2} + k_{32} \cdot T_j + k_{33} \quad (\text{mJ}) \tag{7.4}$$

These coefficients are calculated by substituting the three equations shown above into Equation 7.1. The resultant equation is then curve fitted to the switching energy measured up to the maximum operating temperature of the device (T_j=25°C to 150°C). In this stage, the following currents and voltage are used:

- Device current of 5A and 75A
- DC link voltage of 600V

The calculated coefficients for Equations 7.2 to 7.4 are shown in Table 7.2. In order to maintain the characteristics of the model developed in stage 1, the coefficients in this table are calculated to ensure that when operating at a device temperature of 25°C or 150°C the calculated values of k_1, k_2 and k_3 are the same as the coefficients in Table 7.1.

Table 7.2: Temperature loss coefficients for the IGBT turn-on energy

	T_j^2	T_j^1	T_j^0
k_1 (mJ/A^2)	$2.34e^{-06}$	$9.17e^{-04}$	$4.47e^{-01}$
k_2 (mJ/A)	$4.95e^{-04}$	$1.76e^{-01}$	$9.47e^{+01}$
k_3 (mJ)	$1.38e^{-03}$	$5.11e^{+00}$	$2.65e^{+02}$

For example, when operating at a temperature of 150°C the magnitude of the coefficient k_1 calculated using the values in this table is:

$$k_1 = k_{11} \cdot 150^2 + k_{12} \cdot 150 + k_{13} = 0.637 \text{ mJ/A}^2$$

As shown, the magnitude of k_1 is the same as the value in Table 7.1. A comparison of the measured and curve fitted switching energy is shown in Figure 7.1(b). Like the previous comparison, the polynomial expression provides a good approximation of the switching energy under the defined operating conditions. Although, by using the coefficients calculated in this stage the switching energy can now be estimated at any current or temperature.

Stage 3 - DC Link Voltage

The final stage in this development is to incorporate the effect of the DC link voltage. The change in the switching energy due to a change in voltage is modelled by:

$$k_V = k_{V1} \cdot {V_{DC}}^2 + k_{V2} \cdot V_{DC} + k_{V3} \tag{7.5}$$

Combining this equation with those defined in stage 2 allows the switching energy at any current, temperature or voltage to be calculated:

$$E_{on}(I_C, T_j, V_{DC}) = E_{on}(I_C, T_j) \cdot k_V \quad \text{(mJ)} \tag{7.6}$$

The coefficients in the voltage polynomial are calculated by curve fitting Equation 7.6 (using the coefficients in Table 7.2) to the switching energy measured over the full range of DC link voltage (V_{DC}=500V to 800V) at the following currents and temperature:

- Device current of 5A and 75A
- Device temperature of 150°C

The coefficients for Equation 7.5 are shown in Table 7.3, while the measured and curve fitted switching energy is compared in Figure 7.2(a).

Table 7.3: Voltage loss coefficients for the IGBT turn-on energy

	k_{V1}	k_{V2}	k_{V3}
k_V	0	$2.59e^{-03}$	$-5.45e^{-01}$

Figure 7.2(a) shows that the measured switching energy changes linearly with voltage. Consequently, in the expression for the turn-on energy of the IGBT the coefficient k_{V1} is zero.

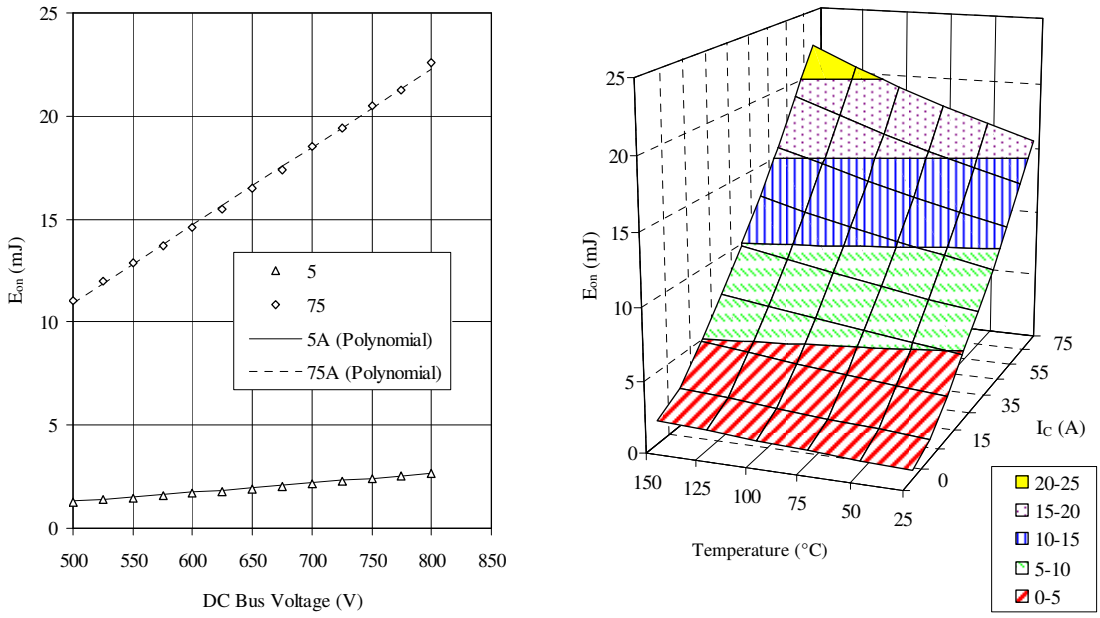

(a) (b)

Figure 7.2: IGBT turn-on energy (a) measured and curve fitted switching energy verses DC link voltage (b) calculated energy verses current and temperature (V_{DC} = 800V)

The complete power loss model developed in this section (Equation 7.6) allows the IGBT turn-on energy to be estimated at any current, temperature or voltage and importantly, only requires the 12 coefficients shown in Tables 7.2 and 7.3. To show the dependency of the switching energy, the complete power loss model is used to estimate the turn-on energy over the full range of operating current and temperature. The results calculated with a fixed DC link voltage of 800V are shown in Figure 7.2(b). These results show that the switching energy of an IGBT is highly dependant on the operating temperature and load current. Furthermore, the DC link voltage has been shown to have a significant effect.

Consequently, none of these can be ignored and the full loss model must be implemented. As discussed, the approach outlined in this section is also used to calculate the coefficients for the other loss parameters and these models are shown in Appendix D.

7.2.2 Investigation into the Accuracy of the Power Loss Models

The accuracy of the power loss models will have a direct impact on the estimated device temperature and it is important that they are accurate in all of the potential operating conditions. To show the accuracy of these models, the difference between the measured and estimated values is calculated in each operating condition in which the switching energy or on-state voltage has been measured. The maximum and average difference calculated from the values measured over the range of operating temperature and current is then determined at each current interval. These results are shown in the figure below:

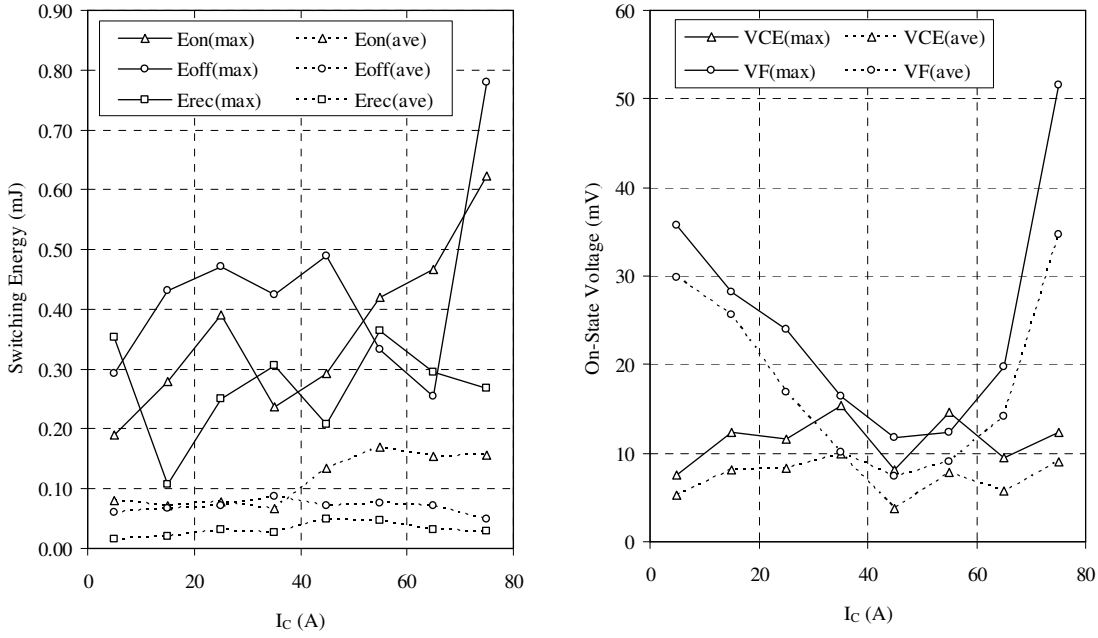

(a) (b)

Figure 7.3: Maximum and average difference between the measured and estimated (a) switching energy (b) on-state voltage

In general, the results show that the differences between the measured and estimated values are relatively small. Although, in these figures it can be see that there are specific operating

conditions where the maximum difference is far greater than the average value. This is due to one of the following reasons:

a) The curve fitting process and the selection of the coefficients used in the models.
b) The ability of the power loss models to model complex characteristics in the measured values.
c) Any errors associated with the initial measurement of the loss parameters.

Considering these, the results in Figure 7.3 reflect the ability of the polynomial expressions to model the measured loss parameters and not necessarily the accuracy of the estimated power loss. In other words, some of the differences may be due to measurement errors. A possible example of this can be seen in Figure 7.1(b), where the turn-on energy of the IGBT measured at a current of 75A and a temperature of 125°C is clearly below the general characteristic of the measured switching energy.

In conclusion, the accuracy of the expression developed to model the switching energy and on-state voltage in a device has been shown to be acceptable over the entire operating range. Furthermore, since the number of input parameters has been reduced, the calculations can be performed on-line using the existing computational resources. Therefore, these expressions are implemented in the thermal model and are used to estimate the total power loss in an IGBT and diode during each sample period.

7.3 Calculation of the Thermal Impedance Parameters

In order to calculate the parameters of the equivalent thermal networks that are used in the thermal model the following stages must be completed:

1. Calculate the parameters of an equivalent thermal network for each of the self and mutual thermal impedances in the inverter (144 matrix elements).
2. Select the elements of the thermal impedance matrix that are to be used in the thermal model for the IGBT and diode (2x12 matrix elements).
3. Combine the mutual impedance from the IGBT and diodes (2x3 matrix elements).

In each stage, the number of matrix elements used to represent the thermal characteristics of the power module is highlighted. Initially, the complete thermal impedance matrix for the twelve devices in the inverter is required. The IGBT and diode that offer the best protection at low frequencies are then selected. This reduces the number of elements to those associated with the chosen devices. Finally, the mutual coupling from the other IGBTs and diodes in the inverter are combined to give the final input parameters for the four Foster networks used by each model. The calculations performed in each of these stages are described in the following sections.

7.3.1 Thermal Network Parameters

As discussed, in order to develop the thermal model, the measured transient thermal impedances must be represented by an equivalent thermal network. In this work, the thermal model is developed using the transfer function for a single element of a Foster network. An equivalent Foster network with four elements (k=4) is shown in Figure 7.4.

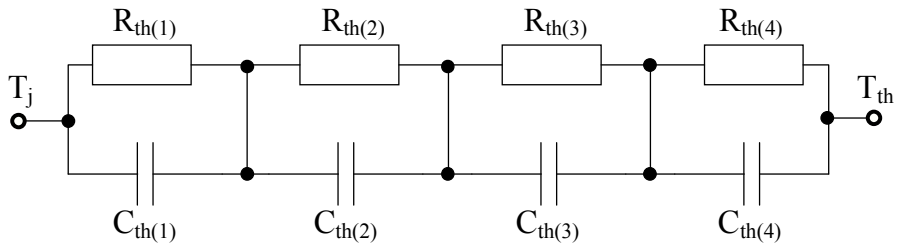

Figure 7.4: Foster network with four elements (k=4)

The thermal resistance (R_{th}) and capacitance (C_{th}) of each element is calculated by curve fitting the response of the network to the transient thermal impedance measured between a device (T_j) and the internal thermistor (T_{th}) in the power module. The method used to calculate these parameters is described in the next section.

7.3.1.1 Curve Fitting Method

The parameters of a Foster network with up to four elements (fourth-order network) are calculated using a program based on the method of least squares. A comparison of the measured self thermal impedance for the upper IGBT in the U phase (I_{UU}) of the inverter and the response of two equivalent Foster networks is shown in Figure 7.5(a). In this figure,

it can be seen that the time constant of the network with a single element (first-order network) has been selected to model the initial rise in the thermal impedance. Consequently, after this initial rise (t>0.1s) the response of the network is significantly higher than the measured thermal impedance.

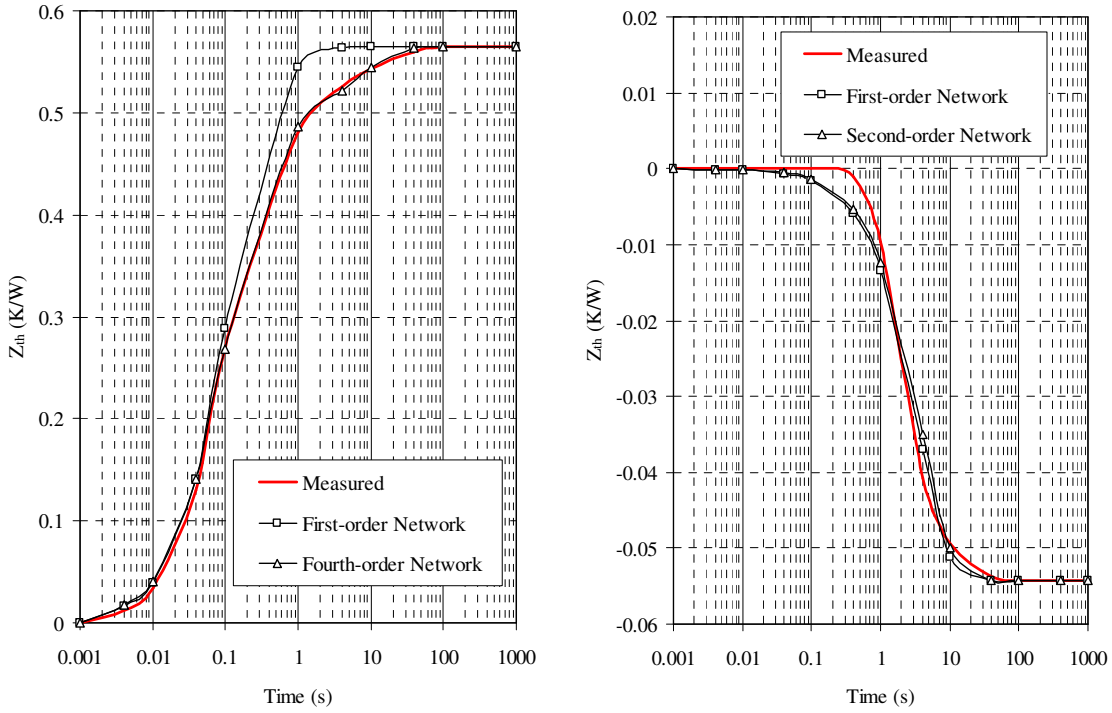

(a) (b)

Figure 7.5: Comparison of the measured transient thermal impedance with the response of an equivalent Foster network (a) self thermal impedance - $Z_{th}(I_{UU}\text{-}I_{UU})$ (b) mutual thermal impedance - $Z_{th}(I_{UU}\text{-}I_{UL})$

In contrast, when an equivalent network with four elements is curve fitted to the measured thermal impedance, the response of the network is significantly improved. The corresponding parameters of a network with up to four elements (fourth-order network) are shown in Table 7.4. These parameters show that the longest time constant in the network increases with the number of network elements, a similar comparison was shown in [118]. However, because of the limitations imposed by the limited computational resource the self thermal impedance is represented by a network with only two elements. Even so, a network with more elements can be used during the selection of the devices since these calculations

are performed off-line. For completeness, the parameters of the equivalent network for the self thermal impedance of every device in the inverter are shown in Appendix B.

Table 7.4: Foster network parameters for $Z_{th}(I_{UU}\text{-}I_{UU})$

Thermal Resistance (K/W)	1st	2nd	3rd	4th	Time Constant (s)	1st	2nd	3rd	4th
$R_{th(1)}$	0.564	0.141	0.071	0.071	$\tau_{(1)}$	0.14	2.180	1.025	0.465
$R_{th(2)}$		0.423	0.071	0.353	$\tau_{(2)}$		0.085	6.312	2.326
$R_{th(3)}$			0.423	0.071	$\tau_{(3)}$			0.105	0.018
$R_{th(4)}$				0.071	$\tau_{(4)}$				8.103

The mutual thermal impedances and any error associated with them are less significant than the self thermal impedance. Therefore, in the thermal model the mutual thermal impedance is modelled by a single network element, although once again, more network elements can be used in the off-line calculations. The mutual thermal impedance measured between the I_{UU} and the internal thermistor in the module when a power loss is applied to I_{UL} is shown in Figure 7.5(b). In this figure, the measured thermal impedance is compared against the response of an equivalent network with up to two network elements. In this example, I_{UU} is further from I_{UL} than the thermistor. Consequently, when a power loss is applied to I_{UL} the temperature measured by the thermistor is hotter than I_{UU}. Consequently, the resulting mutual thermal impedance is negative. Furthermore, due to the diffusion in the power module and heatsink there is a delay before the mutual thermal impedance begins to rise. This characteristic makes it difficult to model the response accurately using conventional network parameters and for this reason, an alternative approach was used in [108]. However, this approach can only be used in networks with more than two elements. Therefore, in this work, a conventional network is used and the calculated parameters for these networks are shown in the table below:

Table 7.5: Foster network parameters for $Z_{th}(I_{UU}\text{-}I_{UL})$

Thermal Resistance (K/W)	1st	2nd	Time Constant (s)	1st	2nd
R_{th1}	-0.054	-0.011	τ_1	3.5	3.5
R_{th2}		-0.043	τ_2		4.5

The network parameters in this table show that for this mutual thermal impedance, the number of network elements has little effect on the accuracy of the response. The calculated network parameters for all of the mutual thermal impedances in the complete matrix for the inverter (132 matrix elements) are shown in Appendix B.

7.3.2 Thermal Impedance Matrix Simplification

The method described in the previous section has been used to calculate the parameters of the equivalent networks for every element in the thermal impedance matrix. However, this is only the first stage in the development process. As described in Chapter 5, the thermal model has been designed to estimate the temperature of a single IGBT and diode in the inverter. Therefore, each model requires the parameters for twelve matrix elements, the self thermal impedance and the eleven mutual thermal impedances associated with each device. Hence, the temperature of a device (i) is calculated using:

$$T_i = \begin{bmatrix} Z_{th,i1} & Z_{th,i2} & \cdots & Z_{th,i12} \end{bmatrix} \cdot \begin{bmatrix} P_1 \\ P_2 \\ \vdots \\ P_{12} \end{bmatrix} \tag{7.8}$$

To select these devices, the complete thermal impedance matrix (formed using the parameters of a network with up to four elements) is used to calculate the temperature of every device in the inverter under a defined operating condition. The IGBT and diode with the largest temperature difference between itself and the thermistor are then selected. In this work the devices are selected from the steady-state temperature calculated in a stationary vector condition (F_{out} = 0Hz). This operating condition was chosen because a device is more likely to exceed its maximum temperature at low output frequencies.

7.3.2.1 Selection of Model Parameters

To select the model parameters, the temperature of every device in the inverter is calculated in the following conditions:

- Load current (I_L) = 50A
- DC link voltage (V_{DC}) = 600V
- Thermistor Temperature (T_{th}) = 80°C
- Switching frequency (F_{SW}) = 3kHz

The IGBT and diode with the largest temperature difference between itself and the thermistor is then calculated at each displacement power factor and modulation depth. These results are shown in Figure 7.6. From this figure, it can be seen that when operating in a stationery vector condition the IGBT and diode that provide the best protection for the inverter, especially with a low modulation index, are I_{UU} and D_{UU}. This suggests that the magnitude of the self thermal impedance calculated for these devices is larger than the other devices in the inverter. This is confirmed by the results shown in Appendix B.

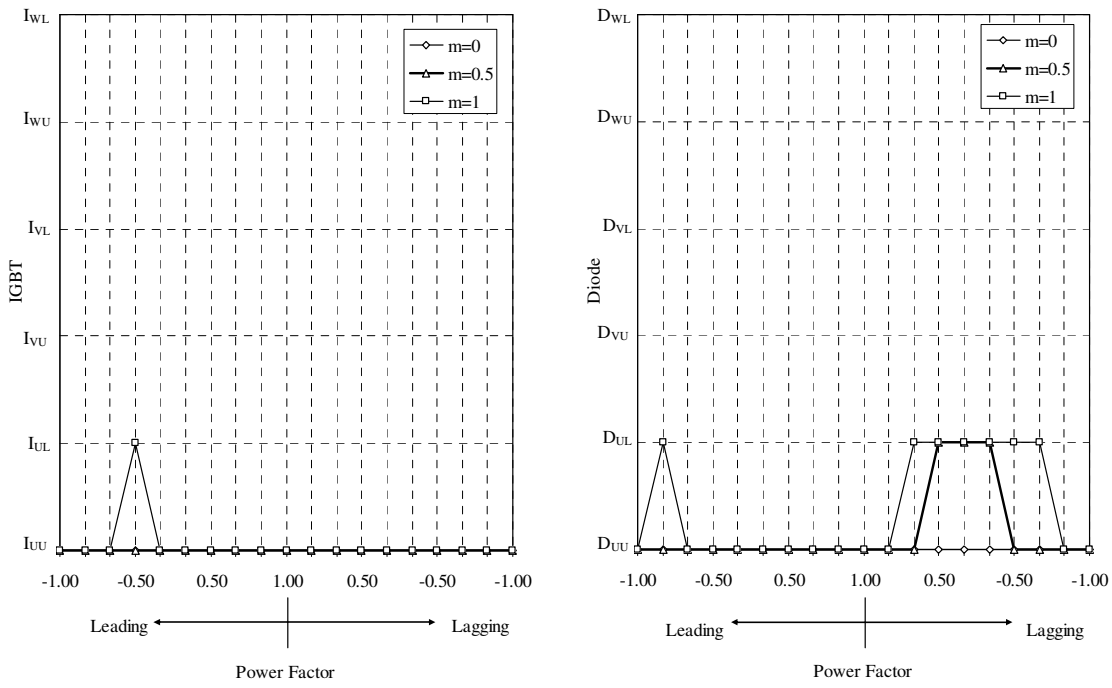

Figure 7.6: Devices in which the peak junction-to-thermistor temperature occurs in a stationary vector (a) IGBT (b) diode (I_L=50A, V_{DC}=600V, T_{th}=80°C, F_{SW}=3kHz)

In a stationary vector condition there is no coupling between an IGBT and its parallel diode, i.e. I_{UU} and D_{UU}. Therefore, as the output frequency is increased the coupling in the

inverter will change. At a very high frequency, where the ripple component of the temperature response is negligible, the thermal coupling will be equal to the DC component (average value) of the response. Under this condition, regardless of the modulation index or displacement power factor, the best protection is offered by I_{VU} and D_{VU}, i.e. the peak junction-to-thermistor temperature always occurs in these devices. Nevertheless, the thermal model can only estimate the temperature of a single IGBT and diode. Therefore, as in Chapter 5, the devices are selected to provide the best protection when the inverter is operating at a low output frequency. In the following sections, the input parameters for the thermal model are calculated from the network parameters for the self and mutual thermal impedances for I_{UU} and D_{UU}, which are shown in the table below.

Table 7.6: Network parameters for the equivalent Foster networks for I_{UU} and D_{UU}

IGBT network parameters							
IGBT	I_{UU}		I_{UL}	I_{VU}	I_{VL}	I_{WU}	I_{WL}
R (K/W)	0.141	0.423	-0.055	0.023	-0.079	-0.061	-0.057
τ (s)	2.18	0.085	3.46	1.58	7.35	3.22	13.15
α (°)	0		180	120	300	240	60
Diode	D_{UU}		D_{UL}	D_{VU}	D_{VL}	D_{WU}	D_{WL}
R (K/W)	0.148		-0.015	-0.0262	-0.129	-0.050	-0.046
τ (s)	1.25		4.12	3.32	2.88	9	17.43
α (°)	180		0	300	120	60	240
Diode network parameters							
IGBT	I_{UU}		I_{UL}	I_{VU}	I_{VL}	I_{WU}	I_{WL}
R (K/W)	0.15		-0.043	0.068	-0.071	-0.044	-0.049
τ (s)	1.81		2.51	1.37	5.66	3.22	11.06
α (°)	180		0	300	120	60	240
Diode	D_{UU}		D_{UL}	D_{VU}	D_{VL}	D_{WU}	D_{WL}
R_1 (K/W)	0.209	0.626	0.026	-0.005	-0.120	-0.038	-0.040
τ (s)	0.81	0.05	1.3	4.48	1.9	9	17.11
α (°)	0		180	120	300	240	60

In this table, the angle between the peak current in the self (modelled device) and mutual devices is defined as α. For example, the angle between the peak current in the upper and lower IGBT in any phase of the inverter is 180°. The same applies for the diode model,

except in this case D_{UU} is the reference device. Therefore, compared with the IGBT model, all of the angles are shifted by 180°, which in this instance is the angle between the peak current in I_{UU} and D_{UU}.

7.3.2.2 Accuracy of the Thermal Model

The thermal model will underestimate the temperature of the hottest device in the inverter in any operating condition where the peak junction-to-thermistor temperature does not occur in either of the selected devices. To show the accuracy of the thermal model, the difference between the estimated temperature and the value calculated using the complete thermal impedance matrix is represented as a percentage of the peak junction-to-thermistor temperature. The error calculated with the inverter operating in a stationary vector condition (F_{out}=0Hz) and at a high output frequency ($F_{out}>>1/\tau_{min}$) is shown in Figure 7.7. In the high frequency condition, it is assumed that the ripple in the temperature response is negligible and the temperature is calculated using only the DC components.

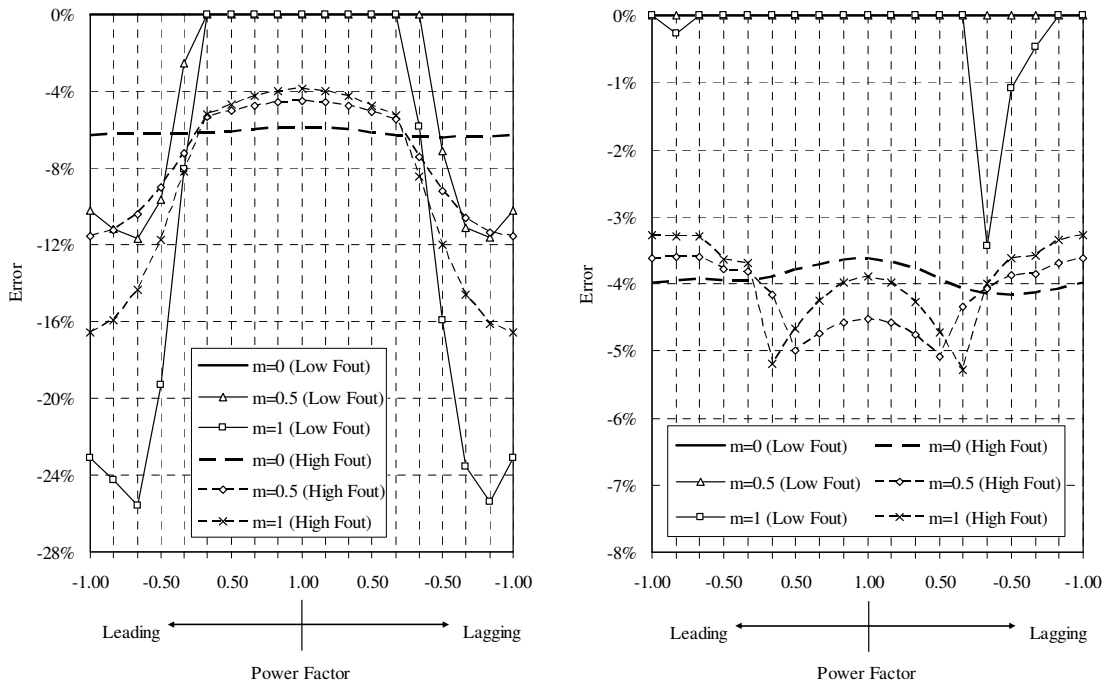

(a) (b)

Figure 7.7: Error calculated when operating in a stationary vector condition and a high output frequency (a) IGBT model (b) IGBT and diode models implemented in parallel (I_L=50A, V_{DC}=600V, T_{th}=80°C)

In Figure 7.7(a), it can be seen that when using the IGBT model to protect the entire inverter the error is significant when operating with a negative displacement power factor. Therefore, as in Chapter 5, to provide sufficient protection the IGBT and diode models must be implemented in parallel. The error corresponding to this approach is shown in Figure 7.7(b). In the stationary vector condition, it can be seen that the temperature of the hottest IGBT and diode is underestimated by less than 3.5% of the peak junction-to-thermistor temperature, although in most operating conditions the error is well below this value. As expected, by comparing these results with those shown in Figure 7.6, it is evident that the error occurs in the operating conditions where the peak junction-to-thermistor temperature does not occur in either of the selected devices.

When operating at a high output frequency the maximum error exceeds 5%. In this condition, the coupling from the neighbouring diodes has a more significant impact on the temperature of the IGBTs and vice versa. Consequently, since there is only a single diode within a device width of I_{UU} (compared to I_{VU} that has three) the peak junction-to-thermistor temperature now occurs in I_{VU}. Consequently, the error in the model is increased. However, for a given power loss, the temperature measured between a device and the thermistor is smaller at high output frequencies. Therefore, it is less likely that a device will exceed its maximum temperature. Thus, any error is less critical.

In summary, by calculating the temperature of a single IGBT and diode the number of network elements used in the thermal model has been reduced. However, the results presented in this section have shown that the device in which the peak junction-to-thermistor temperature occurs is dependant on the operating conditions. Consequently, there are conditions where the temperature of a device could be underestimated. Even so, when using the simplified model all of the devices in the inverter should be protected in a stationary vector condition, where the possibility of a device exceeding its maximum temperature is most likely.

7.3.3 Combination of Mutual Thermal Impedance Terms

In the previous section, the mutual thermal impedances required by the IGBT and diode models were selected, the parameters of these networks were shown in Table 7.6. In order

to reduce the number of network elements in each model, a common time constant is selected for the mutual coupling from the other IGBTs (τ_{IGBT}) and diodes (τ_{Diode}) in the inverter. This allows all of the mutual coupling to be represented by two network elements (two time constants), one representing the thermal coupling from the IGBTs and another from the diodes. The parameters for these networks are calculated using the procedure outlined in Chapter 5. A comparison of the temperature response calculated for the IGBT model is shown in Figure 7.8(a).

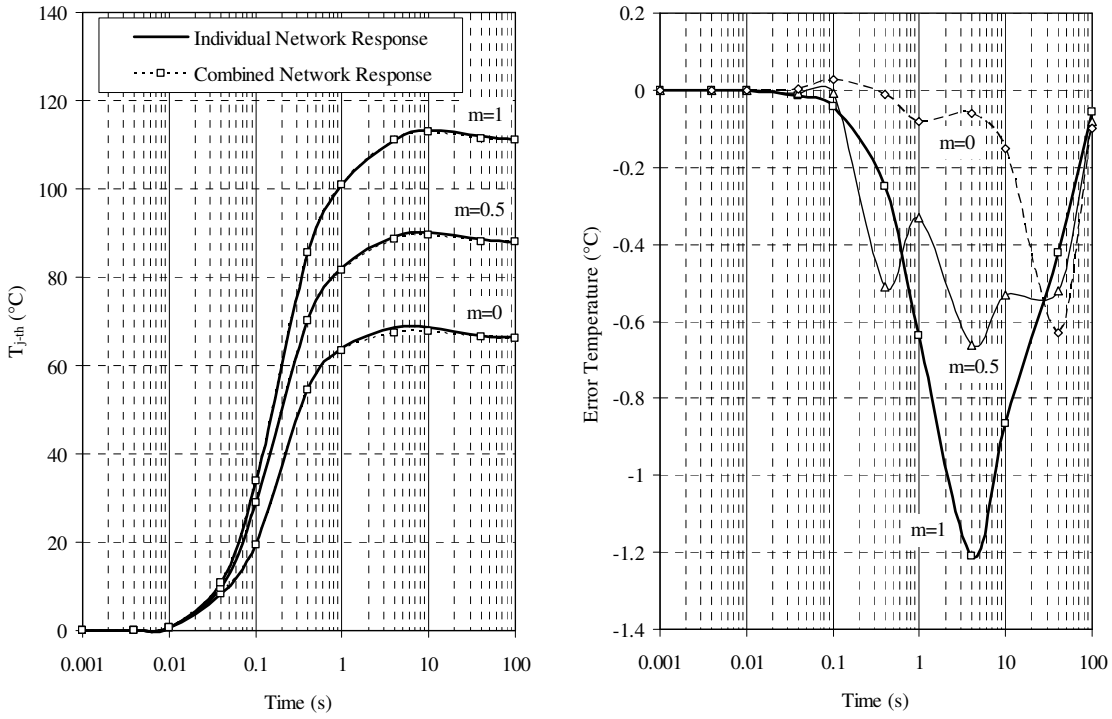

(a) (b)

Figure 7.8: Comparison of the step response calculated using the original network parameters and the common time constants in a stationary vector condition with a unity displacement power factor (a) step response (b) temperature difference

The overshoot seen in each response is caused by the significant coupling between the devices and the internal thermistor, which results in a negative coupling. The difference between the responses is shown in Figure 7.8(b). As previously, if the difference is negative the temperature is underestimated. The selection of a common time constant is only a simple approximation of the complex thermal characteristics that exist within the power

module, thus some error during the transient operation is inevitable. Even so, by carefully selecting the time constants this error can be minimised and for the operating conditions used in this section, the maximum error is just over 1°C. Comparisons in other operating conditions, which include the response of the diode model, are shown in Appendix E. The input parameters for the complete frequency model implemented in the Unidrive SP are shown in the table below:

Table 7.7: IGBT and Diode thermal model parameters

IGBT Thermal Model Network Parameters					
		IGBT Self		IGBT Mutual	Diode Mutual
	Network Element	1	2	1	1
Harmonic (n)	τ (s)	0.085	2.18	15	2.5
0 (DC)	$R_{th,n}$ (K/W)	0.423	0.141	-0.227	-0.118
1		0.423	0.141	0.092	0.147
2		0.423	0.141	0.062	0.263
3		0.423	0.141	0.152	0.261
1	α_n (°)	0	0	86.5	219.1
2		0	0	330.3	5.6
3		0	0	0	60
Diode Thermal Model Network Parameters					
		Diode Self		IGBT Mutual	Diode Mutual
	Network Element	1	2	1	1
Harmonic (n)	τ (s)	0.053	0.812	2.5	10
0 (DC)	$R_{th,n}$ (K/W)	0.626	0.209	0.012	-0.176
1		0.626	0.209	0.167	0.129
2		0.626	0.209	0.174	0.134
3		0.626	0.209	0.338	0.091
1	α_n (°)	0	0	224	130.9
2		0	0	346.8	8.9
3		0	0	60	0

As shown previously, the offset angle for the selected IGBT and diode is zero. Thus, for the self thermal impedance the angle at each harmonic (α_n) is also zero, although for the mutual impedance, $R_{th,n}$ and α_n are different.

7.4 Summary

In this chapter, the input parameters required by the thermal model have been calculated from the measured values. These include the following:

- The coefficients of the power loss models used to estimate the switching energy and on-state voltage for the IGBTs and diodes
- The equivalent network parameters for the thermal impedance used in the thermal impedance matrix

The power loss models developed in this chapter use twelve coefficients to estimate the switching energy and on-state voltage at any current, temperature or voltage. Therefore, compared to the tables of the measured loss data, using these expressions significantly reduces the amount of input data required by the thermal model. Furthermore, in most operating conditions the difference between the measured and estimated values was shown to be negligible.

In order to develop the thermal model, the equivalent network parameters for each element in the thermal impedance matrix must be determined. The method used to calculate these values was described in the second part of this chapter. The procedure outlined in Chapter 5 was then used to select the modelled IGBT and diode, determine the corresponding thermal impedances and calculate the input parameters relating to the thermal characteristics.

From the results in this chapter, the error in a stationary vector condition was shown to be negligible. Although, as the output frequency is increased the error increases due to the additional coupling from the neighbouring devices. For the purpose of evaluating the thermal model this effect has been ignored. Thus, in the comparisons of the estimated and measured device temperatures presented in the next chapter, some underestimation of the temperature is expected when operating at a high output frequency.

Chapter 8: Results and Comparison

8.1 Introduction

In the previous chapters the temperature estimated by the frequency model has been compared with the temperature calculated using the complete thermal impedance matrix. These comparisons were useful when developing the thermal model and provided a means of easily identifying any limitations. However, in this comparison both of the temperatures are calculated from the measured data and as a result, many of the approximations made during the development of the model are ignored. Therefore, in this chapter the thermal model has been implemented in a Unidrive SP and the temperature estimated by this on-line model is compared directly with the instantaneous device temperature measured using an infrared camera. In addition, the temperature is estimated using a basic thermal model which is developed using many of the common assumptions that have been described throughout this work. The basic model is developed and implemented in the same way as the current thermal model used in a Unidrive SP. This model is used to illustrate any weaknesses that exist in the current protection scheme. The development of this basic drive thermal model is described in Section 8.2.

The experimental setup used in this chapter has been designed to allow the device temperatures to be measured while the inverter is operating in a typical operating condition. This is described in Section 8.3. Using this setup, the temperature of every device in the inverter is measured in a range of basic operating conditions and these are compared with the temperature estimated by the thermal models. These comparisons are presented in Section 8.4 and this includes a comparison in each of the following operating conditions:

a) Stationary vector condition F_{out}=0Hz
b) Low output frequency F_{out}<0.1Hz
c) Medium output frequency F_{out}>5Hz

These operating conditions have not only been selected to show the strengths of the frequency model, but to highlight its weaknesses.

In the second part of this chapter, further comparisons are made in operating conditions that are specific to an elevator and a pick and place tool. These applications have been chosen because the characteristics of the load profiles are very different and they include many of the key operating conditions. Consequently, from the comparisons presented in Section 8.5, the protection offered by the thermal models in a typical application can be assessed.

8.2 Basic Thermal Model Development

The basic thermal model is based on the estimation of the IGBT temperature using the thermal impedance quoted in the datasheet of the power module. In order to use this approach, it must be assumed that the case of the power module is at the same temperature as the internal thermistor. The thermal impedance measurements in Chapter 6 showed that this is a poor approximation. In the basic model the peak temperature between the junction and the thermistor over a complete output cycle of the inverter is estimated using:

$$T_{j-th} = \hat{I}_L \left[K_{50Hz} + K_{Fout} \left(K_{0Hz} - K_{50Hz} \right) \right] \tag{8.1}$$

where K_{50Hz} is the temperature rise per amp calculated at an output frequency of 50Hz, K_{0Hz} is the temperature rise per amp calculated at an output frequency of 0Hz (stationary vector condition) and K_{Fout} models the change in the peak junction-to-thermistor temperature with the output frequency. The constants K_{50Hz} and K_{0Hz} are determined from the peak IGBT to thermistor temperature calculated in the operating conditions defined in Table 8.1. The device temperature is calculated by applying the known power loss (calculated using the power loss parameters developed in Chapter 7) to the fourth order Foster network taken from the device datasheet. The peak temperature over the output cycle is then calculated and divided by the known output current, giving the expected temperature rise per amp. In this calculation it is assumed that the temperature rise is linear with output current. To develop the complete model this calculation must be repeated at each of the permissible switching frequencies.

Table 8.1: Operating conditions used to calculate the maximum device temperature

Operating parameters		
Output frequency (Hz)	0	50
Load current (A)	75	75
Device temperature (°C)	150	150
DC link voltage (V)	Maximum allowable	
Datasheet thermal impedance (K/W)	0.35	0.35
Modulation index	0	0.8
Power factor	1	1

An example of the model constants calculated at 3kHz is shown in Figure 8.1. To illustrate the effect that the chosen operating conditions have on the estimated temperature rise, the variation of the constants are shown over the range of output current and at two operating temperatures. Furthermore, since all of the comparisons in this chapter are performed with a DC link voltage of 550V the constants are calculated using the switching and conduction loss parameters measured at this voltage.

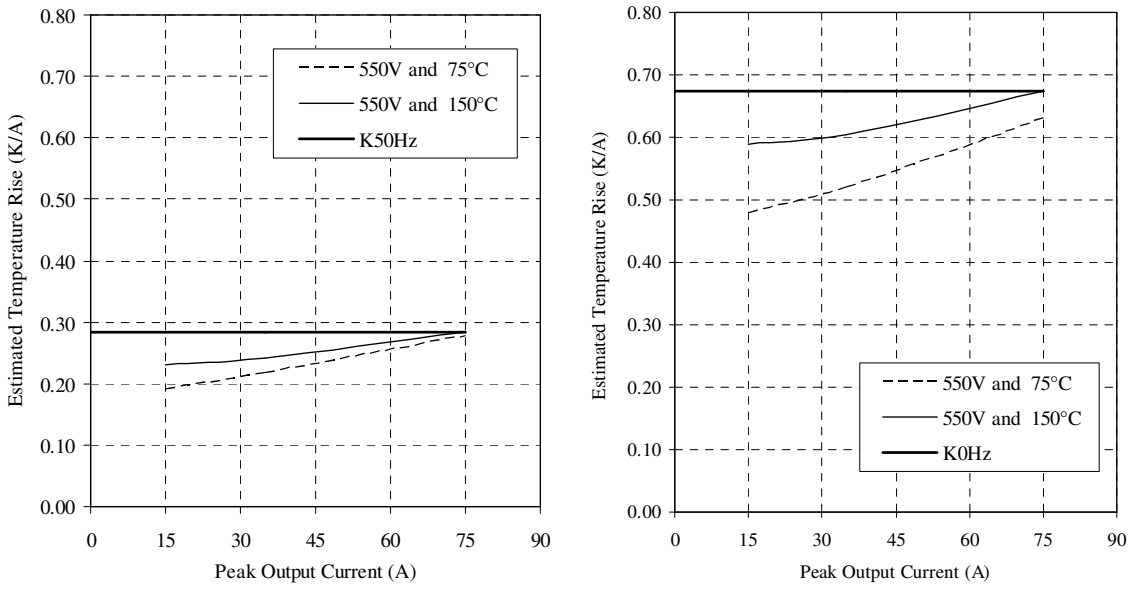

(a) (b)

Figure 8.1: Constants for the basic thermal model calculated at 3kHz (a) K_{50Hz} (b) K_{0Hz}

As described, the constants used in the thermal model are determined from the peak junction-to-thermistor temperature calculated at the maximum operating current (75A) and temperature (150˚C). These constants are then used for all operating conditions. However, when operating at lower currents and temperatures it is evident that this approximation introduces a significant safety margin. For example, when operating at a current of 35A and a temperature of 75°C, the basic thermal model will overestimate the device temperature by approximately 30%.

In order to calculate the temperature at any output frequency, the temperature difference (K_{0Hz} - K_{50Hz}) is multiplied by the factor K_{Fout}. The characteristic of K_{Fout} is shown in Figure 8.2(a). This factor is determined by examining the junction-to-thermistor temperature at different output frequencies. This temperature is calculated for several power modules of different designs and ratings and the maximum value is used. Therefore, this is a general characteristic that can be used with any power module.

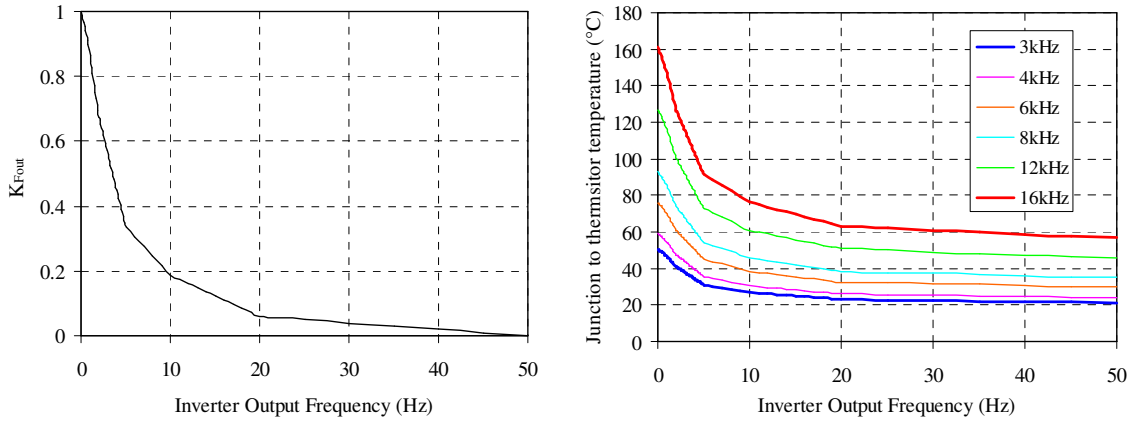

(a) (b)

Figure 8.2: Implementation of the basic thermal model (a) K_{Fout} (b) junction-to-thermistor temperature estimated at 75A

As the output frequency is increased K_{Fout} reduces the contribution of the temperature rise calculated at 0Hz. An example of the junction-to-thermistor temperature estimated using Equation 8.1 is shown in Figure 8.2(b). This figure highlights the dependency of the device temperature with the output and switching frequencies. The method used to implement the

transient model is shown in Figure 8.3. The time constant (τ_{th}) used in this model is 100ms. This time constant is a general value chosen to be between the longest and shortest time constant specified in the datasheet.

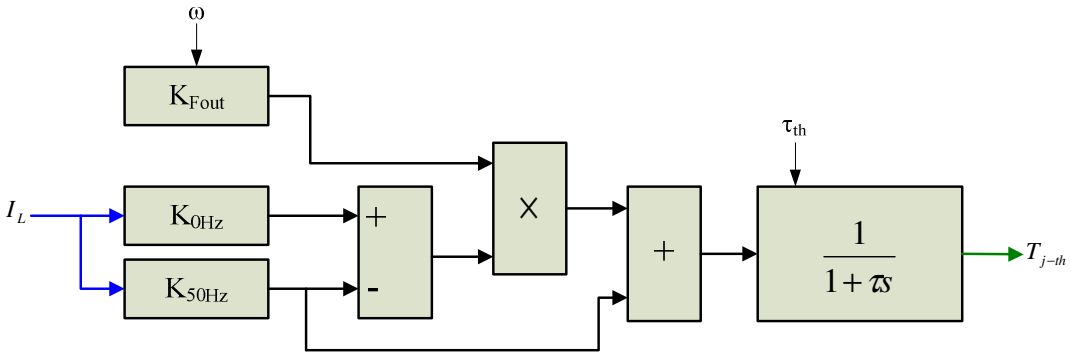

Figure 8.3: Implementation of the basic thermal model in a continuous system

In order to protect the inverter, this model relies on the safety margins introduced during the definition of the operating conditions (Table 8.1) and the calculation of the model constants. These safety margins account for some of the errors due to the following assumptions:

- The thermistor temperature is equal to the case temperature measured directly under each device in all operating conditions.
- No thermal coupling exists between the devices in the power module, thus the thermal impedance in the datasheet (0.35K/W) is used to develop the model.
- The inverter operating conditions are fixed, i.e. the modulation index is always low when operating at a low output frequency.

However, the benefit of this approach is that the temperature can be calculated very quickly using minimum computational resources and only two internal variables (load current and switching frequency) and three input parameters are required (i.e. K_{0Hz}, K_{50Hz}, K_{Fout}). Furthermore, the model can be developed without measuring the thermal impedance and in terms of the product development time, this is a significant advantage.

8.3 Test Setup

To measure the temperature of a device in the inverter during normal operating conditions the power module must be operated outside of the drive and prepared using the procedure

that was described in Chapter 6. Furthermore, since the frequency model has been designed to only protect the devices in the inverter, the rectifier in the power module should not be active during these measurements. For this reason, the dc link voltage is supplied from a second drive. This can be seen in the picture of the test setup shown in Figure 8.4.

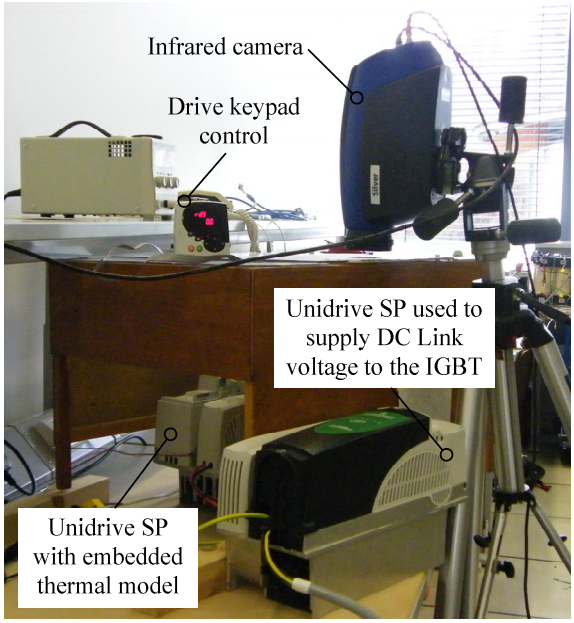

Figure 8.4: Test setup used to measure the temperature under typical operating conditions

This is identical to the setup that was used to measure the loss parameters for the IGBT and diodes in the inverter. The connections between the drive and the external power module that is fitted on a standard heatsink are shown in Figure 8.5. It can be seen that the power and gate drive terminals are connected directly to the drive, which allows the drive to be operated as a standard product. Consequently, the operating conditions can be controlled by simply changing the load that is applied to the motor (induction machine) or the user parameters, which are changed via the keypad. To compare the estimated and measured temperatures, the temperature estimated by the on-line thermal models (both the frequency and basic model) are applied to one of the analogue outputs (voltage range 0 to 10V) on the drive. This voltage is recorded using an oscilloscope and a scaling factor is used to convert the measured voltage to an output temperature. The same method is used to measure the output frequency and load current present in each test.

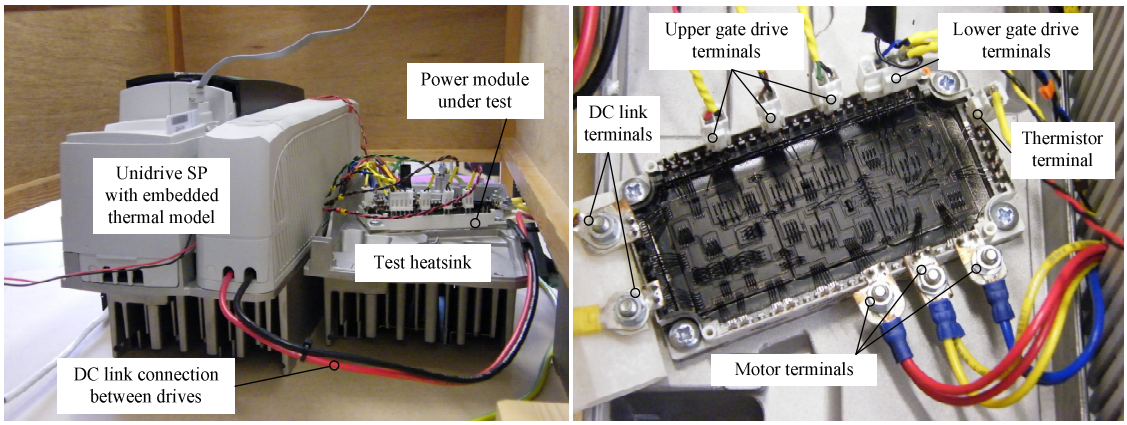

(a) (b)

Figure 8.5: Test setup (a) Unidrive SP with the embedded thermal model (b) power module fitted on a standard heatsink showing the connections between the drive and module

8.4 Comparison of the Estimated and Measured Device Temperature

In this section the temperature estimated by the thermal models are compared with the temperature measured using the infrared camera. These measurements are performed in a number of typical operating conditions. These include operation in a stationary vector condition (F_{out}=0Hz) and at both a low (F_{out}<0.1Hz) and high (F_{out}>5Hz) output frequency.

8.4.1 Stationary Vector Condition

Comparisons of the estimated and measured temperatures determined with the inverter operating in a stationary vector condition at a switching frequency of 8kHz are shown in Figure 8.6. The temperatures estimated by the frequency and basic thermal models are compared with the following measured surface temperatures:

- The upper IGBT in the U phase (Measured I_{UU})
- The upper diode in the U phase (Measured D_{UU})
- Maximum for all IGBTs (Maximum measured IGBT)
- Maximum for all diodes (Maximum measured diode)

In addition, the output frequency (Hz) and output current (rms) are shown, although in this operating condition the output frequency is zero.

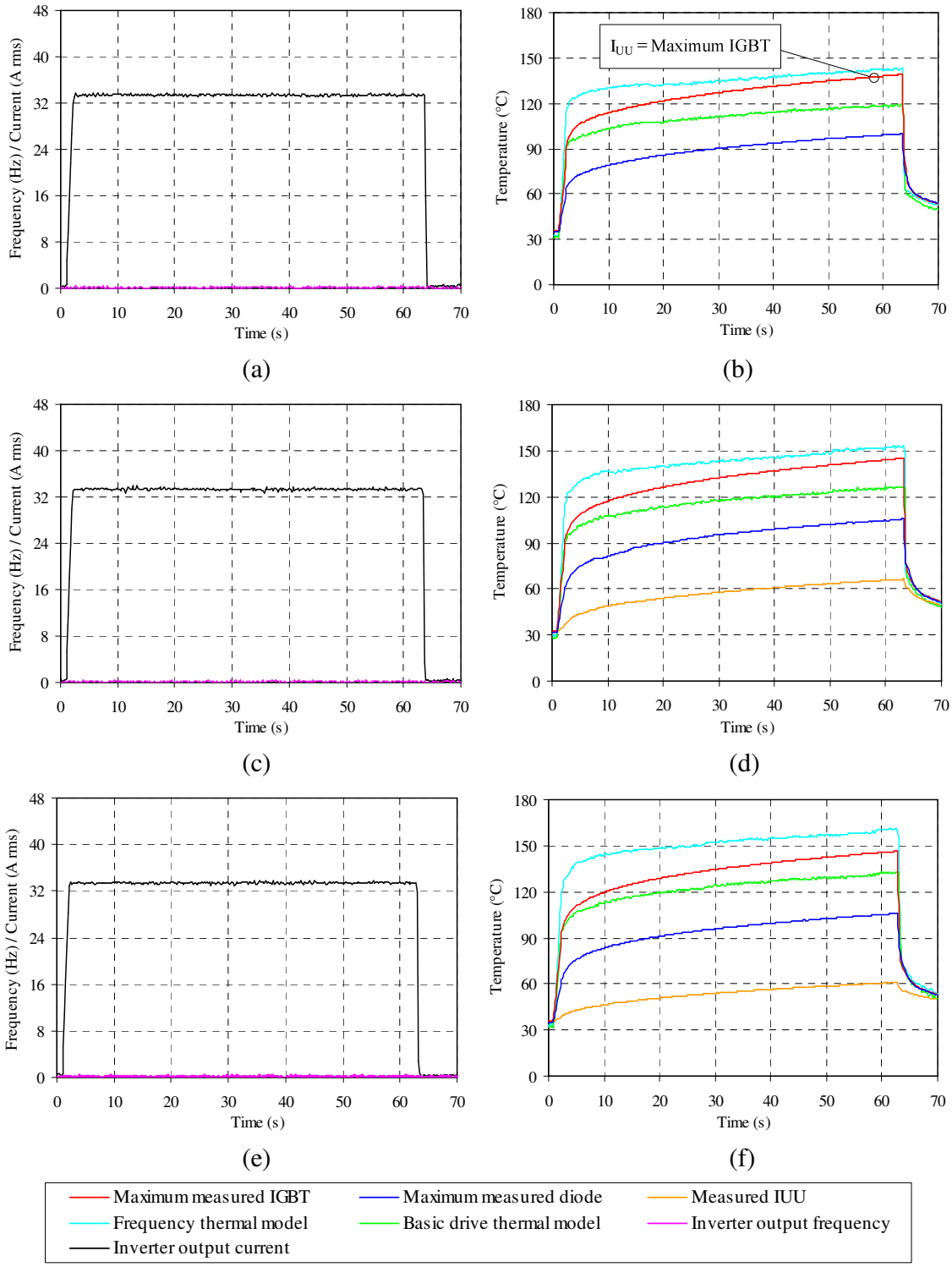

Figure 8.6: Comparison in a stationary vector condition (a) load conditions and (b) comparison with peak current in I_{UU} (c) load conditions and (d) comparison with peak current in I_{VU} (e) load conditions and (f) comparison with peak current in I_{WU}

When developing the frequency model, the modelled devices and the corresponding thermal impedances were selected by examining the temperatures estimated in a stationary vector condition. Therefore, the frequency model should protect all of the devices at the output angle where the peak junction-to-thermistor temperature occurs. A comparison at an output angle of 0˚ (peak power loss in I_{UU}) is shown in Figure 8.6(b). In this comparison it can been seen that as the temperature approaches a steady-state value the difference between the output of the frequency model and the measured temperature of I_{UU} (the hottest IGBT) is only 4°C. In contrast, the basic thermal model underestimates the temperature by nearly 20°C. This is clearly an unacceptable error. Moreover, since the effect of the thermal coupling between the devices is not considered this error could be even higher if the power loss is increased, i.e. if the contribution of the mutual impedances is increased. During the transient period, the temperature estimated by the frequency model is significantly higher than the measured temperature. As discussed in Chapter 4, this effect is caused by the methods used to implement the frequency model.

Similar characteristics are seen as the output angle of the inverter is changed. Although when the peak power loss occurs in a device which is closer to the thermistor, the thermistor temperature increases. As a result, the frequency model begins to overestimate the temperature. For the same reason, the difference between the temperature estimated by the basic thermal model and the hottest IGBT in the inverter is decreased. This effect can be seen in Figure 8.6(d) and Figure 8.6(f). In addition, these results show that the maximum IGBT temperature increases as the output angle of the inverter is changed. When operating at an angle of 240° (peak current in I_{WU}) the temperature of the hottest IGBT approaches 150°C. The higher temperature measured in this condition is caused by the increased thermal coupling between devices.

In each of the comparisons presented in this section the modulation index is very low and over an output cycle, the IGBTs and diodes conduct for a similar period. However, it is possible for the inverter to operate in a stationary vector condition with a modulation index of unity, and more applications are beginning to utilise this operating mode. Therefore, it is essential that the thermal model is capable of protecting the inverter in this condition. In the frequency model the modulation index is an input variable and the estimated temperature

will be increased at a high modulation index. However, in order to develop the basic thermal model it is assumed that the modulation index in a stationary vector condition is zero. Thus, the temperature estimated by this model is independent of the actual modulation index and this assumption will lead to further errors.

In summary, the comparisons performed in a stationary vector condition illustrate the following advantages and disadvantages:

Thermal Model	Advantages	Disadvantages
Frequency model	i) Protects all of the devices in the inverter at any output angle ii) The estimated temperature is accurate (steady-state) when operating at the output angle used to select the devices in the model	i) Overestimates the temperature when the peak power loss occurs in a device close to the thermistor ii) The temperature is overestimated during the transient period and this restricts the maximum short term overload capability of the drive
Basic drive model		i) The devices in the inverter can exceed their maximum temperature by more than 20˚C with a low modulation index ii) Any errors will be significantly increased when the modulation index is above zero

8.4.2 Operation at a Low Output Frequency

To illustrate the effects seen when operating at a low output frequency, the temperatures are compared at an output frequency of 0.033Hz. At this output frequency, the thermal coupling between the devices will still have a significant effect on the device temperature. In these tests the output current is limited to the magnetising current of the induction motor, which is 11A rms. A comparison for the IGBT and diode frequency model with a switching

frequency of 16kHz is shown in Figure 8.7. Since the basic thermal model has only been designed to protect the IGBTs (single output) this temperature is shown in both figures.

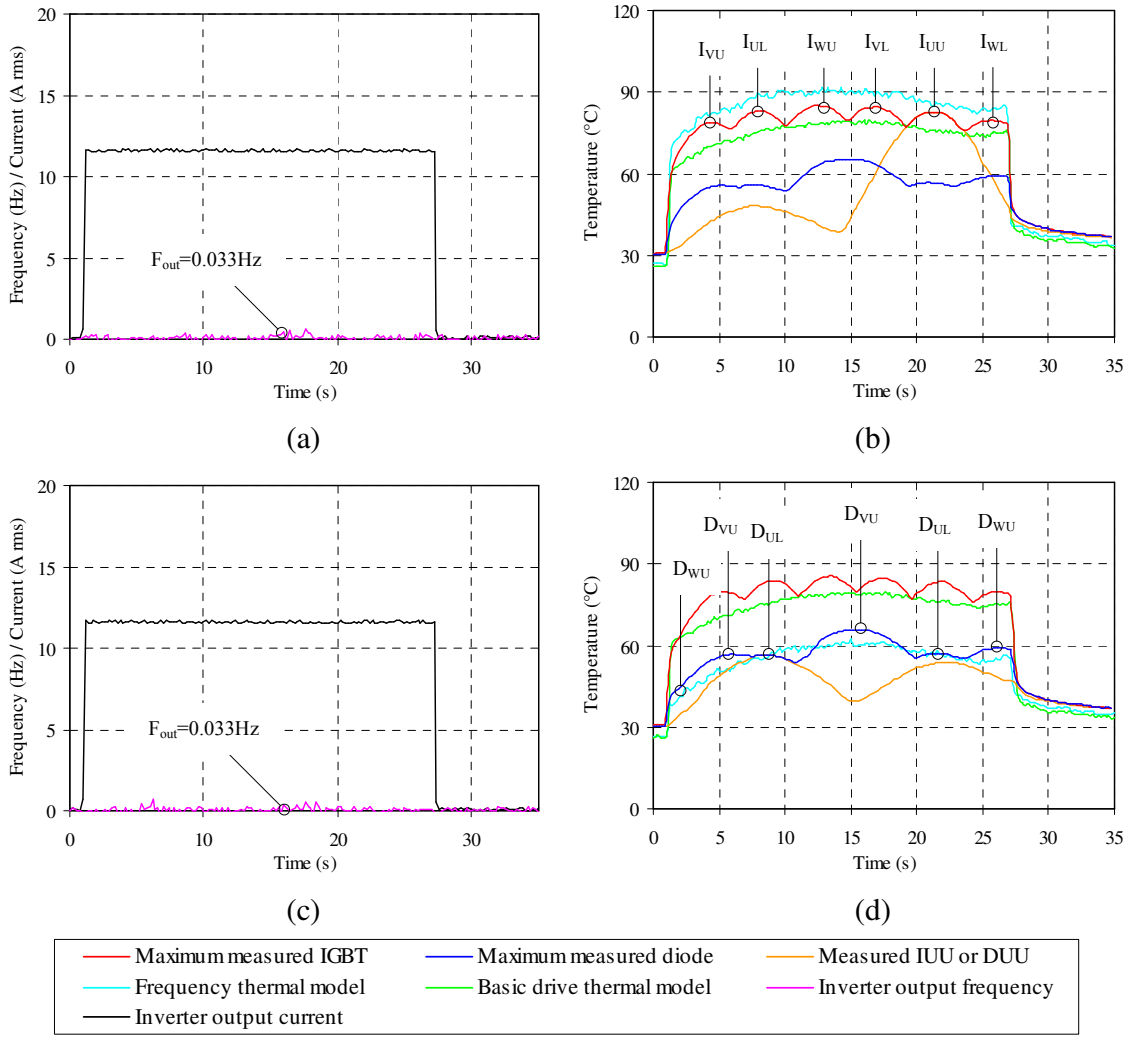

Figure 8.7: Comparison at a low output frequency (a) load conditions and (b) comparison for the IGBT model (c) load conditions and (d) comparison for the diode model

In Figure 8.7(b), it can be seen that the temperature estimated by the IGBT frequency model is higher than the hottest IGBT over the complete output cycle of the inverter. Therefore, this model protects the devices in this condition. Furthermore, since these tests are performed at a high switching frequency (16kHz) the power loss in an IGBT is far greater than a diode. Consequently, the temperature of an IGBT is dominated by its self heating. For this reason the period where the peak current is present in each device can be easily identified, these locations are highlighted by the device labels shown in both

comparisons. As in the previous operating condition, it can be seen that the basic thermal model underestimates the temperature and does not provide adequate protection.

From the comparison of the diode frequency model shown in Figure 8.7(d), it can be seen that the temperatures of the hottest diode is underestimated by the model over the majority of the output cycle. Although, the estimated temperature is comparable to the measured temperature of D_{UU}, which is the diode this model was designed to protect. This device was selected using the power loss and the resulting thermal coupling calculated for a switching frequency of 3kHz. At a high switching frequency the power loss in an IGBT is significantly higher than a diode. Thus, in this instance, the temperature of a diode is dominated by the thermal coupling from any neighbouring IGBTs. To illustrate this effect, the diode in which the peak junction-to-thermistor temperature occurs (between the junction and thermistor) has been calculated in two different operating conditions. These results are shown in Figure 8.8.

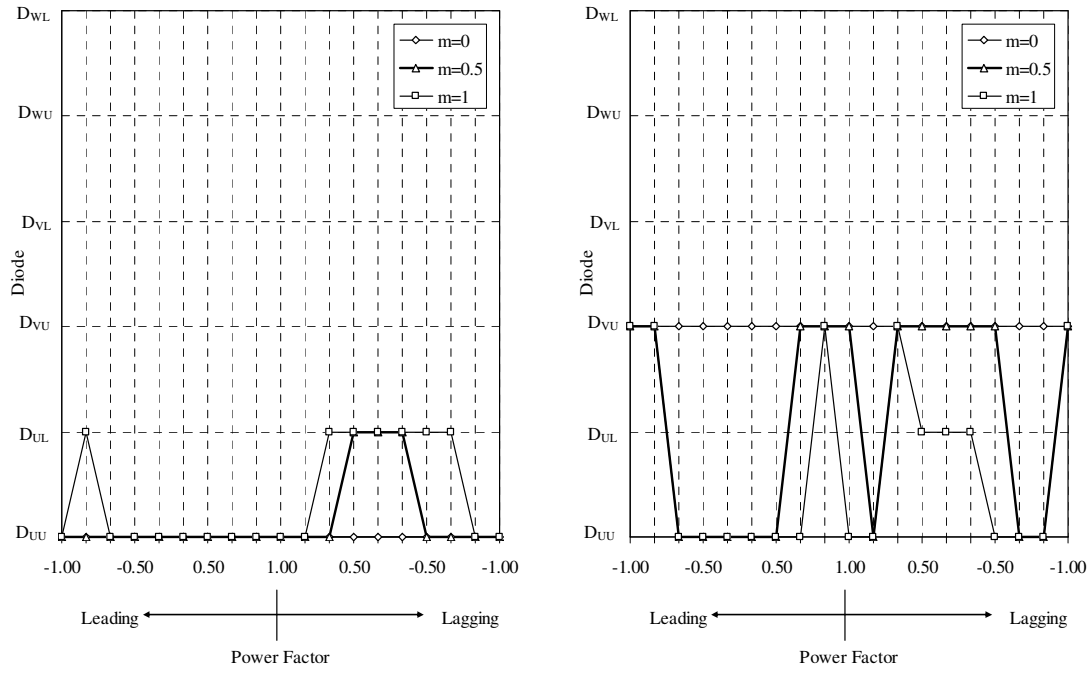

Figure 8.8: Diode in which the peak junction-to-thermistor temperature occurs in a stationary vector condition (a) operating condition A - I_L=50A, V_{DC}=600V, T_{th}=80°C and F_{SW}=3kHz (b) operating condition B - I_L=16A, V_{DC}=550V, T_{th}=40°C and F_{SW}=16kHz

In Figure 8.8(a), the results are calculated using the same operating conditions used in Chapter 7. These results show that when the modulation index is low, the peak junction-to-thermistor temperature always occurs in D_{UU}, hence why this device was initially chosen. However, for the operating conditions used to generate the comparisons in Figure 8.7, with a low modulation index the peak junction-to-thermistor temperature always occurs in D_{VU}. This finding is supported by the measured results in Figure 8.7(d).

In addition to the higher operating temperature, the thermal coupling from a neighbouring IGBT can increase the temperature gradient measured across the surface of the diode. Therefore, since the mutual thermal impedance is calculated using the mean temperature this gradient can have a significant effect on the accuracy of the estimated temperature. To illustrate this, a thermal image of the complete power module (operating at a low output frequency) has been taken when the peak power loss is in I_{WU}. This is shown in Figure 8.9(a). This clearly shows the six devices that are conducting at this output angle and using this data, the temperature gradient across a device can be determined.

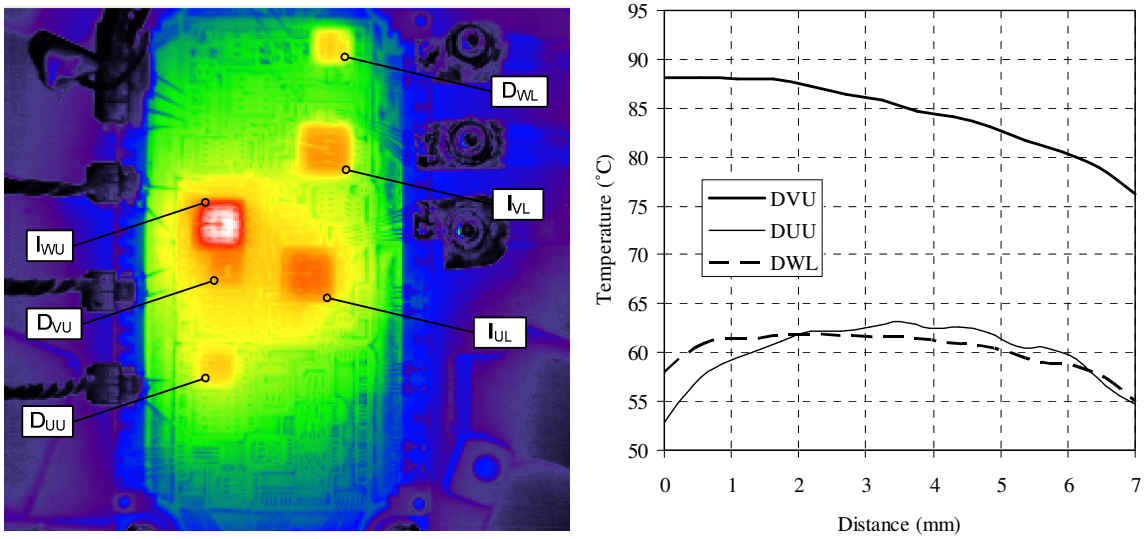

(a) (b)

Figure 8.9: Thermal coupling between I_{WU} and D_{VU} (a) thermal image taken with the peak loss in I_{WU} (b) measured profile temperature along the centre of a diode

The temperature gradient measured across the surface of the diodes is shown in Figure 8.9(b). These results show that the maximum temperature of D_{VU} (88˚C) occurs at the edge of the device and this is considerably higher than the mean temperature (84˚C). Therefore, this effect will contribute towards the underestimation of the device temperature. However, in these conditions, the temperature of the hottest IGBT is far higher than the hottest diode. Consequently, the IGBT model will provide the overall protection for the power module.

In summary, the comparison of the results measured with the inverter operating at a low output frequency and at a high switching frequency illustrates the following advantages and disadvantages:

Thermal Model	Advantages	Disadvantages
Frequency model	i) The thermal model for the IGBTs provides the overall protection for the power module	i) The diode temperature is underestimated ii) The accuracy of the estimated temperature is dependant on the operating conditions used to select the modelled devices
Basic drive model		i) The devices in the inverter can exceed their maximum temperature, an error of more than 10˚C has been observed

8.4.3 Operation at a High Output Frequency

The final comparison in this section shows the effect of operating at a higher output frequency. The results for this operating condition are shown in Figure 8.10. In this figure the measured IGBT temperatures are compared with the estimated temperatures at three output frequencies, ranging from 5Hz to 16.67Hz. The switching frequency used in these measurements was 16kHz. When the output frequency of the inverter is increased the thermal coupling between the devices in the power module changes and as predicted in Chapter 7, the peak junction-to-thermistor temperature no longer occurs in I_{UU}.

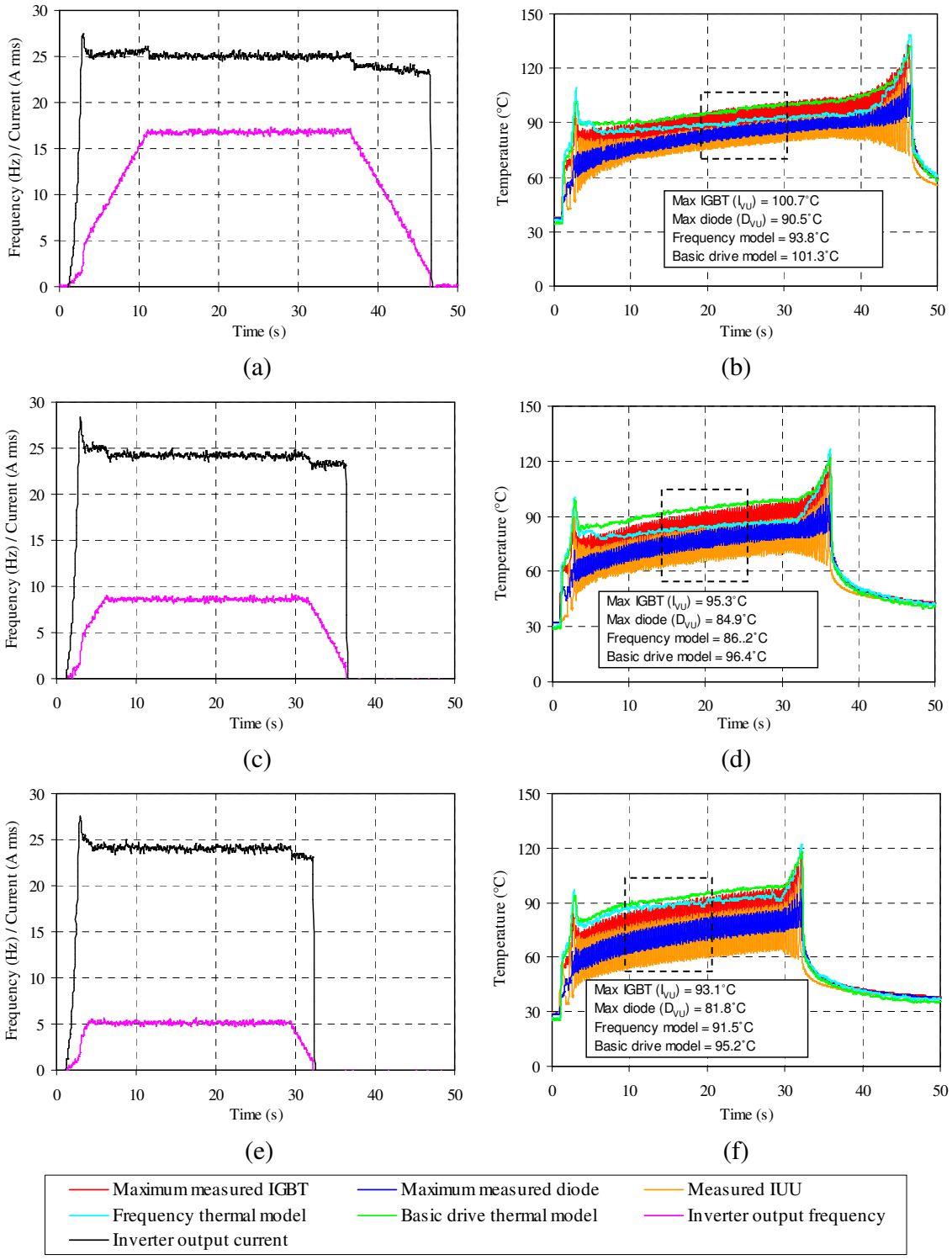

Figure 8.10: Comparison at a high output frequency (a) load conditions and (b) comparison at 16.7Hz (c) load conditions and (d) comparison at 8.3Hz (e) load conditions and (f) comparison at 5Hz

No margins have been added to the frequency model to account for this effect and as expected, the estimated temperature is lower than the hottest device, which in this case is I_{VU}. Even so, the temperature estimated by the frequency model does follow the peak temperature profile of the modelled device (I_{UU}). In contrast to the other operating conditions examined, the basic thermal model provides better protection for the devices in a steady-state condition. This is due primarily to the reduced thermal coupling between the devices and the smaller temperature difference between the case and the thermistor. Although, the characteristics of the factor K_{Fout} and the safety margins in the datasheet thermal impedance will also have an impact. Additional comparisons are presented in Appendix F.

In summary, the comparisons presented in this section highlight the following advantages and disadvantages:

Thermal Model	Advantages	Disadvantages
Frequency model	i) The estimated temperature follows the profile of the modelled IGBT (I_{UU})	i) The temperature of the hottest IGBT is underestimated
Basic drive model	i) In the steady-state, the devices are protected	

Overall, the three operating conditions examined so far have highlighted several key advantages and disadvantages for each model. The main conclusion that can be drawn from these comparisons is that the protection offered by the basic thermal model is not sufficient and the potential underestimation of the device temperature at low output frequencies could lead to the failure of the device. However, further comparisons are made in operating conditions specific to two common applications. These are described in the next section.

8.5 Application Case Studies

In this section the measured and estimated temperatures are compared using a typical load profile for a pick and place tool and an elevator.

8.5.1 Pick and Place Machine

A pick and place machine is designed to perform repetitive picking and placing tasks and these are widely used in factory automation. One of the key performance requirements for these machines is the speed of operation, and as such the motor used to rotate the machine into position must be accelerated rapidly. The load on the motor during this period is highly dependant on the inertia of the machine and a significant load current will only be present when the motor is accelerating or decelerating. The main purpose for choosing this application is that it will identify the ability of the thermal models to estimate the temperature during these very short transient periods.

8.5.1.1 Typical Load Profile

A typical speed and current profile for a pick and place machine is shown in Figure 8.11. This is a very simple application and can be reproduced by accelerating and decelerating a motor (with some added inertia) as fast as possible.

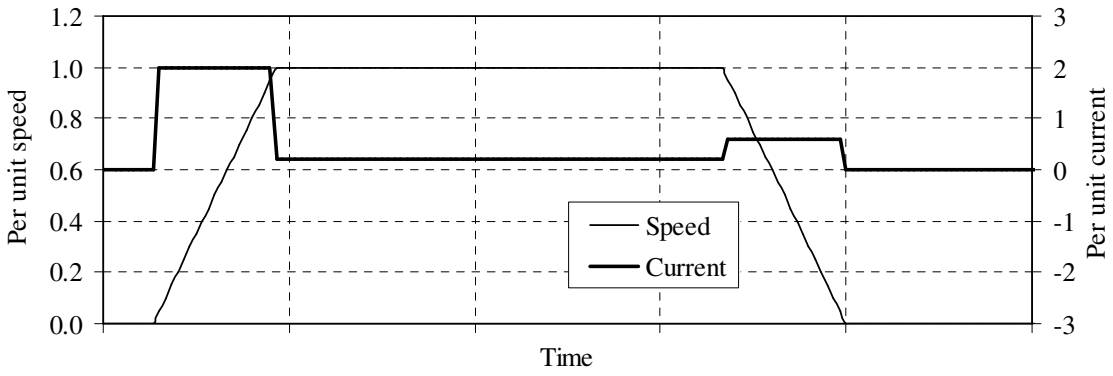

Figure 8.11: Typical pick and place machine load profile

In this application, the load current will be considerable at a low output frequency and this will have a significant impact on the characteristics of the estimated temperatures.

8.5.1.2 Comparison of Results

The comparison of the measured and estimated temperatures with the inverter operating at a switching frequency of 8kHz are shown in Figure 8.12. The comparison over the complete load profile is shown in Figure 8.12(b). In the steady-state the results are comparable to those shown in Section 8.4.3.

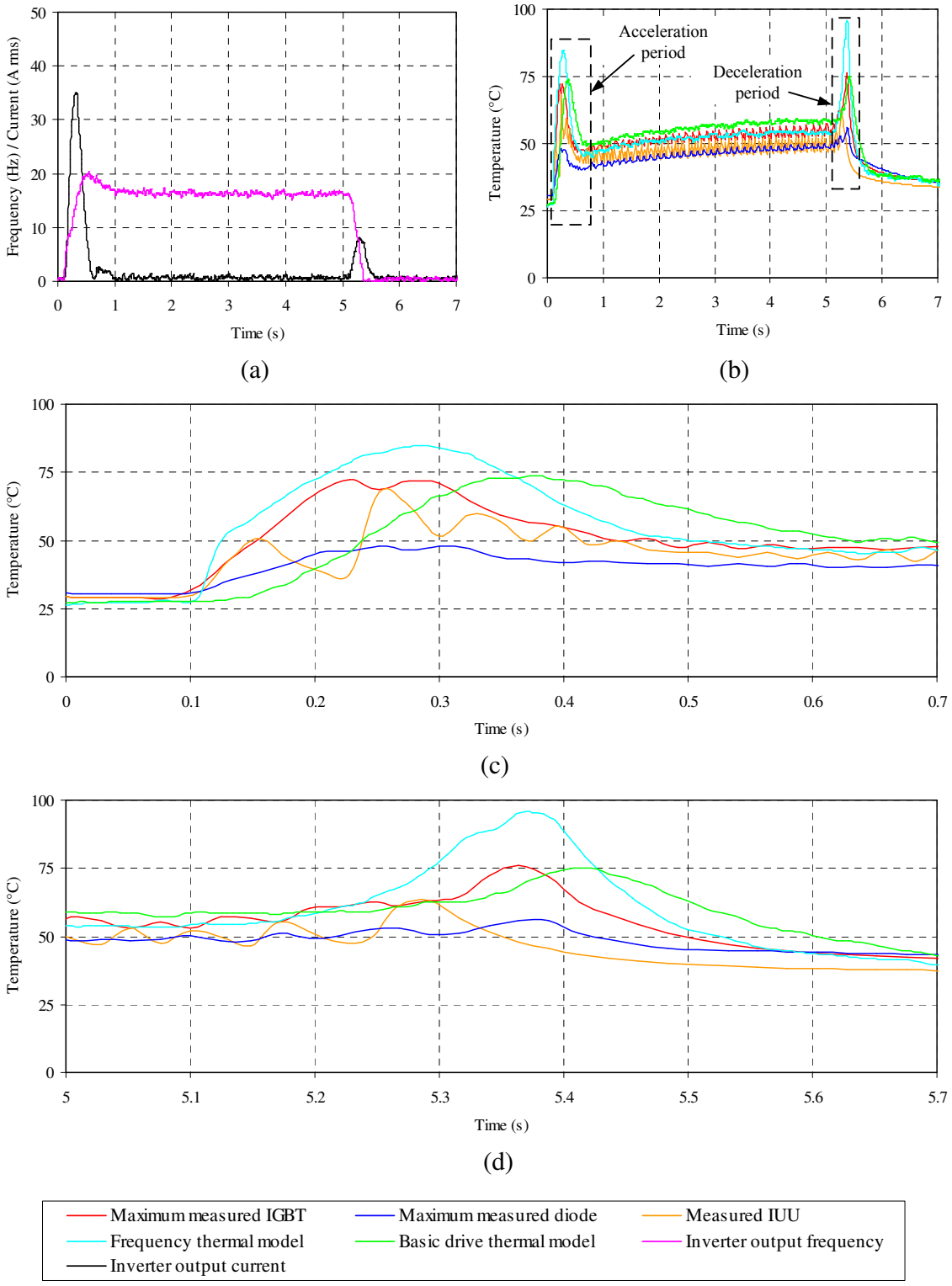

Figure 8.12: Pick and place machine tool comparison (a) load conditions and (b) comparison over the full profile (c) close up of the acceleration period (d) close up of the deceleration period

In this profile the motor is accelerated to full speed within approximately 0.3s. Due to this short time period it is difficult to identify the individual device temperatures in the complete response. Therefore, a close up of the acceleration and deceleration periods is shown in Figure 8.12(c) and Figure 8.12(d) respectively. From the temperatures measured when the motor is accelerating, it can be seen that apart from the initial 10ms, the temperature estimated by the IGBT frequency model is higher than the hottest IGBT. Although during this period, the temperature is overestimated by up to 10˚C. In contrast, due to the selection of the time constant (100ms) the basic thermal model underestimates the temperature by at least 30˚C over the entire acceleration period. Similar characteristics are seen during the deceleration period, although as shown in Chapter 4, in this type of operating condition the frequency model overestimates the device temperature.

In summary, the comparisons presented in this section highlight the following advantages and disadvantages:

Thermal Model	Advantages	Disadvantages
Frequency model	i) Protects all of the devices in the inverter during a fast transient	i) The temperature is overestimated during the transient periods especially when the load current is high and the output frequency is low ii) The temperature is underestimated in the steady-state condition
Basic drive model		i) During a fast transient the devices in the inverter can temporarily exceed their maximum temperature by more than 30˚C

8.5.2 Elevator

The recent trend in the elevator industry has been towards the development of gearless systems using permanent magnet motors. These offer the potential for a reduced space, higher efficiency and superior speed control, with full torque available down to zero speed

(stationary vector condition). To reduce the cost and size of the system, the drives are often selected so that they are operated close to their maximum rating. Furthermore, a high switching frequency is used in order to reduce the acoustic noise generated by the motor. Due to the cyclic nature of this application and the large temperature swings that can occur, the accurate estimation of the device temperature is essential for preventing early failures caused by the degradation of the component.

8.5.2.1 Typical Load Profile

A typical speed and current profile for an elevator application using a permanent magnet motor is shown in Figure 8.13. As shown, this profile includes a hold at floor current, which is required to hold the elevator car in position (at floor) until the mechanical brake is activated. During this period, the output current is dependant on the loading in the system and the inverter is operating in a stationary vector condition.

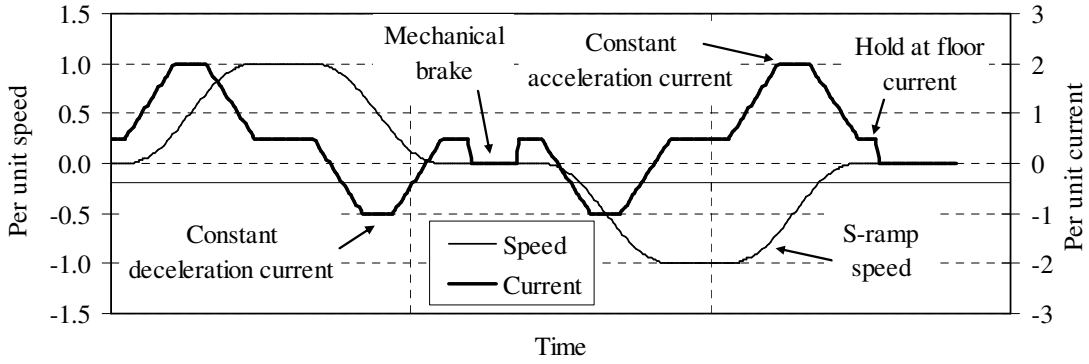

Figure 8.13: Typical elevator profile with hold at floor operation

As with many motion applications, an elevator often uses an S-ramp speed profile during the acceleration and deceleration periods. This is used to provide a smooth ride without significantly increasing the acceleration times.

8.5.2.2 Comparison of Results

The comparison of the measured and estimated temperatures with the inverter operating with a load profile similar to that of an elevator is shown in Figure 8.13. In this figure, three different conditions are shown and in each of these the switching frequency is 16kHz. In the first of these, the temperature is compared for a single profile (no hold at floor current) that represents a loaded elevator car moving up one or more floors.

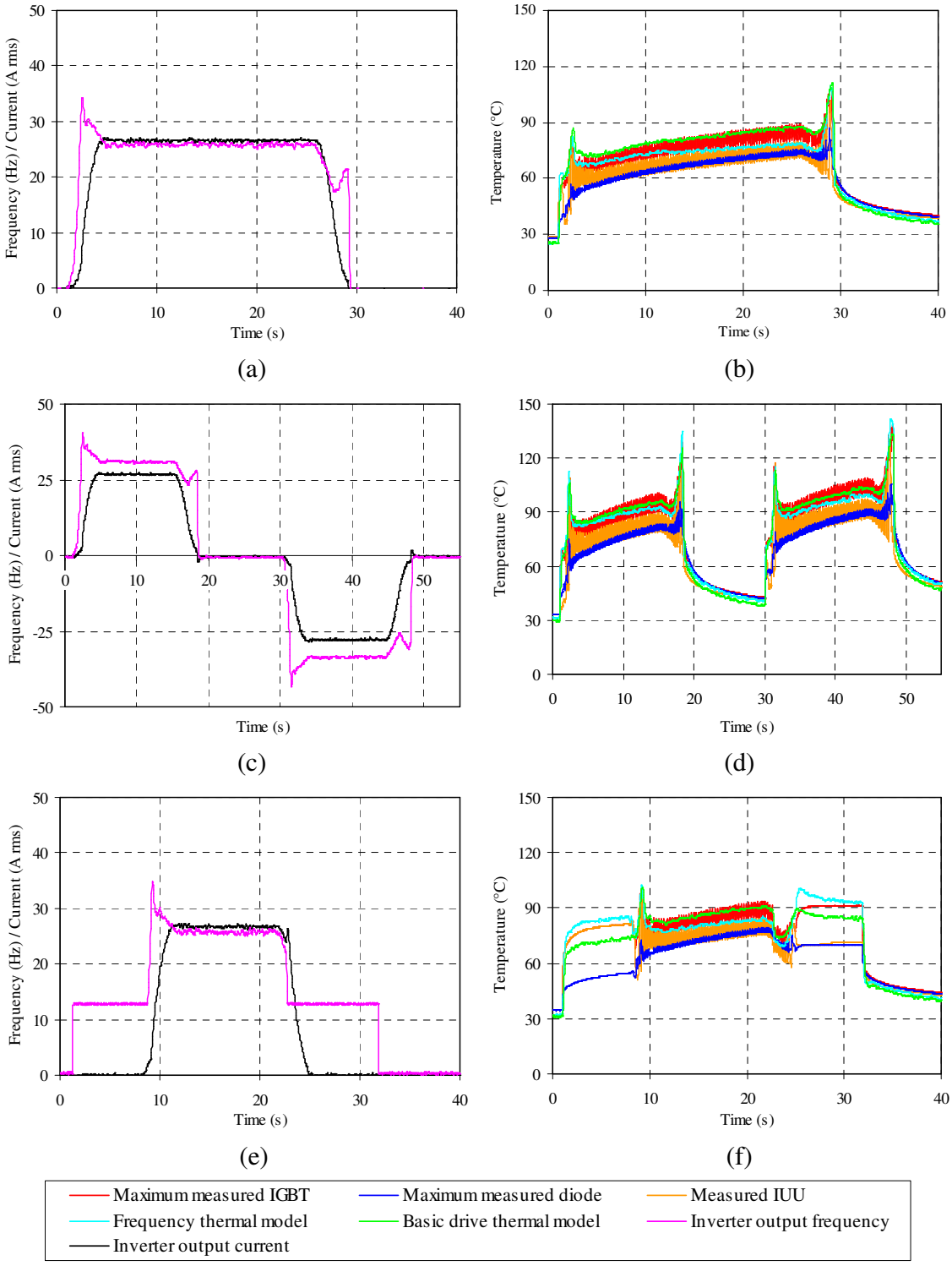

Figure 8.14: Elevator comparison with a steady state output frequency of 25Hz (a) load conditions and (b) comparison for a single profile (c) load conditions and (d) comparison for two profiles (e) load conditions and (f) comparison with hold at floor current

For this profile the frequency model underestimates the device temperature in the steady-state condition, although the protection is once again improved when the inverter is operating at a low output frequency. In Figure 8.13(d), the temperatures are compared over two complete profiles with a higher output current. This comparison shows how the temperature increases over each profile and by the end of the second profile the maximum temperature approaches 150˚C. The final comparison in Figure 8.13(f) includes a hold at floor current. As expected, for this profile the frequency model protects the devices when operating in a stationary vector condition, but begins to underestimate the temperature as the output frequency is increased. The opposite applies for the basic thermal model.

In order to compare the temperatures during the transient periods, a close up of the acceleration and deceleration periods for the second load profile (t=30 to 50s) in Figure 8.13(b) are shown in Figure 8.15. To indicate the demands placed on the power semiconductors in this type of application, the maximum change in temperature (ΔT) during each period has been identified.

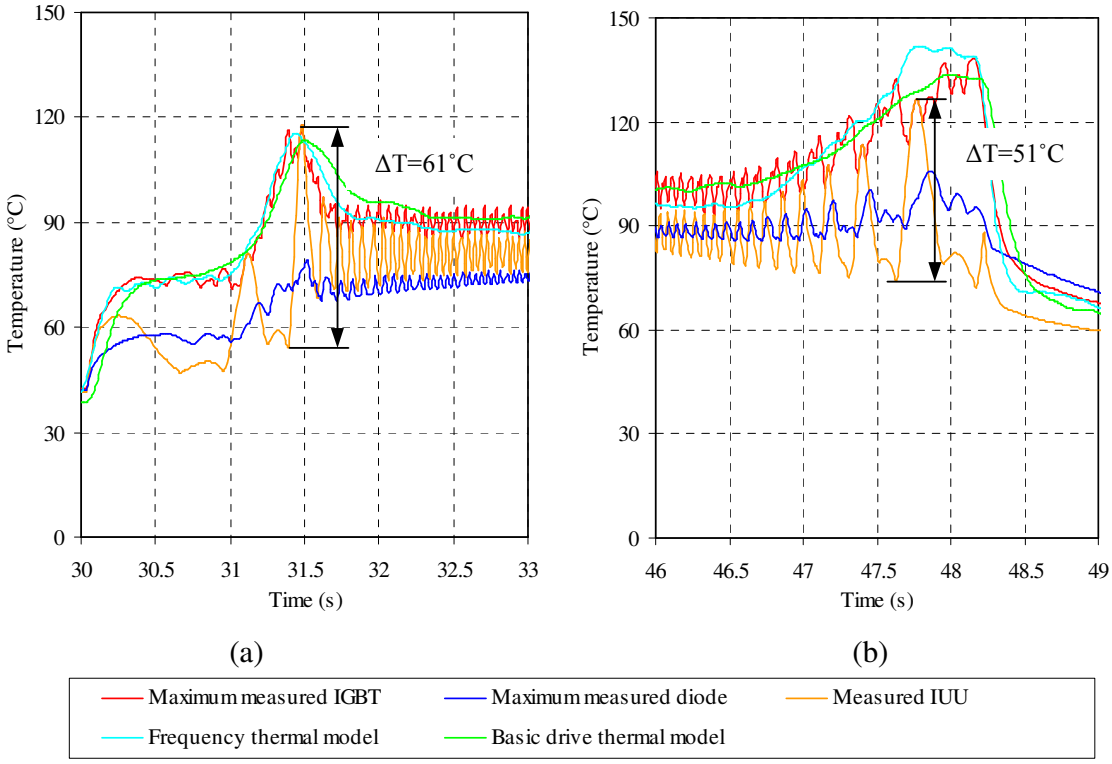

Figure 8.15: Close up of the elevator profile during (a) acceleration (b) deceleration

From these figures, it is evident that both of the thermal models provide similar levels of protection during the acceleration period and even when decelerating, the basic thermal model only underestimates the temperature by approximately 5˚C. Furthermore, as the output frequency is reduced the difference between the peak temperatures of each IGBT can be distinguished.

In summary, the comparisons presented in this section highlight the following advantages and disadvantages:

Thermal Model	Advantages	Disadvantages
Frequency model	i) Protects all of the devices at a low output frequency (hold at floor) and during the transient periods	i) Underestimates the temperature at a high output frequency
Basic drive model	i) Protects all of the devices when operating at a high output frequency	i) The devices in the inverter can exceed their maximum temperature during a hold at floor operation

8.6 Summary

In this chapter, the temperature estimated by the frequency thermal model was compared with the basic thermal model, which is currently implemented in a Unidrive SP, and the temperature measured using an infrared camera. These comparisons were performed under several operating conditions, which include the typical load profile for a pick and place tool and an elevator. The basic thermal model was developed using several assumptions that allow it to be developed using the thermal impedance provided in the datasheet. The development of this model was described in Section 8.2. The main advantage of this approach is that it reduces the time needed to generate the input data for the thermal model, but these approximations will have an impact on the accuracy of this model. This will be more evident in certain operating conditions.

The first operating condition examined in this chapter was a stationary vector condition. When operating in this condition, the effect of the thermal coupling between the devices is significant. This was highlighted in the comparisons performed at the different output angles, which were shown in Section 8.4.1. Due to this thermal coupling, the basic thermal model (based on the self thermal impedance) significantly underestimates the device temperature, whereas the frequency model was shown to protect the devices in each of the operating conditions examined. Similar characteristics were seen in the comparisons in Section 8.4.2, which show the response at a low output frequency. As the output frequency is increased, the effect of the thermal coupling between the devices and the temperature difference between the case, measured directly under a device, and the thermistor is reduced. Consequently, the protection provided by the basic thermal model is improved. This was shown in the comparisons in Section 8.4.3. Furthermore, since the device in which the peak junction-to-thermistor temperature occurs is dependant on the operating condition, at a high output frequency the frequency thermal model underestimates the temperature of the hottest device.

Additional comparisons were shown in Section 8.5, where a load profile similar to that of a pick and place machine and an elevator were defined. These comparisons emphasised many of the characteristics seen in the previous operating conditions, but were also used to highlight the transient characteristics of each model.

Overall, the comparisons in this chapter have shown that the basic thermal model does not prevent the devices in the inverter from exceeding their maximum operating temperature, especially when operating at a low output frequency or during fast transients. In some conditions the model was shown to underestimate the temperature by well over 20˚C. Therefore, with a trip temperature of 150˚C it would be possible for the device temperature to exceed 170˚C, which is not acceptable. In contrast, the frequency model protects the devices at a low output frequency, but due to the selection of the modelled devices it begins to underestimate the temperature as the output frequency is increased. This effect was predicted in Chapter 7. Therefore, the adaptation of the frequency model in order for it to provide adequate protection at both low and high output frequencies is an area for further work.

Chapter 9: Conclusion

9.1 General Overview

The main aim of this work has been to develop a thermal model that can accurately estimate the temperature of the power semiconductors in an inverter. One of the constraints placed on this design is that it must be possible to implement the thermal model using the computational resources available in a commercial drive without introducing the risk of aliasing. This constraint has had a significant impact on the development of the thermal model and several compromises have been made in order to reduce its complexity, although at each stage care has been taken to prevent the temperature from being underestimated. This chapter provides an overview of the work presented in this thesis and examines the extent to which the objectives outlined in Chapter 1 have been achieved.

The scope of this work is limited to the protection of the components in the inverter stage of a drive and does not include protection for the components in the rectifier or brake. Furthermore, the variation of the thermal and electrical characteristics between power modules and the degradation of these over the lifetime of a device has not been considered.

The weaknesses of the existing thermal model implemented in a Control Techniques, Unidrive SP have been identified. This model is based on the thermal impedance provided by the manufacturer and ignores the effect of the thermal coupling between devices and the location of the internal thermistor in the power module. Ignoring these could result in the temperature of the power semiconductor being significantly underestimated, possibly leading to the premature failure of the inverter. This is more likely to occur when the inverter is operating at an output frequency of 0Hz. In this condition, there is no filtering effect due to the thermal capacity of the material in the power module and heatsink, and it is possible for one device to be continuously operated at the peak output current. For these reasons, this operating condition is used to develop and validate the new thermal model.

The temperature of every device in an inverter can be estimated by implementing the complete thermal impedance matrix. However, with the available computational resources it is not possible to implement the complete matrix at a sample rate high enough to avoid aliasing. In [1] a procedure has been described to simplify the thermal impedance matrix by selecting only the key values, although this is still difficult to implement. In this work the thermal impedance matrix is solved in the frequency domain. The main advantage of this approach is that it reduces the computational resource required to avoid aliasing due to the output frequency of the inverter.

9.2 Thermal Model for a Single Device

The thermal model developed in this work is used to estimate the temperature difference between the junction of an IGBT or diode and the internal thermistor in a power module. The temperature of a single device is estimated as follows:

- The self thermal impedance between the junction of a device and the internal thermistor is measured and this is represented by an equivalent Foster network.
- The power loss generated in a device over a complete output cycle of the inverter ($1/F_{out}$) is approximated by a number of frequency components. The magnitude of these components is modified to avoid underestimating the power loss.
- The steady-state temperature over a complete output cycle is calculated by multiplying each of the frequency components with the response of the Foster network. The general response is calculated off-line.
- The peak junction-to-thermistor temperature over the output cycle is calculated using a method based on the Taylor series approximation of each frequency component, this temperature is the steady-state output of the thermal model.
- To model the transient response due to a step change in power loss or output frequency, a transient component is added to the steady-state response.

The main advantage of this approach is that when compared to a model implemented in the time domain the number of on-line calculations is significantly reduced. Furthermore, since the peak junction-to-thermistor temperature is known, the risk of aliasing when the inverter is operating at higher output frequencies has been minimised. However, several

approximations were made during the calculation of the frequency components which can cause the steady-state temperature to be overestimated, although a single device is always protected. The accuracy of the transient response is limited by the implementation of the ripple and transient components, which can lead to the temperature being underestimated for a short period during sudden changes in output frequency.

9.3 Thermal Model for a Multi-chip Device

In a multi-chip device the temperature difference between the junction of a device and the internal thermistor is affected by the thermal coupling from the other devices in the inverter. The single device model has been adapted to model this effect. The temperature of a device in a multi-chip power module is estimated as follows:

- The self and mutual thermal impedance for every device in the inverter is measured and each of these is represented by an equivalent Foster network.
- The measured thermal impedances form the complete thermal impedance matrix for the inverter with 144 elements. This is used to identify the IGBT and diode with the largest temperature difference between itself and the thermistor when the inverter is operating at 0Hz. This calculation is performed off-line.
- The row of thermal impedances (self and mutual) for these devices is selected from the complete matrix, reducing the matrix used in the thermal model to 24 elements.
- By examining the transient response, a common time constant is selected for thermal coupling (mutual impedance) between the selected devices and the other IGBTs and diodes in the inverter. The response of these mutual impedances is then combined off-line, reducing the matrix to 6 elements.
- The temperature rise due to the individual elements for the hottest IGBT and diode is calculated using the general frequency components developed for the single device. Linear superposition is used to calculate the total steady-state temperature.
- The transient response is modelled in the same manner as the single device.

In a multi-chip device operating under constant conditions the temperature difference calculated between the hottest device and the internal thermistor is constant and is equal to the largest temperature difference at any output angle (i.e. the worst case). However, like

the power semiconductors, the temperature of the thermistor is dependant on the thermal coupling between itself and any nearby devices. Thus, combining the constant output of the thermal model with the measured thermistor temperature can result in the temperature being overestimated. Other factors that can have an influence on the accuracy of the thermal model include:

- The power loss generated in a device is dependant on its temperature, but in this model only the temperature of one IGBT and diode is known. Therefore, it is assumed that the peak power loss in the other devices is the same.
- When using the internal thermistor to provide the temperature feedback for the thermal model the mutual thermal impedances can be negative. If so, any overestimation in the power loss can decrease the estimated temperature.
- To combine the mutual thermal impedance a common time constant is selected and this has an impact on the accuracy of the transient response and to a lesser extent, the steady-state temperature.

9.4 Measurements

To implement the thermal model the following parameters have been measured:

Electrical:	Turn on, turn off and reverse recovery switching loss
	On-state and forward voltage
Thermal:	Self thermal impedance between the junction and thermistor
	Mutual thermal impedance between the junction and thermistor

These measurements (electrical and thermal) have been performed with the power module connected externally from the drive, but on a standard heatsink. This configuration allows the temperature of the IGBTs and diodes to be measured by an infrared camera. Each of the electrical parameters are estimated by a polynomial expression, these are generated by curve fitting the expression to the measurements taken at different temperatures, currents and voltages. The accuracy of these expressions is reasonable in all conditions. The thermal impedance is calculated from the cooling response measured by an infrared camera. To implement the thermal model an equivalent Foster network is curve fitted to the measured

values; two network elements are used for the self thermal impedance and a single element for the mutual impedance. These parameters are used to select the modelled devices and for the power module examined in this work, the upper IGBT and diode in the U phase have been selected (I_{UU} and D_{UU}).

9.5 Comparison of the Thermal Model with Measured Temperatures

Two thermal models have been implemented in a Control Techniques, Unidrive SP:

- The frequency thermal model that is described in this work
- A basic thermal model developed from the datasheet thermal impedance (i.e. the thermal model currently used in the Unidrive SP)

The temperature estimated by these models has been compared with the temperature measured by the infrared camera under a range of operating conditions; these conditions have been selected to highlight the key advantages and limitations of both models.

When operating in a stationary vector condition it was shown that the frequency model protects the inverter, but can overestimate the temperature during the initial transient period, or when operating at an output angle other than that where the peak junction-to-thermistor temperature occurs. In contrast, despite the margins within the basic thermal model it can significantly underestimate the temperature, an error of more than 25˚C has been observed.

At higher output frequencies the effect of the thermal coupling between each device is changed. In this condition the temperature estimated by the frequency model continues to follow the peak profile of I_{UU} and D_{UU}. However, these are no longer the hottest devices. Consequently, the frequency model underestimates the temperature. This effect was predicted during the development of the thermal model, but no margins were added to the model to allow the fundamental approach to be evaluated. The protection offered by the basic thermal model is improved at a higher output frequency. This is because the impact of the thermal coupling and the temperature difference between the case and thermistor is reduced to a level where it is smaller that the margins in the model.

Other conditions that have been examined include operating with a load profile similar to that of a machine tool and an elevator; the same conclusions can be drawn from these comparisons.

The frequency model developed in this work has the potential to achieve all of the aims set out in Chapter 1, i.e. to develop a thermal model that can protect an inverter in any operating condition and be implemented using the existing computational resource in a commercial drive.

The only factors preventing the direct application of this model to an industrial application is the underestimation of the temperature at higher output frequencies, but this can be avoided by the calculation of a suitable safety margin.

9.6 Recommendations for Further Work

This research has focused on the development of a thermal model to protect the power semiconductors in the inverter stage. During this development several areas have been identified that would benefit from further work.

1. **Transient component:** The method used to implement the transient component in the frequency model can cause the estimated temperature to increase every time the operating conditions change. This can be a problem in cyclic applications and more work is required to eliminate this effect.
2. **Ripple component:** The peak ripple temperature is calculated from the sum of the frequency components and this is added to the output of the thermal model as a constant value. This can lead to an overestimation of the device temperature. One solution is to apply the ripple component to a first order filter where the time constant is dependant on the output frequency. More work is required to establish the impact of this approximation.
3. **Device selection**: The IGBT and diode with the largest temperature difference between the junction and thermistor are calculated in a stationary vector condition. As the output frequency is increased the device in which the largest temperature difference occurs can change. There are two possible solutions; add a constant

margin to the thermal impedance or select two or more conditions (e.g. 0Hz, 5Hz 10Hz, etc) and change the thermal impedance with the output frequency. Further simulation and experimental work is required to validate these options.

In addition to the development of the thermal model, areas where further work can be applied include:

1. **Extending the frequency model to other devices:** The interaction between the devices in the inverter, rectifier and brake was not considered in this work. More work is required to establish the effect of the thermal coupling between these stages and to develop a model that can also protect the rectifier and brake.
2. **Using the estimated temperature:** The output of the thermal model is used to prevent the components in the inverter from exceeding their maximum temperature by tripping the drive. More sophisticated control of the drive operating parameters (e.g. output current, switching frequency, etc) and the speed of the cooling fan may improve the general performance of the drive.
3. **Improving power semiconductor lifetimes:** The lifetime of the components in the inverter are highly dependant on the thermal cycling present in an application. Even if the temperature of the components is kept below their maximum values the effect of thermal cycling on the lifetime of the inverter can be significant. Existing research has focused on indentifying the causes of failure (e.g. the degradation of the solder layers, bond wire lift off, etc) and the estimation of the life time when operating with predictable load profile. Using the temperature estimated by a thermal model to control the drive operating conditions in order to reduce the temperature swings and prolong the lifetime of the inverter is a novel area of research that would benefit from further work.

Appendix A: Temperature Response of the Frequency Model

A.1 Introduction

In this appendix, the steady-state, DC and transient components of the temperature response due to a step change in power loss and output frequency are calculated for the switching and conduction loss models. To show how these are calculated, a general frequency term representing part of the complete power loss in a device is applied to a Foster network element. The resulting temperature response for this general component is shown in Section A.1.1. This analysis is then used to generate the complete solution for the switching and conduction loss, these are shown in Section A.1.2 and Section A.1.3 respectively.

A.1.1 Calculation of the Frequency Components for a General Term

In this section, the complete temperature response is calculated for a general frequency component (n^{th} harmonic) with an offset (λ):

$$P(\omega t) = \hat{P}\sin\left(n\omega t + \lambda\right) \tag{A.1}$$

This frequency component is applied to a Foster network element, and in the Laplace domain, the response of this element is:

$$Z_{th}(s) = \frac{R_{th}}{\left(1+\tau s\right)} \tag{A.2}$$

To calculate the resulting temperature response the following equation must be solved:

$$T(s) = P(s)Z_{th}(s) \tag{A.3}$$

and for the chosen frequency component (Equation A.1), the temperature response is given by:

$$T(s) = \frac{\hat{P}R_{th}}{1+\varpi s}\left[\frac{n\omega\cos(\lambda) + s\sin(\lambda)}{s^2 + (n\omega^2)}\right] = \frac{A}{s+jn\omega} + \frac{B}{s-jn\omega} + \frac{C}{1+\varpi s} \tag{A.4}$$

This can be rearranged into the form:

$$\hat{P}R_{th}\left[n\omega\cos(\lambda) + s\sin(\lambda)\right] = \begin{array}{r} A(s-jn\omega)(1+\varpi s) + \\ B(s+jn\omega)(1+\varpi s) + \\ C(s+jn\omega)(s-jn\omega) \end{array} \tag{A.5}$$

To solve this equation, the magnitude of each partial faction term (A, B and C) must be calculated. For example, if $s = -jn\omega$ the magnitude of A is given by:

$$A = \frac{\hat{P}R_{th}}{2}\left[\frac{1}{\sqrt{(n\omega\tau)^2+1}}\angle -\lambda - \pi - \tan^{-1}\left(\frac{1}{n\omega\tau}\right)\right] \tag{A.6}$$

This magnitude is shifted by π to account for the imaginary part of the denominator, which in this instance is negative. The phase shift due to the filtering effect of the thermal time constant (τ) can be represented in the form:

$$\tan^{-1}\left(\frac{1}{n\omega\tau}\right) = \frac{\pi}{2} - \tan^{-1}(n\omega\tau) \tag{A.7}$$

and by assigning:

$$\beta_n = -\tan^{-1}(n\omega\tau) \tag{A.8}$$

and

$$A_{Fn} = \frac{1}{\sqrt{(n\omega\tau)^2+1}} \tag{A.9}$$

The magnitude of A can be expressed as:

$$A = \frac{\hat{P}R_{th}A_{Fn}}{2} \angle -\lambda + \frac{\pi}{2} - \beta_n \tag{A.10}$$

or alternatively, in the complex form:

$$A = \frac{\hat{P}R_{th}A_{F1}}{2}\left[\sin(\lambda + \beta_n) + j\cos(\lambda + \beta_n)\right] \tag{A.11}$$

The inverse Laplace transform for partial fraction A is:

$$\left(\frac{A}{s + jn\omega}\right) = Ae^{-jn\omega t} = A\cos(n\omega t) - jA\sin(n\omega t) \tag{A.12}$$

By substituting the magnitude of A (Equation A.11) into this equation, the temperature response for this term is given by:

$$T_A(\omega t) = \frac{\hat{P}R_{th}A_{F1}}{2}\begin{bmatrix}\sin(\lambda + \beta_n)\cos(n\omega t) - j\sin(\lambda + \beta_n)\sin(n\omega t) \\ + j\cos(\lambda + \beta_n)\cos(n\omega t) + \cos(\lambda + \beta_n)\sin(n\omega t)\end{bmatrix} \tag{A.13}$$

Using the procedure outlined above it can be shown that the magnitude of the partial fraction B, in complex form, is given by:

$$B = \frac{\hat{P}R_{th}A_{F1}}{2}\left[\sin(\lambda + \beta_n) - j\cos(\lambda + \beta_n)\right] \tag{A.14}$$

The inverse transform for this partial fraction is:

$$\left(\frac{B}{s - jn\omega}\right) = Be^{jn\omega t} = B\cos(n\omega t) + jB\sin(n\omega t) \tag{A.15}$$

and the corresponding temperature response for this term is:

$$T_B(\omega t) = \frac{\hat{P}R_{th}A_{F1}}{2}\begin{bmatrix}\sin(\lambda+\beta_n)\cos(n\omega t)+j\sin(\lambda+\beta_n)\sin(n\omega t)\\ -j\cos(\lambda+\beta_n)\cos(n\omega t)+\cos(\lambda+\beta_n)\sin(n\omega t)\end{bmatrix} \quad \text{(A.16)}$$

By comparing Equations A.13 and A.16, it can be seen that the magnitude of B is the complex conjugate of A. Consequently, adding the temperature response of A and B together gives:

$$T_{A+B}(\omega t) = \hat{P}R_{th}A_{F1}\left[\sin(\lambda+\beta_n)\cos(n\omega t)+\cos(\lambda+\beta_n)\sin(n\omega t)\right] \quad \text{(A.17)}$$

Combining the frequency components in this response:

$$T_{A+B}(\omega t) = \hat{P}R_{th}A_{F1}\sin(n\omega t+\lambda+\beta_n) \quad \text{(A.18)}$$

This response is defined as the steady-state component and is equivalent to the original input signal (Equation A.1) with a modified magnitude (A_{Fn}) and a phase shift (β_n), both of these are dependant on the time constant of the network element and the output frequency. However, as shown in Equation A.4, there are three partial fraction terms in the complete response. The magnitude of the final term (C) is calculated by assigning $s=-1/\tau$ and is given by:

$$C = \frac{\hat{P}R_{th}\left[n\omega\cos(\lambda)-\frac{1}{\tau}\sin(\lambda)\right]}{\left(\frac{1}{\tau}\right)^2+(n\omega)^2} \quad \text{(A.19)}$$

The inverse Laplace transform for partial fraction C is:

$$\left(\frac{C}{1+\tau s}\right) = \frac{C}{\tau}e^{\frac{-t}{\tau}} \quad \text{(A.20)}$$

and the temperature response for this term is:

$$T_C(\omega t) = \frac{\hat{P}R_{th}\left[n\omega\tau\cos(\lambda) - \sin(\lambda)\right]}{1+(n\omega\tau)^2} e^{\frac{-t}{\tau}} \tag{A.21}$$

As shown in Equation A.20, after the step change the magnitude of this term decays to zero and this is therefore referred to as the transient component of the response. In summary, the complete temperature response due to a sine component of the n^{th} harmonic in the frequency model is given by:

$$T(\omega t) = \hat{P}R_{th}\left[A_{F1}\sin(n\omega t + \lambda + \beta_n) + \frac{\left[n\omega\tau\cos(\lambda) - \sin(\lambda)\right]}{1+(n\omega\tau)^2} e^{\frac{-t}{\tau}} \right] \tag{A.22}$$

or for a cosine component, which is calculated using an offset angle of $\pi/2$:

$$T(\omega t) = \hat{P}R_{th}\left[A_{F1}\cos(n\omega t + \lambda + \beta_n) - \frac{\left[n\omega\tau\sin(\lambda) + \cos(\lambda)\right]}{1+(n\omega\tau)^2} e^{\frac{-t}{\tau}} \right] \tag{A.23}$$

The final component in the complete temperature response is defined as the DC component. For a DC component with a unity magnitude, the temperature response due to a step change in power loss is given by:

$$T(s) = \frac{\hat{P}R_{th}}{s(1+\tau s)} \tag{A.24}$$

and by using the inverse Laplace transform, the temperature response of this component in the time domain is:

$$T(\omega t) = \hat{P}R_{th}\left(1 - e^{\frac{-t}{\tau}}\right) \tag{A.25}$$

In the following sections, Equations A.22, A.23 and A.25 are used to calculate the complete temperature response for the switching and conduction loss models that were described in Chapter 4.

A.1.2 Complete Temperature Response for the Switching Loss Model

For the switching loss model, the power loss over the output cycle of the inverter is approximated by:

$$P_{sw}(\omega t) = \hat{P}_{sw}\begin{pmatrix}\left(\frac{1}{\pi} + A_{p(DC)}\right) + \frac{1}{2}\sin(\omega t + \theta + \alpha) \\ -\left(\frac{2}{3\pi} - A_{p(ac)}\right)\cos(2\omega t + 2\theta + 2\alpha)\end{pmatrix} \tag{A.26}$$

This equation has three components, a DC, fundamental (n=1) and second (n=2) harmonic. Therefore, using the equations developed in Section A.1.1, the DC, steady-state and transient components of the temperature response caused by a step change in the peak switching loss are as shown in Table A.1. For the switching loss the phase shift $\lambda=\theta+\alpha$.

Table A.1: Components of the temperature response due to the device switching loss

Frequency Component	Magnitude	Steady State	Transient
DC	$A_{DC}= \hat{P}_{sw}R_{th}\left(\frac{1}{\pi} + A_{p(DC)}A_{F1}\right)$		
sin(ωt)	$A_{s1}=\frac{\hat{P}_{sw}R_{th}}{2}\cos(\theta+\alpha+\beta_n)$	$A_{s1}A_{F1}$	$\frac{A_{s1}\omega\tau}{1+(\omega\tau)^2}$
sin(2ωt)	$A_{s2}= \hat{P}_{sw}R_{th}\left(\frac{2}{3\pi} - A_{p(ac)}\right)\sin(2\theta+2\alpha+\beta_n)$	$A_{s2}A_{F2}$	$\frac{2A_{s2}\omega\tau}{1+(2\omega\tau)^2}$
cos(ωt)	$A_{c1}=\frac{\hat{P}_{sw}R_{th}}{2}\sin(\theta+\alpha+\beta_n)$	$A_{c1}A_{F1}$	$\frac{-A_{c1}}{1+(\omega\tau)^2}$
cos(2ωt)	$A_{c2}=-\hat{P}_{sw}R_{th}\left(\frac{2}{3\pi} - A_{p(ac)}\right)\cos(2\theta+2\alpha+\beta_n)$	$A_{c2}A_{F2}$	$\frac{-A_{c2}}{1+(2\omega\tau)^2}$

By separating the frequency terms into their sine and cosine components the effect of the phase shift is incorporated into the magnitude of these terms. Therefore, in terms of the transient response there is no phase shift and each term is calculated with λ=0.

A.1.3 Complete Temperature Response for the Conduction Loss Model

For the conduction loss model, the power loss over the output cycle of the inverter with a unity duty cycle is approximated by:

$$P_{con(\delta_m=1)}(\omega t) = \hat{P}_{con}\begin{pmatrix}\left(\frac{1}{\pi}+A_{p(DC)}\right)+\frac{1}{2}\sin(\omega t+\theta+\alpha)\\ -\left(\frac{2}{3\pi}-A_{p(ac)}\right)\cos(2\omega t+2\theta+2\alpha)\end{pmatrix} \tag{A.27}$$

and the duty cycle due to the modulation scheme is approximated by:

$$\delta_m = \left(0.5+\frac{m_{(DC)}A_{F3}}{6\sqrt{3}}\right)+\frac{m}{\sqrt{3}}\sin(\omega t+\alpha) \tag{A.28}$$

Therefore, the power loss that is applied to the Foster network element is given by:

$$P_{con} = \delta_m P_{con(\delta_m=1)} \tag{A.29}$$

By multiplying the frequency components in the power loss and duty cycle, the resulting power loss (P_{con}) will consist of the DC and fundamental components (n=1) as well as the second (n=2) and third (n=3) harmonics. The DC, steady-state and transient components of the temperature response caused by a step change in the peak conduction loss are as shown in Table A.2.

Table A.2: Components of the temperature response due to the device conduction loss

Frequency Component	Magnitude	Steady State	Transient
DC	$A_{DC}=\hat{P}_{con}R_{th}\left[\frac{m}{4\sqrt{3}}\cos(\theta)+\left(\frac{1}{\pi}+A_{P(DC)}A_{F(DC)}\right)\left(\frac{1}{2}+\frac{m_{(DC)}A_{F3}}{6\sqrt{3}}\right)\right]$		
sin(ωt)	$A_{s1}=\hat{P}_{con}R_{th}\left[\begin{array}{l}\frac{1}{2}\left(\frac{1}{2}+\frac{m_{(DC)}A_{F3}}{6\sqrt{3}}\right)\cos(\theta+\alpha+\beta_1)\\+\left(\frac{2}{3\pi}-A_{p(ac)}\right)\frac{m}{2\sqrt{3}}\cos(2\theta+\alpha+\beta_1)\\+\left(\frac{1}{\pi}+A_{p(DC)}A_{F(DC)}\right)\frac{m}{\sqrt{3}}\cos(\alpha+\beta_1)\end{array}\right]$	$A_{s1}A_{F1}$	$\frac{A_{s1}\omega\tau}{1+(\omega\tau)^2}$
sin(2ωt)	$A_{s2}=\hat{P}_{con}R_{th}\left[\begin{array}{l}\left(\frac{2}{3\pi}-A_{P(ac)}\right)\left(\frac{1}{2}+\frac{m_{(DC)}A_{F3}}{6\sqrt{3}}\right)\\\times\sin(2\theta+2\alpha+\beta_2)\\+\frac{m}{4\sqrt{3}}\sin(\theta+2\alpha+\beta_2)\end{array}\right]$	$A_{s2}A_{F2}$	$\frac{2A_{s2}\omega\tau}{1+(2\omega\tau)^2}$
sin(3ωt)	$A_{s3}=-\hat{P}_{con}R_{th}\left(\frac{2}{3\pi}-A_{P(ac)}\right)\frac{m}{2\sqrt{3}}\cos(2\theta+3\alpha+\beta_3)$	$A_{s3}A_{F3}$	$\frac{3A_{s3}\omega\tau}{1+(3\omega\tau)^2}$
cos(ωt)	$A_{c1}=\hat{P}_{con}R_{th}\left[\begin{array}{l}\frac{1}{2}\left(\frac{1}{2}+\frac{m_{(DC)}A_{F3}}{6\sqrt{3}}\right)\sin(\theta+\alpha+\beta_1)\\+\left(\frac{2}{3\pi}-A_{p(ac)}\right)\frac{m}{2\sqrt{3}}\sin(2\theta+\alpha+\beta_1)\\+\left(\frac{1}{\pi}+A_{p(DC)}A_{F(DC)}\right)\frac{m}{\sqrt{3}}\sin(\alpha+\beta_1)\end{array}\right]$	$A_{c1}A_{F1}$	$\frac{-A_{c1}}{1+(\omega\tau)^2}$
cos(2ωt)	$A_{c2}=-\hat{P}_{con}R_{th}\left[\begin{array}{l}\left(\frac{2}{3\pi}-A_{P(ac)}\right)\left(\frac{1}{2}+\frac{m_{(DC)}A_{F3}}{6\sqrt{3}}\right)\\\times\cos(2\theta+2\alpha+\beta_2)\\+\frac{m}{4\sqrt{3}}\cos(\theta+2\delta+\beta_2)\end{array}\right]$	$A_{c2}A_{F2}$	$\frac{-A_{c2}}{1+(2\omega\tau)^2}$
cos(3ωt)	$A_{c3}=-\hat{P}_{con}R_{th}\left(\frac{2}{3\pi}-A_{P(ac)}\right)\frac{m}{2\sqrt{3}}\sin(2\theta+3\alpha+\beta_3)$	$A_{c3}A_{F3}$	$\frac{-A_{c3}}{1+(3\omega\tau)^2}$

Appendix B: Measured Thermal Parameters for the Inverter

B.1 Introduction

The transient thermal impedance curves for every device in the inverter are measured using the experimental methods described in Chapter 6. From these curves, the parameters of an equivalent Foster network are calculated and this is described in Chapter 7. In this appendix, the following parameters are shown:

a) Self thermal resistance for the diodes measured with the fan on and off
b) Self and mutual thermal resistances measured with the fan on
c) Thermal parameters of the equivalent Foster networks

B.2 Diode Thermal Resistance Comparison

The measured thermal resistance for each of the diodes in the inverter is compared with the datasheet value in Figure B.1. The general characteristics shown in this figure are similar to those of the IGBTs that were shown in Chapter 6.

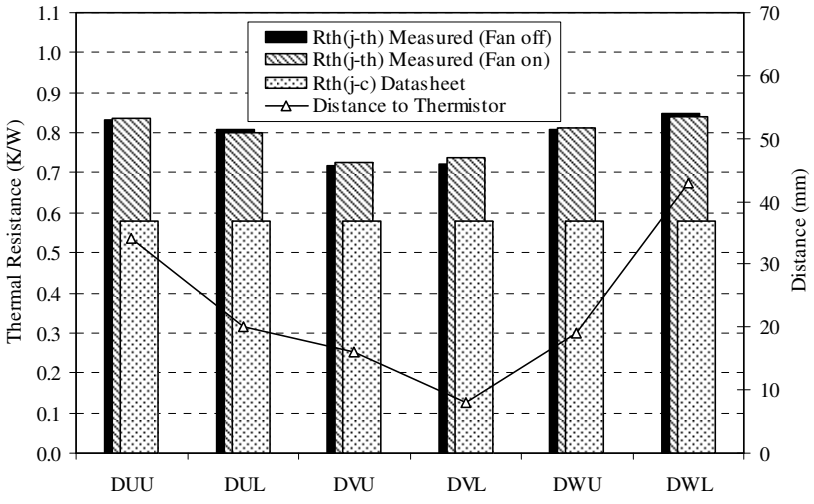

Figure B.1: Comparison of the measured ($R_{th,ii(j\text{-}th)}$) and datasheet ($R_{th(j\text{-}c)}$) self thermal resistance for the diodes in the inverter

B.3 Thermal Impedance Matrix

The self and mutual thermal resistances measured for the devices in the inverter are shown in the table below.

Table B.1: Steady-state thermal impedances between the junction and thermistor (K/W)

	I_{UU}	I_{UL}	I_{VU}	I_{VL}	I_{WU}	I_{WL}	D_{UU}	D_{UL}	D_{VU}	D_{VL}	D_{WU}	D_{WL}
I_{UU}	0.564	-0.054	0.023	-0.079	-0.061	-0.057	0.148	-0.015	-0.026	-0.129	-0.050	-0.046
I_{UL}	0.025	0.456	0.010	-0.032	-0.034	-0.024	0.029	0.073	-0.006	-0.052	-0.028	-0.013
I_{VU}	0.066	-0.024	0.480	-0.058	-0.011	-0.035	0.095	0.045	0.075	-0.103	-0.020	-0.028
I_{VL}	-0.020	-0.053	-0.030	0.475	-0.050	0.030	-0.023	-0.035	-0.039	-0.028	-0.006	0.051
I_{WU}	0.015	-0.030	0.024	-0.034	0.443	-0.005	0.020	-0.008	0.065	-0.082	0.031	-0.008
I_{WL}	-0.028	-0.076	-0.046	-0.010	-0.049	0.481	-0.030	-0.048	-0.057	-0.097	0.038	0.055
D_{UU}	0.150	-0.043	0.068	-0.071	-0.044	-0.049	0.835	0.026	-0.005	-0.120	-0.038	-0.040
D_{UL}	0.053	0.034	0.039	-0.052	-0.040	-0.035	0.063	0.801	-0.006	-0.090	-0.036	-0.025
D_{VU}	0.035	-0.018	0.098	-0.045	0.060	-0.022	0.048	0.030	0.724	-0.089	-0.005	-0.019
D_{VL}	-0.005	-0.012	-0.017	0.030	-0.041	0.002	-0.006	-0.008	-0.026	0.736	-0.016	0.015
D_{WU}	-0.015	-0.064	-0.026	-0.025	-0.008	0.044	-0.014	-0.034	-0.030	-0.092	0.812	0.011
D_{WL}	-0.044	-0.094	-0.067	-0.018	-0.079	0.030	-0.048	-0.068	-0.081	-0.114	-0.024	0.838

The diagonal elements in this table are the self thermal impedances for each device, whereas the off-diagonal are the mutual thermal impedances. Examples of the definition of these impedances are given below:

a) Self thermal impedance for I_{UU} measured when a power loss is applied to this device – $Z_{th}(I_{UU} - I_{UU})$ = 0.564 K/W

b) Mutual thermal impedance measured between I_{WL} and I_{UU} when a power loss is applied to I_{UU} – $Z_{th}(I_{UU} - I_{WL})$ = -0.057 K/W

c) Mutual thermal impedance measured between I_{UU} and I_{WL} when a power loss is applied to I_{WL} – $Z_{th}(I_{WL} - I_{UU})$ = -0.028 K/W

B.4 Curve Fitted Network Parameters for the Transient Thermal Impedance

The parameters of an equivalent Foster network are curve fitted to the measured transient thermal impedance using the method described in Chapter 7.

B.4.1 Self Thermal Impedance Network Parameters

In the thermal model, the self thermal impedance is represented by a second order network and the calculated network parameters (fan on) are shown in this section.

Table B.2: IGBT network parameters

Network Elements		I_{UU}	I_{UL}	I_{VU}	I_{VL}	I_{WU}	I_{WL}
Thermal Resistance (K/W)	R_{th1}	0.141	0.171	0.120	0.238	0.167	0.180
	R_{th2}	0.423	0.285	0.360	0.238	0.278	0.300
Time Constant (s)	τ_1	2.180	0.257	0.860	0.047	0.279	0.535
	τ_2	0.085	0.055	0.090	0.265	0.062	0.064

Table B.3: Diode network parameters

Network Elements		D_{UU}	D_{UL}	D_{VU}	D_{VL}	D_{WU}	D_{WL}
Thermal Resistance (K/W)	R_{th1}	0.209	0.200	0.181	0.368	0.203	0.210
	R_{th2}	0.626	0.601	0.543	0.368	0.609	0.629
Time Constant (s)	τ_1	0.812	0.422	0.398	0.032	0.493	1.098
	τ_2	0.053	0.045	0.092	0.126	0.047	0.048

B.4.2 Mutual Thermal Impedance Network Parameters

In the thermal model, the mutual thermal impedance is represented by a first order network and the calculated network parameters (fan on) are shown in this section.

Table B.4: IGBT to IGBT network parameters

Network Elements		I_{UU}	I_{UL}	I_{VU}	I_{VL}	I_{WU}	I_{WL}
I_{UU}	R_{th1}	0.564	-0.054	0.023	-0.079	-0.061	-0.057
	τ_1	0.122	3.465	1.582	7.349	3.219	13.146
I_{UL}	R_{th1}	0.025	0.456	0.010	-0.032	-0.034	-0.024
	τ_1	5.479	0.129	0.851	5.660	2.268	11.064
I_{VU}	R_{th1}	0.066	-0.024	0.480	-0.058	-0.011	-0.035
	τ_1	4.189	3.148	0.118	5.660	5.639	9.164
I_{VL}	R_{th1}	-0.020	-0.053	-0.030	0.475	-0.050	0.030
	τ_1	20.567	3.817	9.711	0.111	3.219	1.350
I_{WU}	R_{th1}	0.015	-0.030	0.024	-0.034	0.443	-0.005
	τ_1	3.386	2.830	1.269	4.196	0.112	17.852
I_{WL}	R_{th1}	-0.028	-0.076	-0.046	-0.010	-0.049	0.481
	τ_1	20.125	3.986	7.888	4.196	3.219	0.155

Table B.5: Diode to IGBT network parameters

Network Elements		D_{UU}	D_{UL}	D_{VU}	D_{VL}	D_{WU}	D_{WL}
I_{UU}	R_{th1}	0.148	-0.015	-0.026	-0.129	-0.050	-0.046
	τ_1	1.247	4.119	3.321	2.884	9.001	17.429
I_{UL}	R_{th1}	0.029	0.073	-0.006	-0.052	-0.028	-0.013
	τ_1	2.723	0.707	4.479	1.895	5.801	19.991
I_{VU}	R_{th1}	0.095	0.045	0.075	-0.103	-0.020	-0.028
	τ_1	1.898	0.829	0.458	1.895	9.001	15.043
I_{VL}	R_{th1}	-0.023	-0.035	-0.039	-0.028	-0.006	0.051
	τ_1	16.540	6.984	4.479	2.884	7.312	3.182
I_{WU}	R_{th1}	0.020	-0.008	0.065	-0.082	0.031	-0.008
	τ_1	2.533	7.269	0.554	1.895	0.864	12.452
I_{WL}	R_{th1}	-0.030	-0.048	-0.057	-0.097	0.038	0.055
	τ_1	16.361	8.187	4.479	1.895	0.745	4.308

Table B.6: Diode to diode network parameters

Network Elements		D_{UU}	D_{UL}	D_{VU}	D_{VL}	D_{WU}	D_{WL}
D_{UU}	R_{th1}	0.835	0.026	-0.005	-0.120	-0.038	-0.040
	τ_1	0.056	1.301	4.479	1.895	9.001	17.110
D_{UL}	R_{th1}	0.063	0.801	-0.006	-0.090	-0.036	-0.025
	τ_1	2.723	0.141	5.816	1.895	5.800	17.429
D_{VU}	R_{th1}	0.048	0.030	0.724	-0.089	-0.005	-0.019
	τ_1	3.674	0.841	0.144	1.895	20.113	12.599
D_{VL}	R_{th1}	-0.006	-0.008	-0.026	0.736	-0.016	0.015
	τ_1	21.218	11.029	4.479	0.099	5.801	1.344
D_{WU}	R_{th1}	-0.014	-0.034	-0.030	-0.092	0.812	0.011
	τ_1	18.602	6.984	3.320	1.895	0.086	2.504
D_{WL}	R_{th1}	-0.048	-0.068	-0.081	-0.114	-0.024	0.838
	τ_1	18.806	9.485	4.479	1.895	5.801	0.045

Table B.7: IGBT to diode network parameters

Network Elements		I_{UU}	I_{UL}	I_{VU}	I_{VL}	I_{WU}	I_{WL}
D_{UU}	R_{th1}	0.150	-0.043	0.068	-0.071	-0.044	-0.049
	τ_1	1.805	2.513	1.366	5.660	3.219	11.064
D_{UL}	R_{th1}	0.053	0.034	0.039	-0.052	-0.040	-0.035
	τ_1	5.082	0.327	1.354	5.660	2.268	11.064
D_{VU}	R_{th1}	0.035	-0.018	0.098	-0.045	0.060	-0.022
	τ_1	5.887	2.830	0.866	4.196	0.419	9.164
D_{VL}	R_{th1}	-0.005	-0.012	-0.017	0.030	-0.041	0.002
	τ_1	26.482	8.032	9.710	0.519	2.268	0.487
D_{WU}	R_{th1}	-0.015	-0.064	-0.026	-0.025	-0.008	0.044
	τ_1	21.471	3.840	7.888	4.196	19.551	1.597
D_{WL}	R_{th1}	-0.044	-0.094	-0.067	-0.018	-0.079	0.030
	τ_1	21.797	4.201	9.710	5.660	4.342	2.058

Appendix C: Pulse Testing Procedure

C.1 Introduction

To calculate the temperature of a device the power loss in every possible operating condition must be known. In the thermal model, this calculation is performed on-line and the model requires a number of device parameters that must be measured in the exact configuration that will be used to evaluate the thermal model. In this appendix, the configuration used to measure the device parameters and the corresponding test circuit is described. The methods used to measure the switching loss and the on-state voltage for an IGBT and a diode in the inverter stage of the power module are then outlined in detail.

C.1.1 Experimental Setup

The thermal model has been designed to protect the devices in the inverter stage of the power module and does not include the effect that the devices in the rectifier or the brake have on the temperature of these devices. Therefore, to evaluate the thermal model it is important that only the devices in the inverter are active and since the switching loss must be measured in this configuration, the circuit used is as shown in Figure C.1.

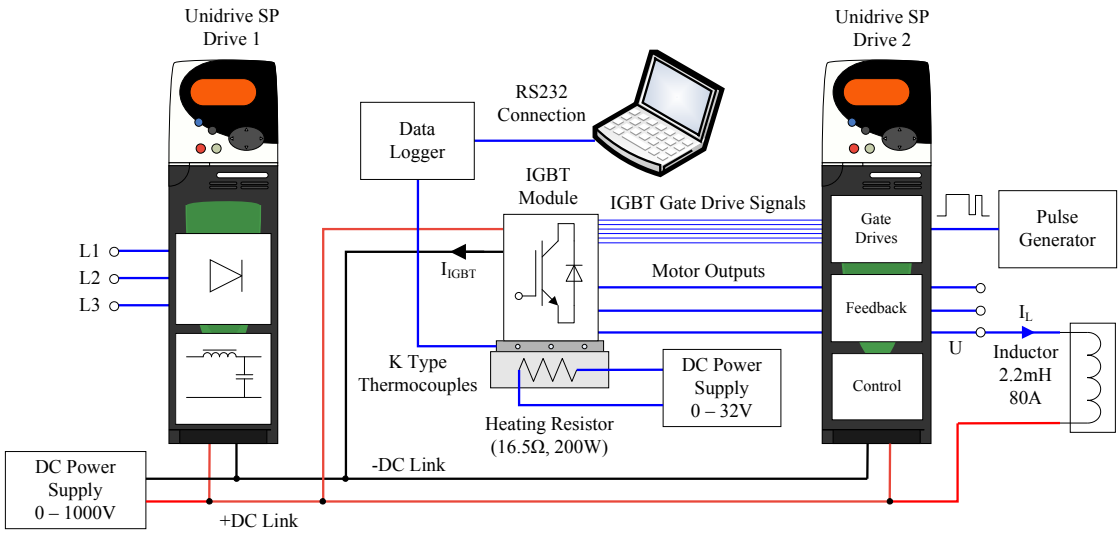

Figure C.1: Physical layout used to measured the switching loss and on-state voltage

In the configuration used to evaluate the thermal model, the power module in an unmodified drive (drive 1) is used to rectify the three phase input. However, in these measurements, the DC link voltage is controlled using a high voltage power supply, which is connected directly to the DC link terminals of both drives. To allow the temperature of the devices to be measured using an infrared camera the power module under test has been removed from drive 2 and the terminals of this module are connected to the drive via fly leads. This drive provides the voltage and current feedback to the controller as well as the gate drive signals for the IGBTs in the inverter (external power module). In order to measure the device parameters, the IGBT is controlled by a pulse generator. For these measurements, the power module is attached to a power resistor and this is used to control the temperature of the module, which is measured using several thermocouples embedded in the case. The corresponding test circuit for this configuration is shown in Figure C.2.

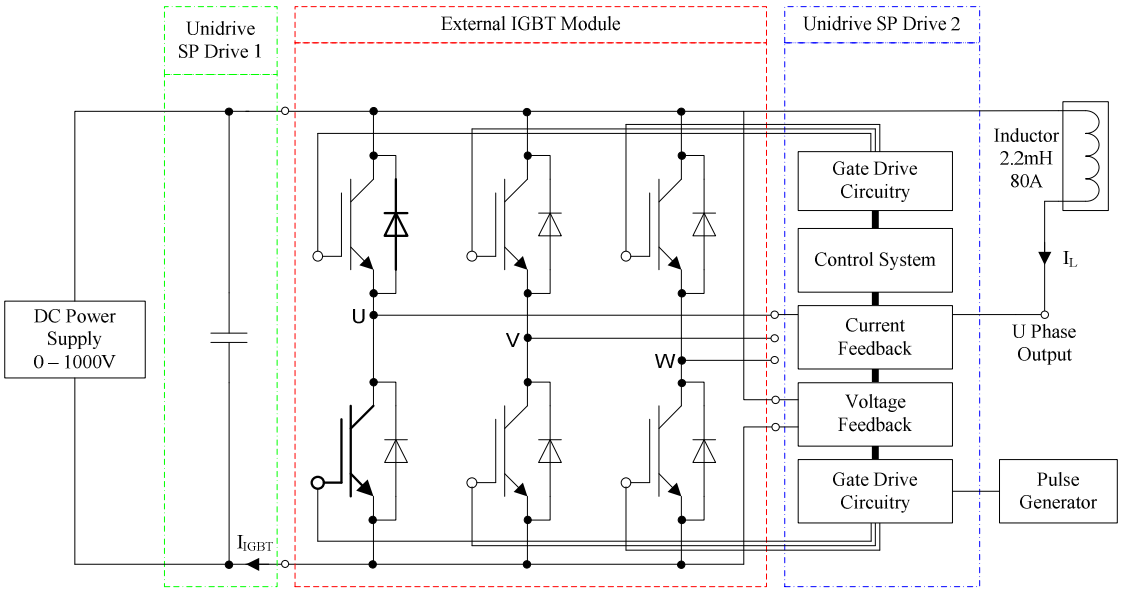

Figure C.2: Test circuit used to measure the switching loss of the lower IGBT and the upper diode in the U phase of the inverter

In this example, the inductor, which is used to provide a constant current during the switching event, is connected between the +DC link and U phase motor terminals. Therefore, using this configuration, the current (I_L) is controlled by varying the on-time of the lower IGBT in the U phase and the switching loss in this device and the upper diode can be measured.

C.1.2 Switching Loss

To measure the switching loss in the IGBT and diode, the IGBT is controlled using a double pulse. This pulse and the typical current in the inductor (I_L), IGBT (I_{IGBT}) and diode (I_L-I_{IGBT}) are shown in Figure C.3.

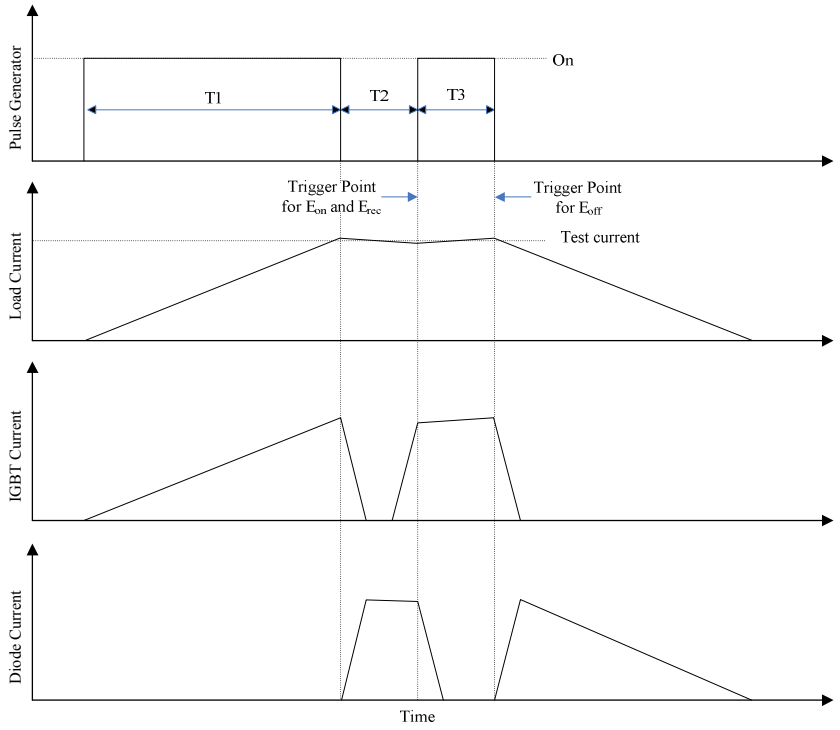

Figure C.3: Double switching pulse used to control the current magnitude for the switching loss measurements

The first pulse is required to increase the current flowing through the load inductance, during this pulse the current flows entirely through the IGBT. The peak magnitude is limited by the on time of the IGBT. The length of T_1 required to reach the target current will depend on the supply voltage and the inductance of the load, although in order to minimise the change in current during the switching event the inductance should be selected so that the pulse length is in the order of 100µs. Once the load current has reached the desired test level the IGBT is turned off and at this point the load current transfers to the anti-parallel diode of the upper device. The length of pulses T_2 and T_3 must be long enough to ensure that the IGBT has fully switched (off or on) before the next event. At the end of the second pulse (T_2) the IGBT is switched on and by triggering on the rising edge of the

output from the pulse generator the turn-on loss in the IGBT (E_{on}) and the turn-off loss in the diode (E_{rec}) can be measured. Similarly, at the end of T_3, the IGBT is switched off and the turn-off energy (E_{off}) is measured. This process is repeated several times at each voltage, current and temperature.

C.1.3 On-State Voltage

Unlike the switching loss measurements the on-state voltage can be measured using a single pulse, this process is shown in Figure C.4.

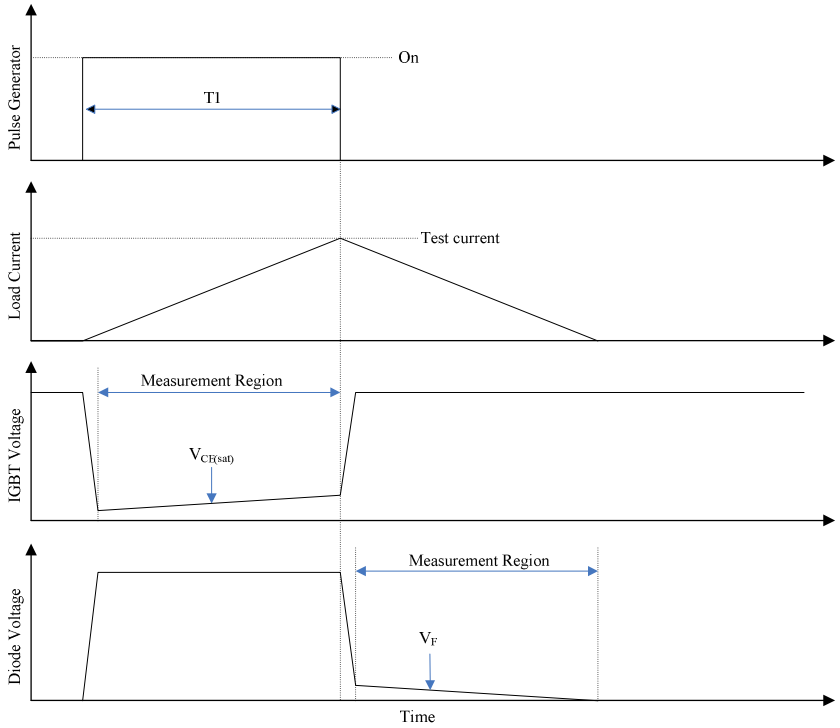

Figure C.4: Single switching pulse used to control the current magnitude for the on-state voltage measurements

In this instance, the pulse length (T_1) is adjusted until the maximum test current is reached. As the load current (I_L) is increased the current flows entirely in the IGBT and the on-state voltage (V_{CE}) rises until the IGBT is turned off, at which point the current is transferred to the diode. The current in the diode and the resulting on-state voltage (V_F) then decays. If the voltage and current is measured over the entire pulse length a single test is required to measure the on-state voltage at each current level, but the measurements must be repeated at each temperature.

Appendix D: Switching and Conduction Loss Parameters

D.1 Introduction

To calculate the power loss in a device the switching energy and on-state voltage for an IGBT and diode must be known over the full range of operating conditions. The procedure used to measure these parameters is described in Chapter 6. To reduce the amount of input data a power loss model is developed for each of the following parameters:

- IGBT turn-on energy loss (E_{on})
- IGBT turn-off energy loss (E_{off})
- Diode turn-off energy loss (E_{rec})
- IGBT on-state (forward) voltage (V_{CE})
- Diode on-state (forward) voltage (V_F)

In this appendix, the measured switching energy and on-state voltage are calculated using the loss model described in Chapter 7. These are compared against the values measured with a DC link voltage of 600V. An example of the model used to calculate the turn-on energy of the IGBT is shown below, although the same model (different parameters) is used to calculate each of the parameters listed above:

$$E_{on}\left(I_L, T_j, V_{DC}\right) = \left(k_1 \cdot {I_L}^2 + k_2 \cdot I_L + k_3\right) \cdot k_V \text{ (mJ)} \tag{D.1}$$

$$k_1 = k_{11} \cdot {T_j}^2 + k_{12} \cdot T_j + k_{13} \quad (\text{mJ/A}^2) \tag{D.2}$$

$$k_2 = k_{21} \cdot {T_j}^2 + k_{22} \cdot T_j + k_{23} \quad (\text{mJ/A}) \tag{D.3}$$

$$k_3 = k_{31} \cdot {T_j}^2 + k_{32} \cdot T_j + k_{33} \quad (\text{mJ}) \tag{D.4}$$

$$k_V = k_{V1} \cdot {V_{DC}}^2 + k_{V2} \cdot V_{DC} + k_{V3} \tag{D.5}$$

D.2 Switching Loss

D.2.1 IGBT Turn-on Energy (E_{on})

Table D.1: Loss parameters

	T_j^2	T_j^1	T_j^0
K_1 (mJ/A^2)	$2.34e^{-06}$	$9.17e^{-04}$	$4.47e^{-01}$
K_2 (mJ/A)	$4.95e^{-04}$	$1.76e^{-01}$	$9.47e^{+01}$
K_3 (mJ)	$1.38e^{-03}$	$5.11e^{+00}$	$2.65e^{+02}$
	k_{V1}	k_{V2}	k_{V3}
k_V	0	$2.59e^{-03}$	$-5.45e^{-01}$

Table D.2: Measured switching energy with a DC Link voltage of 600V (mJ)

Temperature (°C) / Current (A)	25	50	75	100	125	150
5	0.78	1.00	1.16	1.32	1.50	1.68
15	2.15	2.12	2.44	2.69	2.87	3.22
25	3.19	3.43	3.84	4.15	4.41	4.86
35	4.48	4.63	5.11	5.63	6.06	6.46
45	5.82	6.14	6.57	7.08	7.68	8.18
55	7.18	7.63	8.21	8.93	9.43	10.35
65	8.78	9.58	10.22	10.74	11.30	12.26
75	10.60	11.19	11.97	12.76	13.34	14.62

Table D.3: Calculated switching energy with a DC Link voltage of 600V (mJ)

Temperature (°C) / Current (A)	25	50	75	100	125	150
5	0.90	1.06	1.22	1.39	1.56	1.74
15	1.99	2.21	2.43	2.67	2.92	3.19
25	3.17	3.45	3.75	4.07	4.41	4.76
35	4.45	4.80	5.18	5.58	6.01	6.47
45	5.82	6.25	6.71	7.20	7.73	8.30
55	7.29	7.79	8.34	8.94	9.58	10.26
65	8.85	9.44	10.08	10.78	11.54	12.35
75	10.50	11.18	11.93	12.74	13.62	14.56

D.2.2 IGBT Turn-off Energy (E_{off})

Table D.4: Loss parameters

	T_j^2	T_j^1	T_j^0
k_1 (mJ/A^2)	$2.61e^{-06}$	$-3.37e^{-03}$	$1.32e^{-01}$
k_2 (mJ/A)	$1.47e^{-03}$	$5.15e^{-01}$	$7.43e^{+01}$
k_3 (mJ)	$5.56e^{-03}$	$6.34e^{-01}$	$2.81e^{+02}$
	k_{V1}	k_{V2}	k_{V3}
k_V	0	$1.17e^{-03}$	$2.93e^{-01}$

Table D.5: Measured switching energy with a DC Link voltage of 600V (mJ)

Temperature (°C) / Current (A)	25	50	75	100	125	150
5	0.70	0.79	0.84	1.00	1.13	1.38
15	1.66	1.90	2.13	2.41	2.79	3.23
25	2.59	2.89	3.27	3.76	4.23	5.02
35	3.46	3.89	4.41	5.01	5.58	6.48
45	4.36	4.89	5.61	6.24	7.08	8.08
55	5.19	5.92	6.68	7.45	8.43	9.78
65	6.26	6.86	7.83	8.65	9.82	11.20
75	7.21	7.95	8.92	9.99	11.16	12.54

Table D.6: Calculated switching energy with a DC Link voltage of 600V (mJ)

Temperature (°C) / Current (A)	25	50	75	100	125	150
5	0.74	0.84	0.96	1.10	1.25	1.42
15	1.63	1.88	2.15	2.47	2.82	3.20
25	2.53	2.90	3.32	3.80	4.33	4.92
35	3.44	3.92	4.47	5.10	5.80	6.57
45	4.36	4.93	5.60	6.36	7.22	8.17
55	5.29	5.94	6.70	7.58	8.58	9.70
65	6.23	6.94	7.79	8.77	9.90	11.17
75	7.18	7.94	8.85	9.93	11.17	12.57

D.2.3 Diode Turn-off Energy (E_{rec})

Table D.7: Loss parameters

	T_j^2	T_j^1	T_j^0
k_1 (mJ/A^2)	$-1.12e^{-05}$	$-7.76e^{-04}$	$-1.81e^{-01}$
k_2 (mJ/A)	$2.16e^{-03}$	$1.24e^{-01}$	$3.50e^{+01}$
k_3 (mJ)	$4.22e^{-03}$	6.51	$6.85e^{+01}$
	k_{V1}	k_{V2}	k_{V3}
k_V	0	$1.08e^{-03}$	$3.42e^{-01}$

Table D.8: Measured switching energy with a DC Link voltage of 600V (mJ)

Temperature (°C) / Current (A)	25	50	75	100	125	150
5	0.41	0.50	0.66	0.85	1.21	1.54
15	0.83	1.05	1.38	1.75	2.11	2.61
25	1.05	1.34	1.71	2.17	2.70	3.55
35	1.39	1.71	2.15	2.72	3.39	3.93
45	1.54	1.93	2.37	3.01	3.63	4.63
55	1.83	2.28	2.82	3.44	4.16	5.09
65	1.90	2.46	2.91	3.49	4.44	5.34
75	2.03	2.65	3.12	3.87	4.55	5.83

Table D.9: Calculated switching energy with a DC Link voltage of 600V (mJ)

Temperature (°C) / Current (A)	25	50	75	100	125	150
5	0.43	0.63	0.86	1.10	1.36	1.64
15	0.78	1.05	1.36	1.71	2.11	2.55
25	1.09	1.42	1.80	2.26	2.77	3.35
35	1.36	1.73	2.19	2.72	3.34	4.05
45	1.59	2.00	2.51	3.12	3.82	4.63
55	1.78	2.22	2.77	3.44	4.21	5.10
65	1.92	2.39	2.98	3.68	4.51	5.47
75	2.03	2.51	3.12	3.86	4.72	5.72

D.3 Conduction Loss Parameters

D.3.1 IGBT on-state Voltage (V_{CE})

Table D.10: Loss parameters

	T_j^2	T_j^1	T_j^0
k_1 (mJ/A^2)	0	$-1.48e^{-07}$	$-4.75e^{-05}$
k_2 (mJ/A)	0	$6.13e^{-05}$	$1.39e^{-02}$
k_3 (mJ)	0	$-1.19e^{-03}$	$9.26e^{-01}$
	k_{V1}	k_{V2}	k_{V3}
k_V	0	0	1

Table D.11: Measured on-state voltage (V)

Temperature (°C) / Current (A)	25	50	75	100	125	150
5	0.968	0.955	0.936	0.912	0.888	0.857
15	1.121	1.120	1.114	1.106	1.096	1.079
25	1.254	1.266	1.274	1.282	1.287	1.288
35	1.377	1.404	1.426	1.447	1.468	1.480
45	1.488	1.522	1.556	1.591	1.624	1.650
55	1.588	1.633	1.675	1.714	1.754	1.795
65	1.683	1.731	1.785	1.844	1.901	1.951
75	1.773	1.843	1.910	1.972	2.037	2.100

Table D.12: Calculated on-state voltage (V)

Temperature (°C) / Current (A)	25	50	75	100	125	150
5	0.971	0.959	0.939	0.915	0.891	0.860
15	1.131	1.131	1.125	1.117	1.107	1.090
25	1.272	1.285	1.293	1.300	1.305	1.306
35	1.402	1.430	1.452	1.473	1.494	1.505
45	1.521	1.555	1.589	1.624	1.657	1.683
55	1.628	1.674	1.716	1.754	1.795	1.835
65	1.731	1.779	1.833	1.892	1.949	1.999
75	1.829	1.899	1.966	2.027	2.092	2.156

D.3.2 Diode Forward Voltage (V_F)

Table D.13: Loss parameters

	T_j^2	T_j^1	T_j^0
k_1 (mJ/A^2)	0	-1.42e^{-07}	-7.68e^{-05}
k_2 (mJ/A)	0	4.73e^{-05}	1.41e^{-02}
k_3 (mJ)	0	-2.32e^{-03}	9.44e^{-01}
	k_{V1}	k_{V2}	k_{V3}
k_V	0	0	1

Table D.14: Measured forward voltage (V)

Temperature (°C) / Current (A)	25	50	75	100	125	150
5	0.944	0.873	0.821	0.770	0.721	0.674
15	1.117	1.079	1.043	1.002	0.961	0.920
25	1.225	1.202	1.176	1.148	1.120	1.080
35	1.325	1.315	1.298	1.275	1.252	1.219
45	1.409	1.408	1.400	1.385	1.366	1.342
55	1.473	1.489	1.489	1.482	1.472	1.454
65	1.531	1.556	1.567	1.572	1.565	1.543
75	1.594	1.633	1.654	1.657	1.663	1.654

Table D.15: Calculated forward voltage (V)

Temperature (°C) / Current (A)	25	50	75	100	125	150
5	0.961	0.908	0.856	0.804	0.752	0.700
15	1.098	1.056	1.015	0.974	0.933	0.892
25	1.218	1.188	1.157	1.126	1.096	1.065
35	1.323	1.302	1.281	1.260	1.239	1.218
45	1.412	1.400	1.388	1.376	1.364	1.352
55	1.484	1.481	1.477	1.473	1.469	1.466
65	1.541	1.545	1.548	1.552	1.556	1.560
75	1.581	1.592	1.603	1.613	1.624	1.635

Appendix E: Transient Temperature Response

E.1 Introduction

To select the time constants that are used to combine the mutual thermal impedances for the IGBT and diode model the step response is calculated under a range of operating conditions. In this appendix, the results are shown for several conditions that were not included in Chapter 7. These include an investigation into the effect of the switching frequency and displacement power factor.

E.2 IGBT transient response

The following figures show a comparison of the step response calculated using the original network parameters and the common time constants for a stationary vector condition. A negative value indicates that the temperature is underestimated during the transient.

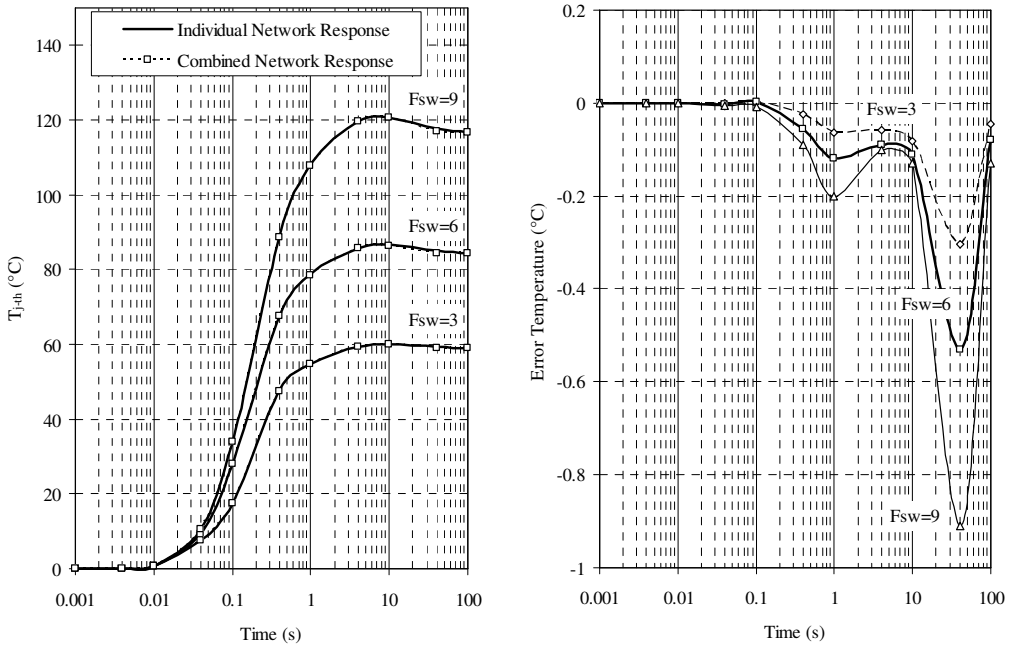

(a) (b)

Figure E.1: Comparison of switching frequencies (a) step response (b) error temperature

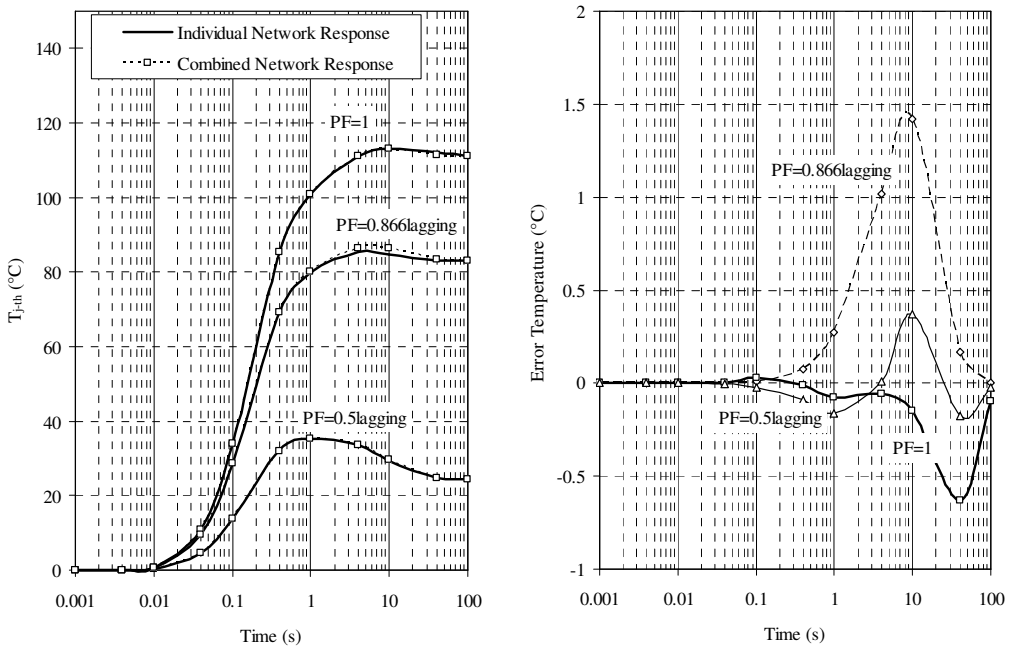

(a) (b)

Figure E.2: Comparison of displacement power factors (a) step response (b) error temperature

The results shown in this section are used to select the common time constants for the IGBT thermal model. Since the process of combining multiple mutual impedances is only an approximation of the complete thermal characteristics some error will always exist. Even so, the error can be minimised by comparing the combined response (two mutual time constants) with the complete response calculated using the full thermal impedance matrix (11 mutual time constants). The common time constants for the two mutual terms that represent the thermal coupling from the other IGBTs and diodes in the inverter can then be selected to minimise the error. This selection process is a compromise between the transient performance (minimising the overestimation of the temperature) and the protection offered by the thermal model (minimising the underestimation of the temperature). The results for the diode model are shown in the next section.

E.3 Diode transient response

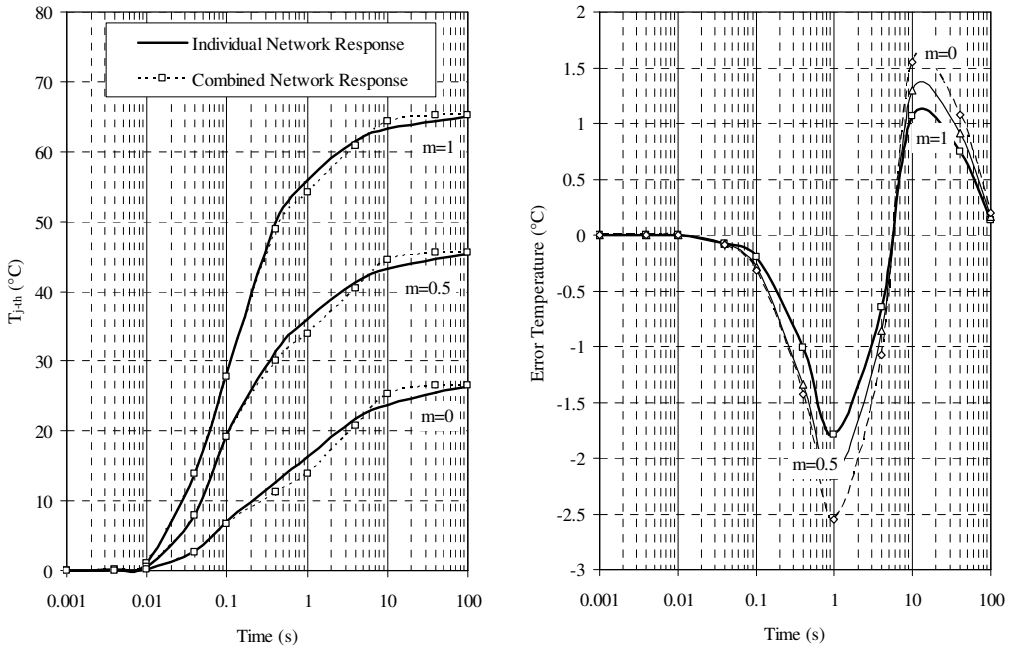

(a) (b)

Figure E.3: Comparison of modulation index (a) step response (b) error temperature

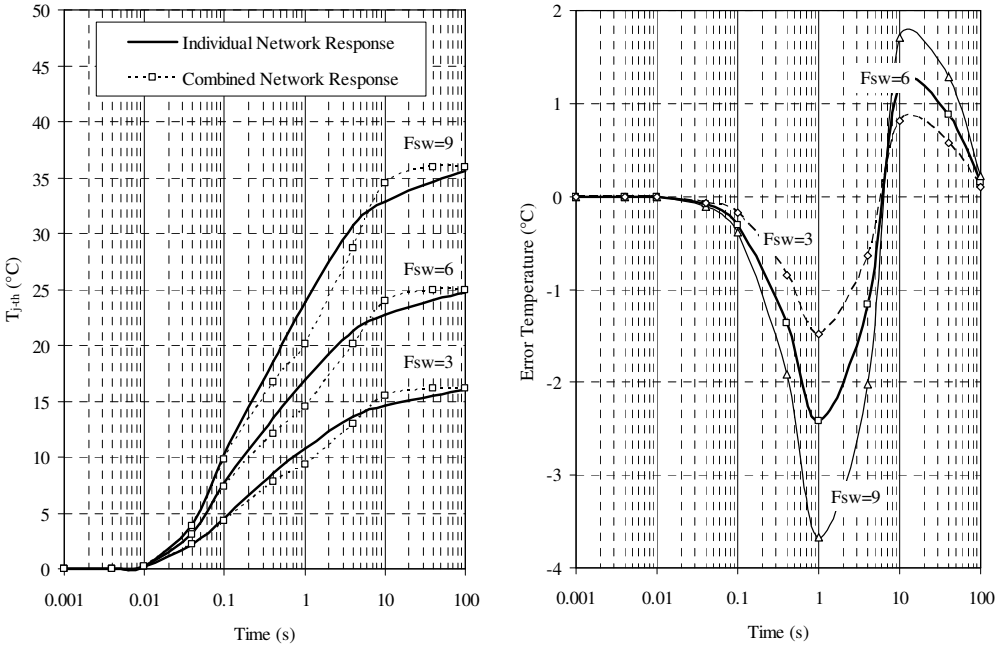

(a) (b)

Figure E.4: Comparison of switching frequencies (a) step response (b) error temperature

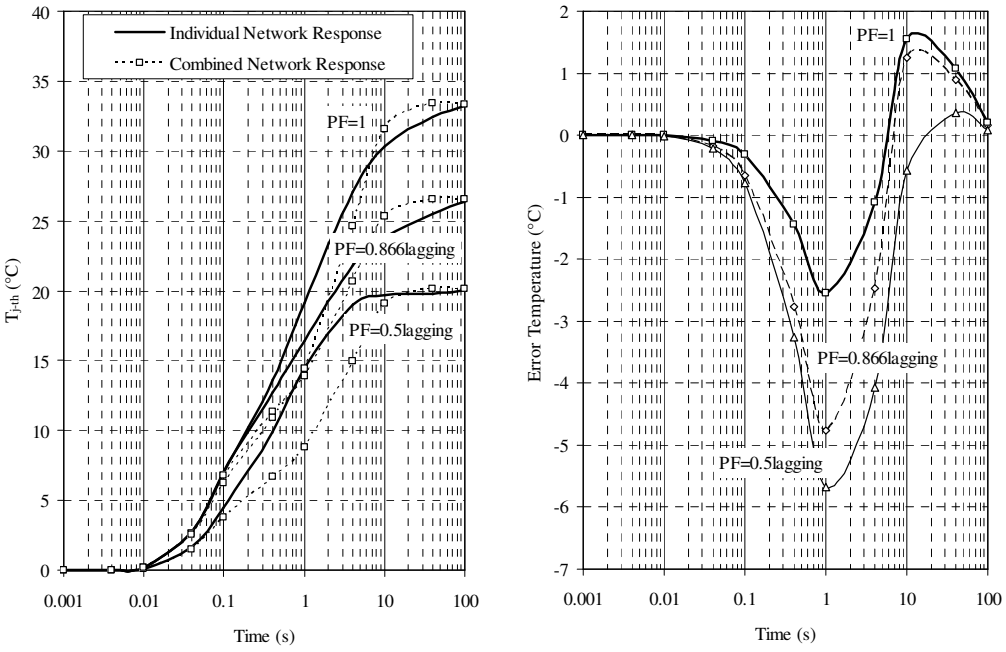

(a) (b)

Figure E.5: Comparison of displacement power factors (a) step response (b) error temperature

The results shown in this section are used to select the common time constants for the diode thermal model. By comparing these results with those for the IGBT model it is evident that the characteristics are very different. This is caused by the different thermal coupling in each model, which is due to the layout of the power module and more specifically, the location of the nearby devices.

Appendix F: Temperature Measurements and Comparison

F.1 Introduction

To develop and validate the thermal model the temperature of the IGBTs and diodes in an inverter were measured under a range of operating conditions. In this Appendix a selection of measurements that were not included in the main body of this thesis are presented and the key observations are described.

F.2 Thermal Coupling between Devices

The thermal coupling between the devices in the inverter has a significant impact on the peak temperature and the temperature profile measured over a complete output cycle ($1/F_{out}$). This can be seen in Figure F.1. With no coupling the peak temperature of each device should be similar, but due to the thermal coupling the peak temperature of every IGBT is different. Under these operating conditions the hottest device is I_{VU}.

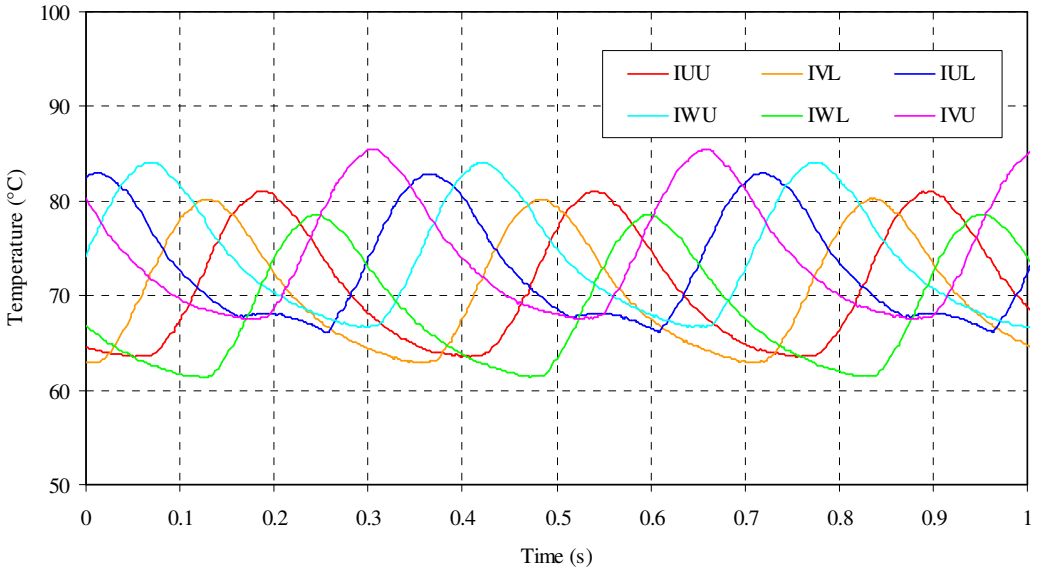

Figure F.1: Maximum IGBT temperature measured at a switching frequency of 16kHz, load current of 25A and an output frequency of 2.5Hz

F.3 Temperature Distribution in a Stationary Vector Condition

The thermal image of the inverter operating in a stationary vector condition is shown in Figure F.2(a). This image was taken with the peak current in the upper IGBT of the U phase. In this condition six devices in the inverter are active. The surface temperature of this IGBT is shown in FigureF.2(b). In this figure, the lower temperature measured from the centre to the edge on one side of the device is caused by the gate lead bond wire.

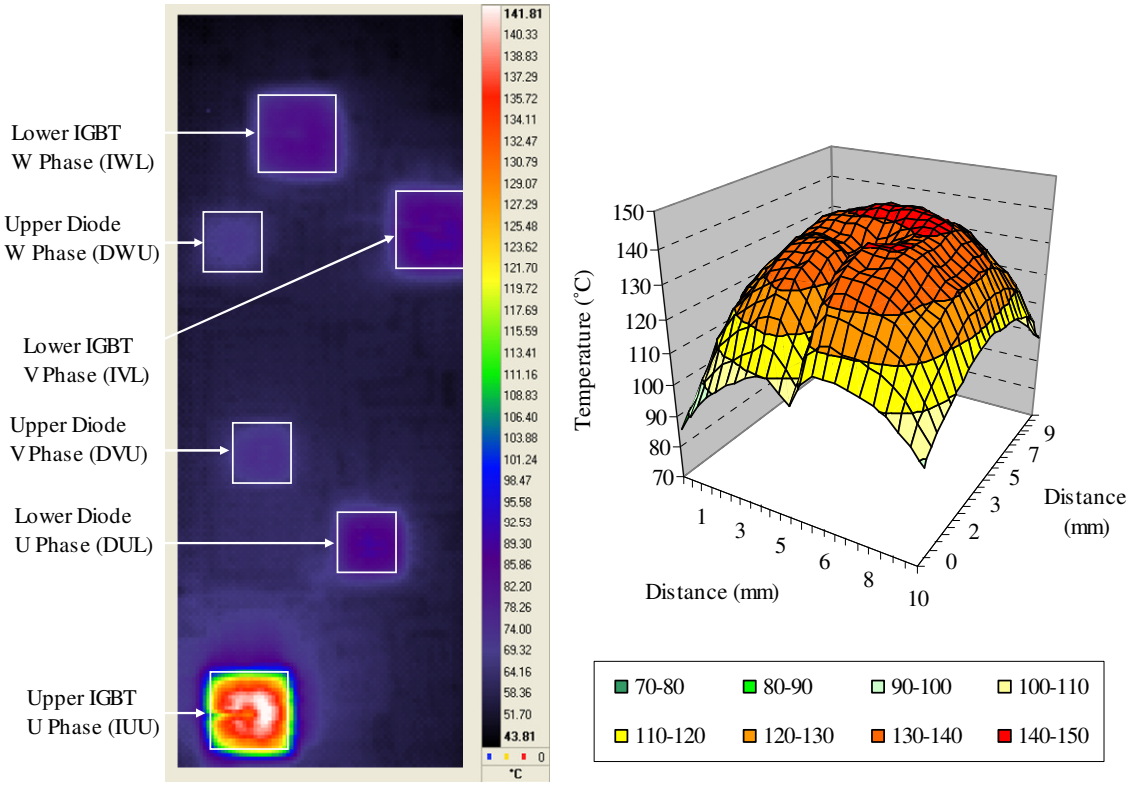

(a) (b)

Figure F.2: Inverter operating in a stationary vector condition at a switching frequency of 16kHz and a current of 19A (a) Infrared image (b) Surface temperature of I_{UU}

Figure F.3 shows the maximum temperature of each IGBT as the devices are heated after a step in output current has been applied to the inverter. As expected, the three IGBTs that are not conducting (I_{UL}, I_{VU} and I_{WU}) have the lowest temperature, the IGBTs conducting half of the load current (I_{VL} and I_{WL}) are the next highest and I_{UU} is the hottest device. The measured temperatures are compared with the output of the frequency model and the basic thermal model.

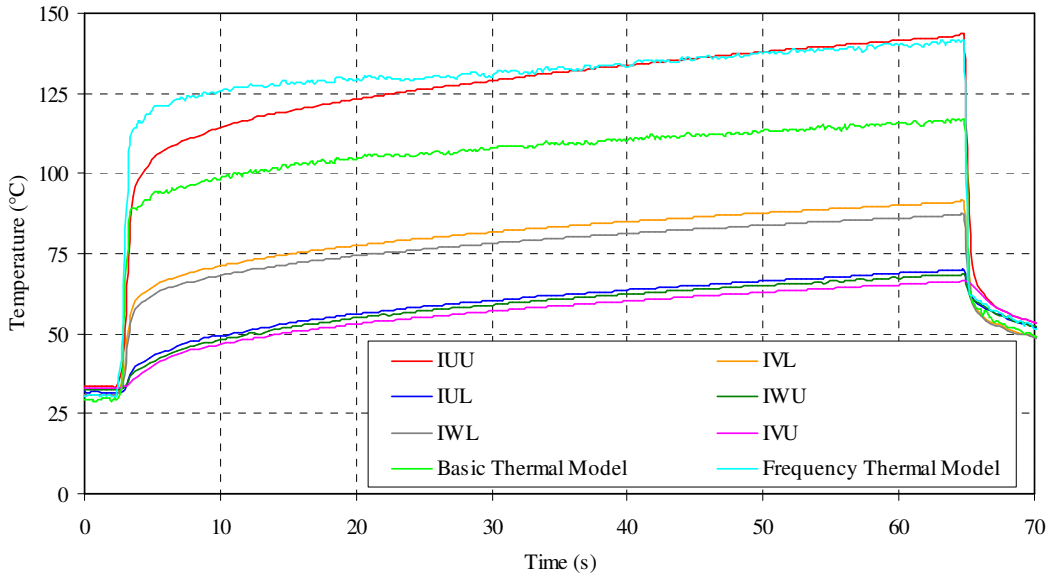

Figure F.3: Comparison of the measured (maximum) and estimated temperature with the inverter operating in a stationary vector condition at a switching frequency of 16kHz and a load current of 19A (Output frequency = 0Hz)

This comparison shows that the basic thermal model underestimates the temperature by over 25˚C and this model would allow the temperature to exceed 175˚C. In contrast, the temperature estimated by the frequency model is only 1˚C lower than the measurement.

F.4 Comparison during an Acceleration, Steady-state and Deceleration Period

The results in Figure F.4 and Figure F.5 show the comparison of the IGBT and diode frequency models with the basic thermal model and the measured temperatures. These results highlight some of the main characteristics of both models. Key points to note are:

1. After the initial acceleration period the output of the frequency model reduces towards the peak junction-to-temperature of the modelled device. This effect is due to the longer time constants associated with the negative mutual thermal impedance.
2. In the steady-state the modelled devices (I_{UU} and D_{UU}) are not the hottest. This is caused by the change in the thermal coupling at higher operating frequencies.
3. As the motor is decelerating the ripple component increases. This is added to the output of the model as a constant value and can cause the temperature to be overestimated.

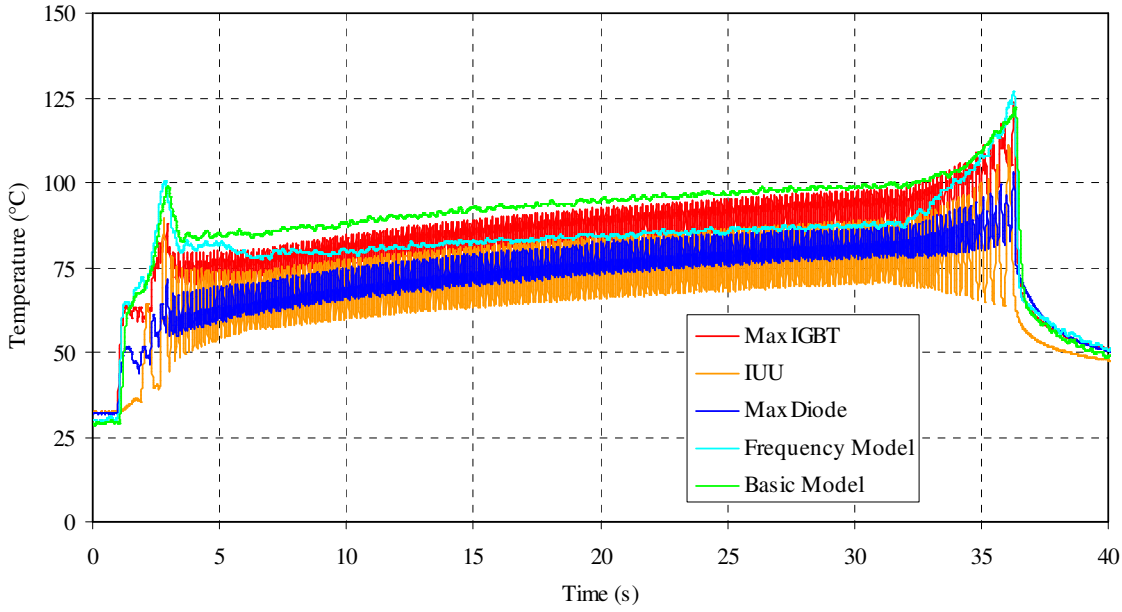

(a)

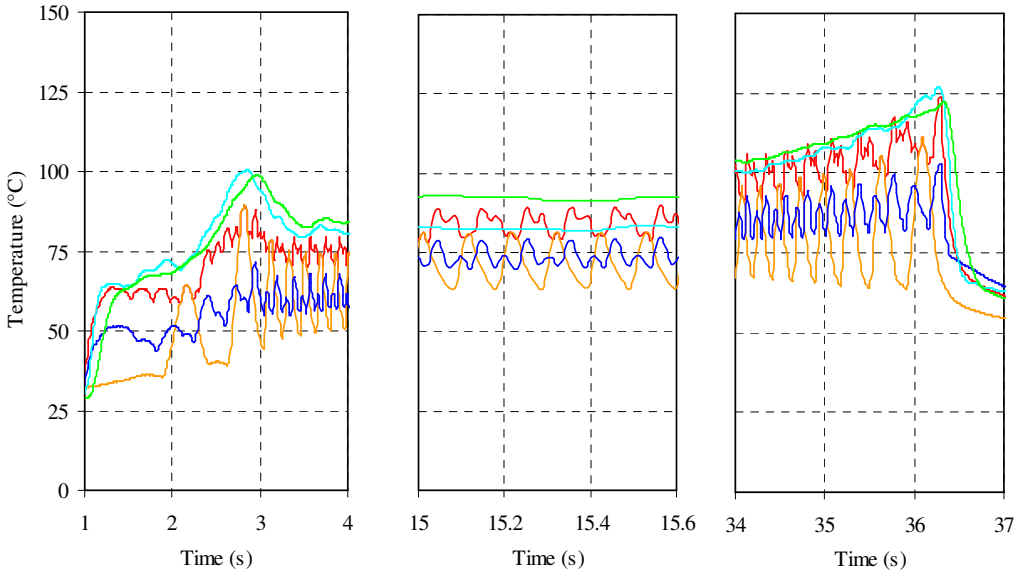

(b) (c) (d)

Figure F.4: Comparison of the IGBT model with the inverter operating at a switching frequency of 16kHz, load current of 25A and an output frequency = 10Hz (a) complete response (b) acceleration period (c) steady state period (d) deceleration period

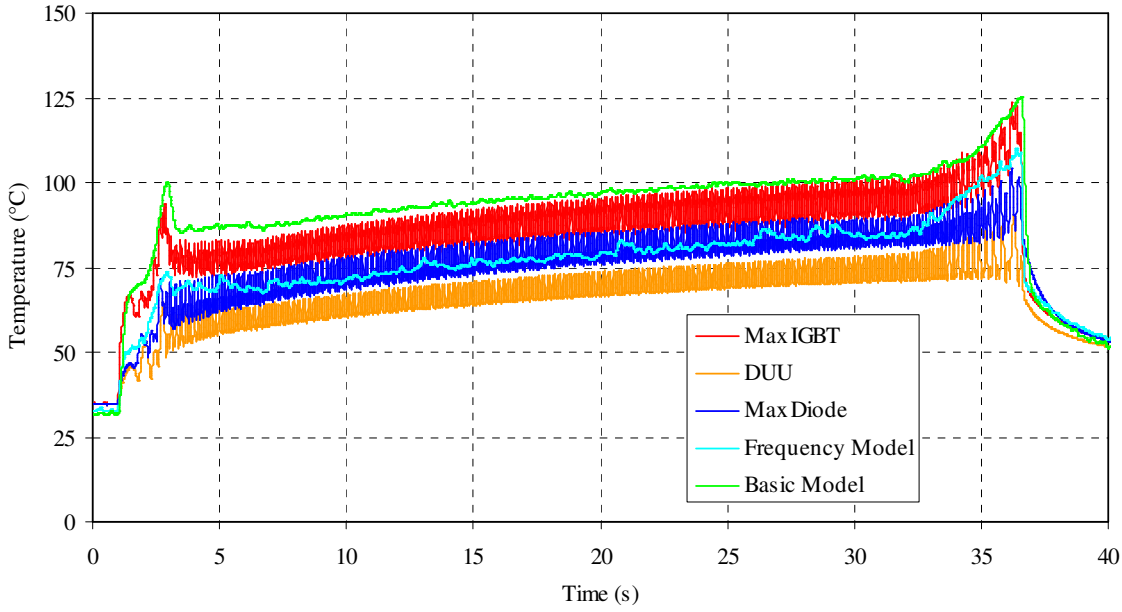

(a)

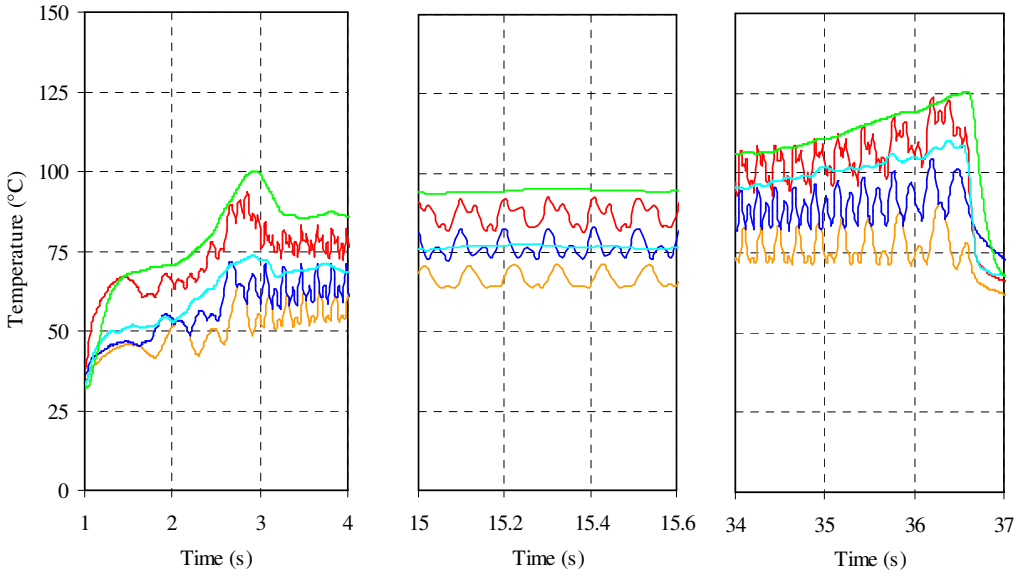

(b) (c) (d)

Figure F.5: Comparison of the diode model with the inverter operating at a switching frequency of 16kHz, load current of 25A and an output frequency = 10Hz (a) complete response (b) acceleration period (c) steady state period (d) deceleration period

List of References

[1] L. Wei, R. J. Kerkman, R. A. Lukaszewski, B. P. Brown, N. Gollhardt, and B. W. Weiss, 'Junction Temperature Prediction of a Multiple-chip IGBT Module under DC Condition', *41st IEEE Industry Applications Society Annual Meeting, IAS '06*, Tampa, FL, USA, 8-12 October 2006, pp. 754-762.

[2] B. Drury, '*The Control Techniques Drive and Controls Handbook'*, Second ed.: The Institution of Engineering and Technology, 2009. ISBN 0852967934.

[3] W. Shepherd, N. L. Hulley, and D. T. W. Liang, '*Power Electronics and Motor Control'*, Second ed. Cambridge: Cambridge University Press, 1995. ISBN 0521478138.

[4] D. G. Holmes and T. A. Lipo, '*Pulse Width Modulation for Power Converters: Principles and Practice '*, First ed. New York: Wiley-IEEE Press, 2003. ISBN 0471208140.

[5] M. H. Rashid, '*Power Electronics Handbook: Devices, Circuits, and Applications '*, Second ed. London: Academic Press, 2007. ISBN 0120884798.

[6] R. Valentine, '*Motor Control Electronics Handbook '*, Third ed. New York: McGraw Hill, 1998. ISBN 0-07066-810-8.

[7] P. J. P. Perruchoud and P. J. Pinewski, 'Power Losses for Space Vector Modulation Techniques', *IEEE Conference on Power Electronics in Transportation*, Dearborn, MI, USA, 24-25 October 1996, pp. 167-173.

[8] B. J. Baliga, M. S. Adler, R. P. Love, P. V. Gray, and N. D. Zommer, 'The Insulated Gate Transistor: A New Three-terminal MOS-controlled Bipolar Power Device', *IEEE Transactions on Electron Devices,* vol. 31, pp. 821-828, June 1984.

[9] V. K. Khanna, '*Insulated Gate Bipolar Transistor: IGBT Theory and Design'*, First ed.: Wiley-IEEE Press 2003. ISBN 0471238457.

[10] L. Lorenz, 'Power Semiconductor Devices-Development Trends and System Interactions', *Power Conversion Conference, PCC '07*, Nagoya, Japan, 2-5 April 2007, pp. 348-354.

[11] L. Lorenz, 'Key Power Semiconductor Devices and Development Trends', *International Workshop on Physics of Semiconductor Devices, IWPSD 2007*, Mumbai, India, 16-20 December 2007, pp. 743-750.

[12] G. Majumdar, 'Recent Technologies and Trends of Power Devices', *International Workshop on Physics of Semiconductor Devices, IWPSD 2007*, Mumbai, India, 16-20 December 2007, pp. 787-792.

[13] B. J. Baliga, 'Trends in Power Semiconductor Devices', *IEEE Transactions on Electron Devices,* vol. 43, pp. 1717-1731, October 1996.

[14] M. Rahimo and S. Klaka, 'High Voltage Semiconductor Technologies', *13th European Conference on Power Electronics and Applications, EPE '09*, Barcelona, Spain, 8-10 September 2009, pp. 1-10.

[15] V. Demuth, 'Power Diodes: More Power at the Same Size', *Power Electronics Europe*, May 2008, pp. 36-37.

[16] T. Stockmeier, 'From Packaging to "Un"-Packaging - Trends in Power Semiconductor Modules', *20th International Symposium on Power Semiconductor Devices and IC's, ISPSD '08*, Orlando, FL, USA, 18-22 May 2008, pp. 12-19.

[17] A. Akdag, 'SOA in High Power Semiconductors', *41st IEEE Industry Applications Society Annual Meeting, IAS '06*, Tampa, FL, USA, 8-12 October 2006, pp. 1473-1477.

[18] M. Aleo, Application Note: 'IGBT Basics', ST, December 2001.

[19] U. Schlapbach, M. Rahimo, C. von Arx, A. Mukhitdinov, and S. Linder, '1200V IGBTs Operating at 200°C? An Investigation on the Potentials and the Design Constraints', *19th International Symposium on Power Semiconductor Devices and IC's, ISPSD '07*, Jeju Island, South Korea, 27-31 May 2007, pp. 9-12.

[20] R. Schnell and N. Kaminski, Application Note: 'Thermal Runaway During Blocking', ABB Switzerland Ltd, Semiconductors, November 2005.

[21] L. Wei-Sun, M. Corfield, L. Hua, S. Hogg, T. Tilford, and C. M. Johnson, 'Wire Bond Reliability for Power Electronic Modules - Effect of Bonding Temperature', *International Conference on Thermal, Mechanical and Multi-Physics Simulation Experiments in Microelectronics and Micro-Systems, EuroSime '07*, 16-18 April 2007, pp. 1-6.

[22] K. Sasaki, N. Iwasa, T. Kurosu, K. Saito, Y. Koike, Y. Kamita, and Y. Toyoda, 'Thermal and Structural Simulation Techniques for Estimating Fatigue Life of an IGBT Module', *20th International Symposium on Power Semiconductor Devices and IC's, ISPSD '08*, Orlando, FL, USA, 18-22 May 2008, pp. 181-184.

[23] R. Amro, J. Lutz, and A. Lindemann, 'Power Cycling with High Temperature Swing of Discrete Components Based on Different Technologies', *35th Annual IEEE Power Electronics Specialists Conference, PESC '04*, Aachen, Germany, 20-25 June 2004, pp. 2593-2598.

[24] A. T. Bryant, P. A. Mawby, P. R. Palmer, E. Santi, and J. L. Hudgins, 'Exploration of Power Device Reliability using Compact Device Models and Fast Electrothermal Simulation', *IEEE Transactions on Industry Applications,* vol. 44, pp. 894-903, May/June 2008.

[25] A. Morozumi, K. Yamada, T. Miyasaka, S. Sumi, and Y. Seki, 'Reliability of Power Cycling for IGBT Power Semiconductor Modules', *IEEE Transactions on Industry Applications,* vol. 39, pp. 665-671, May/June 2003.

[26] S. A. Kharitonov, M. A. Petrov, D. V. Korobkov, M. A. Maslov, and T. Y. Zhoraev, 'A Principle of Calculation Dynamic and Static Power Losses with Hard-Switching IGBT', *6th Annual International Siberian Workshop and Tutorials on Electron Devices and Materials*, Erlagol, Altai, Russia, 1-5 July 2005, pp. 147-149.

[27] M. H. Bierhoff and F. W. Fuchs, 'Semiconductor Losses in Voltage Source and Current Source IGBT Converters Based on Analytical Derivation', *35th Annual IEEE Power Electronics Specialists Conference, PESC '04*, Aachen, Germany, 20-25 June 2004, pp. 2836-2842.

[28] K. Sheng, B. W. Williams, and S. J. Finney, 'A Review of IGBT Models', *IEEE Transactions on Power Electronics,* vol. 15, pp. 1250-1266, November 2000.

[29] P. O. Lauritzen, 'Power Semiconductor Device Models for use in Circuit Simulators', *IEEE Industry Applications Society Annual Meeting*, Seattle, WA, USA, 7-12 October 1990, pp. 1559-1563.

[30] A. N. Githiari, B. M. Gordon, R. A. McMahon, Z.-M. Li, and P. A. Mawby, 'A Comparison of IGBT Models for use in Circuit Design', *IEEE Transactions on Power Electronics,* vol. 14, pp. 607-614, July 1999.

[31] F. Blaabjerg and J. K. Pedersen, 'Optimized Design of a Complete Three-Phase PWM-VS Inverter', *IEEE Transactions on Power Electronics,* vol. 12, pp. 567-577, May 1997.

[32] A. Claudio, M. Cotorogea, and M. A. Rodriguez, 'Parameter Extraction for Physics-Based IGBT Models by Electrical Measurements', *33rd Annual IEEE Power Electronics Specialists Conference, PESC '02*, Queensland, Australia, 23-27 June 2002, pp. 1295-1300.

[33] P. O. Lauritzen, G. K. Andersen, and M. Helsper, 'A Basic IGBT Model with Easy Parameter Extraction', *32nd Annual IEEE Power Electronics Specialists Conference, PESC '01*, Vancouver, BC, Canada, 17-21 June 2001, pp. 2160-2165.

[34] W. Kang, H. Ahn, and M. A. E. Nokali, 'A Parameter Extraction Algorithm for an IGBT Behavioral Model', *IEEE Transactions on Power Electronics,* vol. 19, pp. 1365-1371, November 2004.

[35] P. O. Lauritzen, G. K. Andersen, P. D. Chandana Perera, R. Subramanian, and K. N. Bhat, 'Goals for a Basic Level IGBT Model with Easy Parameter Extraction', *7th Workshop on Computers in Power Electronics, COMPEL '00*, Blacksburg, VA, USA, 16-18 July 2000, pp. 91-96.

[36] M. Cotorogea, A. Claudio, and M. A. Rodriguez, 'Parameter Extraction Method for the Pspice Model of the PT- and NPT-IGBT's by Electrical Measurements', *8th International Conference on Power Electronics Congress, CIEP '02*, Guadalajara, Mexico, 20-24 October 2002, pp. 101-106.

[37] J. Sigg, P. Turkes, and R. Kraus, Application Note: 'Parameter Extraction Methodology and Validation for an Electro-Thermal Physics-Based NPT IGBT Model', Siemens, October 1997.

[38] A. Bryant, P. R. Palmer, J. L. Hudgins, E. Santi, and X. Kang, 'The use of a Formal Optimisation Procedure in Automatic Parameter Extraction of Power Semiconductor Devices', *34th Annual IEEE Power Electronics Specialists Conference, PESC '03*, Acapulco, Mexico, 15-19 June 2003, pp. 822-827.

[39] A. Hefner, Jr. and S. Bouche, 'Automated Parameter Extraction Software for Advanced IGBT Modeling', *7th Workshop on Computers in Power Electronics, COMPEL '00*, Blacksburg, VA, USA, 16-18 July 2000, pp. 10-18.

[40] X. Kang, E. Santi, J. L. Hudgins, P. R. Palmer, and J. F. Donlon, 'Parameter Extraction for a Physics-Based Circuit Simulator IGBT Model', *18th Annual IEEE Applied Power Electronics Conference and Exposition, APEC '03*, Miami Beach, FL, U.S.A, 9-13 February 2003, pp. 946-952.

[41] S. Azuma, M. Kimata, M. Seto, X. Jiang, H. Lu, D. Xu, and L. Huang, 'Research on the Power Loss and Junction Temperature of Power Semiconductor Devices for Inverter', *IEEE International Vehicle Electronics Conference, IVEC '99*, Changchun, China, 6-9 September 1999, pp. 183-187 vol.1.

[42] Z. Zhou, M. S. Khanniche, P. Igic, S. T. Kong, M. Towers, and P. A. Mawby, 'A Fast Power Loss Calculation Method for Long Real Time Thermal Simulation of IGBT Modules for a Three-Phase Inverter System', *11th European Conference on Power Electronics and Applications, EPE '05*, Dresda, Germany, 11-14 September 2005, pp. 10-19.

[43] M. C. Cavalcanti, E. R. da Silva, C. B. Jacobina, D. Boroyevich, and W. Dong, 'Comparative Evaluation of Losses in Soft and Hard-Switched Inverters', *38th IEEE Industry Applications Society Annual Meeting, IAS '03*, Salt Lake City, UT, USA, 12-16 October 2003, pp. 1912-1917.

[44] S. Munk-Nielsen, L. N. Tutelea, and U. Jaeger, 'Simulation with Ideal Switch Models Combined with Measured Loss Data Provides a Good Estimate of Power Loss', *35th IEEE Industry Applications Society Annual Meeting, IAS '00*, Rome, Italy, 8-12 October 2000, pp. 2915-2922.

[45] F. Blaabjerg, J. K. Pedersen, and U. Jaeger, 'Evaluation of Modern IGBT-Modules for Hard-Switched AC/DC/AC Converters', *13th IEEE Industry Applications Society Annual Meeting, IAS '95*, Orlando, FL, USA, 8-12 October 1995, pp. 997-1005.

[46] F. Blaabjerg, J. K. Pedersen, S. Sigurjonsson, and A. Elkjaer, 'An Extended Model of Power Losses in Hard-Switched IGBT-Inverters', *21st IEEE Industry Applications Society Annual Meeting, IAS '96*, San Diego, CA, USA, 6-10 October 1996, pp. 1454-1463.

[47] S. Clemente, 'A Simple Tool for the Selection of IGBTs for Motor Drives and UPSs', *12th Annual IEEE Applied Power Electronics Conference and Exposition, APEC '95*, Dallas, TX, USA, 5-9 May 1995, pp. 755-764.

[48] F. Blaabjerg, U. Jaeger, and S. Munk-Nielsen, 'Power Losses in PWM-VSI Inverter using NPT or PT IGBT Devices', *IEEE Transactions on Power Electronics,* vol. 10, pp. 358-367, May 1995.

[49] P. Salvati, F. Brucchi, and A. D. Medici, Application Note: 'Sinusoidal Inverter using SEMITOP Modules for Electric Vehicles Applications', Semikron.

[50] D. Chen and J. Yang, 'Power Semiconductor Losses and Devices Derating for IGBT based Inverter Drives for Brushless DC Motors', *India International Conference on Power Electronics* Mumbai, India, 20-21 December 2004.

[51] T. Bruckner and S. Bernet, 'Estimation and Measurement of Junction Temperatures in a Three-Level Voltage Source Converter', *IEEE Transactions on Power Electronics,* vol. 22, pp. 3-12, January 2007.

[52] U. Drofenik and J. W. Kolar, 'A General Scheme for Calculating Switching- and Conduction-Losses of Power Semiconductors in Numerical Circuit Simulations of Power Electronic Systems', *International Power Electronics Conference, IPEC '05*, Niigata, Japan, 4-8 April 2005.

[53] B. Backlund, R. Schnell, U. Schlapbach, R. Fischer, and E. Tsyplakov, Application Note: 'Applying IGBTs', ABB, 2007.

[54] M. Ishiko, T. Kondo, M. Usui, and H. Tadano, 'A Compact Calculation Method for Dynamic Electro-thermal Behavior of IGBTs in PWM Inverters', *Power Conversion Conference, PCC '07*, Nagoya, Japan, 2-5 April 2007, pp. 1043-1048.

[55] A. Laprade and R. H. Randal, Application Note: 'Numerical Method for Evaluating IGBT Losses', Fairchild, AN-7520 2000.

[56] A. Odaka, J. Itoh, I. Sato, H. Ohguchi, H. Kodachi, N. Eguchi, and H. Umida, 'Analysis of Loss and Junction Temperature in Power Semiconductors of the Matrix Converter Using Simple Simulation Methods', *39th IEEE Industry Applications Society Annual Meeting, IAS '04*, Seattle, WA, USA, 3-7 October 2004, pp. 850-855.

[57] C. J. M. Lasance, 'Heat Spreading: Not a Trivial Problem', *Electronics Cooling*. vol. 14, May 2008.

[58] J. P. Holman, '*Heat Transfer'*, 7th ed. New York: McGraw-Hill, 1990. ISBN 0079093884.

[59] S. Kakac and K. Yener, '*Heat Conduction'*, 3rd ed. Washington: Taylor and Francis, 1993. ISBN 1560320273.

[60] Z. Luo, H. Ahn, and M. A. El Nokali, 'A Thermal Model for Insulated Gate Bipolar Transistor Module', *IEEE Transactions on Power Electronics,* vol. 19, pp. 902 - 907, July 2004.

[61] A. R. Hefner and D. L. Blackburn, 'Thermal Component Models for Electrothermal Network Simulation', *IEEE Transactions on Components and Packaging Technologies,* vol. 17, pp. 413 - 424, September 1994.

[62] A. Ammous, K. Ammous, H. Morel, B. Allard, D. Bergogne, F. Sellami, and J. Pierre, 'Electrothermal Modelling of IGBT's: Application to Short-Circuit Conditions', *IEE Transactions on Power Electronics,* vol. 15, pp. 778 - 790, July 2000.

[63] P. R. Strickland, 'The Thermal Equivalent Circuit of a Transistor', *IBM Journal of Research and Development,* vol. 3, pp. 35 - 45, January 1959.

[64] F. Profumo, A. Tenconi, S. Facelli, and B. Passerini, 'Instantaneous Junction Temperature Evaluation of High-Power Diodes (Thyristors) During Current Transients', *IEE Transactions on Power Electronics,* vol. 14, pp. 292 - 299, March 1999.

[65] H. A. Mantooth and A. R. Hefner, 'Electrothermal Simulation of an IGBT PWM Inverter', *IEE Transactions on Power Electronics,* vol. 12, pp. 474 - 484, May 1997.

[66] M. Marz and P. Nance, Application Note: 'Thermal Modelling of Power-Electronic Systems', Infineon Technologies AG, Munich, April 2000.

[67] P. E. Bagnoli, C. Cassarosa, M. Ciampi, and E. Dallago, 'Thermal Resistance Analysis by Induced Transient (TRAIT) Method for Power Electronic Devices Thermal Characterization - Part I: Fundamentals and Theory', *IEE Transactions on Power Electronics,* vol. 13, pp. 1208 - 1219, November 1998.

[68] T. Bechtold, E. B. Rudnyi, and J. G. Korvink, 'Dynamic Electrothermal Simulation of Microsystems - A Review', *Journal of Micromechanics and Microengineering,* pp. 17 - 31, October 2005.

[69] A. Ammous, F. Sellami, K. Ammous, H. Morel, B. Allard, and J. Pierre, 'Developing an Equivalent Electrothermal Model for Discrete Semiconductor Packages', *International Journal of Thermal Sciences,* vol. 42, pp. 533 - 539, May 2003.

[70] M. Renze and V. Szekely, 'Studies on the Nonlinearity Effects in Dynamic Compact Model Generation of Packages', *IEEE Transactions on Components and Packaging Technologies,* vol. 27, pp. 124 - 130, March 2004.

[71] Application Note: 'Thermal Equivalent Circuit Models', Infineon, June 2008.

[72] R. David, 'Computerized Thermal Analysis of Hybrid Circuits', *IEEE Transactions on Parts, Hybrids, and Packaging,* vol. 13, pp. 283-290, September 1977.

[73] L. H. Holway, Jr. and M. G. Adlerstein, 'Approximate Formulas for the Thermal Resistance of IMPATT Diodes Compared with Computer Calculations', *IEEE Transactions on Electron Devices,* vol. 24, pp. 156-159, February 1977.

[74] F. N. Masana, 'A Closed Form Solution of Junction to Substrate Thermal Resistance in Semiconductor Chips', *IEEE Transactions on Components, Packaging, and Manufacturing Technology, Part A,* vol. 19, pp. 539-545, December 1996.

[75] F. N. Masana, 'Thermal Characterisation of Power Modules', *Microelectronics Reliability,* vol. 40, pp. 155-161, December 1999.

[76] F. N. Masana, 'A New Approach to the Dynamic Thermal Modelling of Semiconductor Packages', *Microelectronics Reliability,* vol. 41, pp. 901-912, June 2001.

[77] G. N. Ellison, 'Maximum Thermal Spreading Resistance for Rectangular Sources and Plates with Nonunity Aspect Ratios', *IEEE Transactions on Components and Packaging Technologies,* vol. 26, pp. 439-454, June 2003.

[78] C. C. Lee and A. L. Palisoc, 'Real-Time Thermal Design of Integrated Circuit Devices', *IEEE Transactions on Components, Hybrids, and Manufacturing Technology,* vol. 11, pp. 485-492, December 1988.

[79] C. C. Lee, A. L. Palisoc, and Y. J. Min, 'Thermal Analysis of Integrated Circuit Devices and Packages', *IEEE Transactions on Components, Hybrids, and Manufacturing Technology,* vol. 12, pp. 701-709, December 1989.

[80] Y. S. Muzychka, M. M. Yovanovich, and J. R. Culham, 'Thermal Spreading Resistances in Rectangular Flux Channels Part 1 - Geometry Equivalences', *AIAA Thermalphysics Conference*, Orlando, Florida, 23-26 June 2003, pp. 1-10.

[81] Y. S. Muzychka, M. M. Yovanovich, and J. R. Culham, 'Influence of Geometry and Edge Cooling on Thermal Spreading Resistance', *Journal of Thermophysics and Heat Transfer,* vol. 20, pp. PP 247-255, April/June 2006.

[82] A. Bhatt and J. Rhee, 'Thermal Spreading Resistance for Square and Rectangular Entities', *11th International Symposium on Advanced Packaging Materials: Processes, Properties and Interface* Atlanta, GA, USA, 15-17 March 2006, pp. 175-178.

[83] R. D. Lindsted and R. J. Surty, 'Steady-State Junction Temperatures of Semiconductor Chips', *IEEE Transactions on Electron Devices,* vol. 19, pp. 41-44, January 1972.

[84] S. Lee, S. Song, V. Au, and K. P. Morgan, 'Constriction/Spreading Resistance Model For Electronic Packaging', *ASME/JSME Thermal Engineering Conference*, Maui, Hawaii 19-24 March 1995, pp. 199-206.

[85] M. M. Yovanovich, 'Thermal Resistances of Circular Source on Finite Circular Cylinder With Side and End Cooling', *Journal of Electronic Packaging,* vol. 125, pp. 169-177, June 2003.

[86] M. M. Yovanovich, J. R. Culham, and P. Teertstra, 'Analytical Modeling of Spreading Resistance in Flux Tubes, Half Spaces, and Compound Disks', *IEEE Transactions on Components, Packaging, and Manufacturing Technology, Part A,* vol. 21, pp. 168-176, March 1998.

[87] L.-K. Wu and B. Kao, 'A Study of Thermal Spreading Resistance', Innovative Technique Center, Chung-Ho City, 2004.

[88] C. J. M. Lasance, 'The Influence of Various Common Assumptions on the Boundary Condition Independence of Compact Thermal Models', *IEEE Transactions on Components and Packaging Technologies,* vol. 27, pp. 523 - 529, September 2004.

[89] C. Lasance, H. Vinke, H. Rosten, and K. L. Weiner, 'A Novel Approach for the Thermal Characterization of Electronic Parts', *11th Annual IEEE Semiconductor Thermal Measurement and Management Symposium, SEMI-THERM '95*, San Jose, CA, USA, 7-9 February 1995, pp. 1-9.

[90] C. J. M. Lasance, H. Vinke, and H. Rosten, 'Thermal Characterization of Electronic Devices with Boundary Condition Independent Compact Models', *IEEE Transactions on Components, Packaging, and Manufacturing Technology, Part A,* vol. 18, pp. 723-731, December 1995.

[91] C. J. M. Lasance, 'Ten Years of Boundary-Condition- Independent Compact Thermal Modeling of Electronic Parts: A Review', *Heat Transfer Engineering,* vol. 29, pp. 149-168, 2008.

[92] F. Christiaens, B. Vandevelde, E. Beyne, R. Mertens, and J. Berghmans, 'A Generic Methodology for Deriving Compact Dynamic Thermal Models, Applied to the PSGA Package', *IEEE Transactions on Components, Packaging, and Manufacturing Technology, Part A,* vol. 21, pp. 565-576, January 1998.

[93] S. Shidore, V. Adams, and L. Tien-Yu Tom, 'A study of Compact Thermal Model Topologies in CFD for a Flip Chip Plastic Ball Grid Array Package', *7th Intersociety Conference on Thermal and Thermomechanical Phenomena in Electronic Systems, ITHERM '00*, Las Vegas, NV, USA, 23-26 May 2000.

[94] C. J. M. Lasance, 'Two Benchmarks to Facilitate the Study of Compact Thermal Modelling Phenomena', *IEEE Transactions on Components and Packaging Technologies,* vol. 24, pp. 559 - 565, December 2001.

[95] A. Castellazzi, M. Ciappa, W. Fichtner, G. Lourdel, and M. Mermet-Guyennet, 'Comprehensive Electro-Thermal Compact Model of a 3.3kV-1200A IGBT-module', *International Conference on Power Engineering, Energy and Electrical Drives, POWERENG '07*, Setubal, Portugal, 12-14 April 2007, pp. 405-410.

[96] J. Reichl, D. Berning, A. R. Hefner, and S. J. Lai, 'Six Pack IGBT Dynamic Electrothermal Model Parameter Extraction and Validation', *19th Annual IEEE Applied Power Electronics Conference and Exposition, APEC '04*, Anaheim, CA, USA, 22-26 February 2004, pp. 246 - 251.

[97] J. R. Reichl, J. S. Lai, A. R. Hefner, T. R. McNutt, and D. Berning, 'Inverter Dynamic Electro-Thermal Modeling and Simulation with Experimental Verification', *36th Annual IEEE Power Electronics Specialists Conference, PESC 2005*, Recife, Brazil, 5 June 2005, pp. 2208-2215.

[98] J. Reichl, 'Inverter Dynamic Electro-Thermal Simulation with Experimental Verification', *Electrical Engineering*. vol. Master of Science in Electrical Engineering Blacksburg, Virginia: Virginia Polytechnic Institute and State University, November 2005.

[99] J. J. Rodriquez, A. R. Hefner, J. Reichl, Z. Parrilla, D. Berning, S. J. Lai, and M. Velez-Reyes, 'Thermal Component Models for Electrothermal Analysis of Multichip Power Modules', *37th IEEE Industry Applications Society Annual Meeting, IAS '02*, Pittsburgh, PA, USA, 13-18 October 2002, pp. 234 - 241.

[100] R. Stout, 'Linear Superposition Speeds Thermal Modeling - Part 1', *Power Electronics Technology*2007, pp. 20-25.

[101] U. Drofenik, D. Cottet, A. Musing, J.-M. Meyer, and J. W. Kolar, 'Computationally Efficient Integration of Complex Thermal Multi-Chip Power Module Models into Circuit Simulators', *Power Conversion Conference, PCC '07*, Nagoya, Japan, 2-5 April 2007, pp. 550-557.

[102] F. Profumo, A. Tenconi, S. Facelli, and B. Passerini, 'Analysis of the Electrothermal Behaviour of Multichip Power Modules', *33rd IEEE Industry Applications Society Annual Meeting, IAS '98*, St. Louis, MO, USA, 12-15 October 1998, pp. 1031 - 1037.

[103] T. Franke, G. Zaiser, J. Otto, M. Honsberg-Riedl, and R. Sommer, 'Current and Temperature Distribution in Multi-Chip Modules under Inverter Operation', *8th European Conference on Power Electronics and Applications, EPE '99*, Lausanne, Switzerland, 7-9 September 1999.

[104] L. Geng, Z.-m. Chen, R. Kruemmer, T. Reimann, and J. Petzoldt, 'A Precise Model for Simulation of Temperature Distribution in Power Modules', *Chinese Journal of Semiconductors,* vol. 22, pp. 548-553, May 2001.

[105] S. Carubelli and Z. Khatir, 'Experimental Validation of a Thermal Modelling Method Dedicated to Multichip Power Modules in Operating Conditions', *Microelectronics Journal,* vol. 34, pp. 1143 - 1151, December 2003.

[106] Z. Khatir, S. Carubelli, and F. Lecoq, 'Real Time Computation of Thermal Constraints in Multichip Power Electronic Devices', *IEEE Transactions on Components and Packaging Technologies,* vol. 27, pp. 337 - 344, June 2004.

[107] M. J. Whitehead and C. M. Johnson, 'Determination of Thermal Cross-Coupling Effects in Multi-Device Power Electronic Modules', *3rd IET International Conference on Power Electronics, Machines and Drives, PEMD '06*, Dublin, Ireland 4-6 April 2006, pp. 261-265.

[108] M. J. Whitehead and C. M. Johnson, 'Junction Temperature Elevation as a Result of Thermal Cross Coupling in a Multi-Device Power Electronic Module', *Electronics Systemintegration Technology Conference*, Dresden, Germany, 5-7 September 2006, pp. 1218-1223.

[109] Z. Zhou, M. S. Khanniche, P. Igic, S. N. Jankovic, S. G. Batcup, and P. A. Mawby, 'Dynamic Thermal Simulation of Power Devices Operating with PWM Signals', *25th International Conference on Microelectronics, MIEL '06*, Portoroz, Slovenia, 30 August - 2 September 2006, pp. 183-186.

[110] R. Valentine, '*Motor Control Electronics Handbook*', 1st ed.: McGraw-Hill Professional, 1998. ISBN 0070668108.

[111] 'FP75R12KE3 Technical Information', Infineon Technologies, 2002.

[112] V. Blasko, R. Lukaszewski, and R. Sladky, 'On Line Thermal Model and Thermal Management Strategy of a Three Phase Voltage Source Inverter', *34th IEEE Industry Applications Society Annual Meeting, IAS '99*, Phoenix, AZ, USA, 3-7 October 1999, pp. 1423-1431 vol.2.

[113] 'Unidrive SP User Guide', Control Techniques, 2009.

[114] 'http://www.infrared-thermography.com/material-1.htm'.

[115] 'http://www.raytek.com/Raytek/en-r0/IREducation/EmissivityNonMetals.htm'.

[116] 'http://www.omega.com/temperature/Z/pdf/z088-089.pdf'.

[117] D. L. Blackburn and F. F. Oettinger, 'Transient Thermal Response Measurements of Power Transistors', *IEEE Transactions on Industrial Electronics and Control Instrumentation,* vol. IECI-22, pp. 134-141, May 1975.
[118] U. Scheuermann, 'Thermal Impedance of System: Measurement and Evaluation', *ECPE Tutorial: Thermal Engineering of Power Electronic Systems Part II*, Nuremberg 2009.
[119] F. P. Incropera, D. P. DeWitt, T. L. Bergman, and A. S. Lavine, '*Fundamentals of Heat and Mass Transfer '*, 6th Edition ed.: John Wiley & Sons, 2006. ISBN 0471457280
[120] G. Finis and A. Claudi, 'On the Electric Breakdown Behaviour of Silicone Gel at Interfaces', *IEEE Transactions on Dielectrics and Electrical Insulation,* vol. 15, pp. 366-373, April 2008.
[121] Application Note: 'Using Integrated NTC with Reliable Isolation', European Power Semiconductor and Electronics Company (EUPEC).
[122] '34970A Data Acquisition/Switch Unit Product Overview', Agilent, 2005.
[123] 'SC5000-Series Product Guide', Flir, 2009.
[124] 'IGBT Module U-Series Product and Applications Brochure', Powerex 1997.
[125] U.Scheuermann and U.Hecht, 'Power Cycling Lifetime of Advanced. Power Modules for Different Temperature Swings', *Power Conversion Intelligent Motion Conference, PCIM '02*, Nuremberg, Germany, 14-16 May 2002, pp. 59-64.
[126] J. Dodge and J. Hess, Application Note: 'IGBT Tutorial', Advanced Power Technology, July 2002.
[127] 'http://hyperphysics.phy-astr.gsu.edu/hbase/electric/restmp.html'.
[128] U. Scheuermann, 'Design for Reliability', *ECPE Tutorial: Thermal Engineering of Power Electronic Systems Part II*, Nuremberg 2009.
[129] A. Elasser, M. H. Kheraluwala, M. Ghezzo, R. L. Steigerwald, N. A. Evers, J. Kretchmer, and T. P. Chow, 'A Comparative Evaluation of New Silicon Carbide Diodes and State-of-the-art Silicon Diodes for Power Electronic Applications', *IEEE Transactions on Industry Applications,* vol. 39, pp. 915-921, July/August 2003.
[130] 'STGY50NC60WD Technical Information', ST Microelectronics, 2009.
[131] 'http://powerelectronics.com/power_semiconductors/power_mosfets/804PET21test-saturation-voltage.pdf'.
[132] W. Frank, Application Note: 'Next Generation IGBT for Motor Drive Applications', Infineon, October 2004.
[133] T. Laska, L. Lorenz, and A. Mauder, 'The New IGBT Generation a Great Improvement Potential for Motor Drive Systems', *35th IEEE Industry Applications Society Annual Meeting, IAS '00.*, Rome, Italy, 8-12 October 2000, pp. 2885-2889.